Port-Hamiltonian approach for modelling, reduction and control of plasma dynamics in tokamaks

Ngoc Minh Trang Vu

UNIVERSITÉ DE GRENOBLE

THÈSE

Pour obtenir le grade de

DOCTEUR DE L'UNIVERSITÉ DE GRENOBLE

Spécialité : **Automatique et Productique**

Arrêté ministériel : 7 août 2006

Présentée par

VŨ Ngọc Minh Trang

Thèse dirigée par **Laurent LEFÈVRE**
et codirigée par **Rémy NOUAILLETAS**

préparée au sein **Laboratoire de Conception et d'Intégration des Systèmes LCIS EA-3747 –Grenoble INP – UPMF**
et de **l' École Doctorale Électronique, Électrotechnique, Automatique, Traitement du Signal EEATS (220)**

Approche hamiltonienne à ports pour la modélisation, la réduction et la commande des dynamiques des plasmas dans les tokamaks

Thèse soutenue publiquement le **12 Novembre 2014**,
devant le jury composé de :

M. Jacques BLUM
Professeur, Université Nice Sophia Antipolis, Rapporteur
M. Sylvain BRÉMOND
Docteur, STEP/IRFM, CEA, Cadarache, Examinateur
M. Laurent LEFÈVRE
Professeur, Université Grenoble Alpes, Directeur de thèse
M. Bernhard MASCHKE
Professeur, Université Claude Bernard Lyon 1, Président
M. Rémy NOUAILLETAS
Docteur, STEP/IRFM CEA, Cadarache, Co-Directeur de thèse
M. Olivier SAUTER
Professeur, École Polytechnique Fédérale de Lausanne, Suisse, Examinateur
M. Arjan van der SCHAFT
Professeur, University of Groningen, The Netherlands, Rapporteur

The port-Hamiltonian approach for the modelling, reduction and control of plasma's dynamics in tokamaks

Thesis 2014

By
VŨ Ngọc Minh Trang

Supervisor: **Laurent LEFÈVRE**
Co-supervisor: **Rémy NOUAILLETAS**

Jury

Mr. Jacques BLUM	Reviewer, Pr, Univ. Nice Sophia Antipolis, France
Mr. Sylvain BRÉMOND	Member, Dr, STEP/IRFM CEA, Cadarache, France
Mr. Laurent LEFÈVRE	Supervisor, Pr, Univ. Grenoble Alpes, France
Mr. Bernhard MASCHKE	President, Pr, Univ. Claude Bernard Lyon 1, France
Mr. Rémy NOUAILLETAS	Co-supervisor, Dr, STEP/IRFM CEA, Cadarache, France
Mr. Olivier SAUTER	Member, Pr, École polytechnique fédérale de Lausanne, Switzerland
Mr. Arjan van der SCHAFT	Reviewer, Pr, Univ. of Groningen, The Netherlands

Laboratoire de Conception et d'Intégration des Systèmes (LCIS)
- Univ. Grenoble Alpes, LCIS, F-26902, France
CEA, IRFM, Cadarache, F-13108 Saint Paul lez Durance, France

November 12^{th}, 2014

Acknowledgments

This memory of thesis concludes my three and a half-years working in LCIS laboratory in Valence, France. It has been, and will be always a good souvenir in my study time. On this occasion, I'd like to warmly thank to all, who are always by my side.

Firstly, I owe a debt of gratitude to my two supervisors Mr. Laurent LEFÈVRE and Mr. Rémy NOUAILLETAS. Although I haven't had any other supervisors but them and I don't know how wonderful the others are, mine are the best to me. It's my golden chance to be guided by two experts, Laurent on the theoretical side and Rémy on the practical one. The hundreds of long discussions with Laurent contributed many interesting ideas to my thesis, of course, beside many others which were sometimes "out of subject". That made me admire more his rich knowledge in many different research domains. In the other side, the hundreds of hours debugging the tiny errors on Matlab simulink with Rémy taught me to be patient and showed me plenty of useful tips when using Matlab that I can't learn at school.

I truly appreciate their kindness and their friendship that make my thesis a pleasant cooperation. Thanks to them, I can strengthen my slogan: *No matter what you do and no matter where you are, the most important thing is with whom you work.* "Thank you for your availability whenever I need to discuss somethings, for your patience with my stubbornness and my lacking idea". In their eyes, I'm not an under-command-student, a newbie, but a real colleague, who they usually invite for diners with their family. "Let send my big hugs to your family for your warm welcome and your delicious meals".

My thesis can't success without the very significant contribution of the jury members. Let me send my gratefulness to the reviewers Mr. Jacques BLUM and Mr. Arjan van der SCHAFT, who kept patience and courage to accept to review and to try to understand my mixed-french-english (with Vietnamese style) thesis memory. Thanks for their kind reports which encourage me much in my research avenue.

I'd like to thank the president of the jury, Mr. Bernhard MASCHKE, the examiners Mr. Sylvain BRÉMOND and Mr. Olivier SAUTER for their present in my thesis defense to witness this important moment. Moreover, "thanks to Bernhard for your humor communication, your academic advices, and your precious cooperation despite of all your "urgent missions" everytime. We finally finished our 3-year-paper, so-that we can begin another n-year-one (I hope that $n < 3$) in the future". "Thanks to Sylvain for your critical point of view on the practice aspect, which prevents our work going so-far from the reality". "Thanks to Olivier for your experiences and your great cooperation on the TCV experiments, which help to validate one of my control law in my thesis".

A huge thank to all the work-teams of CEA and CRPP/TCV for their warm welcome when I dropped by their laboratories. Especially thanks to Mr. Xavier GARBET and Ms. Clarisse BOURDELLE for their interesting discussions about plasma physics, Mr. Eric NARDON for the bootstrap story, Mr. Philippe MOREAU for accompanying me through the CEA security barrier; Mr. Federico FELICI and Mr. LE Hoang Bao for their numerous helps in the TCV experimental section.

It was not only my work that attached me to the laboratory, but also my dear colleagues in LCIS. A hearty thank is sent to Ms. Jennyfer DUBERVILLE and Ms. Carole SEYVET, the LCIS secretaries for their willing to help me with all the administrative papers in order to simplify my official life. Special thanks to Ms. Florence GALLI, head of International Relations at Grenoble INP - Esisar, who takes care of all the foreign students, like me, and is always by our side in any events, whether joyful or sorrowful. I deeply appreciate the gossips during the coffee breaks with my next-door colleagues Mr. Clément RAIEVSKY, Ms. Divya UNNIKRISHNAN and Mr. Gianfranco ANDIA VERA, thanks to this, I'm always updated with the recent news in our laboratory. I also take this opportunity to thank everyone in the computing service Mr. Joackim PERSE, Mr. Frederic THERON and Mr. Cedric CARLOTTI for their important technical supports. Thanks to my "sensei", "senpai" and "kōhai" Ms. Veronique ANSELIN, Mr. Marc LETI, Mr. Guillaume ANGE, Mr. Nicolas ALLÈGRE in all my sport clubs for all the enjoyable moments all-together. It no doubt strengthens my health but it also reinforces my spirit so-that I've never been under-pressure by my work (though I often heard the contrary from the ancient PhD. students).

Everything would have not been the same without the Vietnam environment in France, I'm grateful to the Vietnamese community, the families of Mr. HIẾU, Ms. TIÊN, Ms. TRANG, Mr.

LAI, Ms. LOAN, Ms. THOA, Ms. KHÂM; the Vietnamese students VY, N.ANH, HỰNG, THÔNG, VUỢNG, V.ANH, LINH. I'll keep in mind everyone's bright face in our unforgettable celebrations: the TET holidays, the Mid-Autumn festivals, the birthday parties, or even the weekend parties to celebrate for nothing. That's when we can enjoy plenty of adorable Vietnamese food. I find myself at home when they're around, whereas my hometown is thousand miles faraway. "I'd like to deeply thank you for sharing my life during five years in this foreign country". There're also two best friends in Vietnam that I can't miss, Ms. THAO and Ms. THU, with whom I can discover the meaning of the youth and the friendship.

Finally, the biggest thank I'd like to dedicate to my family, my daddy HÙNG, my mommy HÀ, my sweethearts CHÂU Dieu and PINKGO, who unconditionally stay with me all the time, encourage me in my work and show me the light whenever I feel lost. Warmly thanks to my dear relatives for trusting me and being always proud of me.

Trang VŨ

Abstract

The port-Hamiltonian approach for the modelling of multiphysics systems is based on the explicit representation of all power exchanges between the multi-domain subsystems. Besides, this approach allows to consider subsystems with complex dynamics, including nonlinear behaviours or spatially distributed phenomena. It is therefore a potential candidate for the modelling of the plasma dynamics in nuclear fusion facilities called Tokamaks.

In this work, a port-Hamiltonian model, using various Dirac structures, is derived for the Thermo-Magneto-HydroDynamics (TMHD) of plasmas in tokamaks. Maxwell field equations as well as balance and closure equations in the material domain are expressed in their covariant form. First a kinetic theory point of view is adopted and transport equations are derived from the Boltzmann equation. Then material derivatives are introduced to deduce macroscopic balance equations of the TMHD fluid model from these kinetic transport equations. Finally, the Gibbs-Duhem equation is used to compute the irreversible entropy source term and to define the interdomain $\mathcal{R}$ - field of the model. All derived interdomain couplings in the material domain are represented using Stokes-Dirac structures and a resistivity $\mathcal{R}$ - field structure. The complete model is summarized in a Bond Graph.

The following stage is a geometric spatial reduction methodology which aims to preserve, throughout the reduction, both the symplecticity of the Dirac interconnection structure and the physical extensive quantities of the original system. It is based on projections which make use of the symmetries and the preservation of the "natural" power pairing for the considered system. The method is applied to a system of two coupled parabolic equations describing the poloidal magnetic flux radial diffusion and the heat radial transport in tokamak reactors. There are two reduction steps, first to reduce the model from *3D* to *1D*, and then from *1D* to *a 0D* finite dimensional approximation. The assumptions of axial symmetry and quasi-static equilibrium of the plasma are used to perform the reduction from *3D* to *1D* by using simple integration formulas on toroidal coordinate surfaces. A Galerkin-type pseudo-spectral spatial reduction method is used to reduce the *1D* model to a *0D* one. Both reductions are symplectic with respect to the power-pairings in the magnetic and thermal domains. Finally, the *0D* plasma control model is obtained by reduction of the multi-domains couplings between the two diffusion PDEs. The obtained model's accuracy is suitable for an efficient control design.

An Interconnection and Damping Assignment - Passivity Based Control (IDA-PBC) , the most general Port-Hamiltonian control, is chosen first to deal with the studied Tokamak system. It is based on a model made of the two coupled PDEs of resistive diffusion for the magnetic poloidal flux and of radial thermal diffusion. The used TMHD couplings are the Lorentz forces (with non-uniform resistivity) and the bootstrap current. The loop voltage at the plasma boundary, the total external current and the plasma heating power are considered as controller outputs. Due to the actuator constraints which imply to have a physically feasible current profile deposits, a feedforward control is used to ensure the compatibility with the actuator physical capability. Then, the IDA-PBC controllers, both finite-dimensional and infinite-dimensional, are designed to improve the system stabilization and convergence speed. The proposed works are validated against the simulation data obtained from the Tore-Supra WEST (CEA/Cadarache, France) test case and from RAPTOR code for the TCV real-time control system (CRPP/ EPFL, Lausanne, Switzerland).

Publications

Journal articles

- Trang.N.M. Vu, L. Lefèvre, R. Nouailletas, and S. Brémond.
"Symplectic Galerkin schemes for the spatial discretization of port-Hamiltonian"
Applied numerical mathematics journal, 2014 (submitted)

- Trang.N.M. Vu, L. Lefèvre, and V. Thang Pham
"Finite rank distributed control for the resistive diffusion equation using damping assignment"
Evolution Equations and Control Theory (EECT) - AIMS, 2014 (accepted)

- Trang.N.M. Vu, L. Lefèvre, and B. Maschke
"Port-hamiltonian formulation for systems of conservation laws: application to plasma dynamics in tokamak reactors"
Mathematical and Computer Modelling of Dynamical Systems, 2014 (submitted)

Conference articles

- Trang.N.M. Vu, L. Lefèvre, R. Nouailletas
"Distributed and backstepping boundary controls to achieve IDA-PBC design"
MATHMOD 2015 - 8th Vienna International Conference on Mathematical Modelling, Vienna, Austria, February 18 - 20 2015 (submitted)

- Trang.N.M. Vu, R. Nouailletas, L. Lefèvre, S. Brémond, and F. Felici
"IDA-PBC control for the coupled plasma poloidal magnetic flux and heat radial diffusion equations in tokamaks"
19th World Congress of the International Federation of Automatic Control, Cape Town, South Africa, August 24-29 2014

- Trang.N.M. Vu, L. Lefèvre, R. Nouailletas, and S. Brémond
"Structure preserving reduction for thermo-magneto plasma control model"
The 21st International Symposium on Mathematical Theory of Networks and Systems, Groningen, Netherlands, July 07-11 2014

- Trang.N.M. Vu, L. Lefèvre, R. Nouailletas, and S. Brémond
"An IDA-PBC approach for the control of 1d plasma prole in tokamaks"
52nd IEEE Conference on Decision and Control, Florence, Italy, December 10-13 2013

- Trang.N.M. Vu and L.Lefèvre
"Material balance and closure equations for plasmas in tokamaks"
IFAC Workshop on Thermodynamic Foundations of Mathematical Systems Theory, Lyon, France, July 13-16 2013

- Trang.N.M. Vu, L. Lefèvre, R. Nouailletas, and S. Brémond
"Geometric discretization for a plasma control model"
IFAC Joint conference: 5th Symposium on System Structure and Control, Grenoble, France, February 2013

- Trang.N.M. Vu, L. Lefèvre, and B. Maschke
"Port-hamiltonian formulation for systems of conservation laws: application to plasma dynamics in tokamak reactors"
4th IFAC Workshop on Lagrangian and Hamiltonian Methods for Non Linear Control, Bertinoro, Italy, August 29-31 2012

Contents

1 Introduction **1**

I Port-Hamiltonian approach for thermonuclear fusion and control challenges 1

II Main contributions of this work 3

III Outline 4

2 *3D* port-Hamiltonian Tokamak model **6**

I Tokamak devices 6

I.1 Tore-Supra 9

I.2 TCV 9

II Related works and motivations 11

III Background: Port-based modelling for distributed parameter systems of conservation laws with boundary energy flows 12

III.1 Co-variant form and exterior calculus notations 12

III.1.1 Differential form 12

III.1.2 Exterior product: 13

III.1.3 Exterior derivation 13

III.1.4 Hodge star operator 13

III.1.5 Contraction 14

III.2 Systems of conservation laws 14

III.3 Stokes-Dirac structures and systems of balance equations 15

III.4 Examples of boundary port-Hamiltonian systems 16

III.4.1 *1D* ideal transmission line 16

III.4.2 *3D* Diffusion 17

IV Co-variant formulation for the dynamics in the electromagnetic domain 17

V Balance equations in the material domain 19

V.1 Kinetic theory and macroscopic transport equations 19

V.1.1 Boltzmann equation 19

V.1.2 Transport equations (balance equations) 20

V.2 Co-variant formulation of the transport equations 21

V.2.1 Time derivative "following the motion" 21

V.2.2 Conservation law equations and closure equation 22

V.3 Closure equations and entropy production 23

V.3.1 Momentum 23

V.3.2 Internal energy 23

V.3.3 Entropy 24

VI Multidomain couplings and resistivity field ($\mathcal{R}$ - field) 24

VI.1 Magneto-hydrodynamic coupling (MHD coupling) 24

VI.1.1 Magnetomotive coupling 25

VI.1.2 Eulerian-Lagrangian transformation 26

VI.2 Interdomain couplings in different material domains 26

VI.3 Resistive field ($\mathcal{R}$ - field) 27

VII Integration of the complete model with port-based approach 27

VIII Conclusion 30

3 Geometric reduction **31**
I Introduction . . . 31
II Reduction assumptions: axis-symmetry and quasi-static equilibrium . . . 32
II.1 Axisymmetry assumption . . . 33
II.2 Quasi-static equilibrium assumption . . . 33
II.3 Magnetic surfaces and magnetic toric coordinate . . . 33
III *3D-1D* Geometric reduction method . . . 34
IV The resistive diffusion equation example . . . 37
IV.1 EM Stokes-Dirac structure . . . 37
IV.2 Reduced constitutive relations in EM domain . . . 39
V The thermal diffusion equation example . . . 41
VI Thermo-Hydro-Dynamic couplings . . . 43
VI.1 Magnetomotive coupling . . . 43
VI.2 Eulerian-Lagrangian transformation . . . 43
VI.3 Parameter identification issues . . . 44
VII Conclusion . . . 44

4 Symplectic discretization **45**
I Introduction . . . 45
II Discretization methodology . . . 46
II.1 Approximation bases for flows and efforts . . . 47
II.2 Bilinear power product and finite dimensional Stokes' theorem . . . 47
II.3 Canonical discrete Dirac structure for the resistive diffusion equation . . . 49
II.4 Storage and dissipation constitutive relations . . . 50
II.4.1 Energy storage element . . . 50
II.4.2 Energy dissipation element . . . 51
II.5 Boundary conditions . . . 51
II.5.1 Homogeneous boundary conditions . . . 51
II.5.2 Non-homogeneous boundary conditions . . . 52
III Choice of effort and flow approximation spaces . . . 52
III.1 Symplectic orthogonal collocation . . . 53
III.1.1 Polynomial approximation's functions choice . . . 53
III.1.2 Numerical oscillations in the magnetic field profile . . . 55
III.2 Symplectic spectral method . . . 55
III.3 Symplectic Galerkin scheme . . . 57
IV Comparison against experimental data . . . 58
IV.1 Test case definition . . . 58
IV.2 Results . . . 58
V Symplectic discretization applied to thermal diffusion equation . . . 60
V.1 Thermal PCH discrete model . . . 60
V.2 Constitutive relations . . . 60
VI Conclusion . . . 62

5 IDA-PBC Controller design **64**
I Introduction . . . 64
II IDA-PBC closed loop control . . . 65
II.1 Methodology overview . . . 65
II.2 Integrator extension . . . 66
II.3 Optimal control . . . 67
II.4 Control strategy . . . 68
II.5 Robustness analysis . . . 69
III First case study: the PCH resistive diffusion model . . . 70
III.1 The resistive diffusion model . . . 70
III.2 Reference state generation for the resistive diffusion model . . . 70
III.3 Controller tuning . . . 71
III.3.1 IDA-PBC simple choice: energy shaping and damping assignment . . . 71
III.4 Simulation results . . . 72

III.4.1 Results for the Tore Supra WEST configuration . . . 72
III.4.2 Results for the TCV configuration . . . 73
III.5 Experimental result . . . 76
IV TMHD Coupled system . . . 78
IV.1 TMHD control system . . . 79
IV.2 Steady state generation for coupled TMHD model . . . 80
IV.3 Controller tuning . . . 81
IV.4 Simulation . . . 81
V Conclusion . . . 84

6 IDA-PBC-like controller for infinite-dimensional PHS 85
I Introduction . . . 85
II IDA-PBC control for infinite-dimensional port-Hamiltonian systems . . . 86
II.1 The class of considered original and target port-Hamiltonian systems . . . 86
II.2 Energy shaping and damping assignment for a subclass of linear port-Hamiltonian systems . . . 88
III Damping assignment design for the resistive diffusion equation . . . 89
III.1 Infinite-dimensional PCH formulation for the resistive diffusion equation . . . 89
III.2 Controller tuning . . . 90
III.3 Simulation result . . . 91
IV IDA-PBC boundary control . . . 93
IV.1 Average matching equation solutions . . . 93
IV.2 IDA-PBC extension: matching equation relaxation . . . 94
IV.3 Solving new matching equation . . . 95
IV.3.1 $k(z, y)$ determination . . . 96
IV.3.2 Find $(\mathcal{R}_d, \mathcal{Q}_d)$ . . . 96
IV.4 Simulation . . . 97
V Conclusion . . . 99

7 Conclusion and perspectives 100

A Tokamak plasma parameters 102

B Covariant form 104
I Differential forms . . . 104
I.1 Exterior product . . . 104
I.2 Exterior Derivative . . . 105
II Hodge star operator . . . 105
III Interior product and Contraction . . . 106
III.1 Contraction and corresponding . . . 106

C Microscopic model (Transport equations) 108
I Equation of continuity (particle transport equation) . . . 108
II Equation of motion (momentum transport) . . . 108
III Energy transport . . . 109
IV Equation of internal energy (heat balance equation) and entropy equation . . . 110

D Magnetic toric coordinate 111
I From Cartesian to magnetic toric coordinate transformation . . . 111
II Derivative operators in magnetic toric coordinate . . . 112

E Theoretical eigenvalues for the diffusion operator 113
I Theoretical eigenvalues for the resistive diffusion equation . . . 113
II Theoretical eigenvalues for the thermal diffusion equation . . . 114

F Error analysis of Symplectic Collocation method **116**
I Influence of collocation point choice 116
II Influence of eigenfunction, base function choice 116
II.1 Symplectic collocation with boundary constraints 117
II.2 Symplectic collocation without boundary constraints 117

G Finite difference approximation scheme **119**

List of Figures

I.1 The fusion reaction between Deuterium and Tritium Hydrogen isotopes which produces Helium, energy and and a high kinetic energy neutron particle 1

I.1 Tokamak design chosen for the ITER project 7
I.2 Schematic view of a tokamak with the electrical solenoids: the magnetic field generated by the three magnets makes the plasma gas ions following helicoidal trajectories along the torus 7
I.3 Multiphysic Tokamak model with main interdonmain couplings 8
I.4 Tore-Supra Tokamak device in CEA/Cadarache 9
I.5 TCV overview in CRPP/EPFL 10
I.6 Plasma shapes in TCV 10
VII.1 Simple Bondgraph 28
VII.2 Bondgraph of thermodynamic tokamak system including electromagnetic domain (blue), mechanic domain (green), thermal domain (red) and hydraulic domain (black) 29

II.1 Magnetic toric coordinates. θ denotes the polar angle and ϕ the azimuth angle. B_θ and B_ϕ are the two magnetic field coordinates ($B_\rho = 0$). R_0 denotes the tokamak major radius and I_p the total plasma current. 32
II.2 The poloidal flux $\psi(R, Z)$ is the magnetic flux traversing the horizontal disk S 33
II.3 Constant level curves of the poloidal flux function for a plasma equilibrium in the toric geometric coordinate (r, θ, ϕ). These curves become the nested toroids in magnetic toric coordinate (ρ, θ, ϕ). 34

III.1 B_θ profile with constant uniform resistivity $\eta = 5.10^{-7}$ controlled using a nonzero boundary condition $V_{loop} \neq 0$; without distributed source term $j_{ni} = 0$ (left) and with distributed source term $j_{ni} \neq 0$ (right) 55
IV.1 In-Output comparison 59
IV.2 Safety factor q comparison 59
V.1 Electronic temperature profiles - time evolution comparison 62
V.2 Electronic temperature profiles - space evolution comparison 63

II.1 The proposed control strategy: a nonlinear feedforward control and a feedback control designed with the help of the linearized model 69
III.1 Open loop system with only the feedforward part of the controller 73
III.2 Closed loop system with the full finite dimensional controller (feedforward and feedback parts) 74
III.3 Open-loop response with feedforward control 75
III.4 The response of the closed loop system with an IDA-PBC controller and a small damping $\mathcal{R}_a$ 75
III.5 The response of the closed loop system with an IDA-PBC controller and a larger damping $\mathcal{R}_a$ 76
III.6 Closed loop system with IDA-PBC controller with integrator effect 76
III.7 Closed loop system with IDA-PBC controller (with the integrator) with perturbations on the resistivity and on the actuator spatial distribution 77
III.8 TCV shock 49514 78

IV.1 Feedforward control of coupled system 82
IV.2 Feedback control of coupled system 82
IV.3 Feedback control of coupled system with a supplementary integrator 83
IV.4 T profiles at $t = 0.7s$ (a) and $t = 1.5s$ (b) 83

III.1 Feedback with the distributed control u_1 92
III.2 Feedback with the distributed control u_1 and the boundary control u_2 92
IV.1 Simulation result of boundary IDA-PBC control for infinite dimensional resistive diffusion equation in Tokamaks 97
IV.2 Error comparison between the presented method, the infinite IDA without boundary control, the (traditional) finite IDA-PBC and the feedforward control 98
IV.3 Simulation result of boundary IDA-PBC control with integrator 99

I.1 Geometric toric coordinate 111

I.1 The Bessel function $J_0(z)$ and its first zeros values 114

II.1 The first and fifth calculated eigenfunctions with boundary conditions $w_i^e = 1-x^2\zeta_i^2 l_i$ vs theoretical Bessel eigenfunctions 118
II.2 Simulation for the case of $we_i = le_i$ with constant $\eta = 5.10^{-7}$, without boundary conditions 118

List of Tables

I.1 Classification of plasma control problems 2

III.1 Contraction and equivalent products 14
IV.1 The vector notation form and the co-variant formulation of the characteristic equations of electrodynamics. 18

III.1 The variables in the 3D model are k-forms α^k of order 0, 1, 2 or 3 35
III.2 Reduced variables definitions in the *1D* domain Π obtained from the integrations of corresponding variables in the *3D* domain (written in toric coordinates) 36

III.1 Eigenvalues using a finite difference scheme and Chebyshev discretization points and a resistivity $\eta = 5.10^{-7}$ 54
III.2 Eigenvalues using the symplectic orthogonal collocation scheme with Lagrangian polynomials as bases functions, Chebyshev collocation points and a uniform resistivity $\eta = 5.10^{-7}$ 55
III.3 Eigenvalues with Bessel basis approximation functions for the case $\eta = 5.10^{-7}$ 57
III.4 Eigenvalues with Bessel base-functions and experimentally provided time varying and non uniform resistivity $\eta(z, t = 11s) \in [2.10^{-8}, 2.10^{-6}]$, discharge TS#47673 58
V.1 Eigenvalues with symplectic and finite different discretization scheme, with $n = 2.10^{19}[m^{-3}]$, $\chi = 5[m^2/s]$ 62

.1 Fixed parameters of tokamak plasma 102
.2 Varying parameters of tokamak plasma 103

I.1 Comparison the precision of the different collocation point choice among the points uniform, Legendre, Chebyshev $\eta = 5.10^{-7}$ 116

Nomenclature

CEA Commissariat à l'Energie Atomique

EM Electromagnetic

IDA-PBC Interconnection and Damping Assignment - Passivity Based Control

IRFM Institut de Recherche sur la Fusion par confinement Magnétique

ITER International Thermonuclear Experimental Reactor

MHD Magneto-Hydro-Dynamics

PCH Port-Control Hamiltonian

PH Port-Hamiltonian

RAPTOR RApid Plasma Transport simulatOR

TCV Tokamak of Configuration Variable

TMHD Thermal-Magneto-Hydro-Dynamics

WEST Tungsten (W) Environment Steady-state Tokamak

Chapter 1

Introduction

I Port-Hamiltonian approach for thermonuclear fusion and control challenges

Nuclear fusion on the sun supplies an immense green energy source to brighten our life everyday. Otherwise, in order to maintain and improve our comfort, we're looking for the energy sources like fossil fuel or nuclear fission, and now we have to deal with the huge amounts of pollution and radiation which threatens back our life. So why not an "artificial sun" on earth?

This such idea lead the Soviet physicists Lev Artsimovitch, Andrei Sakharov and Igor Tamm to invent in the 1950s a fusion reactor called Tokamak (Russian acronym for *toroïdalnaïa kamera s magnitnymi katushkami*, i.e. toroidal chamber with magnetic coils). A Tokamak is a facility constructed with the shape of a torus (or doughnut) in which a plasma (i.e. ionized fuel atoms) is magnetically confined and heated in order to produce nuclear fusion reactions (see Fig. I.2 for a schematic view and the classical Wesson's monograph [106] for a large comprehensive reference textbook on tokamaks).

In thermonuclear fusion at very high temperature, two light atomic nuclei form a heavier one. For instance, Deuterium ${}^2_1D$ (which could be extracted from the sea water) and Tritium ${}^3_1D$ (which is obtained from REE- rare earth element), available in very large quantities, could potentially be used for future fusion reactors. In the fusion reaction, the neutron kinetic energy is converted into electricity, while the rest of the energy should be used to maintain a high temperature for the plasma for future reactions. However, to overcome the Coulomb barrier, in order to merge the two positively charged nuclei, it is required at the same time extremely high temperatures T with sufficiently high density n and large enough confinement time τ. This plasma ignite condition is usually summarized in the empirical Lawson's criterion:

$$n T \tau \geq 3 \times 10^{21} \left(m^{-3} keV s\right)$$

$${}^2_1D + {}^3_1D \longrightarrow {}^4_2 He\,(3.5\text{MeV}) + {}^1_0 n\,(14.1\text{MeV})$$

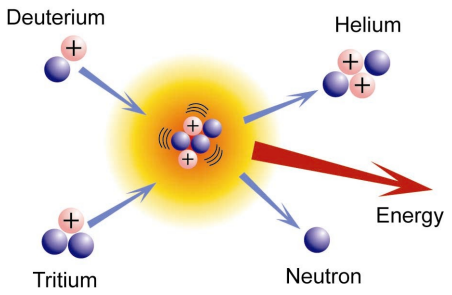

Figure I.1: The fusion reaction between Deuterium and Tritium Hydrogen isotopes which produces Helium, energy and and a high kinetic energy neutron particle

	Basic control	Advanced control	Future control
Magnetic control	plasma positions, shape, current,... or loop voltage[1] (of electric coils)	plasma current profile	Burn control
Kinetic control	plasma density	temperature (coupled with the magnetic domain) MHD instability	

Table I.1: Classification of plasma control problems

In the tokamak strategy, the goal is therefore to optimize the temperature and confinement time in order to compensate the low plasma density. The ITER (International Thermonuclear Experimental Reactor, see http://www.iter.org/) project was born to challenge these controlled fusion problems (cf. [2, 83, 105]). The tokamak feedback control to achieve a stable, well-confined and highly energetic plasma equilibrium is still a large field of research. The table I.1 gives an overview of the possible control problems in the tokamaks from the basic and earlier ones to more involved and recent ones. They are divided into two main categories: the magnetic control (only EM (Electromagnetic) states are considered) and kinetic control (plasma temperature and density are taken into account).

Particularly, in magnetic control the *regulation of the 1D* profile of the safety factor q[2]has become the subject for many control studies. Up to now, the so-called *1D* resistive diffusion model for the poloidal flux (see [10, Chap.6] for the model derivation and details), whose derivation is also inversely proportional to the safety factor, has been extensively used as a "control model" for many control designs related to total plasma current or profiles in the Tokamaks. In this model the plasma is assumed to have reached the hydrodynamic equilibrium profile and displacement currents are neglected in the Maxwell equations (when compared for instance to the inductive current). The model then reduces to a 1D diffusion-like parabolic equation for the radial profile of the plasma poloidal flux (or current density). Readers could refer to [107] for investigations on this model for control purposes or to [81], [80], [1], [39] for different control strategy of the plasma current profile. Note also that two-time-scale extensions have already been considered for simultaneous magnetic and kinetic (temperature) profile control in tokamak [28].

However, it makes very restrictive assumptions on the plasma resistivity (which in fact depends strongly and non-linearly of the temperature) and neglects some nonlinear MHD (Thermal-Magneto-Hydro-Dynamics) couplings which produce the bootstrap current[3]. The next objective for plasma high confinement requires now a better understanding and exploitation (for control purposes) of the TMHD (Thermal-Magneto-Hydro-Dynamics) interdomain couplings. Moreover, a study of the complete TMHD model, including mass and entropy balance equations is necessary to consider the burn control problem (i.e. control of the fusion reaction during the burning phase) which comes next after plasma confinement problems (see for instance preliminary works of [94, 92, 14, 15]). Our goal is to obtain a model simple enough to design a controller but complex enough to capture most of the important (for the here-above considerations) physical properties of the real system. Therefore both kinetic and fluid models will be considered in this work, among others to some MHD and thermal couplings.

The port-Hamiltonian (port-Hamiltonian) approach (cf. [99, 64]) for the modelling of multi-physics systems is quite successful in the recent decades. It's based on the explicit representation of all power exchanges between the multi-domain subsystems.

On one side, this approach is able to describe the complex dynamics systems including nonlinear behaviors or spatially distributed phenomena, such as transmission line models [36], beam equations [55], shallow water equations [42] or models for transport phenomena (adsorption columns [4], fuel

[2]The safety factor yields the ratio of the number of toroidal and poloidal field line turns. It is inversely proportional to the plasma current. The readers may refer to chapter 3, section IV.2 or [106, Chap.3, p.111] for more details.

[3]The boostrap current comes from an magnetohydrodynamical effect which produces an extra current density, due to part of the charged particles bouncing back and forth along their banana orbit. It has been considered in the plasma control literature (until now) as a perturbation. However it is now hoped to be the major source of inductive heating in the ITER project.

cells [34] or Ionic Polymer-Metal Composites [72]).

On the other side, accompanying to the PH modelling, the so-called symplectic reduction methods are also investigated to obtain a control model (cf. [86][18][41]). This geometric spatial reduction may be performed by designing schemes which preserve the geometrical interconnection structure of the model and result in a structured port-controlled Hamiltonian (PCH) model (see [65] for an introduction or [101] for an extensive investigation) with the same balance (conservation) equations and approximated constitutive (closure) equations projected in the reduced spaces.

The discretization methods, reducing the infinite into the finite dimensional control system, which aims at accurate spectral and structure properties and low order models, are also developed for the PH systems. The so-called symplectic discretization is successfully applied to the (mixed) finite elements method [12, 6, 45] or the (mixed) orthogonal collocation with Lagrange polynomials [70].

For the control synthesis, [77] proposes a class of passivity based controls applicable to the PH finite systems, and the IDA-PBC (Interconnection and Damping Assignment - Passivity Based Control) (cf. [76, 78, 88]) can be considered one of the most general methods in this class.

With all the above reasons, we believe that an appropriate (physically meaningful) statement of the simplified distributed diffusion model, like the PH formulation approach presented here, could lead to better results for the tokamak control problems. Moreover, due to the modularity of the port-Hamiltonian formulation, the thermal dispersion model could be refined (if needed) to the necessary level of description by successive inclusions of constitutive equations and coupling effects. At least two key issues are related to nonlinear coupling between electromagnetic, entropy, momentum and material balances: the influence of the temperature on the plasma resistivity and the so-called "bootstrap current". The first is a key effect to control equilibrium profiles in the plasma. The second is a "supplementary source" of plasma current which has to be optimized to improve the plasma confinement. We believe that the port-Hamiltonian formulation of the model developed previously (including energy, momentum and material balance equations) could be used to represent this effect and maybe to handle the related "optimal" control problem.

II Main contributions of this work

A complete control methodology has been developed for the aforementioned plasma control problems. First a *3D* plasma port-Hamiltonian model has been derived in covariant form. It includes the Maxwell field and material balance equations, as well as some TMHD interdomain couplings. The symplectic reduction methods have been designed to derive both *1D* and *0D* control models preserving the geometric structure and some invariants (first integrals) of the original *3D* TMHD model. These models have been validated with the METIS simulator[4] [3] for the Tore-Supra/ WEST (Tungsten (W) Environment Steady-state Tokamak) configuration and with the RAPTOR (RApid Plasma Transport simulatOR) code [30, 29] developed for simulation and real-time control of TCV (Tokamak of Variable Configuration) at EPFL, Lausanne, Switzerland. Then IDA-PBC based controllers have been developed both in finite and infinite dimension. Both controllers aim at controlling the security factor radial profile from boundary (loop voltage) or distributed (current density and heat distribution) control actions. More precisely, the main contributions of the thesis could be summarized as:

- the development of a complete *3D* fluid-like TMHD model with includes energy flows (therefore control actions) from the system to the environment through boundary or distributed controlled port variables, using the port-Hamiltonian extension of Hamiltonian distributed parameter systems suggested in [99].

- the proposal of a spatial reduction methodology which allows to derive *1D* (or *2D*) models from geometric symmetries, still preserving the model structure and invariants and leading to a *1D* (or *2D*) infinite dimensional port-Hamiltonian TMHD model. In the considered plasma application example, axisymmetry and plasma quasi-static equilibrium assumptions

[4] METIS is a tokamak simulator developed for plasma scenario design and analysis [3]. It is a complex simulation code developed at IRFM (Institut de Recherche sur la Fusion par confinement Magnétique) department at CEA-Cadarache (Commissariat à l'Energie Atomique) France.

have been used to derive a *1D* "radial" model from the *3D* model written in toric magnetic coordinates.

- the proposal of a methodology which aims at transforming classical pseudo-spectral spatial discretization schemes into symplectic ones with respect to the power pairing used in the port-Hamiltonian formulation of *1D* distributed parameters systems. In the plasma application case, a symplectic Galerkin scheme has been proposed and the choice of the approximation basis functions has been discussed. A continuous-time finite dimensional approximation has been obtained in the form of a classical PCH system. The obtained reduced model has the same model structure, invariants and accurate spectral properties (both for eigenvalues and eigenfunctions).

- the design of an IDA-PBC controller for the finite dimensional PCH (Port-Control Hamiltonian) approximation of the resistive diffusion and thermal diffusion equations. This design includes a nonlinear feedforward control action based on full steady state computations to handle actuator constraints and the non linearity in the control operator. The IDA-PBC feedback control design includes an optimal strategy for the control parameters selection as well as a robustness analysis w.r.t. errors on critical parameters and external disturbances.

- a proposal for an IDA-PBC-like control design for infinite-dimensional port-Hamiltonian systems and its application to the control of the *1D* resistive diffusion equation with both finite rank distributed input (external current source) and a boundary control (through the loop voltage). The proposed distributed control is derived from the traditional IDA-PBC principle and is indeed an approximate average solution for some matching equation. The boundary control compensates this matching error and is computed using a state feedback Volterra (sometimes referred as backstepping [50]) transformation to prove the stability of the closed-loop system.

- the validation of the different control models and of the control laws for some configurations of the Tore-Supra/WEST and TCV. These validations are based on simulations on the METIS code (Tore-Supra/WEST), on the RAPTOR code (TCV) and on some experimental shocks (TCV).

III Outline

The following of the report is organized as follows.

- Chapter 2 presents the principle of the tokamak device, then details the two tokamaks considered for this work: the Tore-Supra/WEST in Cadarache (France) and the TCV in Lausanne (Switzerland). The port-Hamiltonian (PH) modelling method is revisited before being applied to represent the dynamics of plasmas in tokamaks. A *3D* model based on MHD and energy balance equations is then proposed in covariant form (using the PH formulation). Firstly, PH framework in the covariant form for the electromagnetic domain is recalled. Then, the same structures are derived to the material domain. The novel Dirac structures of the multi-domain couplings are proposed for the magneto-hydro-dynamic couplings (Lorentz force, Joule effect, and the Eulerian-Lagrangian coordinate transformation) in order to complete the *3D* model.

- Chapter 3 suggests a geometric reduction methodology to reduce the model from *3D* to *1D* for the purpose of control synthesis. This spatial reduction method aims at conserving the natural power products and the system interconnection's structures from the original *3D* model. Consequently, the reduced *1D* variables definitions are derived directly from the power conservation relations. The *obtained 1D* reduced models for the electromagnetic and thermal domains are proved equivalent respectively to the resistive diffusion equation and thermal transport equation which are the most commonly used *1D* control models for the control of the security factor profile in tokamaks.

- Chapter 4 adapts an existing symplectic geometric discretization method (see for instance [70]) to derive a finite dimensional *0D* PCH model from the reduced *1D* PH model obtained from in chapter 3. The choice of approximation base functions are discussed. This discussions

leads to the definition of a symplectic Galerkin scheme specifically adapted to the flux and heat diffusion problems investigated in this work. The numerical and dynamical properties of the obtained reduced PCH model are carefully investigated.

- Chapter 5 derives an IDA-PBC control law based on the finite dimensional PCH tokamak model. The control objective is - at first - to regulate the safety factor profile (or plasma current profile) with the finite-dimensional model for the EM domain. Secondly, the thermal diffusion equation is coupled with the resistive diffusion. Another control design is proposed which includes actuators in the thermal domain and couplings between the thermal and EM domains (through the resistivity and the bootstrap current). The control laws are tested with two tokamak simulators METIS and RAPTOR. Results from real-time experimentation on TCV are also provided.

- Chapter 6 develops some ideas to achieve an IDA-PBC control design for infinite dimensional PH systems. A backstepping boundary control action is derived to correct the matching error from the (finite rank) distributed IDA-PBC control. The simple example of the resistive diffusion equation is investigated as a particular example to illustrate the approach. The obtained results are also compared with the ones from the finite dimensional IDA-PBC design in chapter 5.

Chapter 2

3D port-Hamiltonian Tokamak model

In this chapter, a *3D* fluid model - using the port-Hamiltonian extension for distributed parameters suggested in [99] - was developed for the TMHD of plasma in tokamaks. Magnetohydrodynamic and energy balance equations are expressed in their co-variant forms, as well as the balance and closure equations in the material domain. The irreversible entropy (or entropy production) is deduced at last in order to determine the dissipative constitutive relation in the material domain, we call it the resistive$\mathcal{R}$ - field of the model. All derived interdomain couplings in the material domain are sketched using Stokes-Dirac structures and a resistivity $\mathcal{R}$ - field structure.

The first section describes the studied system, the Tokamak construction in general, as well as in detail with two different devices: the Tore Supra WEST and the TCV. Some actual important issues of this system make title for the presented work, our motivations are thus expressed in section II. Section III presents shortly the co-variant formulation for distributed parameter systems with boundary energy flows, using differential forms. Exterior and interior (or contraction) products and Dirac structure definitions are recalled. In section IV, EM domain model for the tokamak system is derived using this port-Hamiltonian formulation. In subsection V, the transport equations (of the mass, momentum, and energy balance) derived from the Boltzmann equation (cf. [11]) are revisited. Then the kinetic theory point of view is adopted in a form which is suitable for the fluid-like port-Hamiltonian formulation of the plasma dynamics. The irreversible entropy is finally deduced, that is to define the $\mathcal{R}$- field. Subsection VI then defines all the multi-domain couplings and the closure equations which are needed to complete the model. A complete *3D* model of Tokamak is then presented in Bond Graph form by integrating all the domains and their couplings to give a general view of the whole system in subsection VII.

I Tokamak devices

Tokamak thermonuclear fusion reactors exist in different versions all around the world: JET in the United Kingdom, JT-60U in Japan, DIII-D in the United States, Tore Supra/WEST in France and TCV in Switzerland are a few examples. They are distinguished by their sizes and their available actuators, but their general architecture remains quite similar and is illustrated in figure I.1.

In a tokamak, a plasma is confined in the shape of a torus by a magnetic field (see figure I.2). The magnetic field is divided into two main components in the toroidal direction and in the poloidal one. It is generated by three sets of electric field coils: a transformer coil in the center of the torus called central solenoid, toroidal and vertical field coils surrounding the plasma and the torus.

The plasma current is generally firstly generated by induction using the central solenoid. It allows heating up the plasma, which behaves as a resistive conductor. However, when the temperature is over 1 keV, ohmic heating becomes practically useless due to the resistivity decreasing with the temperature. Therefore ohmic heating alone does not allow to reach the adequate plasma fusion conditions. Non inductive heating and current drive methods were thus developed to take it over. Auxiliary heating sources which can be considered are:

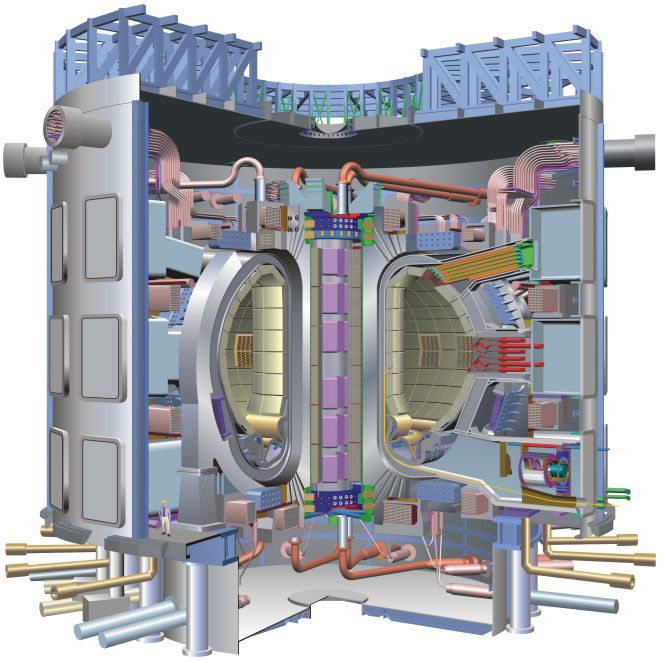

Figure I.1: Tokamak design chosen for the ITER project

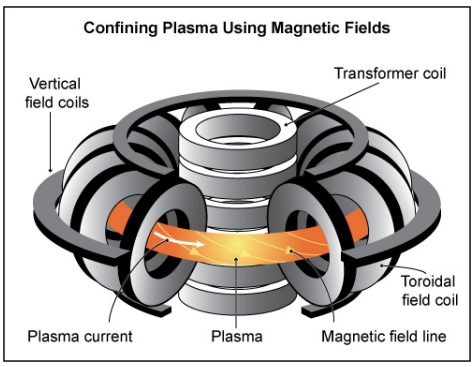

Figure I.2: Schematic view of a tokamak with the electrical solenoids: the magnetic field generated by the three magnets makes the plasma gas ions following helicoidal trajectories along the torus

- Electron Cyclotron Heating and Current Drive (ECRH/ECCD)
  These waves resonate with the electron cyclotron motion around the field lines, heating the electrons and driving bulk current. Radio frequency (RF) waves of $f \sim 100GHz$ range have the advantage that they propagate through vacuum and can therefore be injected from antennas placed farther from the plasma. Their optical properties (such that steering/focusing mirrors) can be used to precisely direct the location of absorption and current drive in the desired location inside the plasma. A disadvantage is their relative inefficiency at driving current, as well as the fact that the electrons are heated instead of ions (as would be useful to stimulate fusion reactions – though this is also the case for LHCD in the following)

- Ion Cyclotron Heating and Current Drive (ICRH/ICCD)
  They use low-frequency RF waves ($f \sim 40MHz$) which are coupled to the ion cyclotron frequency or a hybrid frequency of a given ion species in the plasma. While the RF sources use conventional technology, the waves must be driven directly at the plasma/vacuum interface since they do not propagate in vacuum or low-density plasmas. This can cause problems related to the plasma/antenna interface. Specially designed antennas have been tested on tokamaks over the years

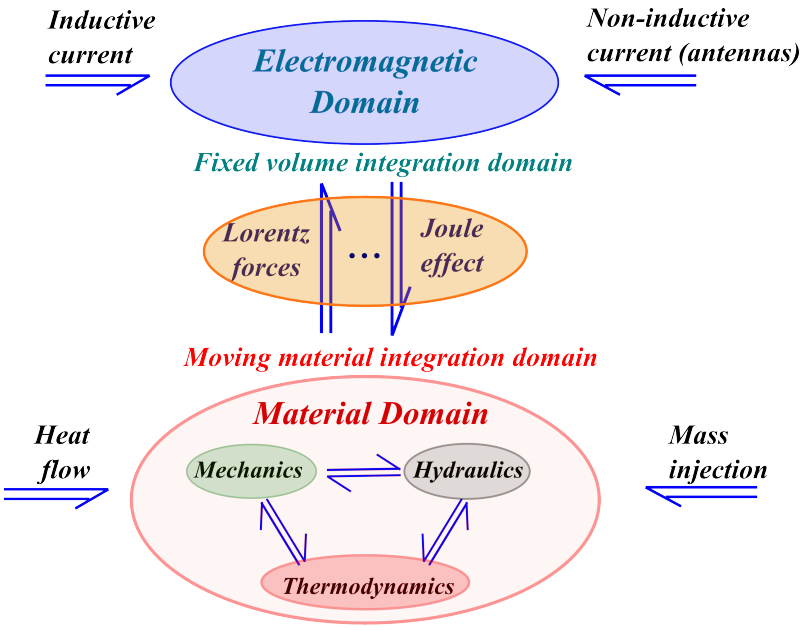

Figure I.3: Multiphysic Tokamak model with main interdonmain couplings

- Lower Hybrid Heating and Current Drive (LHCD)
  It is yet another method for plasma heating, relying on resonant coupling of a RF wave in the plasma. LHCD is technologically and conceptually simple on the source side ($f \sim 5GHz$), and is able to drive significant amounts of current which can be easily controlled. It also requires antennae placed in proximity to the plasma, providing similar engineering challenges as ICRH

- Neutral Beam Injection (NBI)
  Neutral atoms are injected into a plasma travel in straight lines. They are initially not affected by the magnetic field until the particles ionize in collisions with plasma particles. Neutral Beams injecting tens of megawatts have been successfully used and provide the bulk heating of many tokamaks worldwide. One of their main disadvantages is the large scale and complexity of the injectors, as well as the difficulty to vary where the heat and current are deposited. (NBIs also inject momentum, which can have important physical consequences)

A complete review of these heating source's principles and technologies may be found in [106, Chap.5, p.243].

In other words, with a simple point of view, a Tokamak system can be described in the figure I.3

The value of the total plasma current may be controlled using the central magnetic coil. This defines a boundary control problem (the controlled variable being either the total plasma current or the equivalent loop voltage). Contrarily, the magnetic field, defining equivalently the so-called safety factor profile (chapter 3, section IV.2 or [106, Chap.3, p.111]), necessary to avoid MHD instabilities and to obtain a satisfying confinement for the plasma, may only be controlled using distributed non inductive sources. These distributed control actions are usually non-linear, and have specific shapes (or spatial distributions) being non linearly related to the state (e.g. the total plasma current) and to some control inputs (e.g. the total non inductive power or the beam deflection angle). Only a few control inputs (also termed as engineering control parameters) are available and strong restrictions on the admissible shapes are therefore imposed. Moreover modelling and optimizing the bootstrap current effect ([106, Chap.4, p.172]), as well as a better understanding of all thermal phenomena in the tokamak (cf. [27, 38]), are the key issues for the success of the ITER project. Both require an explicit representation of electromagnetic, material, momentum and entropy balance equations (possibly in 3D models) as well as coupling constitutive equations between these energy domains.

Two Tokamaks are briefly presented hereafter: the Tore-Supra at CEA-IRFM Cadarache, France and the TCV at CRPP-EPFL Lausanne, Switzerland. Experimental data and detailed knowledge-

based simulation models of these two tokamaks have been used for the numerical (simulations) and experimental validations of the control models, numerical methods and control laws presented in this report. However only TCV has been used for real-time control experiments within the context of this thesis.

I.1 Tore-Supra

Figure I.4: Tore-Supra Tokamak device in CEA/Cadarache

Built in 1988 in CEA Cadarache France, Tore Supra[1] is one of the largest tokamaks in the world, with a diameter of $11.5m$ and a height of $7.2m$, a major radius of $2.25m$ (from the machine center to the plasma center) and a minor radius of $0,70m$. Its main feature is the superconducting toroidal magnets which enable generation of a permanent toroidal magnetic field. Tore Supra is also the only tokamak with plasma facing components actively cooled. These two features allow the study of plasma with long duration. Until now, it has produced more than 40 000 plasma discharges, mastery of long-duration plasmas (a record duration plasma of 6 minutes and 30 seconds was achieved on 04/12/2003).

In Tore Supra, different auxiliary heating sources by radiowaves are used, such as ECRH/ECCD, ICRH/ICCD, LHCD and NBI. Improvements on existing systems are being considered so as to initially raise the injection capacity up to $12MW$ for 1000 seconds.

Working on this experimental facility are about 250 researchers in the IRFM department from the CEA. Since 2013, within the WEST project, Tore-Supra is being transformed to test ITER plasma facing component. The operations on this machine are thus postponed until 2016.

This is the reason why in this thesis there are no experimental results on the Tore-Supra tokamak but only simulations using data given by METIS, the tokamak simulator developed in [3] for plasma scenario design and analysis.

I.2 TCV

The TCV[2] came into operation in November 1992 at the Centre de Recherches en Physique des Plasmas, Ecole Polytechnique Fédérale de Lausanne (CRPP/EPFL). About 140 specialists are actually contributing to manifold activities of the CRPP. Since then it has produced plasma currents above $1MA$ for pulse lengths longer than a second.

TCV is a medium size Tokamak with $1.44m$ height, $0.48m$ width and $0.875m$ of major radius; it is not designed to produce a significant number of fusion reactions (nor is Tore Supra).

TCV possesses an interesting property which makes it unique in the zoo of existing tokamaks in the world: the plasma cross section can be 3 times higher than wide. This feature opens the door

[1] website: www-fusion-magnetique.cea.fr/gb/cea/ts/description/ts_description01.htm
[2] website: crppwww.epfl.ch/crpp_tcv.html

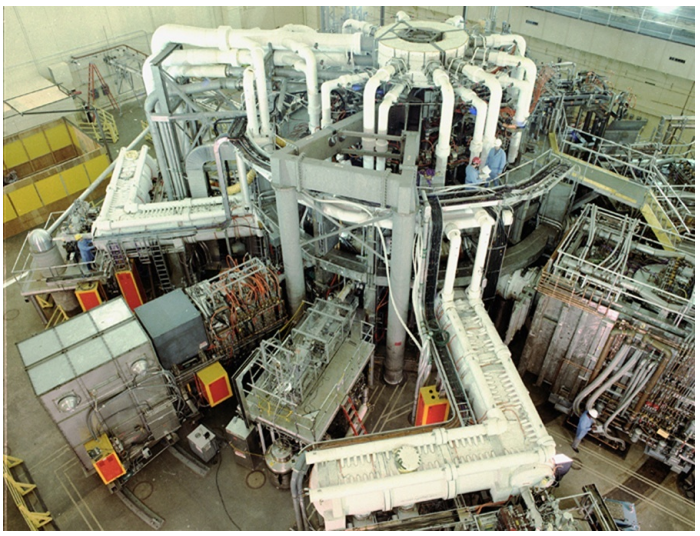

Figure I.5: TCV overview in CRPP/EPFL

to studies on plasmas of very different shapes. A series of plasma configurations (cross-sections) which have been produced in TCV are shown in figure I.6. The interests of the elongated plasma are that no part of the plasma touches the inner wall and that the plasma can be bounded by a seperatrix. It is also called diverted plasma, that creates an $X-point$, where the poloidal motion of the field lines is almost eliminated, that improves the plasma confinement (cf.[106, Chap.3, p.115]). Other tokamaks in the world are generally limited to a more or less fixed shape which is given by the shape of vacuum vessel. With TCV, fusion research has a versatile tool to study the influence of the plasma shape on confinement and stability.

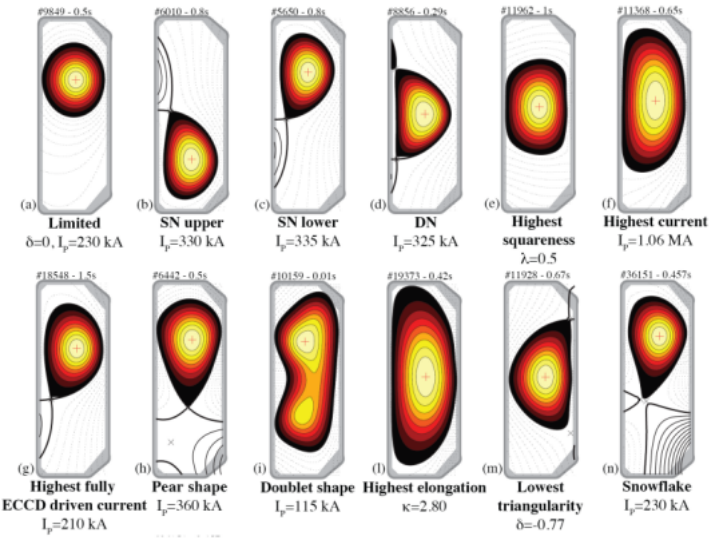

Figure I.6: Plasma shapes in TCV

Another important objective of TCV is to study this variety of plasma shapes with microwave heating, more precisely with Electron Cyclotron Resonance Heating (ECRH). For this purpose up to 9 strong microwave sources, called gyrotrons, have been installed representing a power of 4.5MW additional heating for the plasma.

However, the gyrotrons reached the end of their life by 2013. These old gyrotrons have been disassembled and are being replaced by new ones. At the same time, a NBI heating source is being implanted. TCV is expected returning with full function in 2016. Fortunately we got the precious

chance to test our very first (and simple) control laws on TCV in the last campaign on October 2013 before the machine has been stopped. Nevertheless, we're pleased to try our designed controllers with RAPTOR developed by [30, 29]. RAPTOR is a Real-time model-based reconstruction and control of Tokamak, which has been proved the be consistent with the real plant TCV.

II Related works and motivations

Many model-based control designs are based on the *1D* resistive diffusion equation for poloidal magnetic flux (refered to chapter 5 for the explication and related works). In this model all TMHD dynamical couplings such as the bootstrap current are neglected as well as the significant variation of the plasma resistivity with the temperature. Static models (or "scaling laws") are usually used in approaches based on the resistive diffusion equation to determine the value of the necessary system parameters (see [13] or [67]).

On the other hand, the fundamental laws governing charged particle dynamics can be well represented by both kinetic theory of gases[3] and Hamiltonian formulation. Nevertheless, the structured approach Hamiltonian can also stands for a fluid description of the system. Therefore the preservation of the Hamiltonian structure provides some confidence that the truncations that are used to derive the fluid model have not introduced unphysical phenomena. Hamiltonian formulations have already been used in the plasma dynamics context, such as in [68] for ideal fluid models, in [69] for magnetohydrodynamics models or in [26] to represent the Grad-Shafranov equations using a Lie-Poisson bracket. However some of these earlier works either make use of the "microscopic" (six dimensional) kinetic theory to represent the plasma dynamics, while all of them (to the best of our knowledge) considered only closed systems without any explicit input-output variables. Therefore these previous models, although they bring much more insights into the "geometry" of the magnetohydrodynamics equations, were not convenient for control or observation purposes.

In this work we aim at developing a complete *3D* fluid model which includes thermal phenomena (energy balance equation) since the plasma profiles control problem should take into account the strong variation of the plasma resistivity with the temperature and since non linear coupling effects between the thermal and electromagnetic domains are essential to capture the bootstrap current effect. Moreover we would like to keep the Hamiltonian structure of the physical model and, more precisely, we would like in some sense to extend the Lie-Poisson structure (i.e. brackets) for closed MHD systems to TMHD models with energy flows from the system to the environment through the boundary and through the distributed (field) controls. These extensions required by mixed boundary and control actions will be achieved using the port-Hamiltonian extension for distributed parameter systems suggested in [99]. It will be based on Dirac interconnection structures (including the previously defined canonical Stokes-Dirac structures [99]) an elementary sub-models rather than on complex brackets as those defined in [69, 62] for the kinetic model or in [26] for a fluid model. The reasons of this choice are the following:

- in this structured modelling approach, each elementary interconnection structure is the formulation of a fundamental conservation principle. It is then usually closed with a "natural" constitutive equation suggested by modelling considerations and which satisfies physical constraints and principles (conservation, reciprocity, symmetry, etc.).
- the Stokes-Dirac structures and other Dirac interconnection structures used in the model are stable under interconnection. The global connected model is still a port-controlled Hamiltonian model (partially) defined with a global power preserving Dirac interconnection structure [82][4].
- the Stokes-Dirac interconnection structures, as well as simple constitutive equations, may be spatially reduced using geometric reduction algorithms [40, 42, 87] which preserve both the structural and energetic properties of the infinite dimensional model, including the Dirac structure, conservativeness and dissipativeness of each sub-models.

[3] Kinetic theory explains macroscopic properties of gases, such as pressure, temperature, viscosity, thermal conductivity, and volume, by considering their molecular composition and motion.

[4] The work also derives the conditions for the achievable closed loop Dirac structures, analogous to the finite dimensional case and then characterize the set of achievable Casimir.

- the proposed approach for modelling leads trivially to an explicit port-controlled Hamiltonian realization which is essential to apply non linear control techniques based on energy or structural property of the model such as IDA-PBC [77] or mixed PCH interconnection methodologies [101, Chap.6, p.309]. Such approaches have already been successfully applied to various examples of distributed parameter systems such as the control of Timoschenko beam [55], the control of water flows and levels in the shallow water equations [44] or the control of a passive charge connected through a transmission line [56].

III Background: Port-based modelling for distributed parameter systems of conservation laws with boundary energy flows

In this section, the port-Hamiltonian formulation for systems of conservation laws is recalled. Port-based modelling techniques and languages have been extensively used these last decades to model, simulate and control a wide variety of lumped parameters physical systems [49, 97, 95, 51, 101, Chap.6, p.309]. When dealing with distributed parameter systems, first "series" - like expansion models were derived from various kind of finite difference, modal or finite element methods. These already appear in many textbooks such as [49]. More recently, a more intrinsic formulation of port-based models for distributed parameter systems (i.e described by partial differential state space equations) with boundary energy flows have been proposed [64, 99]. They are based on the definition of the state variables as the densities of some thermodynamical extensive variables. The time derivatives of these variables and their distributed conjugated intensive variables[5] form together the pairs of variables which are used to define a power pairing form and a port-Hamiltonian formulation for systems of conservation laws.

It is known that Stokes-Dirac structures allow to extend the Hamiltonian description of distributed parameter systems to include *variable boundary conditions*, leading to *open* distributed-parameter port-Hamiltonian systems with boundary ports [99]. We shall now briefly recall the definitions of these Stokes-Dirac structures and port-Hamiltonian extensions for distributed parameter systems in the 3-dimensional case, with a spatial domain Ω. We will make use of the exterior differential formalism [89, 20] (also called *k-forms*) both to remain general and to highlight the fundamental geometric ideas throughout the work.

This modelling approach has been applied successfully to many hyperbolic systems as varied as transmission line models [40], beam equations [55] or shallow water equations [42, 43]. The same canonical Stokes-Dirac structure may be used to build port-Hamiltonian formulations of parabolic models issued from (linear) irreversible thermodynamics such as in the case of heat and mass transport phenomena in adsorption columns [4, 6] or ionic diffusion in fuel cell [33] or Ionic Polymer-Metal Composites [37, 72]. A more surprising parabolic plasma resistive diffusion model in the next section will show the interest of the approach in multi-physics (e.g. Thermo-MagnetoHydroDynamics) models and more involved geometries (e.g. toroidal).

III.1 Co-variant form and exterior calculus notations

Let us first recall some exterior calculus definitions and notations used in the sequel. In vector analysis, a new algebra, the co-variant form, also called the differential form, introduced by Grassmann at the middle of nineteenth century. It's a generalization of scalar and vector products in space of any dimension. We shall give a brief reminder on this algebra, [35] [101, chap.4].

III.1.1 Differential form

Definition III.1. On a n-dimensional spatial domain $\Omega \ni \xi$, a *k-form* ($k \leq n$), is the field ω^k_ξ of *k-alternated forms* on $T_\xi\Omega$, that is k-linear (i.e. linear with respect to each of its arguments) forms

[5] Such pairs of conjugated variables are, for instance, the entropy density flow and the temperature in the thermal domain, the momentum density and the velocity in the kinetic domain, the pressure and the volumic flow in the hydraulic domain, etc. Examples of conjugated pairs of variables are presented hereafter for the transmission line and resistive diffusion.

on the tangent vectors: $\omega_\xi^k : (T_\xi\Omega)^k \to \mathbb{R}$ that satisfy for any permutation π in $\{1,..,k\}$ and for any k-duple $(\xi_1,\ldots,\xi_k) \in (T_\xi\Omega)^k$:

$$\omega_\xi^k\left(\xi_{\pi(1)},\ldots,\xi_{\pi(k)}\right) = \sigma(\pi)\,\omega_\xi^k(\xi_1,\ldots,\xi_k)$$

where $\sigma(\pi)$ denotes the signature of the permutation π. The set of *k-forms* is denoted by $\Lambda^k(\Omega)$.

Differential *k-forms* are endowed with a product, called exterior product, denoted by $\wedge$, which we use to compute the power and define the passivity properties, and a derivation which is called exterior derivation, denoted by d. These operators are defined as follows.

III.1.2 Exterior product:

Consider a *k-form* $\omega^k \in \Lambda^k(\Omega)$ and a *l-form* $\omega^l \in \Lambda^l(\Omega)$, their *exterior product* (also called *wedge product* or *Grassman product*) is the $(k+l)$*-form* $\omega^k \wedge \omega^l$:

$$\wedge : \ \Lambda^k(\Omega) \times \Lambda^l(\Omega) \quad \to \quad \Lambda^{k+l}(\Omega)$$

such that for any $(k+l)$-tuple of vector fields $(\xi_1,\ldots,\xi_{k+l})$:

$$\begin{array}{l}\left(\omega^k \wedge \omega^l\right)(\xi_1,\ldots,\xi_{k+l}) = \\ \sum_{\pi\in\mathfrak{S}} \sigma(\pi)\,\omega^k\left(\xi_{\pi(1)},\ldots,\xi_{\pi(k)}\right)\omega^l\left(\xi_{\pi(k+1)},\ldots,\xi_{\pi(k+l)}\right) \ \in \Lambda^{k+l}(\Omega)\end{array}$$

where $\mathfrak{S}$ denotes the sets of shuffle permutation that is the permutation π satisfying $\pi(1) < \ldots < \pi(k)$ and $\pi(k+1) < \ldots < \pi(k+l)$.

III.1.3 Exterior derivation

The exterior derivation (also called *co-boundary map*) of a *k-form* $\omega^k \in \Lambda^k(\Omega)$, denoted $\mathrm{d}\omega^k$, is a derivation of degree 1 which maps $\Lambda^k(\Omega)$ into $\Lambda^{k+1}(\Omega)$

$$\mathrm{d} : \ \Lambda^k(\Omega) \quad \to \quad \Lambda^{k+1}(\Omega)$$

and satisfies:

- linearity $\mathrm{d}(\omega+\eta) = \mathrm{d}\omega + \mathrm{d}\eta$
- anti-derivation $\mathrm{d}\left(\omega^k \wedge \omega^l\right) = (-1)^k\left(\mathrm{d}\omega^k \wedge \omega^l\right) + \left(\omega^k \wedge \mathrm{d}\omega^l\right) \qquad \omega^k \in \Lambda^k(\Omega)\,,\ \omega^l \in \Lambda^l(\Omega)$
- if ω^0 is a smooth function, $\mathrm{d}\omega^0$ is the differential of the function
- $\mathrm{d} \wedge \mathrm{d} = 0$
- the derivation is local: for any open set $U \subset \Omega$, if the restrictions to U of two *k-forms* coincide then also the restrictions of their exterior derivatives.

Another operator associated with an inner product on the exterior differential forms is the Hodge star operator, and the (anti-)derivation is given by the contraction of a *k-form* with some vector field. They are defined as follows.

III.1.4 Hodge star operator

The Hodge star (cf. [20, V.A.,p.295]) is essential in the definition of the Hamiltonian (or energy) functions of many physical systems which admits "quadratic" energy. Assume that the vector space $\Lambda^k(\Omega)$ of *k-forms* on Ω is endowed with an inner product denoted by $(\,,\,)$, then the *Hodge star* is a linear map that transforms a *k-form* ω^k into a $(n-k)$*-form,* also called the *dual* or *the pseudo* $(n-k)$*-form* $\star\omega^k$:

$$\star : \ \Lambda^k(\Omega) \quad \to \quad \Lambda^{n-k}(\Omega)$$

Thus:

$$\left(\alpha,\,\omega^k\right) = \int_\Omega \alpha \wedge \left(\star\omega^k\right) \quad \forall\alpha \in \Omega^k(\Omega)$$

It relies on both the inner product and the orientation, that means the sign is changed in a reversing orientation.

III.1.5 Contraction

The contraction of a *k-form* $\omega^k \in \Lambda^k(\Omega)$ by some vector field $v \in T_\xi\Omega$, denoted by $i_v\omega^k$, is a derivation of degree -1 which maps:

$$i_v : \Lambda^k(\Omega) \rightarrow \Lambda^{k-1}(\Omega)$$

such that for any $(k-1)$-tuple of vector fields $(\xi_1, \ldots, \xi_{k-1})$:

$$i_\xi\omega^k(\xi_1, \ldots, \xi_{k-1}) = \omega^k(\xi, \xi_1, \ldots, \xi_{k-1})$$

Contraction	Exterior product	Vectorial product
$i_v\alpha^1$	$\star(v^1 \wedge \star\alpha^1)$	$\overrightarrow{v}.\overrightarrow{\alpha}$
$i_v\alpha^2$	$-(\star(v^1 \wedge \star\alpha^2))$	$-\overrightarrow{v} \times \overrightarrow{\alpha}$
$i_v\alpha^3$	$\star\left(v^1 \wedge \star\alpha^3\right)$	$\alpha.\overrightarrow{v}$

Table III.1: Contraction and equivalent products

Remark 1. In general, the *1-forms* are usually identified with the vector fields (cf.[84, 20, V.A.,p.295-296]). As in [84], the authors clearly distinguish a *1-form* and its vector field by the additional notation $.^\sharp$, so-that the velocity vector field should be $v^\sharp$ corresponding to the *1-form* $v \in \Lambda^1(\Omega)$. However, for the sake of simplicity, and only for our studied case in $\mathbb{R}^3$, we shall use the *1-forms* equivalently to the vector fields. Hence, the vector product of a *1-form* $v \in \Lambda^1(\Omega)$ and a $(n-k)$-*form* $\alpha \in \Lambda^{n-k}(\Omega)$ leads to an alternative expression (equivalent to the more usual vector calculus) of these relations using the contraction of a *k-form* by a vector field, using the Hodge star operator:

$$\star\left(v \wedge \alpha^{n-k}\right) = \star\left(v \wedge \star\alpha^k\right) = \varepsilon i_v\alpha^k$$

where $\varepsilon \in \{-1, +1\}$. The contraction of the differential forms of degree *1* to *3* with a vector field v is summarized in the table III.1. The vector calculus can be found in detail in appendix B.

Finally we shall recall Stokes' theorem which is fundamental for the definition of the port variables defined on the boundary and which gave the name to the Dirac structure underlying systems of conservation laws with energy flux at the boundary.

Theorem III.2. *Consider a spatial domain $\Omega \in \mathbb{R}^n$ being an k-dimensional smooth manifold with smooth $(k-1)$-dimensional boundary $\partial\Omega$. Then for any $(k-1)$-form ω^{k-1} with compact support in $\mathbb{R}^n$, one has:*

$$\int_\Omega d\omega^{k-1} = \int_{\partial\Omega} \omega^{k-1} \tag{III.1}$$

Note that from here, the spatial domain Ω is considered the 3D domain $\Omega \in \mathbb{R}^3$. The port-Hamiltonian formulation is derived hereafter using the Dirac-structure for systems of conservation laws.

III.2 Systems of conservation laws

Consider now systems of two conservation laws in canonical interaction and then we will represent them using Dirac structures in the open case (i.e. with boundary energy flows).

Definition III.3. Consider the two conserved quantities as being two *2-forms*: $q \in \Lambda^2(\Omega)$ and $p \in \Lambda^2(\Omega)$. Consider also the system of conservation laws, with flux variables $\beta_q \in \Lambda^1(\Omega)$ and $\beta_p \in \Lambda^1(\Omega)$ for each conserved quantity, defined by the *Hamiltonian density function* $\mathcal{H} : \Lambda^2(\Omega) \times \Lambda^1(\Omega) \rightarrow \Lambda^3(\Omega)$ resulting in the total Hamiltonian $\mathbb{H} := \int_\Omega \mathcal{H}(q, p) \in \mathbb{R}$. The *system of two canonically interacting conservation laws* is then defined by:

$$\frac{\partial}{\partial t}\begin{pmatrix} q \\ p \end{pmatrix} + \mathrm{d}\begin{pmatrix} \beta_q \\ \beta_p \end{pmatrix} = 0 \quad \text{and} \quad \begin{pmatrix} \beta_q \\ \beta_p \end{pmatrix} = \varepsilon\begin{pmatrix} 0 & 1 \\ 1 & 0 \end{pmatrix}\begin{pmatrix} \frac{\delta\mathcal{H}}{\delta q} \\ \frac{\delta\mathcal{H}}{\delta p} \end{pmatrix} \tag{III.2}$$

where $\varepsilon \in \{-1, +1\}$ depends on the fluxes sign convention on the physical domain.

This system of two conservation laws may be also written as follows:

$$\frac{\partial}{\partial t}\begin{pmatrix} q \\ p \end{pmatrix} = \varepsilon \begin{pmatrix} 0 & \mathrm{d} \\ \mathrm{d} & 0 \end{pmatrix} \begin{pmatrix} \frac{\delta \mathcal{H}}{\delta q} \\ \frac{\delta \mathcal{H}}{\delta p} \end{pmatrix} \tag{III.3}$$

that is as an infinite-dimensional Hamiltonian system defined with respect to the *matrix differential operator*:

$$\mathcal{J} = \varepsilon \begin{pmatrix} 0 & \mathrm{d} \\ \mathrm{d} & 0 \end{pmatrix} \tag{III.4}$$

and generated by the Hamiltonian function $\mathbb{H}$ [73].[6]

In order to generate a Hamiltonian systems, the matrix differential operator $\mathcal{J}$ defined in (III.4) should satisfy the properties of a *Hamiltonian operator*, that is it should be skew-symmetric and satisfy the Jacobi identities. A short calculus shows that the skew-symmetry holds only for functions *with compact support in the spatial domain* Ω or satisfying Dirichlet or Neumann *homogeneous boundary conditions*.

III.3 Stokes-Dirac structures and systems of balance equations

Interested in observation and control problems, one must consider more general (dynamic) boundary conditions where some energy is exchanged through the boundary of the spatial domain. Therefore the matrix differential operator $\mathcal{J}$ must be extended to a Dirac structure, called Stokes-Dirac structure [99, 63, 54]. Dirac structures [21, 23] are a geometric perspective to skew-symmetric tensors, actually corresponding to their *graph*, which generalize the tensors associated with Poisson brackets or pre-symplectic forms. They have been introduced in classical mechanics to represent systems with constraints. Then they have been used to include input-output port variables in finite dimensional port-Hamiltonian models [98]. Finally an infinite dimensional extension, called Stokes-Dirac structures, has been defined to represent distributed parameter systems of conservation laws with boundary energy flows [99].

Proposition III.4. *Consider the product spaces of* k-forms*:*

$$\begin{aligned} \mathcal{F} = &\quad \Lambda^2(\Omega) \times \Lambda^2(\Omega) \times \Lambda^1(\partial\Omega) \ni \quad (f_p, f_q, f_b) \\ \mathcal{E} = &\quad \Lambda^1(\Omega) \times \Lambda^1(\Omega) \times \Lambda^1(\partial\Omega) \ni \quad (e_p, e_q, e_b) \end{aligned} \tag{III.5}$$

Consider the linear subspace $\mathscr{D}$ *of the bond space* $\mathcal{B} = \mathcal{F} \times \mathcal{E}$*:*

$$\begin{aligned} \mathscr{D} \quad = \quad & \{(f_p, f_q, f_b, e_p, e_q, e_b) \in \mathcal{F} \times \mathcal{E} | \\ & \begin{bmatrix} f_p \\ f_q \end{bmatrix} = \varepsilon \begin{bmatrix} 0 & d \\ d & 0 \end{bmatrix} \begin{bmatrix} e_p \\ e_q \end{bmatrix}, \\ & \begin{bmatrix} f_b \\ e_b \end{bmatrix} = \begin{bmatrix} \varepsilon & 0 \\ 0 & -1 \end{bmatrix} \begin{bmatrix} e_{p|\partial\Omega} \\ e_{q|\partial\Omega} \end{bmatrix} \Big\} \end{aligned} \tag{III.6}$$

where $\varepsilon \in \{-1, +1\}$ *and* $|_{\partial\Omega}$ *denotes restriction to the boundary* $\partial\Omega = [0, L]$*. Then* $\mathscr{D}$ *is a Dirac structure with respect to the non degenerated bilinear form between* $\mathcal{F}$ *and* $\mathcal{E}$*:*

$$\langle (e_p, e_q, e_b) \,|\, (f_p, f_q, f_b) \rangle = \int_\Omega [e_p \wedge f_p + e_q \wedge f_q] + \langle e_b,\, f_b \rangle_{\partial\Omega} \tag{III.7}$$

As a consequence of proposition III.4 one may define a Hamiltonian system with respect to this Stokes-Dirac structure as follows.

Definition III.5. The boundary *port-Hamiltonian system of two conservation laws* with state space $\Lambda^2(\Omega) \times \Lambda^2(\Omega) \ni (q, p)$ and boundary port variables spaces $\Lambda^1(\partial\Omega) \times \Lambda^1(\partial\Omega) \ni (f_b, e_b)$, is

[6] In the coordinates z, the Hamiltonian system (III.4) may be written using functions as:

$$\frac{\partial}{\partial t}\begin{pmatrix} q(z) \\ p(z) \end{pmatrix} = \varepsilon \begin{pmatrix} 0 & \nabla\times \\ \nabla\times & 0 \end{pmatrix} \begin{pmatrix} \frac{\delta \mathcal{H}}{\delta q}(z) \\ \frac{\delta \mathcal{H}}{\delta p}(z) \end{pmatrix}$$

the Hamiltonian system defined with respect to the Stokes-Dirac structure $\mathscr{D}$ given in proposition III.4 and generated by the Hamiltonian functional $\mathbb{H}(q,\, p)$, as follows:

$$\left(\left(\left(-\frac{\partial p}{\partial t}, -\frac{\partial q}{\partial t}\right), f_b\right), \left(\left(\frac{\delta \mathcal{H}}{\delta p}, \frac{\delta \mathcal{H}}{\delta q}\right), e_b\right)\right) \in \mathscr{D}$$

The choice of boundary conditions has obviously to be added to the definition of a boundary port-Hamiltonian system in order to define a Cauchy problem. In fact, in the linear case, a boundary port-Hamiltonian system defines a class of well-posed systems. For any solution, the isotropy condition of the Dirac structure implies the balance equation on the Hamiltonian:

$$\frac{d\mathbb{H}}{dt} = \langle e_b,\, f_b \rangle_{\partial} \tag{III.8}$$

III.4 Examples of boundary port-Hamiltonian systems

The examples of the ideal transmission line (cf. [99]) in 1 dimensional space, and the canonical diffusion equation (cf. [5]) in the domain of 3 dimensions, as the simple case, are useful to illustrate, the relation between the classical formulation of Hamiltonian systems in mechanics and the proposed port-based modelling approach (using Stokes-Dirac structures) of macroscopic multiphysics systems described by sets of balance and closure equations (following the classical thermodynamics approach).

III.4.1 *1D* ideal transmission line

Consider an ideal lossless transmission line defined on the interval $\Omega = [0,\, L]$. The state variables are the charge density *1-form* $q = q(t,z)\mathrm{d}z \in \Lambda^1(\Omega)$, and the flux density *1-form* $p = p(t,z)\mathrm{d}z \in \Lambda^1(\Omega)$ where $t \geq 0$ denotes the time variable. The total energy stored at time t in the transmission line is given as:

$$\begin{aligned} \mathbb{H}(q,\, p) &= \int_0^L \frac{1}{2}\left(\star_{\frac{1}{C(x)}} q \wedge q + \star_{\frac{1}{L(x)}} p \wedge p\right) \mathrm{d}z \\ &= \int_0^L \frac{1}{2}\left(\frac{q^2(t,z)}{C(z)} + \frac{p^2(t,z)}{L(z)}\right) \mathrm{d}z \end{aligned} \tag{III.9}$$

where $C(z)$, $L(z)$ are respectively the distributed capacitance and inductance of the line. Its variational derivatives with respect to the state variables are:

$$\begin{aligned} \tfrac{\delta \mathcal{H}}{\delta q} &= \star_{\frac{1}{C(z)}} q = V(t,z) \quad \text{(voltage)} \\ \tfrac{\delta \mathcal{H}}{\delta p} &= \star_{\frac{1}{L(z)}} p = I(t,z) \quad \text{(current)} \end{aligned} \tag{III.10}$$

The dynamics of the transmission line equation may be expressed as the Hamiltonian system, with the derivative operator d is equivalent to the spatial derivative ∂_z:

$$\frac{\partial}{\partial t}\begin{pmatrix} q \\ p \end{pmatrix} = \begin{pmatrix} 0 & \mathrm{d} \\ \mathrm{d} & 0 \end{pmatrix} \begin{pmatrix} \frac{\delta \mathcal{H}}{\delta q} \\ \frac{\delta \mathcal{H}}{\delta p} \end{pmatrix} \tag{III.11}$$

augmented, according to (III.3), with the boundary variables:

$$\begin{aligned} f_b^0(t) &= V(t,0), \quad f_b^1(t) = V(t,L) \\ e_b^0(t) &= -I(t,0), \quad e_b^1(t) = -I(t,L) \end{aligned} \tag{III.12}$$

which are simply the voltage and the currents at both boundary points of the spatial domain. The resulting energy-balance is:

$$\frac{d\mathbb{H}}{dt} = \langle e_b,\, f_b \rangle_{\partial} = -\left(I(t,L)V(t,L) - I(t,0)V(t,0)\right) \tag{III.13}$$

III.4.2 *3D* Diffusion

We denote hereafter Ω the $3D$ spatial domain and $\partial\Omega$ its closed boundary. The *3-form* $c \in \Lambda^3(\Omega)$ is the molar density (concentration), the *2-form* $J \in \Lambda^2(\Omega)$ is the molar flux. The mass conservation states:

$$\frac{d}{dt}\int_\Omega c \;=\; -\int_{\partial\Omega} J = -\int_\Omega \mathrm{d}J \;\text{ or in local vectorial form }\; \frac{\partial c}{\partial t} = -\nabla.J$$

Although there is only one energy state space variable $c(x,t)$, the mass conservation may be completed with the phenomenological diffusion relation:

$$J \;=\; J(F)$$

$$\text{and } F \;=\; -\mathrm{d}(\mu) \text{ or in vectorial form } F = -\nabla\mu$$

with the internal energy (here the Gibbs free energy density) $u(c) \in \Lambda^3(\Omega)$, the driving force $F \in \Lambda^1(\Omega)$, and J a phenomenological relation between the flux and the driving force. The chemical potential $\mu \in \Lambda^0(\Omega)$ is usually defined from the energy $\mathbb{H}(\mu, c)$ as the Langmuir chemical potential:

$$\mu(c) \;=\; \delta_c \mathbb{H}$$

Hence, the canonical model for the diffusion equation, including boundary condition can be expressed in Hamiltonian formulation as:

$$\begin{bmatrix} -\frac{\partial c}{\partial t} \\ -F \end{bmatrix} = \begin{bmatrix} 0 & \mathrm{d} \\ \mathrm{d} & 0 \end{bmatrix} \begin{bmatrix} \mu \\ J \end{bmatrix} \;\text{ and }\; \begin{bmatrix} e_\partial \\ f_\partial \end{bmatrix} = \begin{bmatrix} -\mu|_\partial \\ J|_\partial \end{bmatrix}$$

where $\mu|_\partial$ and $J|_\partial$ denotes respectively the chemical potential and the molar flux at the boundary $\partial\Omega$. One can easily derive from the previous structure the traditional diffusion equation:

$$\frac{\partial c}{\partial t} = -\nabla.\left(J\left(\nabla\left(\mu(c)\right)\right)\right)$$

Finally, the power balance reads:

$$\frac{d\mathbb{H}}{dt} = \int_{\partial\Omega} e_\partial \wedge f_\partial = \int_{\partial\Omega} \mu \wedge J$$

This example demonstrates that the proposed Stokes-Dirac structure may be used as well for parabolic problem (here fundamentally a diffusion type problem) which may seem quite unusual for a Hamiltonian approach. In the next subsection, we derive a boundary port-Hamiltonian formulation for the resistive diffusion equation which describes the diffusion of the poloidal magnetic flux in the tokamaks. Then it illustrates the powerfulness of the geometric approach and the co-variant formulation of the state equations in the case with a more complex (toroidal) geometry.

IV Co-variant formulation for the dynamics in the electromagnetic domain

We recall hereafter the port-Hamiltonian co-variant formulation of electrodynamics in the differential forms which allow a compact, independent coordinate formulation [99] [101, chap.4]. The model presented is a slight adaptation from the model presented in [99] and [71] which includes additional Lorentz forces. The main equations of electromagnetism are summarized in vector calculus notation in the Table IV.1 below.

Let denote by Ω the smooth connected and bounded spatial domain of the system and by $\partial\Omega$ its smooth boundary, then the electric and magnetic field intensities are naturally identified in [99] with the *1-forms*: E, $H \in \Lambda^1(\Omega)$; the magnetic, electric flux and free current densities are identified

with the *2-forms*: $B, D, J \in \Lambda^2(\Omega)$; and the charge density is written as a *3-form*: $\rho_e \in \Lambda^3(\Omega)$. Finally we shall identify the velocity of the plasma with a *1-form*, $v \in \Lambda^1(\Omega)$, obtained classically using the Riemannian structure of the spatial domain (stemming for instance from the Euclidean metric of $\mathbb{R}^3$) and keep both identifications throughout this work. The same choice is found in [84] and note that as stated in the remark 1, this *1-form* will be considered as the velocity vector field in the contraction calculus.

Name	Vector calculus formulation	Co-variant formulation
Gauss's law	$\nabla.D = \rho_e$	$dD = \rho_e$
Gauss's law for magnetism	$\nabla.B = 0$	$dB = 0$
Maxwell- Faraday	$\nabla \times E = -\frac{\partial B}{\partial t}$	$dE = -\frac{\partial B}{\partial t}$
Maxwell- Ampere	$\nabla \times H = J + \frac{\partial D}{\partial t}$	$dH = J + \frac{\partial D}{\partial t}$
Constitutive equations	$D = \epsilon E$ $B = \mu H$	$D = \star_\epsilon E$ $B = \star_\mu H$

Table IV.1: The vector notation form and the co-variant formulation of the characteristic equations of electrodynamics.
where $\star_\epsilon, \star_\mu$ denote the Hodge star products associated with *the permittivity* and *permeability tensors* respectively.

The electrodynamic equations may be formulated, using the co-variant formulation [89], as a port-Hamiltonian system [99] hereafter. The Hamiltonian functional is defined as the total electromagnetic energy $\mathbb{H}(D, B)$ in the domain Ω which is the integration of the energy density $\mathcal{H} = \frac{1}{2}[E \wedge D + H \wedge B]$:

$$\mathbb{H}(D, B) = \int_\Omega \mathcal{H} = \frac{1}{2}\int_\Omega [\star_{\frac{1}{\varepsilon}} D \wedge D + \star_{\frac{1}{\mu}} B \wedge B] \tag{IV.1}$$

The electric field intensity and magnetic field intensity are therefore intensive variables defined as variational derivatives of $\mathbb{H}(D, B)$, that is respectively the two *1-forms:* $E, H \in \Lambda^1(\Omega)$:

$$\begin{aligned} \frac{\delta \mathcal{H}}{\delta D} &= E(t, x) \\ \frac{\delta \mathcal{H}}{\delta B} &= H(t, x) \end{aligned} \tag{IV.2}$$

From the power continuity and Stokes theorem, one may derive the following Stokes-Dirac structure (see [99] for the definition and details) on the space of flows $\mathcal{F} = \Lambda^2(\Omega) \times \Lambda^2(\Omega) \times \Lambda^2(\Omega) \times \Lambda^1(\partial\Omega)$ and efforts $\mathcal{E} = \Lambda^1(\Omega) \times \Lambda^1(\Omega) \times \Lambda^2(\Omega) \times \Lambda^1(\partial\Omega)$:

$$\mathcal{D}_{EM} = \left\{ \begin{array}{c} (f_{el}, f_{mg}, f_d, f_{\partial\Omega}, e_{el}, e_{mg}, e_d, e_{\partial\Omega}) \in \mathcal{F} \times \mathcal{E} \mid \\ \begin{pmatrix} f_{el} \\ f_{mg} \end{pmatrix} = \begin{pmatrix} 0 & -\mathrm{d} \\ \mathrm{d} & 0 \end{pmatrix} \begin{pmatrix} e_{el} \\ e_{mg} \end{pmatrix} + \begin{pmatrix} 1 \\ 0 \end{pmatrix} f_d, \\ e_d = \begin{pmatrix} 1 & 0 \end{pmatrix} \begin{pmatrix} e_{el} \\ e_{mg} \end{pmatrix} \text{ and } \begin{pmatrix} f_{\partial\Omega} \\ e_{\partial\Omega} \end{pmatrix} = \begin{pmatrix} e_{el}|_{\partial\Omega} \\ e_{mg}|_{\partial\Omega} \end{pmatrix} \end{array} \right\} \tag{IV.3}$$

where $\omega^1|_{\partial\Omega}$ denotes the restriction of the *1-forms* at the boundary of the domain. Then the electromagnetic field equations may be implicitly defined as a port-Hamiltonian systems:

$$\left(-\frac{\partial D}{\partial t}, -\frac{\partial B}{\partial t}, f_d, f_{\partial\Omega}, E, H, e_d, e_{\partial\Omega}\right) \in \mathcal{D}_{EM} \tag{IV.4}$$

with boundary port variables:

$$\begin{cases} f_{\partial\Omega} &= E|_{\partial\Omega} \\ e_{\partial\Omega} &= H|_{\partial\Omega} \end{cases}$$

whose wedge product forms the Poynting vector at the boundary of the spatial domain $\partial\Omega$. The distributed port variables in the domain Ω are:

$$\begin{cases} f_d &= J \\ e_d &= E \end{cases}$$

where $J = J_\Omega + J_{ni}$ is the total current density including the Ohmic and the external non-inductive current (created by the RF waves). This distributed port is terminated with the Ohm's resistive $\star_\eta J_\Omega$ (with $\star_\eta$ the Hodge star related to the plasma resistivity) and connected to the material domain via the Lorentz force equation. The Lorentz force E_L is usually written using the Hodge star product and the exterior product, as:

$$E_L = \star(v \wedge \star B) \tag{IV.5}$$

with $v \in \Lambda^1(\Omega)$ the plasma velocity field then according to the remark 1 in the previous subsection (see appendix B for the calculus detail), we can use the equivalent contraction $E_L = -i_v B$ and derive the relation:

$$E = \star_\eta J_\Omega - i_v B \tag{IV.6}$$

The implicit formulation (IV.4) reveals to be extremely useful for the systems and control theory [101]. Among others, it satisfies following energy balance equation:

$$\frac{d\mathbb{H}}{dt} = -\int_{\partial\Omega} e_{\partial\Omega} \wedge f_{\partial\Omega} - \int_\Omega e_d \wedge f_d$$

In other words, with the appropriate choice of input-output variables, the system passivity is hold, that means the energy evolution is governed by the external energy through the boundary and its own dissipation.

A common Tokamak control model is so-called the $1D$ resistive diffusion equation, which can be reduced from the previous $3D$ model in the next chapter. However, it should be noticed that the influence of material balance equation on certain parameters in the electromagnetic domain, like the resistivity η and the bootstrapcurrent J_{bt} (which is considered as a non-inductive current source), is ignored in this resistive diffusion control model. We expect, in the sequel, to determine the coupling between electromagnetic and the material domains which affects the resistivity η via irreversible entropy source term. The bootstrap current source still remains unmodelled source term in this work but it will be our prospect.

V Balance equations in the material domain

In this section, the material balance equations for mass, momentum, energy and entropy are derived from the Boltzmann equation, the kinetic theory. These balance equations are computed for a moving material domain. The connection between the classical macroscopic transport equation and the port-based formulation is made by using the material derivative in co-variant form and the Gibbs-Duhem relation for the internal energy (cf. [101, Chap. 3, p. 154]). The result is a port-based fluid-like model expressed in terms of pairs of power conjugated variables. The couple with the volumic balance equation in the EM domain will also be investigated in the next section.

V.1 Kinetic theory and macroscopic transport equations

Using a kinetic description for the plasma dynamics, the material balance equations (mass, momentum, and energy balances) may be obtained from the integrals of the Boltzmann equation [16, p. 205]. The operators are written here in vectorial form ($\nabla, \nabla\times, \nabla.$). This step is a preamble for the fluid approach coming later.

V.1.1 Boltzmann equation

The Boltzmann equation is a state equation which describes the time evolution of the distribution functions $f_a(t, x, v)$ for particles with position x and velocity v in the coordinate β:

$$\frac{\partial f_a}{\partial t} + \frac{\partial}{\partial x_\beta}(v_\beta f_a) + \frac{\partial}{\partial v_\beta}\left(\frac{F_{a\beta}}{m_a} f_a\right) = C_a \tag{V.1}$$

Here the subscript a stands for the different considered species, such as electrons $a = e$, ions $a = i$, or neutral particles $a = n$ in our case. The external force:

$$F_a = e_a E + \frac{e_a}{c}[vB] \tag{V.2}$$

is caused by electric and magnetic fields, respectively E and B. The collision term is usually of the form $C_a = \sum_b C_{ab}(f_a, f_b)$ where C_{ab} denotes the rate of change for the distribution function of particles a due to elastic and/or inelastic collisions with b[7]. Averaging momenta of the distribution function over all possible velocities, the average or macroscopic classical (fluid-like) quantities may be derived:

$$\begin{aligned} n_a(t,r) &= \int f_a(t,r,v)\,dv \\ \overline{v}_a(t,r) &= \frac{1}{n_a}\int v f(t,r,v)\,dv = \langle v\rangle_a \\ T_a(t,r) &= \frac{1}{n_a}\int \frac{m_a}{3}(v-\overline{v}_a)^2 f(t,r,v)\,dv \\ &= \frac{m_a}{3}\left\langle (v-\overline{v}_a)^2\right\rangle \end{aligned} \tag{V.3}$$

which are the a-particles density, average velocity and temperature. The third equation is obtained by considering the thermal equilibrium (when $\overline{v}_a = 0$) $m\langle v^2\rangle/2 = 3T/2$. In this work, there is no fusion reaction considered. Hence balance equations for one species in the plasma may be usually derived from those for the other species (although there are some neglected interaction terms). Macroscopic variables related to only one representative species will be considered in this work. There will be no more use of the species subscripts a for electrons, ions, and neutral particles. In other words, $T, P, v, ...$ will be representative average temperature, pressure, velocity, ... for all species.

V.1.2 Transport equations (balance equations)

Three macroscopic balance equations may be derived by multiplying the Boltzmann equation (V.1) with 1, mv, and $\frac{mv^2}{2}$ respectively, and integrating these three resulting products over the domain of possible velocities (calculation detail from cf. [16, p.208] are detailed in the appendix C). Let's denote the usual material derivative:

$$\frac{d}{dt} = \frac{\partial}{\partial t} + \overline{v}.\nabla \tag{V.4}$$

we obtain with the calculations described hereover:

- the equation of continuity (particle transport):

$$\frac{dn}{dt} = -n\nabla.\overline{v} \tag{V.5}$$

  which is obtained assuming the density conservation (no external source term), and the assumption that the third term in (V.1) vanishes rapidly as $v \to \infty$.

- the equation of motion (momentum transport):

$$n\frac{d\overline{v}}{dt} = -\nabla P - \nabla\times\tau - en\left(E + \frac{1}{c}[\overline{v}B]\right) \tag{V.6}$$

  where P denotes the scalar pressure, τ the stress tensor, and electron charge $e = 1.6\,10^{-19}C$.

- the (total) energy transport equation:

$$\frac{d\epsilon}{dt} = -\nabla.[nT\overline{v} + \tau\overline{v} + \mathbf{q}] + en(E\overline{v}) \tag{V.7}$$

  where $\mathbf{q}$ is defined as the "heat" flux density, T is the average temperature and the total energy is defined as:

$$\epsilon = \frac{mn}{2}\overline{v}^2 + \frac{3}{2}nT \tag{V.8}$$

[7] This collision term is neglected in this work. It is a quite usual assumption since the plasma gas in tokomak is low density and usually considered as a perfect gas (cf. [16, p.206] or [10, Chap.6]).

The internal energy (or heat balance) equation may be obtained when the total energy (V.8) is replaced in equation (V.7), using the continuity and momentum equations:

$$\frac{3}{2}n\frac{dT}{dt} = -P\nabla.\overline{v} - \nabla.\mathbf{q} - \tau\left(\nabla\times\overline{v}\right) \tag{V.9}$$

Defining the entropy in the perfect gas case as $\mathbf{s} = ln\left(T^{3/2}/n\right) = ln\left(P^{3/2}/n^{5/2}\right)$, the heat balance equation may be written:

$$Tn\frac{d\mathbf{s}}{dt} = -\nabla.\mathbf{q} - \tau\left(\nabla\times\overline{v}\right) \tag{V.10}$$

The balance equations (V.5), (V.6) , (V.9) and (V.10)) will now be written in co-variant form for a representation in the port-Hamiltonian formulation.

V.2 Co-variant formulation of the transport equations

The properties and dynamics of the plasma considered as a fluid will be described in this section. The mass, momentum, energy and entropy balance equations will be derived in the co-variant form. We shall follow closely the general frame presented in [101, Chap.3, p.154] and drive to the corresponding results expressing in terms of differential forms.

The material properties are defined by the total material energy $\mathbb{H}_M$ which is the integral over the material domain $\mathcal{M}$ of total energy density ϵ. It consists the sum of the kinetic and internal energy of the system which depends on the specific quantity (per unit mass) of *the momentum density* $\mathbf{p}\in\Lambda^1(\mathcal{M})$[8], the *entropy* $\mathbf{s}\in\Lambda^3(\mathcal{M})$ and the *volume* $\mathbf{v}\in\Lambda^3(\mathcal{M})$.

This subsection gives a definition of the material derivative in terms of differential form which will be used in the following to write the balance equations on a moving material domain. Some features are simplified in our studied case, thanks to the assumptions no chemical reaction, and homogeneous mono-particle fluid[9]. In other words, $T, P, v, ...$ represent the average temperature, pressure,velocity... of all species.

V.2.1 Time derivative "following the motion"

The material properties must be described for a fixed amount of mass which, due to some velocity field, is described on a time-dependent spatial domain which is called a moving material domain. We denote ϕ_t the flow associated with the velocity field v (i.e. $v = d/dt\left(\phi_t z\right)$). Then any moving material domain with a fixed mass may be defined by $V\left(t\right) = \phi_t\left(\Omega\right)$ where Ω denotes the same material domain at time $t = 0$. Then the variation of some conserved material quantity α^k (a *k-form,* on some time dependent spatial domain $V(t)$ of dimension n satisfies [35, Chap.1, sec.4]) becomes:

$$\frac{d}{dt}\int_{V(t)}\alpha = \int_{V(t)}\frac{\partial\alpha}{\partial t} + \mathfrak{L}_v\alpha \tag{V.11}$$

where $\mathfrak{L}_v\alpha$ denotes the Lie derivative of the *k-form* α. Using Cartan's formula:

$$\mathfrak{L}_v = i_v\circ\mathrm{d} + \mathrm{d}\circ i_v \tag{V.12}$$

one may define *the material derivative* $\frac{D\alpha}{Dt}$ in term of the variation of some conserved quantity α such that:

$$\int_{V(t)}\frac{D\alpha}{Dt} = \frac{d}{dt}\int_{V(t)}\alpha \tag{V.13}$$

Therefore:

$$\frac{D\alpha}{Dt} := \frac{\partial\alpha}{\partial t} + i_v\mathrm{d}\alpha + \mathrm{d}(i_v\alpha) \tag{V.14}$$

For a volume form α^n in an n-dimensional spatial domain ($\mathrm{d}\alpha^n = 0$) and (V.14) becomes:

$$\frac{D}{Dt}\alpha = \frac{\partial\alpha}{\partial t} + \mathrm{d}i_v\alpha \tag{V.15}$$

which is equivalent to the usual $\partial_t + v\cdot\nabla$ vectorial form.

[8] Momentum density is actually equal to the velocity $\mathbf{p} = v$ [101, section 3.4]

[9] That means the average value of all parameters will be used instead of distinguishing different species a (electron, ions, neutral particles) like in kinetic theory.

V.2.2 Conservation law equations and closure equation

A balance equation for the material quantity α in a fixed frame generally takes form:

$$\frac{\partial \alpha}{\partial t} = -\mathrm{d}f_\alpha + \sigma_\alpha \tag{V.16}$$

where f_α defines the flux of α, and σ_α represents the external α source (by unit mass, as α is a density). Therefore, when considering a moving material domain, the balance equation becomes (using (V.15) and (V.16)):

$$\frac{D}{Dt}\alpha = -\mathrm{d}f_\alpha^R + \sigma_\alpha \tag{V.17}$$

where $f_\alpha^R = f_\alpha - i_v\alpha$ is now the relative flux of α and $\dfrac{D}{Dt}$ the material derivative. We can now express in co-variant form all the balance equations obtained from the kinetic theory in a moving material domain.

Mass balance The mass balance (continuity) equation may be written (fluid-like description) as:

$$\frac{\partial \rho}{\partial t} = -\mathrm{d}f_\rho + \sigma_\rho \tag{V.18}$$

or using (V.5) and (V.17):

$$\frac{D}{Dt}\rho = -\mathrm{d}f_\rho^R + \sigma_\rho \tag{V.19}$$

with the mass density $\rho = mn$, the relative particle flux $\mathrm{d}f_\rho^R = \mathrm{d}\left(f_\rho - i_v\rho\right) \equiv \rho \wedge \mathrm{d}\left(\star v\right)$, and the material source term σ_ρ per unit volume.

Remark 2. If $\mathbf{v} := 1/\rho$ denotes the specific massic volume and $\sigma_\mathbf{v}$ as the massic source term, then from equation (V.19) we have another corresponding volume balance equation, with the relative volume flux $\mathrm{d}f_\mathbf{v}^R \equiv -\mathbf{v}\mathrm{d}\left(\star v\right) \equiv \mathrm{d}\left(-i_v\mathbf{v}\right)$:

$$\frac{D}{Dt}\mathbf{v} = \mathrm{d}\left(i_v\mathbf{v}\right) + \sigma_\mathbf{v} \tag{V.20}$$

Momentum conservation The material derivative may be used as well to write the momentum balance equation in a moving material domain:

$$\frac{1}{\mathbf{v}}\frac{D\mathbf{p}}{Dt} = -\mathrm{d}f_\mathbf{p}^R + \sigma_\mathbf{p} \tag{V.21}$$

where $\mathbf{p}$ is the momentum per unit mass (that is $\mathbf{p} \equiv v$) and $\sigma_\mathbf{p}$ is the source term caused by external body force per unit mass, considered in this work to be the electromagnetic pressure:

$$\sigma_P = -\star\left(\star J \wedge \star B\right) \tag{V.22}$$

It may immediately be seen that these two relations are power continuous as:

$$\begin{aligned} \star v \wedge \sigma_P &= \star v \wedge \left(-\star\left(\star J \wedge \star B\right)\right) \\ &= \star v \wedge \left(\star\left(\star B \wedge \star J\right)\right) \\ &= \star\left(v \wedge \left(\star B \wedge \star J\right)\right) \\ &= \star\left(E_L \wedge \star J\right) \\ &= \left(\star E_L \wedge J\right) \end{aligned} \tag{V.23}$$

Note that one could also use a more usual identification of both the velocity v and the current J would be identified with vector fields (see remark 1 and appendix B), leading to an alternative expression of these relations using the contraction of a *2-form* by a vector field. The electromagnetic pressure is then expressed as:

$$\sigma_P = -i_{(\star J)}B \tag{V.24}$$

Energy balance The classical approach of the first principle of thermodynamic states that the total energy of the system is considered as a conserved quantity. Then the energy balance can also be written in material derivative as:

$$\frac{D\epsilon}{Dt} = -\mathrm{d}f_{\epsilon}^{R} + \sigma_{\epsilon} \tag{V.25}$$

where the source term σ_ϵ represents the inductive (ohmic) heat source term which is $\mathbf{v}\,(E \wedge J) = \mathbf{v}\,({}_{\star\eta}J \wedge J)$.

V.3 Closure equations and entropy production

In this subsection, we consider the closure equations for the momentum and energy balance equations. Then, since the entropy is not a conserved quantity, the irreversible entropy production term must be computed (from the previous balance and closure equations using to the Gibbs-Duhem relation) and from the entropy production deduced by identifying the total energy in (V.25) with internal energy.

V.3.1 Momentum

We first consider the momentum closure equation. According to (V.6), the tensor $f_{\mathbf{p}}^{R}$, representing the momentum flux per unit of surface area, is the sum of a pressure P and viscous force τ terms:

$$f_{\mathbf{p}}^{R} = (P\mathbf{I} + \tau) \tag{V.26}$$

Considering that P is a scalar (in an isotropic domain), while $\tau \in \Lambda^1$ is the non-diagonal part of stress tensor, or the so-called shear stress tensor, we have:

$$\mathrm{d}f_{\mathbf{p}}^{R} = \mathrm{d}P + \star\mathrm{d}\tau \tag{V.27}$$

V.3.2 Internal energy

The total energy density (per unit mass) is:

$$\epsilon = \frac{\star\mathbf{p} \wedge \mathbf{p}}{2} + \mathbf{u} \tag{V.28}$$

with u is the internal energy, then its time variation is defined according to:

$$\begin{aligned} \frac{D\epsilon}{Dt} &= \star v \wedge \frac{D\mathbf{p}}{Dt} + \frac{D\mathbf{u}}{Dt} \\ &= i_v\mathbf{v} \wedge \frac{1}{\mathbf{v}}\frac{D\mathbf{p}}{Dt} + \frac{D\mathbf{u}}{Dt} \end{aligned} \tag{V.29}$$

where the material derivative of internal energy u is applied from (V.17):

$$\frac{D}{Dt}\mathbf{u} = -\mathrm{d}f_{\mathbf{u}}^{R} + \sigma_{\mathbf{u}} \tag{V.30}$$

Thanks to equations (V.21) and (V.30), the total energy transfer in (V.29) is thus:

$$\begin{aligned} \frac{D\epsilon}{Dt} &= i_v\mathbf{v} \wedge \left(-\mathrm{d}f_{\mathbf{p}}^{R} + \sigma_{\mathbf{p}}\right) + \left(-\mathrm{d}f_{\mathbf{u}}^{R} + \sigma_{\mathbf{u}}\right) \\ &= -\mathrm{d}\left(i_v\mathbf{v} \wedge f_{\mathbf{p}}^{R} + f_{\mathbf{u}}^{R}\right) + f_{\mathbf{p}}^{R} \wedge \mathrm{d}\left(i_v\mathbf{v}\right) + i_v\mathbf{v} \wedge \sigma_{\mathbf{p}} + \sigma_{\mathbf{u}} \end{aligned} \tag{V.31}$$

with

$$\begin{cases} f_{\mathbf{u}}^{R} &= f_{\epsilon}^{R} - i_v\mathbf{v} \wedge f_{\mathbf{p}}^{R} \\ \sigma_{\mathbf{u}} &= \sigma_{\epsilon} - f_{\mathbf{p}}^{R} \wedge \mathrm{d}\left(i_v\mathbf{v}\right) - i_v\mathbf{v} \wedge \sigma_{\mathbf{p}} \\ &= \mathbf{v}\left({}_{\star\eta}J \wedge J\right) - \left(P \wedge \mathrm{d}\left(i_v\mathbf{v}\right) + \tau \wedge \mathbf{v}\mathrm{d}v\right) \end{cases} \tag{V.32}$$

V.3.3 Entropy

The internal energy is also determined by the Gibbs-Duhem equation:

$$\mathrm{d}\mathbf{u} = T \wedge \mathrm{d}\mathbf{s} - P \wedge \mathrm{d}\mathbf{v} \tag{V.33}$$

which will allow us to compute the irreversible entropy production source term σ_s (without nuclear fusion reaction in the studied case). We can deduce the entropy production rate:

$$\frac{D\mathbf{s}}{Dt} = \frac{1}{T}\left(\frac{D\mathbf{u}}{Dt} + P \wedge \frac{D\mathbf{v}}{Dt}\right) \tag{V.34}$$

Applying the material derivative formula for s, u and $\mathbf{v}$ in (V.34), we get:

$$\begin{aligned}
\frac{D}{Dt}\mathbf{s} \quad &= \frac{1}{T}\left(\frac{Du}{Dt} + P \wedge \frac{D\mathbf{v}}{Dt}\right) \\
\Leftrightarrow -\mathrm{d}f^R_{\mathbf{s}} + \sigma_{\mathbf{s}} \quad &= \frac{1}{T}\left(-\mathrm{d}f^R_u + \sigma_{\mathbf{u}} + P \wedge \mathrm{d}\left(i_v\mathbf{v}\right)\right) \\
\Leftrightarrow -\mathrm{d}\left(\frac{f_q}{T}\right) + \sigma_{\mathbf{s}} &= \frac{1}{T}\left(-\mathrm{d}f_q - \left(P \wedge \mathrm{d}\left(i_v\mathbf{v}\right) + \tau \wedge \mathbf{v}\mathrm{d}v\right)\right) + \\
&\quad + \frac{1}{T}\left(\mathbf{v}\left(\star_\eta J \wedge J\right) + P \wedge \mathrm{d}\left(i_v\mathbf{v}\right)\right)
\end{aligned} \tag{V.35}$$

where the heat flux f_q is related to the entropy and internal energy fluxes:

$$\begin{cases} f^R_{\mathbf{u}} = & f_q \\ f^R_{\mathbf{s}} = & \dfrac{1}{T} f_q \end{cases} \tag{V.36}$$

Thus the irreversible entropy source term $\sigma_{\mathbf{s}}$ is obtained with the help of the internal energy source term in equation (V.32):

$$\begin{aligned}
\sigma_{\mathbf{s}} &= \mathrm{d}\left(\frac{f_q}{T}\right) + \frac{1}{T}\left(-\mathrm{d}f_q - \tau \wedge \mathbf{v}\mathrm{d}v + g \wedge f^R_\rho\right) \\
&= -\frac{1}{T^2} f_q \wedge \mathrm{d}T - \frac{1}{T}\tau \wedge \mathrm{d}v + \frac{\mathbf{v}}{T} \star_\eta J \wedge J
\end{aligned} \tag{V.37}$$

This irreversible entropy source term contains the heat conduction $-\frac{1}{T^2} f_q \wedge \mathrm{d}T$, the viscous dissipation $-\frac{1}{T}\tau \wedge \mathrm{d}v$ and the Joule (ohmic) terms $\frac{\mathbf{v}}{T} \star_\eta J \wedge J$. The three of them define the constitutive relations for the $\mathcal{R}$ - field (see next section) which is needed to "close" the heat balance equation.

VI Multidomain couplings and resistivity field ($\mathcal{R}$ - field)

In this section, all power conservative multi-domain couplings are detailed as well as a dissipative $\mathcal{R}$ - field multi-domain coupling element. It's worthwhile noting that all conservative multi-domain couplings may be represented using Dirac structures (cf. [99]).

VI.1 Magneto-hydrodynamic coupling (MHD coupling)

MHD coupling is one of the important multi-domain couplings in tokamak system. It concludes a magnetomotive Dirac structure (which couples the two domains: EM and material one) and an Eulerian-Lagrangian coordinate transformation to link the volumetric and massic domains together.

VI.1.1 Magnetomotive coupling

Proposition VI.1. *Let us now prove that the two relations (IV.5) and (V.22) may be associated with a Dirac structure. Therefore, using the identification* $(f_J, e_J) = (J, E_L)$ *and* $(f_v, e_v) = (\sigma_P, \star v)$*, we shall define the space of flow variable* $\mathcal{F}_1 = \Lambda^2(\Omega) \times \Lambda^1(\Omega) \ni (f_J, f_v)$ *and the space of effort variables* $\mathcal{E}_1 = \Lambda^1(\Omega) \times \Lambda^2(\Omega) \ni (e_J, e_v)$*. For a fixed magnetic induction* B *, the two equations (V.24) and (IV.6) define two anti-adjoint maps:*

$$\begin{array}{rcl} \Lambda^2(\Omega) & \to & \Lambda^1(\Omega) \\ f_J & \mapsto & f_v = -\star(\star f_J \wedge \star B) \end{array}$$

and

$$\begin{array}{rcl} \Lambda^1(\Omega) & \to & \Lambda^2(\Omega) \\ e_v & \mapsto & \star(\star e_v \wedge \star B) \end{array}$$

The linear subspace $\mathcal{D}_1(B)$ *with* $B \in \Lambda^2(\Omega)$*, defines a Dirac structure in the bond space in* $\mathcal{F}_1 \times \mathcal{E}_1$*:*

$$\mathcal{D}_1(B) = \left\{ \begin{array}{l} (f_J, f_v, e_J, e_v) \in \mathcal{F}_1 \times \mathcal{E}_1 \mid \\ \left\{ \begin{array}{l} f_v = -\star(\star f_J \wedge \star B) \\ e_J = \star(\star e_v \wedge \star B) \end{array} \right. \end{array} \right\} \tag{VI.1}$$

Proof. Let us precise that the Dirac structure is defined with respect to the symmetrized pairing of the pairing on $\mathcal{F}_1 \times \mathcal{E}_1$ defined by:

$$\left\langle \begin{pmatrix} e_J \\ e_v \end{pmatrix}, \begin{pmatrix} f_J \\ f_v \end{pmatrix} \right\rangle = \int_\Omega e_v \wedge f_v - e_J \wedge f_J$$

Firstly let us show that $\mathcal{D}_1(B) \subset \mathcal{D}_1(B)^\perp$ which is equivalent to show that:

$$\left\langle \begin{pmatrix} e \\ e_v \end{pmatrix}, \begin{pmatrix} f_J \\ f_v \end{pmatrix} \right\rangle = 0\,, \qquad \forall (f_J, f_v, e_J, e_v) \in \mathcal{F}_1 \times \mathcal{E}_1$$

and this follows by using the calculation (V.23).

Secondly let us prove that $\mathcal{D}_1(B)^\perp \subset \mathcal{D}_1(B)$. Assume that $(f_J, f_v, e_J, e_v) \in \mathcal{F}_1 \times \mathcal{E}_1$ satisfies:

$$\left\langle \begin{pmatrix} e'_J \\ e'_v \end{pmatrix}, \begin{pmatrix} f_J \\ f_v \end{pmatrix} \right\rangle + \left\langle \begin{pmatrix} e_J \\ e_v \end{pmatrix}, \begin{pmatrix} f'_J \\ f'_v \end{pmatrix} \right\rangle = 0\,, \qquad \forall (f'_J, f'_v, e'_J, e'_v) \in \mathcal{D}_1(B)$$

This is equivalent to:

$$\left\langle \begin{pmatrix} \star(\star e'_v \wedge \star B) \\ e'_v \end{pmatrix}, \begin{pmatrix} f_J \\ f_v \end{pmatrix} \right\rangle + \left\langle \begin{pmatrix} e_J \\ e_v \end{pmatrix}, \begin{pmatrix} f'_J \\ -\star(\star f'_J \wedge \star B) \end{pmatrix} \right\rangle = 0\,, \qquad \forall (f'_J, e'_v) \in \Lambda^2(\Omega) \times \Lambda^1(\Omega)$$

or

$$\int_\Omega (e'_v \wedge f_v - \star(\star e'_v \wedge \star B) \wedge f_J) - (e_J \wedge f'_J - e_v \wedge \star(\star f'_J \wedge \star B)) = 0\,, \qquad \forall (f'_J, e'_v) \in \Lambda^2(\Omega) \times \Lambda^1(\Omega) \tag{VI.2}$$

Using the fact $\int_\Omega \star\alpha \wedge \beta = \int_\Omega \alpha \wedge \star\beta$ that $\star\star\alpha = \alpha$ one calculates:

$$\begin{array}{rcl} \int_\Omega \star(\star e'_v \wedge \star B) \wedge f_J & = & \int_\Omega \star e'_v \wedge \star B \wedge \star f_J \\ & = - & \int_\Omega \star e'_v \wedge \star f_J \wedge \star B \\ & = - & \int_\Omega e'_v \wedge \star(\star f_J \wedge \star B) \end{array}$$

and choosing $f'_J = 0$, the preceding equation becomes:

$$\int_\Omega e'_v \wedge (f_v + \star(\star f_J \wedge \star B)) = 0\,, \qquad \forall e'_v \in \Lambda^1(\Omega)$$

hence $f_v = -\star(\star f_J \wedge \star B)$.

In a similar way, choosing $e'_v = 0$, (VI.2) becomes:

$$\int_\Omega (e_J \wedge f'_J + e_v \wedge \star(\star f'_J \wedge \star B)) = 0\,, \qquad \forall f'_J \in \Lambda^2(\Omega)$$

or with similar calculus:

$$\begin{array}{rcl} \int_\Omega e_v \wedge \star(\star f'_J \wedge \star B) & = & -\int_\Omega e_v \wedge \star(\star B \wedge \star f'_J) \\ & = & -\int_\Omega \star e_v \wedge \star B \wedge \star f'_J \\ & = & -\int_\Omega (\star e_v \wedge \star B) \wedge \star f'_J \\ & = & -\int_\Omega \star(\star e_v \wedge \star B) \wedge f'_J \end{array}$$

$$\int_\Omega (e_J - \star(\star e_v \wedge \star B) \wedge f'_J) \wedge f'_J = 0\,, \qquad \forall f'_J \in \Lambda^2(\Omega)$$

yielding $e_J = \star(\star e_v \wedge \star B)$. Hence $(f_J, f_v, e_J, e_v) \in \mathcal{D}_1(B)$which completes the proof. □

VI.1.2 Eulerian-Lagrangian transformation

We shall define hereafter a Dirac structure associated with the change from Eulerian to Lagrangian coordinates (that is from integration on a fixed domain Ω to a moving domain $M = \phi_t(\Omega)$). Therefore let us write the power product between the effort and the flow variables in the two coordinates and look for the following equality:

$$\int_{M=\phi_t(\Omega)} e_2 \wedge f_2 = \int_\Omega \phi^*(e_2 \wedge f_2) = \int_\Omega \phi^*(e_2) \wedge f_1 \tag{VI.3}$$

with $\phi^*(e_2) = 1/\star\mathbf{v} e_2 \circ \phi^{-1}$, where $\mathbf{v}$ is the specific massic volume of the plasma. This defines the following vector subspace :

$$\mathcal{D}(\mathbf{v}) = \left\{ \begin{array}{c} (f_1, e_1;\, f_2, e_2) \in \Lambda^1(\Omega) \times \Lambda^2(\Omega) \\ \times \Lambda^1(M) \times \Lambda^2(M) \\ f_2 = f_1 \circ \phi^{-1};\, e_1 = \phi^*(e_2) \circ \phi; \\ f_1 \in \Lambda^1(\Omega)\,,\, e_2 \in \Lambda^2(\phi(\Omega)) \end{array} \right\} \tag{VI.4}$$

Subspaces $\mathcal{D}_1$ and $\mathcal{D}(\mathbf{v})$, as well as their interconnection, may be proved to be Dirac structures using the power products in the material domain suggested in (VI.3) and following arguments similar to those in [99]. In the Tokamak model the pairs of flow and effort variables are identified as follows: $(f_1, e_1;\, f_2, e_2)_1 = (-i_{\star J} B, \star v;\, -i_{\star J} B, i_v \mathbf{v})$ and $(f_1, e_1;\, f_2, e_2)_2 = (J, {}_{\star\eta} J;\, J, {}_{\star\eta} J\mathbf{v})$.

VI.2 Interdomain couplings in different material domains

The material domains includes the mechanical, hydraulic and thermal domains, interconnected together via canonical Stokes-Dirac structures (subsection III.3) of the form:

$$\mathcal{D}_i = \left\{ \begin{array}{c} (f_p, f_q, f_{i\partial M}, e_p, e_q, e_{i\partial M}) \in \mathcal{F}_\mathrm{i} \times \mathcal{E}_\mathrm{i} \mid \\ \begin{pmatrix} f_p \\ f_q \end{pmatrix} = \begin{pmatrix} 0 & \mathrm{d} \\ \mathrm{d} & 0 \end{pmatrix} \begin{pmatrix} e_p \\ e_q \end{pmatrix}, \\ \begin{pmatrix} f_{i\partial M} \\ e_{i\partial M} \end{pmatrix} = \begin{pmatrix} 0 & 1 \\ 1 & 0 \end{pmatrix} \begin{pmatrix} e_p \\ e_q \end{pmatrix} |_{\partial M} \end{array} \right\} \quad i = \{2,3,4\} \tag{VI.5}$$

- The Dirac structure $\mathcal{D}_2$ is the hydrodynamical coupling between mechanical and hydraulic domains:

$$(-\mathrm{d}P, \mathrm{d}(\star v), f_{2\partial M}, \star v, -P, e_{2\partial M}) \qquad = (f_p, f_q, f_{2\partial M}, e_p, e_q, e_{2\partial M}) \in \mathcal{F}_2 \times \mathcal{E}_2$$

$$\text{where } \begin{cases} \mathcal{F}_2 = \Lambda^1(M) \times \Lambda^3(M) \times \Lambda^0(M) \\ \mathcal{E}_2 = \Lambda^2(M) \times \Lambda^0(M) \times \Lambda^2(M) \end{cases}$$

- The Dirac structure $\mathcal{D}_3$ is the mechanical-thermal coupling, with:

$$(\star \mathrm{d}\tau, \mathbf{v}\mathrm{d}v, f_{3\partial M}, i_v \mathbf{v}, \tau, e_{3\partial M}) \qquad = (f_p, f_q, f_{3\partial M}, e_p, e_q, e_{3\partial M}) \in \mathcal{F}_3 \times \mathcal{E}_3$$

$$\text{where } \begin{cases} \mathcal{F}_3 = \Lambda^2(M) \times \Lambda^2(M) \times \Lambda^1(M) \\ \mathcal{E}_3 = \Lambda^1(M) \times \Lambda^1(M) \times \Lambda^1(M) \end{cases}$$

- The thermodynamic coupling $\mathcal{D}_4$ represents the irreversible heat flows in the thermal domain:

$$\left(\mathrm{d}\left(\frac{f_q}{T}\right), \mathrm{d}T, f_{4\partial M}, T, \left(\frac{f_q}{T}\right), e_{4\partial M}\right) \qquad = (f_p, f_q, f_{3\partial M}, e_p, e_q, e_{3\partial M}) \in \mathcal{F}_4 \times \mathcal{E}_4$$

where $\begin{cases} \mathcal{F}_4 = \Lambda^3(M) \times \Lambda^1(M) \times \Lambda^2(M) \\ \mathcal{E}_4 = \Lambda^0(M) \times \Lambda^2(M) \times \Lambda^0(M) \end{cases}$

VI.3 Resistive field ($\mathcal{R}$ - field)

According to the expression for the irreversible entropy source term in (V.37), the entropy creation is contributed by different resistivity sources: the heat conduction, the ohmic diffusion and the viscosity, with dissipation terms identified to $\left(-\frac{1}{T} f_q \wedge \mathrm{d}T,\ \mathbf{v}\left(\star_\eta J \wedge J\right),\ -\tau \wedge \mathbf{v}\mathrm{d}v\right)$ respectively, and notice that the nuclear reaction which has been neglected in this thesis. This leads to define a 3-port resistivity field, $\mathcal{R}$- field.

However, let us remind to the entropy production, derived from (V.35) as:

$$\frac{D\mathbf{s}}{Dt} = -\frac{1}{T} \wedge \mathrm{d}f_q - \tau \wedge \mathbf{v}\mathrm{d}v + \frac{1}{T}\left(\mathbf{v}\left(\star_\eta J \wedge J\right)\right) \tag{VI.6}$$

According to [74] and [11] or [38], this entropy production is composed by the power product of efforts and fluxes and there is a transport matrix Γ which yields the "linear" relation between efforts and fluxes:

$$f = \Gamma \mathrm{d}e \tag{VI.7}$$

Onsager's theory [74] implies that transport matrix Γ is symmetric, if one makes a special choice for the fluxes and their conjugated efforts.

In other words, it is more complicated to explicit the entropy irreversible term in our studied case than the one stated in the $\mathcal{R}$- field, since we made an assumption, as well as in [11], to diagonalize our transport matrix Γ:

$$\begin{pmatrix} f_q \\ \tau \\ J \end{pmatrix} = \begin{pmatrix} \star_\chi & \times & \times \\ \times & \star_\kappa & \times \\ \times & \times & \star_{1/\eta} \end{pmatrix} \mathrm{d} \begin{pmatrix} T \\ v \\ V_{loop} \end{pmatrix} \tag{VI.8}$$

where the diagonal terms $\star_\chi$, $\star_\kappa$, $\star_{1/\eta}$ represent respectively the *thermal diffusion coefficient*, *viscosity*, and *electrical resistivity*, V_{loop} is the *loop voltage* so ohmic electrical intensity is $E_\Omega = \mathrm{d}V$. This constitutive relation completes our model with the dissipation power in the $\mathcal{R}$- field is determined in (VI.6).

Remark 3. The non-diagonal terms "$\times$" in (VI.8) may play significant roles in the multidomain couplings. Nevertheless, their calculus formulations are not yet well defined . Our multiphysics modular model could help in this work.

VII Integration of the complete model with port-based approach

In this section, we describe the tokamak system in a graphical way by using Bondgraph (see [101, Chap.2]). It models the power exchange between elements in a systems, and between the system and its environment. The power exchanges are represented by arrows. The direction of the arrow is the "relative" direction of power flow. Each arrow is labeled by one pair of effort and flow variables, whose product defines the power of energy exchange between two elements: $\mathcal{P}(t) = e \wedge f$.

There are three basic types of elements: energy storage element $\mathcal{C}$, energy dissipative element $\mathcal{R}$, and interconnection element (Dirac structure, junctions, transformers and gyrators). The principle of energy conservation provides a fundamental basis for characterizing such elements, especially the interconnections ([101, Chap.2]).

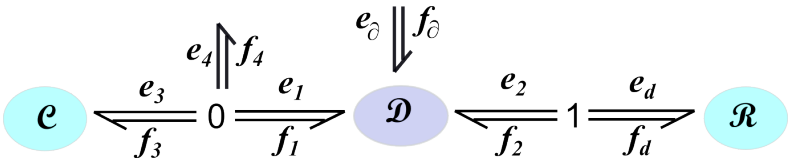

Figure VII.1: Simple Bondgraph

A very simple example in the figure VII.1 can help to clarify the Bondgraph utility. This example represents many common physical systems such as electric RLC circuit, or mechanic mass-spring system.

The energy storage element $\mathcal{C}$ and dissipative element $\mathcal{R}$ simply "receive"[10] energy from other elements:

$$\begin{cases} \mathcal{P}(\mathcal{C}) & := e_3 \wedge f_3 \\ \mathcal{P}(\mathcal{R}) & := e_d \wedge f_d \end{cases}$$

The Stokes-Dirac structure $\mathcal{D}$ defined in subsection III.3 is a conserving energy element, which holds:

$$\langle (e_1, e_2, e_\partial) \mid (f_1, f_2, f_\partial) \rangle = \int_\Omega [e_1 \wedge f_1 + e_2 \wedge f_2] + \langle e_\partial,\, f_\partial \rangle_{\partial\Omega} = 0$$

Then two types of junctions are used to connect the different elements together. They neither store or dissipate power. A $0-junction$ is a point where flows are distributed:

$$\begin{cases} e_1 = e_3 = e_4 \\ f_1 + f_3 + f_4 = 0 \end{cases}$$

while a 1-junction is where efforts are distributed:

$$\begin{cases} e_2 + e_d = 0 \\ f_2 = f_d \end{cases}$$

But in both case, we have energy conservation:

$$\sum_i e_i \wedge f_i = 0$$

Remark 4. In this simple example, we even can introduce the input-output control variables. The external energy source, can directly modify the system states via the junction 0 by the power $e_4 \wedge f_4$ or affect the system through the boundary as $e_\partial \wedge f_\partial$.

In figure VII.2, we present the complete Tokamak *3D* model including all the domains and subdomains, as well as their inter-domain and multi-domain couplings: electromagnetic, magneto-hydrodynamic, thermal-mechanic and hydrodynamic multi-domain couplings (using Stokes-Dirac and interconnection structures).

The blue part describes the electromagnetic domain. The Dirac structure $\mathcal{D}_{EM}$ in (IV.3) couples the electric and magnetic domains, which are based on Maxwell's equations (*0-junctions*), and Ohm's law (*1-junction*). The electromagnetic energy is accumulated in energy storage elements $\mathcal{C} :: \mathbb{H}(D)$ and $\mathcal{C} :: \mathbb{H}(B)$. It is dissipated by Joule effect via the $\mathcal{R}$-field element (section VI.3). Moreover, this Bondgraph also indicates two possible control ports which are the boundary input-output control (V_{loop}, I_p) and distributed control non-inductive current drive(J_{ni}, $\star_\eta J_{ni}$). The system actuators will be mentioned in the next chapters.

The red, green, and black parts of the Bondgraph respectively sketch the thermal, mechanical and hydraulic subdomains of the material domain. There is a common storage source in this domain denoted $\mathcal{C} :: \mathbb{H} = \int_\mathcal{M} \frac{\star\mathbf{p} \wedge \mathbf{p}}{2} + u$. All the transport equations developed in section V are implied at

[10] Note that, unlike the reversible element $\mathcal{C}$, which can receive as well as supply energy to the system, $\mathcal{R}$ is an irreversible element, that means one cannot inverse the energy exchange flow via this element.

0-junctions in each subdomain. *1-junctions* link the subdomains to the dissipative $\mathcal{R}$-field, which transfers all its energy as the irreversible entropy source term to the thermal domain. In each material subdomain, there is a Stokes-Dirac structure (VI.5) (section VI.2) such as the structure $\mathcal{D}_2$ for the hydraulic domain, $\mathcal{D}_3$ for the mechanic domain, and $\mathcal{D}_4$ for the thermal one. At each Stokes-Dirac structure, the boundary control signals are determined, however, we don't use them all in actual control of tokamak. Two other important control actions in the material domain is the distributed heating source S_{heat} in thermal domain, and material injection source $\sigma_{\mathbf{v}}$ in hydraulic domain.

The electromagnetic volumetric balance equations in the blue part are related to the material domain through the Dirac structure $\mathcal{D}(\mathbf{v})$ defined in (VI.4) and the transformer $\mathcal{TF} :: B = \mathcal{D}_1$ as in (VI.1).

The Bondgraph sketches out the complete tokamak system in the manner of modular multi-physics. On one hand, we can separately study an (some) interesting subdomain(s) with the appropriate assumptions, that will be illustrated in the next chapter 3. On the other hand, it's also convenient to couple the subdomains together which guarantees the system passivity conservation of the ensemble.

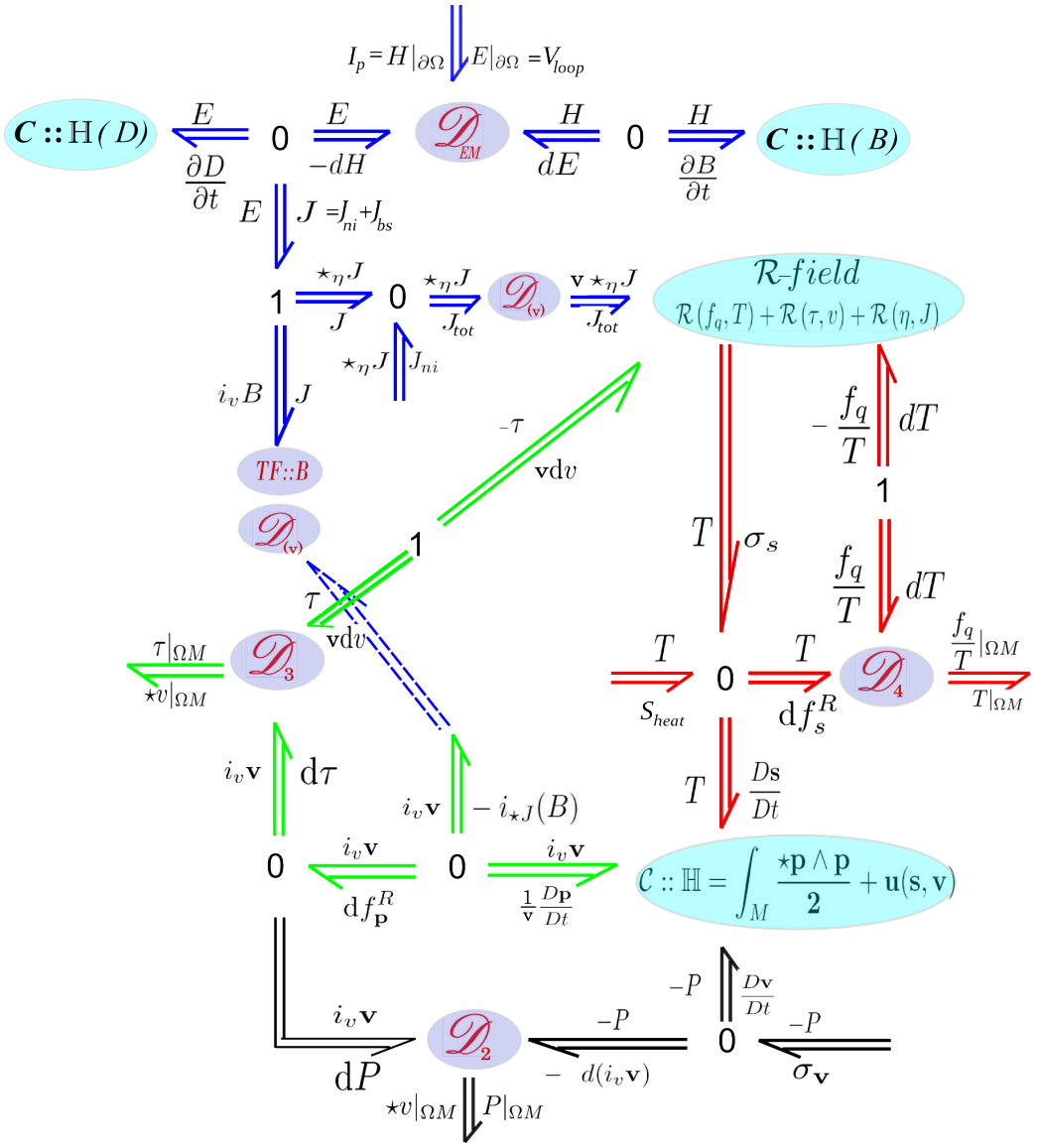

Figure VII.2: Bondgraph of thermodynamic tokamak system including electromagnetic domain (blue), mechanic domain (green), thermal domain (red) and hydraulic domain (black)

VIII Conclusion

In this section we developed the balance and constitutive equations for the material domain, a part of the plasma fluid model for tokamaks. These equations are derived from the Boltzmann equation, using the classical kinetic theory approach. They have been written in a port-Hamiltonian form with the help of material derivatives (balance equations for a moving material domain).

The entropy balance and the Gibbs-Duhem equations allowed us to compute the irreversible entropy production (source) term. We obtain finally a modular structured model which is split into different parts. This result allows us to be able to gradually complete the resistive diffusion equation control model, which corresponds only to the electromagnetic balance equations. The first step will be to include a simple thermal model with the heat production from the Joule effect (ohmic resistivity), a simple heat transport diffusion (dispersion) model and the variation of the resistivity with the temperature. This model will allow us to consider the important effect of temperature variations on the resistivity and also to use the non inductive actuators for the heating of the plasma. The second step will be to consider the magneto-hydrodynamic and hydrodynamic part to obtain a control model which includes the bootstrap current effect. Finally, the third step will be the inclusion of the mass balance equation and the supplementary terms and equations related to the fusion reaction.

The next chapter will propose a geometric reduction method for our *3D* Hamiltonian system in order to derive an ideal control model which includes all these supplementary physical phenomena.

Chapter 3

Geometric reduction

I Introduction

For the purpose of system analysis, simulation or control synthesis, a reduced model well-reflecting the original one - in some desired aspects - may be looked for. The term "geometric reduction" for Hamiltonian system appeared in the 1980s in the works of J.E. Marsden ([60, 61, 48, 59]). Dedicated to the reduction of finite dimensional mechanics, it made use of system symmetries and invariant variables to reduce the phase space. For instance the method called momentum reductions (cf. [100, 59]) for Lagrangian or Hamiltonian systems was based on tangent and cotangent maps. The work of Blankenstein in [9] presented the reduction of Dirac Structure including application to the reduction of implicit Hamiltonian systems. The projection map was applied on symmetry Lie group. However, in these previous works, the Hamiltonian was also projected in the reduced space and the system invariants, which can play a central role of control action, sometimes disappeared in the reduction.

On the other hand, during the 1990s, related to the discretization of PDEs, the idea of geometric structure conservation was studied for the so-called multi-symplectic systems[1]. For many PDEs, the multi-symplectic formulation has revealed important features for stability analysis. The series of papers ([17] [86]) endowed the system geometric structure to understand the interaction and stability of nonlinear waves (the nonlinear Schrödinger equation and the water-wave problem) as Hamiltonian systems. [47] showed that multi-symplectic systems of PDEs may be derived from Hamilton's principle without higher-order derivatives[2]. The multi-symplectic structure preservation in numerical simulation of Hamiltonian dynamics (i.e. multi-symplectic integrators) was for instance investigated in [18], and detailed in [41, Chap. 6,7].

The geometric reduction method presented in this thesis aims only at the spatial reduction and spatial discretization of a system which reduces the dimension of the spatial domain: from a three dimensional model to a finite dimensional one. Quite surprisingly this symplectic semi-discretization problem has not been studied extensively in the literature. However, this is understood by the fact that our main motivation in the derivation of continuous time spatial approximation is the further design of non linear control laws based on the model structure. In the port-Hamiltonian approach, a model is determined by a specific interconnection structure (Dirac structure) and its Hamiltonian function (normally derived from the energy function). The proposed reduction aims also at the preservation of the main dynamical properties (as for instance the spectrum qualitative properties and quantitative values) and the main energetic properties (conservativeness, dissipativeness, and symplecticity, etc) of the considered system. The corresponding reduced variables are defined in order to preserve the "natural" power pairing. The proposed method applies mostly to port-

[1] Roughly speaking, multi-symplectic (or multi-Hamiltonian) systems may be written in the form $Kx_t + Lx_\rho = \nabla_x S(x)$ where K and L are skew-symmetric matrices and $\nabla_x S$ denotes the gradient of some smooth scalar function S. This is a a way of generalizing Hamiltonian systems of ODEs of the form $Jx_t = \nabla H(x)$. Such systems have a structural conservation law from which scalar conservation laws may be derived such as energy and or momentum conservation (cf. [47]). In this context, multi-symplectic integrators are numerical integration methods that exactly preserve some discrete analogue of the multi-symplectic conservation law (a symplectic structure in both space and time).

[2] This can be achieved by introducing auxiliary variables to eliminate the derivatives.

Hamiltonian models for open systems of balance equations and will be applied to the *3D* fluid-like model of the fusion tokamak reactor developed in chapter 2. The obtained *1D* and *0D* models will be used later in the thesis to apply successfully passivity or energy based control approaches (such as IDA-PBC control [77]).

The main idea of the spatial reduction method - i.e. preserving the natural power product which is used to define the Dirac interconnection structures - is applied twice: first to reduce the model from *3D* to *1D*, the key feature of this chapter, then from *1D* to *0D* discrete system in the next chapter. Both reductions are symplectic with respect to the power-pairings in the magnetic and thermal domains. In section II the assumptions of axial symmetry and quasi-static equilibrium of the plasma are used to perform the reduction from *3D* to *1D* by using simple integration formulas on toroidal coordinate surfaces. The geometric reduction methodology is then deduced in section III. Two application examples, representing all the possible cases in a *3D* model, are derived: for the resistive diffusion equation in section IV and for the thermal diffusion equation in section V. Once the projections have been defined to preserve the power pairing forms, the coupling structures and closure equations will be reduced - using the same projections - in section VI to complete the *1D* model. Some discussions are carried out in the last section in order to explicit the dependencies of the coupling parameters on the system states in different domains.

II Reduction assumptions: axis-symmetry and quasi-static equilibrium

A *3D* TMHD tokamak model has been developed in chapter 2 for the dynamics of a plasma gas in a toroidal chamber. It is based on the mass, entropy, momentum and electromagnetic balance equations. With the help of Dirac and Stokes-Dirac interconnection structures, balance and closure (constitutive) equations are organized in a structured port-Hamiltonian model.

In this chapter we derive a *1D* model more suitable for control issues than the full *3D* TMHD one. There are two main reduction assumptions: axial symmetry with respect to the main torus axis (see figure II.1) and quasi-static equilibrium for the plasma. With these two assumptions, it may be proved that the magnetic flux surfaces form a set of nested toroids which are simultaneously isobaric, isothermal and iso-poloidal flux[3] (cf. [106, sec. 3.2] and [10, chap. 1]). After a continuous mapping, these surfaces may be matched into nested regular toroidal surfaces with circular cross-sections and a set of magnetic toric coordinates (ρ, θ, ϕ) (see figure II.1) may be defined such that ρ denotes the index of the considered magnetic surface (the new "radial" coordinate; subsection II.3 will explain how to determine this ρ index) and such that all the system variables are independent of θ and ϕ. Therefore the model may be projected onto the *1D* domain $\Pi = [0, a] \ni \rho$, $a = \rho_{max}$.

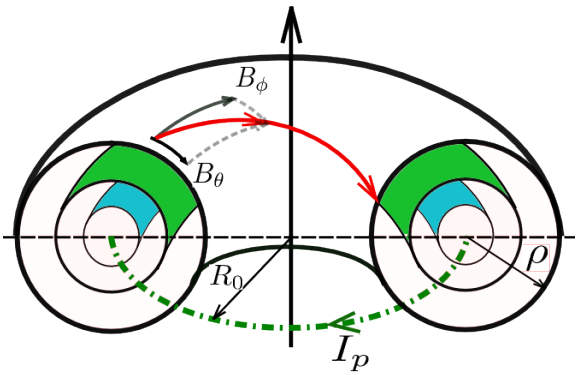

Figure II.1: Magnetic toric coordinates. θ denotes the polar angle and ϕ the azimuth angle. B_θ and B_ϕ are the two magnetic field coordinates ($B_\rho = 0$). R_0 denotes the tokamak major radius and I_p the total plasma current.

[3] The poloidal flux $\psi(R, Z)$ is defined as the flux through a circular horizontal disk S determined by the radius R from the torus axis and the height Z in cylindrical coordinate in the figure II.2.

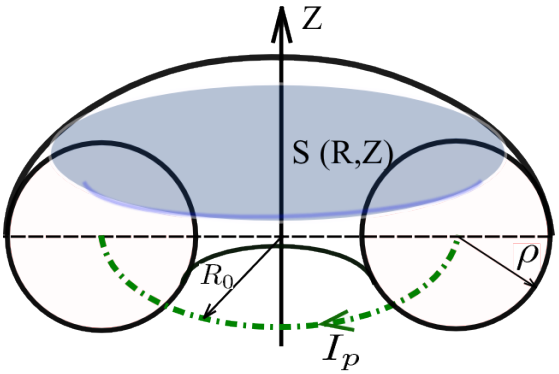

Figure II.2: The poloidal flux $\psi(R, Z)$ is the magnetic flux traversing the horizontal disk S

Although the "symmetry" assumptions are specific to the tokamak *3D* TMHD model, the proposed methodology could be applied to other examples with other symmetries. Roughly speaking, this methodology simply consists in using spatial symmetries in the *3D* model in order to (spatially) reduce the power pairing to an "equivalent" *2D* or *1D* power pairing (with the same value).

II.1 Axisymmetry assumption

The symmetric position of all the electric coils allows to carry out an axisymmetric magnetic field around the principle axis of the torus. This means that all the variables in the equilibrium states may be considered as independent of the toroidal angle ϕ. Using this assumption we get a *2D* model with all variables depending only on the ρ and θ spatial coordinates. Note that, because there is only a finite number of non-continued external coils, a dissymmetric effect (named magnetic ripple) should be added. It may be treated as a perturbation acting on the *2D* model obtained with the axisymmetric equilibrium assumption.

II.2 Quasi-static equilibrium assumption

Following [10, Chap.6], we consider that the Alfvén time constant τ_A[4] is much smaller than the one for plasma diffusion τ_p[5]. The time constant τ_A is in the order of a microsecond while τ_p is in the order of a millisecond. Therefore the plasma may be assumed to have reached a "mechanical" stationary profile at every instant t considered for the heat or magnetic flux diffusion phenomena. Otherwise stated, since the pressure and material transport is established much faster than the current transport process, we consider a quasi static plasma in Tokamak which neglects the dynamics $\frac{\partial \mathbf{p}}{\partial t}$ in momentum conservation. In this case the magnetic force balances the pressure forces and

$$-i_{\star J} B = \mathrm{d}P \text{ or in vectorial form } J \times B = \nabla P \tag{II.1}$$

where J, B, P are the plasma current, magnetic field and plasma pressure respectively. Besides, in the resistive diffusion equation which will be considered as a particular example hereafter, the other "material" dynamics are also ignored such as no material source is added $\frac{D\mathbf{v}}{Dt} = 0$. Hence, in the resistive diffusion equation which is sometimes used as a *1D* control model for the poloidal flux profile regulation, the internal energy accumulation is neglected.

II.3 Magnetic surfaces and magnetic toric coordinate

The magnetic surfaces made with constant field lines of B (where also lies the plasma current density J), thanks to the quasi-static assumption (II.1), are also surfaces of constant pressure P.

[4] the Alfvén time is an important timescale for wave phenomena. It is related to the Alfvén velocity by: $\tau_A = \frac{a}{v_A}$, where a denotes the minor radius of the torus

[5] τ_p is in fact defined as the smallest among the diffusion time constants of the particle density τ_n(millisecond), of the electron and ion heat diffusion τ_e, τ_i (millisecond), and the one of the diffusion of current density and magnetic field τ_r (second).

Furthermore, it's proved in [106, sec 3.2, p.108] and [10, Chap.1], that these surfaces are iso-thermal and iso-poloidal flux as well. Therefore, we define a new variable - the ρ index[6] which determines

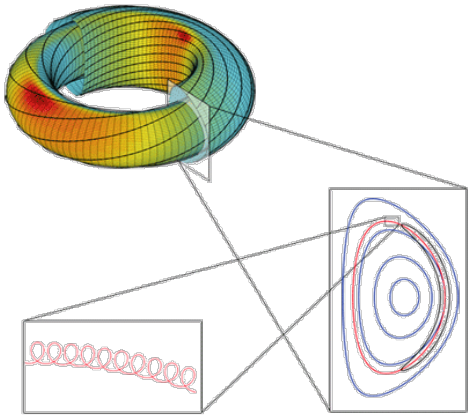

Figure II.3: Constant level curves of the poloidal flux function for a plasma equilibrium in the toric geometric coordinate (r, θ, ϕ). These curves become the nested toroids in magnetic toric coordinate (ρ, θ, ϕ).

the magnetic surfaces:

$$\rho = \sqrt{\frac{\Phi}{\pi B_0}} \tag{II.2}$$

where B_0 denotes the toroidal magnetic field amplitude at the center of plasma flux ($\rho = 0$) (considered as a constant) and Φ is the toroidal magnetic flux (the flux through a vertical section of the plasma). The ρ index admits the unit of a spatial variable and the choice of the new coordinates system (ρ, θ, ϕ) deforms the set of magnetic surfaces into a set of nested tori as represented in the figure II.1. Moreover, in many recent Tokamaks, the toroidal field Φ varies much less than the poloidal flux ψ. This Φ is almost invariant during the plasma discharge and so is the "mean radius" ρ of each magnetic surface defined from Φ. In the sequel, we will adopt this new coordinates system (ρ, θ, ϕ) - named *magnetic toric coordinates*[7] to derive the *1D* model from the *3D* one with the spatial reduction method that we propose.

III *3D-1D* Geometric reduction method

The *3D* TMHD model in chapter 2 is stated in covariant form, that is the state and port variables are not defined as vector fields but rather as differential *k-forms* corresponding to the integral calculus (cf. [35]). It is assumed in this approach that the total energy in *3D* spatial domain Ω may be written $\mathbb{H} = \int_\Omega \mathcal{H}^3$ where the energy density $\mathcal{H}^3 \in \Lambda^3(\Omega)$ is the external product of two *k-forms*, either $\mathcal{H}^3 = \alpha^1 \wedge \beta^2$ or $\mathcal{H}^3 = \alpha^0 \wedge \beta^3$. The idea is then to partially integrate $\mathcal{H}$ on *2D* coordinate surfaces such that the total energy reads:

$$\mathbb{H} = \int_\Omega \mathcal{H}^3 = \int_\Pi \overline{\alpha}^0 \wedge \overline{\beta}^1 \tag{III.1}$$

leading to the definition of the *1D* reduced variables $\overline{\alpha}^0$ and $\overline{\beta}^1$ and their external product (power pairing) $\overline{\alpha}^0 \wedge \overline{\beta}^1$ in the *1D* domain $\Pi = [0, a]\,;\, a = \rho_{max}$. We discuss hereafter how to determine

[6] Notice that in the toric geometric coordinate (r, θ, ϕ), the equilibrium equation for the axis-symmetric system can be written as a differential equation for the poloidal flux ψ. This differential equation is usually called Grad-Shafranov equation ([106, sec 3.3] and [10, Chap.1]), which also helps to determine the profiles of the plasma pressure P and plasma current J. This choice is made by [46] and used by [10, Chap.6], since it's was the simplest idea to take ψ as the independent variable in the flux and transport diffusion equations in tokamak systems. However, in conventional tokamaks, ψ varies with plasma current as well as loop voltage in the primary loop.

[7] note that this is not a purely geometric fixed coordinates system since it is closely related to the plasma magnetic surfaces

k-form	Examples
α^0	T, P
α^1	$E, H, v, \mathbf{p}$
α^2	D, B, J
α^3	$\mathbf{s}, \mathbf{v}, \mathbf{u}, \sigma$

Table III.1: The variables in the 3D model are k-forms α^k of order 0, 1, 2 or 3

these variables.

Let g_ρ, g_θ, g_ϕ, and $g = g_\rho g_\theta g_\phi$ denote the transformation coefficients between geometric toric coordinates (r, θ, ϕ) and magnetic toric coordinates (ρ, θ, ϕ) (see appendix D for a detailed computation of this coordinates transformation and the expression of volume forms and differential operators in toric coordinates), and the volume element is $dV = \sqrt{g} d\rho d\theta d\phi$. For instance, the integration in (III.1) in magnetic toric coordinate reads in toric coordinates:

$$\int_\Omega \mathcal{H}^3 = \int_V \alpha\beta \, dV \tag{III.2}$$

Therefore , the corresponding reduced variables α and β may be obtained by grouping the variables into two parts and performing integration on suitable integration domains: a curve coordinate for *1-forms* and *2-forms* and a surface coordinate for *3-forms*. These integrations are summarized in table III.2. Note that most of the variables "lie" on the magnetic surfaces, since the component in the radial direction ρ vanishes with the quasi-static equilibrium assumption.

We will detail the concept in (III.1) via an example hereafter. First of all, let's remind all the *3D* variables in our system in the table III.1. Since the equivalent variables in the *1D* model are deduced via the power conservation (III.1), we now look at the dissipation due to the Joule effect in EM domain as a first example of reduced variables definitions. The dissipated power is defined as the power product of the electric field intensity $E \in \Lambda^1(\Omega)$ and the plasma current $J \in \Lambda^2(\Omega)$:

$$\mathcal{P}_{Joule} = \int_\Omega E^1 \wedge J^2 = \int_V EJ \, dV \tag{III.3}$$

The *1-form* E is integrable over a contour C. We denote $E_t = E_\theta + E_\phi$ the tangential component of the vector field E and dl the length element along the contour C. Then the loop voltage on C reads:

$$V_C = \int_C E_t dl \tag{III.4}$$

with $dl = dl_\theta + dl_\phi = \sqrt{g_\theta} d\theta + \sqrt{g_\phi} d\phi$ (see appendix *D*). Then:

$$\begin{array}{rcccc} V_C & = & \int_0^{2\pi} E_\theta \sqrt{g_\theta} d\theta & + & \int_0^{2\pi} E_\phi \sqrt{g_\phi} d\phi \\ & = & \overline{E}_\theta & + & \overline{E}_\phi \end{array} \tag{III.5}$$

The result proves that $E^1 \in \Lambda^1(\Omega)$ becomes a function in our *1D* model: $\Lambda^0(\Pi) \ni V_C \equiv E^0 = \overline{E}_\theta + \overline{E}_\phi$ with

$$\begin{cases} \overline{E}_\theta & = \int_0^{2\pi} E_\theta \sqrt{g_\theta} d\theta \\ \overline{E}_\phi & = \int_0^{2\pi} E_\phi \sqrt{g_\phi} d\phi \end{cases}$$

Remark 5. In the tokamaks, one of the simple measurements is the loop voltage called V_{loop} (cf. [106, Chap.10, p.502]). It is defined as the voltage of the external toroidal loop (the contour on the magnetic surface of ρ_{max}), that is $V_{loop} = \overline{E}_\phi(\rho_{max})$. It's one of the important control variables which determines the Joule heating of plasma [25, 2, 107].

From (III.3) we may determine that the reduced form of the conjugated variable $J \in \Lambda^2(\Omega)$ is a *1-form* in the *1D* spatial domain: $\overline{J}^1 \in \Lambda^1(\Pi)$. We focus again on the dissipated power in (III.3)

k-form	new variables	corresponding values
0-form	α^0	f
1-form	$\overline{\alpha}^0 = \left(\overline{A_\theta}, \overline{A_\phi}\right)$	$\left(\int_0^{2\pi} \sqrt{g_\theta} A_\theta d\theta,\ \int_0^{2\pi} \sqrt{g_\phi} A_\phi d\phi\right)$
2-form	$\overline{\alpha}^1 = \left(\overline{A_\theta}, \overline{A_\phi}\right) d\rho$	$\left(\int_0^{2\pi} \sqrt{g_\rho g_\phi} A_\theta d\phi,\ \int_0^{2\pi} \sqrt{g_\rho g_\theta} A_\phi d\theta\right) d\rho$
3-form	$\overline{\alpha}^1 = \overline{A} d\rho$	$\left(\int_0^{2\pi} \int_0^{2\pi} \sqrt{g} A d\theta d\phi\right) d\rho$

Table III.2: Reduced variables definitions in the *1D* domain Π obtained from the integrations of corresponding variables in the *3D* domain (written in toric coordinates)

to determine the corresponding value of $\overline{J}^1$ in the Π domain:

$$\begin{aligned} \mathcal{P}_{Joule} &= \int_V \left(E_\rho J_\rho + E_\theta J_\theta + E_\phi J_\phi\right) \sqrt{g} d\rho \wedge d\theta \wedge d\phi \\ &= \int_0^a \int_0^{2\pi} \int_0^{2\pi} \left[\left(E_\theta \sqrt{g_\theta}\right) \left(J_\theta \sqrt{g_\rho g_\phi}\right) d\theta d\phi + \left(E_\phi \sqrt{g_\phi}\right) \left(J_\phi \sqrt{g_\rho g_\theta}\right) d\theta d\phi\right] d\rho \\ &= \int_0^a \left[\left(\overline{E}_\theta\right) \left(\overline{J}_\theta\right) + \left(\overline{E}_\phi\right) \left(\overline{J}_\phi\right)\right] d\rho \\ &= \int_\Pi \overline{E}^0 \wedge \overline{J}^1 \end{aligned} \tag{III.6}$$

Note that $J_\rho = 0$ as the plasma currents lie on the magnetic surfaces (subsection II.2) and that the *1D* corresponding variables (like $\overline{E}^0$ in (III.5)) are independent from the θ, ϕ coordinates. The reduced variable of J is thus:

$$\Lambda^1(\Pi) \ni \overline{J}^1 = \overline{J}_\theta d\rho + \overline{J}_\phi d\rho \tag{III.7}$$

with

$$\begin{cases} \overline{J}_\theta &= \int_0^{2\pi} J_\theta \sqrt{g_\rho g_\phi} d\phi \\ \overline{J}_\phi &= \int_0^{2\pi} J_\phi \sqrt{g_\rho g_\theta} d\theta \end{cases}$$

We may get the corresponding *1D* variables for others *k-forms* in *3D* domain (namely the *0-forms* and *3-forms*) thanks to the similar calculus (see section V hereafter for the detailed computations on the temperature/entropy density product example). The result are summarized in the table III.2.

Remark 6. A relation may be established between these definitions of the reduced variables in the *1D* domain Π and the spatial averaging process used in [10, Chap.6, p.242] to perform the *3D-1D* reduction. In this latter work average quantities $\langle A \rangle$ are defined over the magnetic surfaces in the form:

$$\langle A \rangle = \frac{\partial}{\partial V} \int_V A dV \tag{III.8}$$

The average values of a function A and a vector field W in his proposition VI.1 ([10, Chap.6, p.242]) is defined as:

$$\begin{aligned} \langle A \rangle &= \frac{1}{V'} \int_S \frac{A dS}{|\nabla \rho|} \\ \langle \nabla . W \rangle &= \frac{1}{V'} \frac{\partial}{\partial \rho} \left[V' \langle W . \nabla \rho \rangle\right] \end{aligned} \tag{III.9}$$

where S is the surface of the horizontal disk in the figure II.2. In fact, his term $V' = \frac{\partial V}{\partial \rho}$ is equivalent to our volume element of each unit of ρ: $\frac{\partial V}{\partial \rho} = \sqrt{g} d\theta d\phi$. Thus this idea can be summarized by our calculus for each *k-form*, such as:

- for the 1-*form* $A^1 \in \Lambda^1$, an average value around the toric boundary line:

$$\left\langle A^1 \right\rangle = \frac{\int_0^{2\pi} A \sqrt{g_\theta} d\theta}{\int_0^{2\pi} \sqrt{g_\theta} d\theta} \tag{III.10}$$

- for the 2-*form* $A^2 \in \Lambda^2$, an average value on the vertical section of plasma flux $\langle A^2 \rangle$ is defined as:

$$\begin{aligned} \int_0^\rho d\tau \int_0^{2\pi} A\sqrt{g_\rho g_\theta} d\theta &= \int_0^\rho d\tau \langle A^2 \rangle \int_0^{2\pi} \sqrt{g_\rho g_\theta} d\theta \\ \Rightarrow \langle A^2 \rangle &= \frac{\int_0^{2\pi} A\sqrt{g_\rho g_\theta} d\theta}{\int_0^{2\pi} \sqrt{g_\rho g_\theta} d\theta} \end{aligned} \tag{III.11}$$

- for the 3-*form* $A^3 \in \Lambda^3$, an average value in an element volume:

$$\begin{aligned} \int_0^{2\pi} d\phi \int_0^\rho d\tau \int_0^{2\pi} A\sqrt{g} d\theta &= \int_0^{2\pi} d\phi \int_0^\rho d\tau \langle A^3 \rangle \int_0^{2\pi} \sqrt{g} d\theta \\ \Rightarrow \langle A^3 \rangle &= \frac{\int_0^{2\pi} A\sqrt{g} d\theta}{\int_0^{2\pi} \sqrt{g} d\theta} \end{aligned} \tag{III.12}$$

It's easy to note that our average value of a 3-*form* stands for the case of function A in (III.9), while those of the 1-*form* and 2-*form* correspond to the case of vector field W in (III.9).

However, there's a different point between our *1D variable* definitions. As reminded previously, the proposition in III.9 used the average values as reduced variables, while ours count on the total integral value of each variable (in other words, our *1D corresponding variables* are defined by integrating them over their domain as in table III.2.

The definitions of reduced variables based on the conservation of the power pairings for conjugated pairs of variables is applied hereafter to derive the reduced *1D* models for two examples. Firstly the Stokes-Dirac structure for Maxwell's equations in the electromagnetic domain is reduced. Since the electromagnetic energy density is defined as a product

$$\mathcal{H}_{EM} = \alpha^1 \wedge \beta^2 \tag{III.13}$$

the corresponding *1D* variables for the *1-forms* and the *2-forms* are derived. This case is similar to the previous example of the dissipative element $\mathcal{P}_{Joule}$.

Secondly, the *1D* model for the thermal diffusion equation will be obtained by deducing the corresponding *1D* variables of the *0-forms* and the *3-forms*, since the thermal energy power product is:

$$\mathcal{H}_T = \alpha^0 \wedge \beta^3 \tag{III.14}$$

IV The resistive diffusion equation example

The EM model of tokamak plasma (chapter 2, equation (IV.3)) is used as an example to illustrate the proposed reduction method. The EM Stokes-Dirac structure as well as the constitutive relations are all projected in the reduced coordinate. The result is also validated by comparing to the existence models.

IV.1 EM Stokes-Dirac structure

The plasma electromagnetic *3D* model was figured out in port-Hamiltonian form in the previous chapter in (IV.3). It is defined in the following covariant formulation for the Maxwell's equations with the help of the effort-flow variable notations:

$$\begin{pmatrix} f_{el} \\ f_{mg} \end{pmatrix} = \begin{pmatrix} 0 & -\mathrm{d} \\ \mathrm{d} & 0 \end{pmatrix} \begin{pmatrix} e_{el} \\ e_{mg} \end{pmatrix} + \begin{pmatrix} 1 \\ 0 \end{pmatrix} f_d \tag{IV.1}$$

or using explicitly the electromagnetic variable notations:

$$\begin{pmatrix} -\partial_t D \\ -\partial_t B \end{pmatrix} = \begin{pmatrix} 0 & -\mathrm{d} \\ \mathrm{d} & 0 \end{pmatrix} \begin{pmatrix} E \\ H \end{pmatrix} + \begin{pmatrix} 1 \\ 0 \end{pmatrix} J \tag{IV.2}$$

Here d denotes the external spatial derivative of the *1-forms* which corresponds to the curl operator in the vectorial notation. The electromagnetic energy is:

$$\mathbb{H}_{EM} = \frac{1}{2} \int_\Omega [E^1 \wedge D^2 + H^1 \wedge B^2] \tag{IV.3}$$

Let us now apply the geometric reduction described previously only to the magnetic domain to determine the corresponding *1D* variables:

$$\begin{array}{rcl}
\mathbb{H}(B) & = & \frac{1}{2}\int_\Omega H^1\wedge B^2 \\
& = & \frac{1}{2}\int_\Omega \left(H_\rho B_\rho + H_\theta B_\theta + H_\phi B_\phi\right)\sqrt{g}d\rho d\theta d\phi \\
& = & \frac{1}{2}\int_0^a d\rho[\int_0^{2\pi}\left(\sqrt{g_\theta}H_\theta\right)d\theta\int_0^{2\pi}\left(\sqrt{g_\rho g_\phi}B_\theta\right)d\phi \\
& & +\int_0^{2\pi}\left(\sqrt{g_\phi}H_\phi\right)d\phi\int_0^{2\pi}\left(\sqrt{g_\rho g_\theta}B_\phi\right)d\theta] \\
& = & \frac{1}{2}\int_0^a d\rho\left[\left(\overline{H}_\theta\right)\left(\overline{B}_\theta\right)+\left(\overline{H}_\phi\right)\left(\overline{B}_\phi\right)\right] \\
& = & \frac{1}{2}\int_\Pi \overline{H}^0\wedge\overline{B}^1
\end{array} \tag{IV.4}$$

The same reduction is applied to the electric domain with the energy density $\mathbb{H}(D)=\frac{1}{2}\int_\Omega E^1\wedge D^2$ and leads to the definition of the reduced variables $\overline{E}^0$, $\overline{D}^1$ which are derived similarly. The Maxwell's equations (or EM Dirac structure) in Π domain are then simply written:

$$\left[\begin{array}{c} -\frac{\partial}{\partial t}\overline{D}^1 \\ -\frac{\partial}{\partial t}\overline{B}^1 \end{array}\right] = \left[\begin{array}{cc} 0 & -\mathrm{d}_\Pi \\ \mathrm{d}_\Pi & 0 \end{array}\right]\left[\begin{array}{c} \overline{E}^0 \\ \overline{H}^0 \end{array}\right]+\left[\begin{array}{c} 1 \\ 0 \end{array}\right]\overline{J}^1 \tag{IV.5}$$

Hence the *exterior derivator* d becomes $\mathrm{d}_\Pi=\left(\begin{array}{cc} 0 & -1 \\ 1 & 0 \end{array}\right)\frac{\partial}{\partial\rho}$ in the *1D* reduced spatial domain Π.

The Stokes-Dirac structure of the EM domain must be completed with the choice of a pair of reduced variables for the boundary energy flow. In case of an exterior product of two *1-forms* in *3D* model, the right result is slightly different from the product of two reduced *0-forms* in *1D* model. We explain hereafter the reason and propose some definitions to ensure the conservation property in the reduction.

Let us examine in some details the energy flux $\int_{\partial\Omega}H^1\wedge E^1$ which goes through the boundary. The considered boundary in our system is the magnetic surface at the plasma external radius $\rho_{max}=a$. Since $E_\rho=H_\rho=0$ on the magnetic surfaces, we get:

$$\begin{array}{rcl}
\int_{\partial\Omega}H^1\wedge E^1 & = & \int_{\partial\Omega}\left(H_\rho E_\theta - H_\theta E_\rho\right)\sqrt{g_\rho}d\rho\wedge\sqrt{g_\theta}d\theta+\left(H_\phi E_\rho - H_\rho E_\phi\right)\sqrt{g_\phi}d\phi\wedge\sqrt{g_\rho}d\rho \\
& & +\left(H_\theta E_\phi - H_\phi E_\theta\right)\sqrt{g_\rho}\rho d\theta\wedge\sqrt{g_\phi}d\phi \\
& = & \int_0^{2\pi}d\phi\int_0^{2\pi}d\theta\sqrt{g_\theta g_\phi}\left(H_\theta E_\phi - H_\phi E_\theta\right)|_0^a \\
& = & \left(\int_0^{2\pi}\sqrt{g_\phi}E_\phi d\phi\right)\left(\int_0^{2\pi}d\theta\sqrt{g_\theta}H_\theta\right)|_0^a-\left(\int_0^{2\pi}\sqrt{g_\phi}H_\phi d\phi\right)\left(\int_0^{2\pi}d\theta\sqrt{g_\theta}E_\theta\right)|_0^a \\
& = & \int_{\partial\Pi}\overline{H}_\theta\overline{E}_\phi-\overline{H}_\phi\overline{E}_\theta \\
& = & \int_{\partial\Pi}\overline{H}^0\wedge\overline{E}^0
\end{array} \tag{IV.6}$$

Then on the space of reduced flows (augmented with the boundary flow) $\overline{\mathcal{F}}=\Lambda^1(\Pi)\times\Lambda^1(\Pi)\times\Lambda^1(\Pi)\times\Lambda^0(\partial\Pi)$ and reduced efforts (augmented with the boundary efforts) $\overline{\mathcal{E}}=\Lambda^0(\Pi)\times\Lambda^0(\Pi)\times\Lambda^0(\Pi)\times\Lambda^0(\partial\Pi)$, one may define the reduced *1D* model with the help of a reduced Stokes-Dirac structure which is basically the same as before (except for the fact that it is written explicitly for the θ and ϕ components of the reduced variables):

$$\begin{array}{c}
\overline{\mathcal{D}}_{EM}= \\
\left\{\begin{array}{c}
(f_{el},f_{mg},f_d,f_{\partial\Pi},e_{el},e_{mg},e_d,e_{\partial\Pi})\in\overline{\mathcal{F}}\times\overline{\mathcal{E}}\mid \\
\left(\begin{array}{c} f_{el} \\ f_{mg}\end{array}\right)=\left(\begin{array}{cc} 0 & -\mathrm{d}_\Pi \\ \mathrm{d}_\Pi & 0\end{array}\right)\left(\begin{array}{c} e_{el} \\ e_{mg}\end{array}\right)+\left(\begin{array}{c} 1 \\ 0\end{array}\right)f_d, \\
e_d=\left(\begin{array}{cc} 1 & 0\end{array}\right)\left(\begin{array}{c} e_{el} \\ e_{mg}\end{array}\right)\text{ and }\left(\begin{array}{c} f_{\partial\Pi} \\ e_{\partial\Pi}\end{array}\right)=\left(\begin{array}{c} e_{el}|_{\partial\Pi} \\ e_{mg}|_{\partial\Pi}\end{array}\right)
\end{array}\right\}
\end{array} \tag{IV.7}$$

Thus the *3D* model (IV.2) transforms into a *1D* model with a similar power pairing product. In fact, this *1D* EM model can be split into two decoupled submodels: the poloidal submodel (describing the dynamics of B_θ, H_θ, E_ϕ, J_ϕ) and the toroidal one (describing the relations between

B_ϕ, H_ϕ, E_θ J_θ). In order to prove the equivalence between our approach and the existing resistive diffusion equation, we will focus on the poloidal submodel which may be written:

$$\begin{pmatrix} f_{el\phi} \\ f_{mg\theta} \end{pmatrix} = \begin{pmatrix} 0 & -\dfrac{\partial}{\partial\rho} \\ -\dfrac{\partial}{\partial\rho} & 0 \end{pmatrix} \begin{pmatrix} e_{el\phi} \\ e_{mg\theta} \end{pmatrix} + \begin{pmatrix} 1 \\ 0 \end{pmatrix} f_{d\phi} \tag{IV.8}$$

where $f_{el\phi} = -\partial_t\left(\overline{D}_\phi\right)$, $f_{mg\theta} = -\partial_t\left(\overline{B}_\theta\right)$, $e_{el\phi} = \overline{E}_\phi$, $e_{mg\theta} = \overline{H}_\theta$ and $f_{d\phi} = \overline{J}_\phi$. In the following subsection, we aim to derive the resistive diffusion equation from our reduced system (IV.8) with the help of the constitutive relations in *1D* domain.

IV.2 Reduced constitutive relations in EM domain

We consider here the *3D* constitutive relations for the induction field and Ohm's law. These two constitutive equations may be written in coordinates:

$$\begin{cases} B^2 = & {}_{\star\mu}H^1 \\ E^1 = & {}_{\star\eta}J^2 \end{cases} \Rightarrow \begin{cases} B_\theta & = \mu H_\theta \\ E_\phi & = \eta\left(J_\phi - J_{ni}\right) \end{cases} \tag{IV.9}$$

We define the non inductive current J_{ni} as the sum of the bootstrap current J_{bs} and external current source J_{ext} which is controlled through external heating sources. The above constitutive equations may be written equivalently:

$$\begin{cases} \dfrac{1}{\mu}\dfrac{\sqrt{g_\theta}}{\sqrt{g_\rho g_\phi}}\left(\sqrt{g_\rho g_\phi}B_\theta\right) & = \left(\sqrt{g_\theta}H_\theta\right) \\ \eta\sqrt{g_\rho g_\theta}\left(J_\phi - J_{ni}\right) & = \dfrac{\sqrt{g_\rho g_\theta}}{\sqrt{g_\phi}}\left(\sqrt{g_\phi}E_\phi\right) \end{cases} \tag{IV.10}$$

Integrating the left and right hand sides of IV.10 over the domain $\theta \in [0, 2\pi]$ and $\phi \in [0, 2\pi]$, using the previous definitions of the *1D* reduced variables, we get the new constitutive equations in the Π domain:

$$\begin{cases} \underbrace{\left[\displaystyle\int_0^{2\pi} \frac{\sqrt{g_\theta}}{\sqrt{g_\rho g_\phi}} d\theta\right]}_{A_1} & \overline{B}_\theta = \mu\overline{H}_\theta \\ \eta\left(\overline{J}_\phi - \overline{J}_{ni}\right) & = \overline{E}_\phi \underbrace{\left[\displaystyle\int_0^{2\pi} \frac{\sqrt{g_\rho g_\theta}}{\sqrt{g_\phi}} d\theta\right]}_{A_2} \end{cases} \Rightarrow \begin{cases} \overline{B}^1 = & {}_{\star\mu}\overline{H}^0 \\ \overline{E}^0 = & {}_{\star\eta}\overline{J}^1 \end{cases} \tag{IV.11}$$

where the $\bar{J}_{ni}$ term added in the second constitutive equation of (IV.10) is in fact the $\bar{J}_{ni\phi}$component.

Until then the derived model is a classical system of two conservation laws which would result in a hyperbolic system, very similar for instance to the classical transmission line example. However, in the resistive diffusion model, the displacement current $f_{el\phi}$ is considered negligible when compared to the inductive current. This assumption[8] will result in a system of only one conservation law (related to the magnetic field intensity storage) which can be written as an algebro-differential[9] system using the same *1D* structure (IV.8).

With this assumption, (IV.8) becomes:

$$\begin{aligned} \frac{\partial\overline{B}_\theta}{\partial t} &= \frac{\partial}{\partial\rho}\overline{E}_\phi \\ &= \frac{\partial}{\partial\rho}\left(\eta\frac{1}{A_2}\left(\overline{J}_\phi - \overline{J}_{ni}\right)\right) \\ &= \frac{\partial}{\partial\rho}\left(\eta\frac{1}{A_2}\frac{\partial}{\partial\rho}\left(\frac{1}{\mu}A_1\overline{B}_\theta\right)\right) - \frac{\partial}{\partial\rho}\frac{1}{A_2}\left(\eta\overline{J}_{ni}\right) \end{aligned} \tag{IV.12}$$

[8] The same assumption is made in the Maxwell-Ampère law in [10, Chap.6] and [106, sec 3.3], to find the flux diffusion equation

[9] In this context, "algebro-differential" is an improper term since the dissipation equation also makes use of an exterior derivative. It only means that the dissipation equation contains no time derivative

Using the definition of the poloidal plasma flux ψ, Faraday theory gives:

$$\begin{array}{rcccc} & -\dfrac{\partial\psi}{\partial t} & = & \overline{E}_\phi & \\ \Rightarrow & -\dfrac{\partial\dfrac{\partial\psi}{\partial t}}{\partial\rho} & = & \dfrac{\partial\overline{E}_\phi}{\partial\rho} & = \dfrac{\partial\overline{B}_\theta}{\partial t} \\ \Rightarrow & -\dfrac{\partial\psi}{\partial\rho} & = & \overline{B}_\theta & \end{array} \tag{IV.13}$$

Thus we obtain finally the classical resistive diffusion equation for the poloidal flux:

$$\begin{array}{rcccc} \dfrac{\partial\left(-\dfrac{\partial\psi}{\partial\rho}\right)}{\partial t} & = & -\dfrac{\partial}{\partial\rho}\left(\eta\dfrac{1}{A_2}\dfrac{\partial}{\partial\rho}\left(\dfrac{1}{\mu}A_1\dfrac{\partial\psi}{\partial\rho}\right)\right) & -\dfrac{\partial}{\partial\rho}\dfrac{1}{A_2}\left(\eta\overline{J}_{ni}\right) \\ \Leftrightarrow \quad \dfrac{\partial\psi}{\partial t} & = & \eta\dfrac{1}{A_2}\dfrac{\partial}{\partial\rho}\left(\dfrac{1}{\mu}A_1\dfrac{\partial\psi}{\partial\rho}\right) & +\dfrac{1}{A_2}\left(\eta\overline{J}_{ni}\right) \end{array} \tag{IV.14}$$

Remark 7. The safety factor q spatial profile is really important for MHD-stability. Recent works on advanced tokamak control are based on the control of this safety factor profile [1, 39]. In first approximation, the q-profile is given by the expression [10, Chap.6]:

$$q = -\frac{1}{2\pi}\frac{\partial\Phi}{\partial\psi} \tag{IV.15}$$

where Φ is the toroidal magnetic flux, which is considered static in comparing with the evolution of the poloidal flux ψ in (IV.14). In the simplest point of view, the condition to prevent MHD instabilities in the plasma is $q > 1$. However, in some cases of interest, such as in the case of a saw-teeth profile for the plasma current, it may happen that the q-profile crosses the critical value $q = 1$.

The chosen boundary conditions may be written equivalently in term of the poloidal flux:

$$\begin{cases} f_{mg\theta}|_{\rho=0} \sim \frac{\partial\psi}{\partial z}|_{\rho=0} & = 0 \\ e_{el\phi}|_{\rho=a} = -\frac{\partial\psi}{\partial t}|_{\rho=a} & = -V_{loop} \end{cases} \tag{IV.16}$$

The first one expresses the smoothness and symmetry with respect to the central circular axis (magnetic axis) of the Tokamak torus. The second one defines the boundary control action.

Remark 8. There is an equivalence between (A_1, A_2) and the coefficients (C_2, C_3) first used in [10, Chap.6] or later in [107] for the resistive diffusion equation. Firstly remind that the volume element may be written in the magnetic coordinates system $dV = r\lambda.d\rho.d\theta.d\phi$ (appendix D). Hence $V' = \dfrac{\partial V}{\partial\rho} = 4\pi^2\left\langle r\lambda\right\rangle$. From equation (I.7) $r = \sqrt{g_\rho g_\theta}$, and $\dfrac{\partial r}{\partial\rho} = \sqrt{g_\rho} = \delta_\rho$, $\sqrt{g_\phi} = \lambda = R_0 + rcos\theta$. Thus we have:

$$\Rightarrow \begin{cases} A_1 & = \int_0^{2\pi}\dfrac{r}{\lambda\delta_\rho^2}d\theta \\ A_2 & = \int_0^{2\pi}\dfrac{r}{\lambda}d\theta \end{cases} \Rightarrow \begin{cases} A_1 & = \left\langle\dfrac{r}{\lambda\delta_\rho^2}\right\rangle \\ A_2 & = \left\langle\dfrac{r}{\lambda}\right\rangle \end{cases} \tag{IV.17}$$

The coefficients (C_2, C_3) are defined as:

$$\begin{cases} C_2 = & V'\left\langle\dfrac{|\nabla\rho|^2}{\lambda^2}\right\rangle \\ C_3 = & V'\left\langle\dfrac{1}{\lambda^2}\right\rangle \end{cases} \Leftrightarrow \begin{cases} C_2 & = & 4\pi^2\left\langle\dfrac{r\,|\nabla\rho|^2}{\lambda}\right\rangle & = & 4\pi^2 A_1 \\ C_3 & = & 4\pi^2\left\langle\dfrac{r}{\lambda}\right\rangle & = & 4\pi^2 A_2 \end{cases} \tag{IV.18}$$

where $\dfrac{\partial\rho}{\partial r} = \dfrac{1}{\delta_\rho} = \nabla\rho$.

As a partial conclusion we see that assuming the classical axial symmetry and quasi-static equilibrium assumptions, neglecting the displacement current and considering the same constitutive relations as in the classical approach, the port-Hamiltonian model provides the resistive diffusion equation as a by-product (basically equivalent to the poloidal submodel) with a direct computational definition of the coefficients A_1 and A_2 corresponding to the magnetic toric geometry.

The plasma resistive diffusion model (IV.8) and (IV.16) may thus be represented in the port-Hamiltonian formalism using a Stokes-Dirac skew-symmetric structure. This seemingly unusual feature is in fact a characteristic of all diffusion-like models relies on a fundamental assumption from thermodynamics: flows are generated by generalized forces which may be written as gradients of generalized potentials. Once this assumption holds, then a similar transformation into port-Hamiltonian model may be successfully operated with the two formally adjoint operator *div* (used for the conservation law) and *grad* (used for the flux law). This approach has already been applied for the modelling of transport phenomena [5] and leads to very nice properties of reduction schemes for parabolic equations using spatially symplectic reduction schemes [7]. This idea for the port-Hamiltonian formulation of diffusion like parabolic equations is again applied in the next section for the thermal diffusion equation.

The plasma resistivity η, and the bootstrap current $\overline{J}_{bs}$ are significantly varying with the plasma temperature T (cf. [10, p.172]). However, in most existing control designs (for the poloidal flux control) these TMHD couplings have been neglected and the temperature T has been considered as an external parameter. Therefore $\eta := \eta(z,t)$ and $\overline{J}_{bs} := \overline{J}_{bs}(z,t)$ have been considered as time and space dependent parameters. In the next section, we will consider therefore an explicit port-Hamiltonian formulation for a simplified heat transport equation in the Tokamak. This *1D* "thermal diffusion equation" will allow in the sequel to consider (for control purposes) explicitly the dependance of the plasma resistivity and bootstrap current with the new state variable T.

V The thermal diffusion equation example

In chapter 2, the material domain balance equations for mass, momentum, energy and entropy were derived from the Boltzmann equation. The connection between the classical macroscopic transport equation and the port-based formulation has been made by using the material derivative definition written in covariant form. We then derived the irreversible entropy source terms (from the Gibbs-Duhem relation, following the "port-based" approach in [101, Chap.3] or [24]) which contains the heat conduction term, the viscous dissipation term, the Joule (ohmic) term and the external heating source. All of these terms are necessary to define the constitutive relations for the heat balance equation or "thermal diffusion equation".

Let $\sigma_{\mathbf{s}} \in \Lambda^3(\mathcal{M})$ denote the entropy source term, $\mathbf{s} \in \Lambda^3(\mathcal{M})$ the entropy density and $T \in \Lambda^0(\mathcal{M})$ the temperature[10]. These variables are all defined in the material domain (the moving massic frame $\mathcal{M}$). The entropy balance equation reads (see chapter 2, section V.3.3):

[10] Note that the above considered variables are in fact average values since the real plasma consists of different species of ions and electrons. Each species has its own temperature and entropy/energy balance equations should also consider interactions between species (see [10, Chap.6]). However it will only become necessary to separate these species transport equations once the fusion reaction will be considered and separate material balance equations will be required to account for the species transformations. This is the reason why coupled models of ionic and electronic energy transport equations are usually used in the burn control problem (see [93, 94]). However, in our case (no reaction), some average variables may be used and only one energy balance equation may be considered for the sake of simplicity and without loss of generality. Following [107], we will consider that the electronic temperature T_e may be deduced from the average temperature T thanks to the assumptions of the linear dependencies between electronic-ionic temperatures T_e, T_i and their densities n_e, n_i :

$$\begin{gathered} T_i = \alpha_{T_i} T_e \\ n_i = \alpha_i n_e \\ T = \frac{n_e T_e + n_i T_i}{n_e + n_i} = \frac{1 + \alpha_i \alpha_{T_i}}{1 + \alpha_i} T_e \end{gathered}$$

where α_i and α_{Ti} are the ratios defined in [107].

$$\begin{pmatrix} T\dfrac{d\mathbf{s}}{dt} \\ F \end{pmatrix} = \begin{pmatrix} 0 & -\mathrm{d} \\ -\mathrm{d} & 0 \end{pmatrix} \begin{pmatrix} T \\ f_q \end{pmatrix} + \begin{pmatrix} \sigma_{\mathbf{s}} \\ 0 \end{pmatrix} \tag{V.1}$$

with the heat flux $f_q \in \Lambda^2(\mathcal{M})$ and the thermal force $F \in \Lambda^1(\mathcal{M})$. The entropy balance equation (V.1) is written for a moving material domain $\mathcal{M}$ (chapter 2, section V). Therefore, a transformation from Lagrangian to Eulerian coordinates (whose details are given in section VI) will be necessary to connect this balance equation to the EM balance equations written in the fixed volumic domain Ω.

Applying the proposed *3D-1D* reduction in subsection III, using as well magnetic toric coordinates for the thermal domain, the *1D* reduced port-conjugated variables in the thermal domain may be defined in the following way:

$$\begin{aligned} \mathbb{H}(T) &= \int_M T^0 \wedge \sigma^3_{\mathbf{s}} = \int_\Omega T^0 \wedge n\sigma^3_{\mathbf{s}} \\ &= \int_\Omega T n \sigma_{\mathbf{s}} \sqrt{g} d\rho d\theta d\phi \\ &= \int_0^a d\rho \left[T \int_0^{2\pi} \int_0^{2\pi} \left(n\sqrt{g}\sigma_{\mathbf{s}} \right) d\theta d\phi \right] \\ &= \int_0^a T \overline{\sigma}_{\mathbf{s}} d\rho = \int_\Pi \overline{T}^0 \wedge \overline{\sigma}^1_{\mathbf{s}} \end{aligned} \tag{V.2}$$

Therefore the *3D* thermal model in (V.1) may be transformed into the *1D* port-Hamiltonian model:

$$\begin{pmatrix} f_1 \\ e_2 \end{pmatrix} = \begin{pmatrix} 0 & -\partial_\rho \\ -\partial_\rho & 0 \end{pmatrix} \begin{pmatrix} e_1 \\ f_2 \end{pmatrix} + \begin{pmatrix} \overline{\sigma}_{\mathbf{s}} \\ 0 \end{pmatrix} \tag{V.3}$$

where f_1, f_2, e_1, e_2 are the flows and efforts which are respectively defined by $\overline{nT(D_t s)}$, $\overline{nf_q}$, T and $\overline{F}$ (where the factor n is the average particle density). One of the associated closure relation is the Fourier's law in *3D* and its corresponding *1D* reduction reads:

$$f_q^2 =_{\star\chi} F^1 \Rightarrow f_2 = n\chi \frac{\sqrt{g_\theta g_\phi}}{\sqrt{g_\rho}} e_2 \tag{V.4}$$

where χ is the diffusion coefficient. The ideal gas law is used as the second constitutive equation, relating e_1 and f_1, by considering no particle source injection $\dfrac{dn}{dt} = 0$:

$$s = \ln\left(\frac{T^{3/2}}{n}\right) \Rightarrow \frac{ds}{dt} = \frac{\partial s}{\partial T}\frac{dT}{dt} = \frac{3}{2}\frac{1}{T}\frac{dT}{dt} \tag{V.5}$$

One can notice that our port-Hamiltonian model for heat transport derived from (V.3) is formally equivalent to the usual thermal diffusion equation (c.f [29]) (see remark 9):

$$\sqrt{g}\frac{3}{2}\frac{\partial nT}{\partial t} = \partial_\rho \left(\frac{\sqrt{g_\theta g_\phi}}{\sqrt{g_\rho}} \left(n\chi \partial_\rho T \right) \right) + \overline{\sigma}_{\mathbf{s}} \tag{V.6}$$

Furthermore, the continuity condition at $z = 0$ gives:

$$f_1(0) = e_2(0) = 0 \tag{V.7}$$

The boundary conditions will be chosen as:

$$\begin{cases} f_2(0) \sim \frac{\partial T}{\partial z}|_{z=0} & = 0 \\ e_1^1 = T|_{z=1} & = T_1 \end{cases} \tag{V.8}$$

The smoothness and symmetry of the tokamak torus are also respected thanks to the first boundary condition. The second boundary condition defines a boundary control action T_1. In practice, it's impossible to regulate the plasma temperature at the boundary, it is usually fixed at $T_1 = 0$. This control signal is thus not used in the sequel. Otherwise, a distributed control is represented by the source term $\overline{S}$, including possible ohmic heating or non-inductive heating sources.

Remark 9. The electronic heat transport equation in [29] states:

$$V'\partial_t\left(n_eT_e\right)=\partial_\rho\left(G_1V'n_e\chi_e\partial_\rho T_e\right)+V'P_e \tag{V.9}$$

where the terms V', $G_1=\langle\nabla\rho\rangle^2$, and P_e are equivalent respectively to our parameters $\sqrt{g}$, g_ρ^{-1}, and $n\sigma_{\mathbf{s}}$ which are the magnetic toric coordinate coefficients and the source terms in (V.6).

All possible cases for the reduction of the power pairing from *3D* to *1D* spatial domains have been studied through two previous examples with the transformations in equations (IV.4,V.2, and IV.6). Other interconnection structure equations or element constitutive equations in the system (expressed in terms of relations between *0, 1, 2* and *3-forms*) can be reduced using the same reduction principle summarized in the table III.2. However, for the sake of clarity and completeness, we will now carry out the reduction of MHD coupling in the flowing section.

VI Thermo-Hydro-Dynamic couplings

In this section we will apply first the reduction methodology to the magneto-hydrodynamic couplings, that is to the magnetomotive coupling and the pull-back transformation between the Eulerian and Lagrangian coordinates. Then, we will also explicit some relations actually used in the recent works on tokamaks in order to parametrize the resistivity η, the bootstrap current J_{bs} and the thermal diffusion coefficient χ. These estimated parameters play an important role in the control synthesis in the next chapters.

VI.1 Magnetomotive coupling

The Dirac structure (VI.1) is used to represent the (Lorentz) magnetomotive transducer. The power conservation in this transducer reads:

$$\int_\Omega e_v\wedge f_v-e_J\wedge f_J=0 \tag{VI.1}$$

with $(f_J,e_J)=(J,\,E_L)$ and $(f_v,e_v)=(\sigma_P,\,\star v)$. The reduction of this Dirac structure is therefore straightforward since it is directly expressed as a power pairing. We make use of the correspondence between *3D* and *1D* variables in table III.2 to obtain these power products reduced in the form:

$$\begin{cases}\int_\Omega J\wedge E_L &=\int_\Pi \overline{J}\wedge\overline{E}_L\\ \int_\Omega \sigma_P\wedge\star v &=\int_\Pi \overline{\sigma}_P\wedge\overline{\star v}\end{cases} \tag{VI.2}$$

Therefore the *1D* power conservation for the *1D* transducer reads:

$$\int_\Pi \overline{\sigma}_P\wedge\overline{\star v}-\overline{J}\wedge\overline{E}_L=0 \tag{VI.3}$$

and the Dirac structure (VI.1) keeps the same form with the new reduced variables.

VI.2 Eulerian-Lagrangian transformation

Remind that, to reverse the relation described in Magneto-Hydrodynamic coupling $\mathcal{D}(\mathbf{v})$ (chapter 2, subsection VI.1.2), the transformation from the fix volumic frame Ω into the moving massic one $\mathcal{M}$is defined:

$$\int_{\mathcal{M}=\phi_t(\Omega)} e_2\wedge f_2=\int_\Omega \phi^*\left(e_2\wedge f_2\right)=\int_\Omega \phi^*\left(e_2\right)\wedge f_1 \tag{VI.4}$$

with $\phi^*\left(e_2\right)=\dfrac{1}{\star\mathbf{v}}e_2\circ\phi^{-1}$, and note that $n=\dfrac{1}{\star\mathbf{v}}$ the particle density (considered constant by the quasi-static assumption $\partial_t\mathbf{v}=0$).

The thermal inter-structure in (V.1) is written in *1D* magnetic toric coordinates, when one considers $\partial_t g=0$ as follows:

$$\begin{cases}\sqrt{g}nT\left(D_t\mathbf{s}\right)= & -\partial_\rho\left(n\sqrt{g_\theta g_\phi}f_q\right)+\sqrt{g}n\sigma_{\mathbf{s}}\\ \sqrt{g_\rho}F_\rho= & -\partial_\rho T\end{cases} \tag{VI.5}$$

VI.3 Parameter identification issues

We discuss here the dependence with the electronic temperature and induction field of the resistivity $\eta(T)$, the bootstrap current $J_{bs}(T, \partial_z T)$ and the thermal diffusion coefficient $\chi\left(T, \overline{B}_\theta\right)$ which appear in the resistive and thermal diffusion submodels and play a central role in the coupling of these two submodels.

- The analytic expression for η given in [90] is:

$$\eta(T) = C_\eta(B_\theta)\, T^{-3/2} \tag{VI.6}$$

  where C_η is the specific coefficient varying with the magnetic field B_θ, but the evolution of η by B_θ (whose value is about unity ~ 1) may be neglected in comparison with the strong impact of the plasma temperature T ($\sim 10^5 KeV$).

- The bootstrap current is also determined via experimental data. Its estimated value is given by the simplified expression below [29, 90, 107]:

$$J_{bs} = q\left(\beta_1 T + \beta_2 \partial_z T\right) \tag{VI.7}$$

  where β_1 and β_2 are the constants determined in [107] in the case of a steady state particle density n.

- Thermal diffusion coefficient, whose analytic expression given in [107], is:

$$\chi(\partial_z T, B_\theta) = C_\chi(B_\theta)\, \partial_z T \tag{VI.8}$$

  where C_χ is the specific coefficient of χ which also depends on the magnetic field B_θ.

However, the diffusion processes in plasma systems may be subdivided into different time scales as mentioned in the subsection II.2. As it will be shown in the next chapter, the spectral properties (eigenvalues) of the two diffusion port-Hamiltonian control models still exhibit this time scale separation property.

As a result, the plasma temperature T profile in the thermal diffusion PDE (V.6) is established thousands times faster than the magnetic field profile in the resistive diffusion PDE (IV.8). This "separation" assumption allows to decouple the two-PDE-solvers. The coupling elements $\eta(T_e)$ and $J_{bs}(T_e, \partial_z T_e)$ in the resistive diffusion model may be computed statically from some analytic expressions (see e.g.[107]) once T_e, the electronic temperature, is determined. The coupling via the thermal diffusion coefficient $\chi(T, B_\theta)$ may also be determined by an analytic expression which depends on T and the state of resistive model B_θ, which is considered invariant.

VII Conclusion

A *3D-1D* symplectic geometric reduction methodology has been proposed in this chapter. The resistive and thermal diffusion equations were used as illustrations of the approach because they cover all of the possible cases in a *3D-1D* reduction.

At this stage, the *1D* tokamak control models are established. On one side, they are compatible with the "traditional" widely used resistive diffusion equation and heat transport equation. On the other side, they admit Dirac interconnection structures analogous to the ones in the original *3D* port-Hamiltonian models and preserve the power-pairing for each pairs of port-conjugated variables (hence also preserve energetic properties of the *3D* model such as conservativeness, dissipativeness, passivity, etc.). The control synthesis, based on the obtained *1D* model, will be split into two approaches. For the first approach (indirect approach), a symplectic discretization method will be developed in chapter 4 in order to obtain the finite dimensional PCH systems. Then, the obtained finite dimensional PCH model will be used to derive IDA-PBC control laws in chapter 5. In the second approach (direct approach), we will deduce an infinite dimensional IDA-PBC-like control law in chapter 6 which can be applied directly on the *1D* reduced models developed in this chapter.

A more detailed *1D* model, including separated ionic and electronic thermal transport phenomena as well as nuclear reactions (featuring the burn-control problem) are among the prospects of this work.

Chapter 4

Symplectic discretization

I Introduction

In this chapter, a method to derive geometric discretization schemes from existing solution approximation methods (for PDEs) is presented. It is then applied to the pseudo-spectral spatial discretization of the *1D* plasma control model derived in the previous chapter.

In the spatial reduction of distributed parameter systems, i.e. dynamical systems described by state partial differential equations, pseudo-spectral methods are often chosen because they lead to low order approximated models, with accurate spectral properties (in the linear case, see for instance [32]). These objectives are obviously the key features for the design, supervision and control engineering problems although they are sometimes not sufficient: a finite-dimensional approximated model has also to share some (most) of the other qualitative dynamical properties with the actual infinite-dimensional model. To achieve such a goal could be viewed as performing a geometric reduction scheme in the spatial domain, in a sense very similar to geometric numerical time integration for systems of ordinary differential equations [41].

In the case of port-Hamiltonian models, this geometric spatial reduction may result a structured finite-dimensional port-controlled Hamiltonian (PCH) model (see [65] for an introduction or [101] for an extensive investigation). The discrete schemes is expected to preserve the geometrical *interconnection structure* of the model and with the same balance (conservation) equations and approximated constitutive (closure) equations projected in the chosen approximation spaces. To achive this goal, one may simply require that the power pairing (symplectic) form defining the port-Hamiltonian system is preserved when effort and flow variables are projected into the chosen approximation spaces (we will then speak about a *symplectic* spatial reduction scheme). To guarantee this symplecticity, one has to consider different approximation spaces for the dynamical variables according to their "physical nature", that is the kinds of differential forms used to represent them. It should be noticed that using different approximation spaces according to the nature of differential forms to be approximated is not a new idea. It may be found in the literature for some specific approximation methods such as the (mixed) finite elements method [12, 40, 45, 6] or the (mixed) orthogonal collocation with Lagrange polynomials [70]. In this chapter we define how it may be applied to build systematically a symplectic spatial reduction scheme from any given classical pseudo-spectral method (see for instance [31] for a general presentation of classical pseudo-spectral methods).

Besides this generalization, this work provides a theoretical interpretation of implicit choices made in these earlier works. Except that the chosen approximation spaces (usually different for effort and flow variables) have to be compatible to guarantee the preservation of the symplectic power pairing form (they are then *conjugated* in some sense), they could theoretically be chosen quite freely. Classical choices for the approximation spaces are those spanned by Fourier, wavelets or polynomial bases. Not much has been written however about how to choose practically a couple of approximation spaces among these ones, in the general case. In this work, a symplectic collocation scheme using Lagrange polynomials is first derived and investigated. Although the scheme is indeed symplectic, numerical results show unwanted oscillations in the transient response in the case of non-homogeneous boundary conditions or sharp distributed control actions.

Therefore, we generate a method suggesting that a natural way to do so for the *symplectic reduction of port-Hamiltonian models* could be to choose - as one of the compatible approximation space - the space generated by eigenfunctions of a simplified (canonical) model for which the eigenfunctions may be exactly computed (from the *skew-symmetry* of the canonical interconnection structure). Then the other (conjugated) approximation space may be computed using an exact spatial differentiation condition which ensures the conservation of the power pairing. These two approximation spaces may still be used with the unsimplified model. Doing so then results in a symplectic Galerkin scheme. Besides nice spectral properties, this scheme leads to (by construction) the accurate approximation of eigenfunctions which can solves the numerical oscillation problem encountered with distributed action and arbitrary initial conditions.

In the considered example (the resistive and thermal diffusion equations from chapter 3) eigenfunctions are Bessel functions which could be used easily to build the two desired approximation spaces. It is then shown how this Bessel-Galerkin choice reduces numerical oscillations in the presence of non homogeneous initial conditions or sharp distributed control actions. Simulation results are obtained with the proposed symplectic reduction scheme and besides are validated against experimental data from the tokamak Tore Supra.

The chapter is organized as follows. In the section II we present the proposed methodology to transform a pseudo-spectral method for the approximation of the PDE solution into a symplectic one. The compatibility condition between the approximation bases which guarantees exact spatial differentiation is presented, as well as the finite dimensional version of the Stokes theorem and the resulting symplecticity of the corresponding spatial reduction scheme. The generic explicit Port-Controlled Hamiltonian (PCH) formulation for the finite-dimensional model approximation is proposed, independently from the chosen approximation bases. In section III we investigate a first symplectic method which is developed from the classical collocation scheme, following ideas in [70]. The method is adapted to fit to the case of a toroidal symmetric geometry and to the resulting non-canonical Stokes-Dirac interconnection structure (or bilinear product). Besides the expected nice spectral properties for the eigenvalues, we show that the eigenfunctions are poorly approximated. This results in unwanted numerical oscillations in the magnetic field profile in the case of non homogeneous initial conditions or sharp distributed non inductive current profiles. To solve this problem a Galerkin scheme with Bessel's approximation bases is specifically designed. We show that (as expected) the symplecticity is preserved (still resulting in accurate approximate eigenvalues) while the unwanted numerical oscillations are canceled. We show briefly, in section IV, that the obtained discrete model may be validated against experimental data with scenarios where non uniform resistivity and distributed non inductive current occur. In this case, Bessel's functions are no more the eigenfunctions for the considered problems but still accurate and satisfying results are obtained. In section V, the same methodology is then applied to the thermal diffusion equation. At the end, the whole discrete scheme of the thermal domain is obtained. Our discrete model is ready for the next step, control synthesis in chapter 5

II Discretization methodology

In order to get a finite-dimensional approximation for the original distributed parameter system written in port-Hamiltonian form, we will define different specific approximation spaces for the flow and effort variables. In the *1D* case, these approximation spaces will be respectively spaces of differential forms of order 0 and 1.

This allows to guarantee that the reduced (finite dimensional approximation) variables also satisfy the Stokes-Dirac interconnection relations by performing exact spatial differentiation in the conjugated approximation spaces.

Therefore, the original (spectral, Galerkin, collocation or any other pseudo-spectral) approximation scheme will be transformed into a symplectic one in the sense that the bilinear power pairing form used to define the Stokes-Dirac structure is preserved. Symplecticity with respect to this form ensures that balance equations (and thus conservativeness, dissipativeness and qualitative properties of the spectrum, in the linear case) are satisfied by the finite dimensional approximation even in the case of systems with boundary energy flow[1] which is not the case with classical symplecticity

[1] This case is fundamental for control engineering systems where interactions with the environment through measurements and actuation are necessary

(used for instance for closed Hamiltonian systems).

Further in this section the methodology will be applied on the resistive diffusion example (chapter 3, equation (IV.8)) to illustrate how the closure relations may be projected into the approximation bases once they have been chosen (in order to preserve to power bilinear form). Although presented for the tokamak resistive diffusion model, results in this the section are generic and the symplectic discretization methodology may be applied to many examples which have been written in the port-Hamiltonian form and for many approximation bases.

II.1 Approximation bases for flows and efforts

The flows (f_{el}, f_{mg}, f_d) and efforts (e_{el}, e_{mg}, e_d) are approximated in the *1D* Π domain using a classical expansion:

$$\begin{array}{rcl} f(t,z) & = & \sum_{k=1}^{N-1} \left(\mathbf{f}(t)\right)_k w_k^f(z) \\ e(t,z) & = & \sum_{i=1}^{N} \left(\mathbf{e}(t)\right)_i w_i^e(z) \end{array} \tag{II.1}$$

in which $\mathbf{f}(t) \in \mathbb{R}^{N-1}$, $\mathbf{e}(t) \in \mathbb{R}^N$ are respectively the flow and the effort time dependent coefficients while $w_k^f(z)$ and $w_i^e(z)$ are the approximation base generating functions satisfying the exact differentiation condition:

$$\begin{cases} \overline{\mathcal{E}} & = span\left(w_i^e(z)\right) \\ \overline{\mathcal{F}} & = span\left(w_k^f(z)\right) \\ \mathrm{d}\left(\overline{\mathcal{E}}\right) & = \overline{\mathcal{F}} \end{cases} \tag{II.2}$$

where d denotes the spatial exterior derivative for the corresponding differential form (here, in the *1D* case, it is simply the usual derivative with respect to the reduced spatial coordinate z and applies to effort variables which are 0-forms or functions). From (II.1) and (II.2), we may project the relation $f(t,z) = \mathrm{d}(e(t,z))$ in the finite dimensional approximation bases as:

$$\sum_{k=1}^{N-1} w_k^f(z)\mathbf{f}_k(t) = \sum_{i=1}^{N} \partial_z\left(w_i^e(z)\right)\mathbf{e}_i(t) \tag{II.3}$$

Since the approximation bases have been chosen to satisfy the exact differentiation condition, the quantities $\partial_z w_i^e(z)$ may be expanded in the flow space. This results in a finite-dimensional derivative operator represented by the differentiation matrix $D \in \mathbb{R}^{(N-1)\times N}$ such that:

$$\mathbf{f}(t) = D\mathbf{e}(t) \tag{II.4}$$

II.2 Bilinear power product and finite dimensional Stokes' theorem

On the *1D* domain Π with boundary $\partial\Pi$, canonical Stokes-Dirac structure may be defined as self-orthogonal subspace $\mathscr{D}$ of the bond space $\mathcal{B} = \mathcal{F} \times \mathcal{E}$ with respect to the inner product defined by symmetrization of the non degenerated bilinear form (or power pairing, see proposition III.4 in chapter 2):

$$\begin{array}{rccc} \langle .|. \rangle : & \mathcal{F} \times \mathcal{E} & \longrightarrow & \mathbb{R} \\ & (f,e) & \longmapsto & \langle e|f \rangle \end{array} \tag{II.5}$$

with

$$\langle e|f \rangle = \left\langle \left(e_p, e_q, e^\partial\right) \mid \left(f_p, f_q, f^\partial\right) \right\rangle := \int_\Pi \left[e_p \wedge f_p + e_q \wedge f_q\right] - \int_{\partial\Pi} e^\partial \wedge f^\partial \tag{II.6}$$

This inner product is then the *symmetric positive definite bilinear form*:

$$\begin{array}{rccc} \langle\langle .,. \rangle\rangle : & \mathcal{B} \times \mathcal{B} & \longrightarrow & \mathbb{R} \\ & ((f_1,e_1),(f_2,e_2)) & \longmapsto & \langle\langle (f_1,e_1),(f_2,e_2) \rangle\rangle := \langle e_1|f_2 \rangle + \langle e_2|f_1 \rangle \end{array} \tag{II.7}$$

It has been noted previously that every pairs (f,e) belonging to the Stokes-Dirac structure (thus satisfying the balance equations) also satisfy $\langle e|f \rangle = 0$. As a consequence, balance equations (and conservations laws) will be satisfied also in the finite dimensional approximation spaces if the bilinear form (II.6) is preserved by the discretization. If this happens, we will call the reduction scheme

symplectic with respect to the power pairing by analogy with symplecticity of time integrators for Hamiltonian (finite dimensional) systems. The relation $\langle e|f\rangle = 0$ (and the resulting symplecticity) will be satisfied for pairs of approximated flow and effort variables defined in the previous section provided that the boundary variables (e^∂, f^∂) are correctly defined. We will obtain this result for the considered schemes because they perform exact spatial derivation in the chosen compatible conjugated approximation spaces.

In our example of Tokamak electromagnetic system, we can identify:

$$(e,f) = \left(\left(e_p, e_q, e^\partial\right), \left(f_p, f_q, f^\partial\right)\right) = \left(\left(e_{el}, e_{mg}, e^\partial_{el}\right), \left(f_{el}, f_{mg}, e^\partial_{mg}\right)\right) \tag{II.8}$$

Note that each of the efforts and flows have both poloidal θ and toroidal ϕ components.

To perform an exact integration of the power pairing integral (and thus preservation of the inner product in the Bond space) we define the (integral) matrix $M \in \mathbb{R}^{N\times(N-1)}$ such as:

$$M_{ik} = \int_\Pi w_i^e(z) w_k^f(z) \mathrm{d}z \tag{II.9}$$

and the (trace) matrices $T_k \in \mathbb{R}^{N\times N}$ as:

$$(T_k)_{ij} = w_i^e\left(z=k\right) w_j^e\left(z=k\right) \text{ where } k \in \{0,1\} \tag{II.10}$$

We may replace the effort and flow variables by their approximation (II.1) in the chosen conjugated approximation spaces and force the reduced variables to satisfy the Stokes-Dirac equations (using exact spatial differentiation in the approximation spaces). We may still apply the Stokes theorem (on the power pairing integral) to prove that the bilinear power product computed with the reduced variables coordinates is again zero. Therefore, one gets for every pairs of reduced variables $(e_1, f_1), (e_2, f_2)$ in the Stokes-Dirac structure:

$$\begin{aligned} &\mathbf{e}_p^{1T} \begin{pmatrix} 0 & MD + D^T M^T - T_1 + T_0 \\ -D^T M^T - MD + T_1 - T_0 & 0 \end{pmatrix} \mathbf{e}_q^2 + \\ &-\mathbf{e}_q^{1T} \begin{pmatrix} 0 & MD + D^T M^T - T_1 + T_0 \\ -D^T M^T - MD + T_1 - T_0 & 0 \end{pmatrix} \mathbf{e}_p^2 = 0 \end{aligned} \tag{II.11}$$

where $\mathbf{e}_p = (\mathbf{e}_{p\theta}, \mathbf{e}_{p\phi})$ and $\mathbf{e}_q = (\mathbf{e}_{q\theta}, \mathbf{e}_{q\phi})$ are any real vector values in the toric coordinates of the effort variables in the finite dimensional approximation spaces. Therefore we can deduce a "finite dimensional" version of the Stokes theorem in the selected conjugated approximation spaces for reduced efforts and flows:

$$MD + D^T M^T - T_1 + T_0 = 0 \tag{II.12}$$

We will call hereafter this result the discrete Stokes theorem. It simply states in coordinates the power conservation in the interconnection structure resulting from the projection of the Stokes-Dirac structure equations in the approximation spaces selected for the reduced efforts and flows.

Remark 10. Note that for homogeneous boundary conditions, the efforts are zero at the boundary and therefore the trace matrices may be selected as $T_1 = T_0 = 0$. In this case, there's no energy exchange through the boundary and the discrete Stokes theorem reduces to $MD + D^T M^T = 0$. In this case the matrix MD is skew-symmetric and defines a Poisson tensor. The condition (II.12) may thus be viewed as the extension of a skew-symmetry property characterizing finite dimensional reduced Dirac structures.

Remark 11. The proposed "mixed" pseudo-spectral scheme may be viewed as a classical scheme if we consider that only one approximation basis is chosen: the approximation basis used for the effort variables. In this case, the port-Hamiltonian formulation for the resistive diffusion equation (as an example) and the definition of an auxiliary approximation basis for the flows may be viewed as a "trick" to obtain a symplectic Galerkin scheme for the second order diffusion equation. On one hand, the discrete Stokes theorem (II.12) ensures the symplecticity with respect to the "natural" power pairing of the considered system. On the other hand, the exact integration formula and the resulting discrete Stokes theorem also ensure that the residual is zero in the approximation space (spanned by "effort" base functions). Therefore, the proposed mixed pseudo-spectral methods may be also viewed as a family of *symplectic Galerkin-type methods* realizing the projection of the actual dynamics in the approximation space spanned by the effort basis.

II.3 Canonical discrete Dirac structure for the resistive diffusion equation

In the case of the resistive diffusion[2] model (IV.8) in chapter 3, it is possible to study only the poloidal subsystem describing the dynamics of the variables

$$\left(\left(e_p, e_q, e^{\partial}\right), \left(f_p, f_q, f^{\partial}\right)\right) = \left(\left(e_{el\phi}, e_{mg\theta}, e^{\partial}_{el\phi}\right), \left(f_{el\phi}, f_{mg\theta}, e^{\partial}_{mg\theta}\right)\right)$$

Indeed the poloidal and toroidal subsystems are totally decoupled and the finite dimensional approximation of the poloidal subsystem may be written independently from the toroidal variables in the form:

$$\begin{cases} \begin{pmatrix} \mathbf{f}_{el\phi} \\ \mathbf{f}_{mg\theta} \end{pmatrix} = \underbrace{\begin{pmatrix} 0 & -D \\ -D & 0 \end{pmatrix}}_{\textbf{Interconnection matrix}} \begin{pmatrix} \mathbf{e}_{el\phi} \\ \mathbf{e}_{mg\theta} \end{pmatrix} + \begin{pmatrix} 1 \\ 0 \end{pmatrix} \mathbf{f}_{d\phi} \\ \underbrace{\begin{pmatrix} f_{1\phi} \\ f_{0\phi} \\ e_{1\theta} \\ e_{0\theta} \end{pmatrix}}_{\textbf{Boundary variables}} = \begin{pmatrix} w^e(1) & 0 \\ w^e(0) & 0 \\ 0 & w^e(1) \\ 0 & w^e(0) \end{pmatrix} \begin{pmatrix} \mathbf{e}_{el\phi} \\ \mathbf{e}_{mg\theta} \end{pmatrix} \end{cases} \tag{II.13}$$

Therefore, for the sake of simplicity, we will consider throughout the rest of this work only the poloidal subsystem (II.13). Since the flow variables are obtained from the effort variables through a spatial derivation, the two approximation spaces do not have the same dimension and system (II.13) is not in minimal form. This minimal form is of prime importance because it is required to provide a "causality free" reduced Dirac structure and finite dimensional model, that is a model which may be connected to any other compatible port-controlled Hamiltonian system where any of the flow or effort variables may be freely chosen as an input. To obtain such a minimal form for the system (II.13) - corresponding to an invertible representation of the reduced Dirac structure - it will be necessary figure out a projection which cancels the kernel of the exterior derivative (in the space of reduced effort coordinates) but without affecting the power pairing value and the resulting symplecticity of the reduction scheme. Such a projector is built hereafter based on the exact integration of the power product, which can pull the system back to a square invertible one.

Using the $\{w^e_i, w^f_k\}$ bases integration matrix M defined in (II.9), the power balance equation for the poloidal electromagnetic energy may be exactly evaluated (in the chosen approximation spaces) with the expression:

$$\begin{aligned} \frac{\partial \mathbb{H}_{pol}}{\partial t} &= \int_{\Pi} e_{el\phi} \wedge f_{el\phi} + e_{mg\theta} \wedge f_{mg\theta} \\ &= \mathbf{e}^T_{el\phi} M \mathbf{f}_{el\phi} + \mathbf{e}^T_{mg\theta} M \mathbf{f}_{mg\theta} \end{aligned} \tag{II.14}$$

where $\mathbb{H}_{pol}$ stands for the total "poloidal" Hamiltonian, that is the part of the electromagnetic energy stored in the poloidal subsystem. As mentioned above, the bilinear power product in (II.14) is degenerated and admits the kernel $ker\left(M^T\right)$. Therefore a projection:

$$\tilde{\mathbf{e}} = M^T \mathbf{e} \tag{II.15}$$

allows to obtain an invertible system in the new Bond space of reduced effort and flow variables $\mathbb{R}^{N-1} \times \mathbb{R}^{N-1} \ni (\tilde{\mathbf{e}}, \mathbf{f})$. The degenerated bilinear product (II.14) becomes non degenerated in this new Bond space and the power balance becomes:

$$\frac{\partial \mathbb{H}}{\partial t} = \int_{\Pi} e \wedge f = \mathbf{e}^T M \mathbf{f} = \tilde{\mathbf{e}}^T \mathbf{f} \tag{II.16}$$

The symmetrization of this power pairing results in a bilinear form in the Bond space which is symmetric positive definite, that is defines an inner product. It may be observed that the reduced

[2] Remind that the resistive diffusion equation is obtained by neglecting the displacement current $f_p = f_{el\phi} = 0$. The parabolic resistive diffusion model results from the magnetic balance equation and the closure (diffusion) constitutive equation relating the diffusive flow $-\mathrm{d}\left(e_{mg\theta}\right)$ and the magnetic field intensity $e_{mg\theta}$.

(invertible) Dirac structure corresponding to this inner product may be written using its image representation, in the form

$$\begin{pmatrix} \mathbf{f}_{el\phi} \\ \mathbf{f}_{mg\theta} \\ f^1_{\partial\phi} \\ f^0_{\partial\phi} \end{pmatrix} = \underbrace{\begin{pmatrix} 0 & -D \\ -D & 0 \\ w^e(1) & 0 \\ w^e(0) & 0 \end{pmatrix}}_{E^T} \begin{pmatrix} \mathbf{e}^q \\ \mathbf{e}^p \end{pmatrix} \quad \text{and} \quad \begin{pmatrix} \tilde{\mathbf{e}}_{\mathbf{el}\phi} \\ \tilde{\mathbf{e}}_{\mathbf{mg}\theta} \\ e^1_{\partial\theta} \\ e^0_{\partial\theta} \end{pmatrix} = \underbrace{\begin{pmatrix} M^T & 0 \\ 0 & M^T \\ 0 & w^e(1) \\ 0 & w^e(0) \end{pmatrix}}_{F^T} \begin{pmatrix} \mathbf{e}_{\mathbf{el}\phi} \\ \mathbf{e}_{\mathbf{mg}\theta} \end{pmatrix} \tag{II.17}$$

The discrete Stokes theorem (II.12) allows to prove that $[E : F]$ is full rank and that $EF^T + FE^T = 0$. These are "classical" necessary and sufficient conditions for (II.17) defining a well-posed Dirac structure (see e.g. [23]). The relations (II.17) defining the Dirac structure may also be written in explicit ("input-output") form:

$$\begin{bmatrix} \begin{pmatrix} \mathbf{f}_{el\phi} \\ e^1_{\partial\theta} \end{pmatrix} \\ \begin{pmatrix} \mathbf{f}_{mg\theta} \\ -f^0_{\partial\phi} \end{pmatrix} \end{bmatrix} = \underbrace{\begin{bmatrix} 0 & \begin{pmatrix} -D \\ w^e(1) \end{pmatrix} \begin{pmatrix} M^T \\ w^e(0) \end{pmatrix}^{-1} \\ \begin{pmatrix} -D \\ -w^e(0) \end{pmatrix} \begin{pmatrix} M^T \\ w^e(1) \end{pmatrix}^{-1} & 0 \end{bmatrix}}_{\mathcal{J}} \begin{bmatrix} \begin{pmatrix} \tilde{\mathbf{e}}_{\mathbf{el}\phi} \\ f^1_{\partial\phi} \end{pmatrix} \\ \begin{pmatrix} \tilde{\mathbf{e}}_{mg\theta} \\ e^0_{\partial\theta} \end{pmatrix} \end{bmatrix} \tag{II.18}$$

where $\mathcal{J}$ is a skew matrix as $\mathcal{J} + \mathcal{J}^T = 0$ thanks to (II.12).

II.4 Storage and dissipation constitutive relations

Relations between effort and flow variables coming from the balance equations and realized with the Dirac interconnection structure have to be completed with closure relations. These come from the constitutive equations considered in each specific example. Usually they are storage and dissipation phenomenological laws. They may be projected in the finite-dimensional approximation spaces which have been previously chosen to guarantee symplecticity of the spatial reduction scheme. This means that the energy stored and dissipated in the actual dynamics will evolve in the reduced dynamics although the values of these energies will only be approximated ones. Energy storage and dissipation reductions are illustrated hereafter on the plasma model example.

II.4.1 Energy storage element

From (II.14), the poloidal magnetic power may be written:

$$\frac{d\mathbb{H}\left(\overline{B}_\theta\right)}{dt} = \int_\Pi e_{mg\theta} \wedge f_{mg\theta} = \tilde{\mathbf{e}}^T_{mg\theta} \mathbf{f}_{mg\theta} \tag{II.19}$$

On the other hand, the quadratic form for the magnetic energy results in a linear constitutive equation with the magnetic effort variable defined as: $e_{mg\theta} = \frac{C_2}{\mu} \overline{B}_\theta$. Hence the poloidal magnetic power may be projected in the chosen flow basis according to:

$$\begin{aligned} \frac{d\mathbb{H}\left(\overline{B}_\theta\right)}{dt} &= \int_\Pi e_{mg\theta} \wedge f_{mg\theta} = \int_\Pi \frac{C_2}{\mu} B_\theta \wedge \frac{\partial \overline{B}_\theta}{\partial t} \\ &\simeq \mathbf{b}^T G \mathbf{f}_{mg\theta} \end{aligned} \tag{II.20}$$

with

$$G_{ij} = \int_\Pi \frac{C_2}{\mu} w^f_i(z) w^f_j(z) \mathrm{d}z,\ G = G^T > 0 \tag{II.21}$$

and $B_\theta(t, z) = \sum_{k=1}^{N-1} (\mathbf{b}(t))_k w^f_k(z)$. This results in the finite dimensional magnetic constitutive equation:

$$\tilde{\mathbf{e}}_{mg\theta} = G\mathbf{b} \tag{II.22}$$

II.4.2 Energy dissipation element

The dissipated poloidal power is defined as:

$$\mathbb{P}_{d\phi} = \int_\Pi e_{d\phi} \wedge f_{d\phi} = \tilde{\mathbf{e}}_{el\phi}^T \mathbf{f}_{d\phi} \tag{II.23}$$

using for instance Ohm's law for the electrical diffusion

$$e_{d\phi} = \frac{\eta}{C_3} J_\Omega = \frac{\eta}{C_3} \left(f_{d\phi} - J_{ni} \right) \tag{II.24}$$

this poloidal dissipation may be approximated in the same flow basis:

$$\begin{aligned} \mathbb{P}_{d\phi} &= \int_\Pi e_{d\phi} \wedge f_{d\phi} = \int_\Pi \tfrac{\eta}{C_3} \left(f_{d\phi} - J_{ni} \right) \wedge f_{d\phi} \\ &\simeq \left(\mathbf{f}_{d\phi} - \mathbf{J_{ni}} \right)^T R \mathbf{f}_{d\phi} \end{aligned} \tag{II.25}$$

with the dissipation matrix R is defined as

$$R_{ij} = \int_\Pi \frac{\eta}{C_3} w_i^f(z) w_j^f(z) \mathrm{d}z, \; R = R^T > 0 \tag{II.26}$$

Hence the dissipative constitutive equation may be written:

$$\tilde{\mathbf{e}}_{el\phi} = R \left(\mathbf{f}_{d\phi} - \mathbf{J_{ni}} \right) \tag{II.27}$$

II.5 Boundary conditions

When dealing with boundary control systems, two kinds of boundary conditions have to be distinguished: homogeneous and time varying boundary conditions. Most often homogeneous boundary conditions are used for symmetry considerations or permanent physical interconnections (contact condition, isolated systems, etc.). On the contrary, time varying boundary conditions are used to represent external control actions of the system. These boundary control actions correspond to the boundary energy flows and are realized by forcing time varying efforts and/or flows values at the system boundary.

In our approach, the homogeneous boundary conditions (no power exchange with the environment) will be integrated in the approximation bases choice: all homogeneous boundary conditions on the effort or flow values (and their spatial derivatives) will be satisfied by all functions in the corresponding approximation bases. This common choice very often allows to get better results in terms of accuracy, minimizing of the boundary effects introduced by the boundary conditions. Besides, it leads to some symplectic reduction schemes for homogeneous problems as it may be seen from the results in the next section or in [70].

Otherwise, non homogeneous boundary conditions - precisely since they describe "action-reaction" like interactions - have to be considered as relations between additional boundary port variables in the finite dimensional state space model. Otherwise, once substituted in the state space model, these non homogeneous boundary conditions break the model symmetries and lead to a lack of symplecticity in the considered spatial reduction scheme [70]. In our approach these boundary conditions are time varying values either for the effort or flow boundary values. The proposed family of schemes remain symplectic because symplecticity is defined with respect to a bilinear form which "embed" the boundary variables (this is precisely the aim of the extension from the Poisson to the Dirac structure).

These ideas are illustrated hereafter on the plasma example, both for homogeneous boundary conditions and for boundary control actions.

II.5.1 Homogeneous boundary conditions

We consider that there is no flow source inside the domain at $z = 0$ (the central magnetic axis inside the toroidal plasma chamber). Therefore the following symmetry boundary conditions apply

$$f_{d\phi}(0) = f_{mg\theta}(0) = 0 \tag{II.28}$$

since $f_{d\phi} \approx azJ_\phi$ and $f_{mg\theta} = \partial_t B_\theta = -\partial_t \dfrac{\partial \psi}{\partial z}$ with $\dfrac{\partial \psi}{\partial z}|_{z=0} = 0$. On the other hand, the constitutive relation $e_{mg\theta} = \dfrac{C_2}{\mu} B_\theta$, $C_2(0) = 0$ leads to:

$$e_{0\theta} = e_{mg\theta}(0) = 0 \tag{II.29}$$

II.5.2 Non-homogeneous boundary conditions

The loop voltage will be considered as the controlled boundary input. Therefore we will consider non homogeneous boundary conditions at the boundary $z = 1$:

$$f_{1\phi} = e_{el\phi}(1) \quad = -\partial_t \psi|_1 = \quad -V_{loop}(t) \tag{II.30}$$

Taking into account the quasi-static assumption $f_{el\phi} = 0$, the interconnection equations (II.18), together with the energy storage constitutive equation (II.22), the energy dissipation constitutive equation (II.27) and the boundary conditions here above, we may the complete reduced state space in the following PCH form:

$$\begin{pmatrix} \begin{pmatrix} -\mathbf{f}_{d\phi} \\ e_{1\theta} \end{pmatrix} \\ \begin{pmatrix} -\dot{\mathbf{b}} \\ -f_{0\phi} \end{pmatrix} \end{pmatrix} = \mathcal{J} \begin{pmatrix} \begin{pmatrix} R(\mathbf{f}_{d\phi} - \mathbf{J}_{\mathbf{ni}\phi}) \\ -V_{loop} \end{pmatrix} \\ \begin{pmatrix} G\mathbf{b} \\ 0 \end{pmatrix} \end{pmatrix} \tag{II.31}$$

where the derivative operator is represented by the skew symmetric interconnection matrix:

$$\mathcal{J} := \begin{pmatrix} 0 & \begin{pmatrix} -D \\ w^e(1) \end{pmatrix} \begin{pmatrix} M^T \\ w^e(0) \end{pmatrix}^{-1} \\ \begin{pmatrix} -D \\ -w^e(0) \end{pmatrix} \begin{pmatrix} M^T \\ w^e(1) \end{pmatrix}^{-1} & 0 \end{pmatrix} \tag{II.32}$$

The finite-dimensional approximated PCH model (II.31) will be analyzed in the sequel for different bases function choices. Each of these chosen approximation bases lead to a symplectic scheme (i.e. preserving the power pairing form or the Dirac interconnection structure) although they have very different properties, for instance related with the approximation accuracy of the spectrum and eigenfunctions.

III Choice of effort and flow approximation spaces

In this section we investigate the selection of conjugated effort-flow approximation bases. This problem of choosing the approximation space is common to any pseudo-spectral method (whatever it is symplectic or not). Its solution is usually dependent both of the the properties of the actual system and the expected properties for the reduced one. We will first employ a choice of collocation bases spanned by Lagrange interpolation polynomials. This choice corresponds to a definition of the state space variables which are simply the values of the infinite dimensional state space variables at the collocation points. The corresponding symplectic collocation scheme which is derived with the method proposed in section II will then produce a finite dimensional PCH model easy to manage for subsequent control problems since it is low order, its state space variables have an immediate intuitive interpretation and its spectral properties should be close to the actual ones (in fact, this is a common feature for most of the pseudo-spectral schemes). However, as it will be shown hereafter, this choice does not allow - in the considered plasma control problem - to handle the distributed control action (non-inductive current deposit). This will be explained by a poor approximation of the eigenfunctions of the considered operators although the approximation of its eigenvalues is indeed quite accurate (provided that the homogeneous boundary conditions are integrated in the Lagrange's polynomials basis functions choice).

Therefore we will choose another approximation basis for the efforts and flows. It is suggested by the observation that, with an uniform resistivity η and homogeneous boundary conditions, the eigenvalues problem for the plasma resistive diffusion equation gives rise to a Bessel equation. Hence eigenfunctions for this problem are Bessel functions and the eigenvalues can be explicitly evaluated from the zeros of Bessel functions (details of these computations are in appendix E). We will thus select a basis as Bessel functions and its power-conjugated basis (compatible with the

exact derivation condition) to propose a new spectral symplectic reduction scheme. This choice will of course result in an accurate approximation of the homogeneous problem eigenfunctions. It will also improve the approximation accuracy for the solution in this case of non uniform resistivity and distributed control actions where Bessel's functions are no more eigenfunctions of the problem, as it will be shown in section III.3.

III.1 Symplectic orthogonal collocation

In this section we generate the flow approximation basis with Lagrange polynomials and then a corresponding symplectic collocation scheme with the proposed method. We analyze the accuracy of the resulting spectrum approximation and also observe numerical oscillations in the non homogeneous case. This problem will be solved in the next sections by considering other conjugated approximation bases.

III.1.1 Polynomial approximation's functions choice

Let's $\xi_j\,(j=1..N-1)$ be the $N-1$ chosen collocation points for the flows and $\zeta_i\ (i=1..N)$ the N collocation points for the efforts. In the sequel to improve the order of the interpolation formulas and minimize the oscillations of the interpolation errors, zeros of respectively $(N-1)^{th}$ and N^{th} orders Chebyshev polynomials will be carried out. Both notations $\mathbf{f}\in\mathbb{R}^{N-1}$ and $\mathbf{e}\in\mathbb{R}^{N}$ will be used to denote respectively the coordinates' vectors of the approximated flows and efforts in the corresponding approximation spaces. In particular, with the chosen orthogonal collocation method, the approximation basis for the flows is made with Lagrange interpolation polynomials at the collocation points $\xi_j\,(j=1..N-1)$ which satisfy the interpolation conditions

$$w_k^f(\xi_j)=\begin{cases}1 & \text{if } j=k\\ 0 & \text{else}\end{cases} \tag{III.1}$$

Therefore the exact spatial derivation equation (II.4) (compatibility condition between the flow and effort conjugated approximation bases) becomes:

$$\mathbf{f}\,(t)=\overline{D}\,(z)\,\mathbf{e}\,(t) \tag{III.2}$$

where $\overline{D}$ is a $(N-1)\times N$ derivation matrix with elements $\overline{D}_{ji}:=\partial_z\left(w_i^e\right)|_{\xi_j}$.

Embedding the homogeneous boundary conditions in the approximation bases definitions

Most often, it is necessary to include boundary conditions in the approximation bases definitions to get satisfying results for the spectrum approximation. In the plasma resistive diffusion example, the boundary condition at $x=0$ states that there is no flows source term at the center of the tokamak. The efforts at $x=0$ however may be non zero (but in fact usually is). Therefore we will consider the following additional conditions on the flow and effort bases:

$$\begin{aligned} w_k^f(0)&=0\\ \frac{\partial w_i^e(z)}{\partial z}|_{z=0}&=0\end{aligned} \tag{III.3}$$

These conditions may be fulfilled with the choice of effort and flow approximations bases presented hereafter. Let l_i^{N-1} denotes the $(n-1)^{th}$ order Lagrange interpolation polynomial defined with:

$$l_i^{N-1}(z):=\prod_{j=1,\,j\neq i}^{N}\frac{z-\zeta_j}{\zeta_i-\zeta_j} \tag{III.4}$$

Conditions (III.3) on the effort values at the boundary $z=0$ are satisfied by the functions

$$w_i^e(z)=1-z^2\zeta_i^2 l_i^{N-1} \tag{III.5}$$

which may be used to generate the effort approximation space. The components of derivation matrix in the exact derivation formula (III.2) are then:

$$D_{ji} = \frac{\partial}{\partial z}\left(w_i^e\right)|_{\xi_j} = \left(-2z\zeta_i^2 l_i^{N-1} - z^2\zeta_i^2 \frac{\partial}{\partial z}\left(l_i^{N-1}\right)\right)|_{\xi_j} \tag{III.6}$$

Using this derivation matrix, a basis function for the flows which satisfies the exact derivation condition in (II.2) is:

$$w^f(z) = \left(\frac{\partial}{\partial z} w^e(z)\right) D^+ \tag{III.7}$$

where D^+ is the pseudo-inverse of D.

Projections of the constitutive equations

As $w^e(z)$ and $w^f(z)$ are both polynomial bases, the integral matrix M:

$$M_{ik} = \int_0^1 w_i^e(z) w_k^f(z) \mathrm{d}z \tag{III.8}$$

may be easily exactly evaluated. Therefore, the projections of the storage and dissipation relations which result in the matrices G and R whose elements are:

$$\begin{aligned} G_{ij} &= \int_0^1 \frac{C_2}{\mu} w_i^f(z) w_j^f(z) \mathrm{d}z \\ R_{ij} &= \int_0^1 \frac{\eta}{C_3} w_i^f(z) w_j^f(z) \mathrm{d}z \end{aligned} \tag{III.9}$$

and may be as well explicitly computed. The complete input-output model (II.31) has been derived for the case with uniform resistivity η and homogeneous boundary conditions (both at $z = 0$ and $z = 1$). Then, eigenvalues of this model have been computed and compared with the theoretical ones (eigenvalues of the resistive diffusion operator with homogeneous boundary conditions, see appendix E) and with the ones obtained by a finite difference formula (see appendix G). Results are shown respectively on tables III.2 and III.1 hereafter. The symplectic orthogonal collocation method is, from this spectrum approximation point of view, clearly more accurate, as it was expected. Besides, in the case of non homogeneous boundary conditions (in our case at $z = 1$) and with the distributed term source, the finite difference approximation scheme introduces imaginary (oscillation) parts in the approximated eigenvalues and even numerically unstable modes. This is not the case with the symplectic orthogonal collocation, precisely because it is symplectic with respect to the Dirac structure and the corresponding inner product derived from the natural power product which embeds the boundary values of efforts and flows.

Theoretical	Numerical eigenvalues		
eigenvalues	N=5	N=8	N=10
-2.301056852	-3,965414997	-3,885480574	-3,860185392
-12.12413006	-19,18940482	-18,95845463	-19,00658467
-29.79659326	-40,14692865	-38,34709614	-39,98776146
-55.32237139	-53,82013956	-58,53622826	-61,19522543
-88.70194524		-85,81642985	-82,15362798
-129.9354296		-120,7439326	-112,9192769
-179.0228628		-127,9196240	-155,4380422
-235.9642604			-180,4468519
-300.7596298			-215,9294060

Table III.1: Eigenvalues using a finite difference scheme and Chebyshev discretization points and a resistivity $\eta = 5.10^{-7}$

Theoretical eigenvalues	Numerical eigenvalues N=5	N=8	N=10
-2.301056852	-2.350753323	-2.310110425	-2.304769649
-12.12413006	-12.63581394	-12.22630390	-12.23545753
-29.79659326	-33.62142541	-30.15754539	-30.39891094
-55.32237139	-227.3150319	-56.03293217	-56.51610868
-88.70194524		-92.85175835	-88.81543981
-129.9354296		-159.9060543	-127.9699944
-179.0228628		-1170.918746	-176.7315844
-235.9642604			-317.0613604
-300.7596298			-2547.963503

Table III.2: Eigenvalues using the symplectic orthogonal collocation scheme with Lagrangian polynomials as bases functions, Chebyshev collocation points and a uniform resistivity $\eta = 5.10^{-7}$

III.1.2 Numerical oscillations in the magnetic field profile

We are now considering a controlled scenario where stationary values are chosen for the loop voltage V_{loop} control action and the distributed source term J_{ni}. The obtained radial profiles of the magnetic field component B_θ are illustrated on figure III.1 (on the left, the simulation case is without distributed source term $J_{ni} = 0$ and on the right with $J_{ni} \neq 0$ the distributed source term whose profile takes the Gaussian form as in [107]) and compared with the profiles supplied by the finite different method.

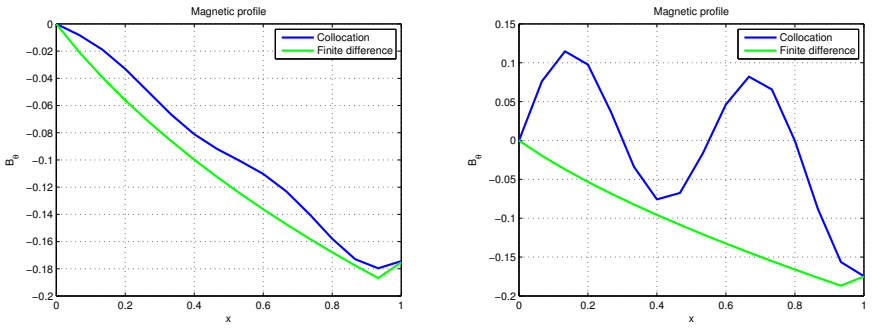

Figure III.1: B_θ profile with constant uniform resistivity $\eta = 5.10^{-7}$ controlled using a nonzero boundary condition $V_{loop} \neq 0$; without distributed source term $j_{ni} = 0$ (left) and with distributed source term $j_{ni} \neq 0$ (right)

It may be observed that the magnetic profile B_θ presents an oscillation profile (figure III.1, right) in the case of a non zero distributed control action, when using the symplectic collocation scheme. In fact, this is also the case - for the first time steps - with some certain initial profiles are chosen for the state variables. These numerical oscillations are not found in higher order FD schemes and are of course undesired numerical oscillations.

As it is shown in appendix F, these numerical oscillations come from a poor approximation of the eigenfunctions in the chosen Lagrange's polynomials basis. These eigenfunction approximations themselves exhibit large oscillations (see figure II.1, appendix F). These large oscillations arise mainly from the boundary conditions imposed to the polynomial approximation bases. They disappear when classical Lagrange's polynomials are used rather than those in (III.5) which satisfy the problem boundary conditions. Obviously, in this case, part of the boundary conditions are not satisfied by the approximation (in fact they are not satisfied by the reference finite difference solution as well).

III.2 Symplectic spectral method

To solve the eigenfunction approximation problem, instead of seeking better - but unknown - basis functions, we will use the theoretical eigenfunctions of the resistive diffusion operator with

homogeneous boundary conditions, computed for the uniform case (i.e. with a spatially uniform resistivity η). This will result in a symplectic spectral scheme since the approximation will be spanned in the basis of Bessel functions, which are then exact eigenfunctions of the (simplified) problem. In this section, we show how to derive this symplectic spectral scheme and how it solves the numerical oscillations problem.

Choice of the conjugated bases of eigenfunctions

Computing the eigenfunctions of the operator appearing in the right hand side of the resistive diffusion equation (IV.14), chapter 3 - in the constant and uniform resistivity case - is equivalent to solve a Bessel equation (see appendix E for details). Eigenvalues λ_k may be computed from the zeros s_k, $k = 1...N-1$ of the first kind Bessel functions of order 0, J_0 and eigenfunctions w_k^f may be written in terms of first kind Bessel functions of order 1, J_1, as:

$$w_k^f(z) = J_1(\lambda_k z), \text{ with } \lambda_k = \sqrt{s_k \frac{\eta}{\mu}} \tag{III.10}$$

Therefore we will choose for the effort approximation basis functions:

$$w_i^e(z) = \begin{cases} -\frac{1}{\lambda_i} J_0(\lambda_i z), & i = \overline{1..N-1} \\ 1 & i = N \end{cases} \tag{III.11}$$

in such a way that the exact differentiation (compatibility) condition is satisfied. Indeed, with the previous choices:

$$\begin{cases} \partial_z w_k^e(z) & = w_k^f(z), \forall k = \overline{1..N-1} \\ \partial_z w_N^e(z) & = 0 \end{cases} \tag{III.12}$$

Hence the derivation matrix D in equation $\mathbf{f} = D\mathbf{e}$ here reduces to $[\mathbb{I}_{N-1}|\,0] \in \mathbb{R}^{(N-1)\times N}$ where $\mathbb{I}_{N-1}$ is the identity matrix of order $N-1$. Indeed

$$\begin{array}{rccccc} & f & = & \partial_z e & & \\ \Rightarrow & \sum_{k=1}^{N-1} w_k^f(z)\mathbf{f}_k & = & \sum_{i=1}^{N} [\partial_z w_i^e(z)]\,(\mathbf{e})_i & = \sum_{i=1}^{N-1} w_i^f(z)\,(\mathbf{e})_i & \\ \Rightarrow & \mathbf{f} & = & [\mathbb{I}_{N-1}|\,0]\,\mathbf{e} & & \end{array} \tag{III.13}$$

Projections of the constitutive equations

The integration matrix, used in the power pairing (II.9) and needed to get the finite-dimensional representation of the Dirac interconnection structure, has to be computed. Elements in the diagonal and in the last row in this integration matrix may be computed exactly using Bessel's function properties:

$$\begin{array}{rccccc} M_{Nk} & = & \int_0^1 w_k^f(z)\mathrm{d}x & = & w_k^e(z)\,|_0^1 & = \frac{1}{\lambda_k} \\ M_{kk} & = & \int_0^1 w_k^e(z)\partial_x w_k^e(z)\,\mathrm{d}z & = & \frac{1}{2}\left(w_k^e(z)\right)^2|_0^1 & = -\frac{1}{2}\left(\frac{1}{\lambda_k}\right)^2 \end{array} \tag{III.14}$$

For the other elements (when $j \neq i$, hereafter) the Gauss quadrature formula with Chebyshev points will be used:

$$\begin{array}{rccc} M_{ij} = \int_0^1 f_{ij}(z)\,\mathrm{d}x & = & \frac{1}{2}\int_{-1}^1 f(z)\,\mathrm{d}(1-2z) & \\ & = & \frac{1}{2}\frac{\pi}{n}\sum_{k=1}^m \sqrt{1-(1-2z_k)^2}\, f(z_k) & \end{array} \tag{III.15}$$

where

$$f(x) = w_i^e(z) w_k^f(z) \text{ and } z_k = \frac{1 - \cos\left(\frac{(2k-1)\pi}{2(m-1)}\right)}{2}. \tag{III.16}$$

Unlike in the polynomial case, it is not possible here to perform exact integration for a product of Bessel functions of different orders. Chebyshev quadrature points have been chosen to get a finite dimensional PCH model which may be easily compared to the previous ones (obtained from FD or symplectic collocation at the very same points). The quadrature formula (III.15) is also used to determine the matrices G and R used in the finite dimensional storage and dissipation constitutive equations (III.9).

This previous choice of conjugated base functions obviously guarantees accurate eigenfunction approximation for the problem with homogeneous boundary conditions and uniform resistivity since the approximation functions are the eigenfunctions. As it may be expected, it gives also still more accurate results for the eigenvalue approximations as illustrated in table III.3 for the case $\eta = 5.10^{-7}$.

Theoretical	Numerical eigenvalues		
eigenvalues	N=5	N=8	N=10
-2.301056852	-2.305253100	-2.301848126	-2.301466232
-12.12413006	-12.25659915	-12.14481967	-12.13359575
-29.79659326	-30.92406956	-29.93017370	-29.85455494
-55.32237139	-81.24868031	-55.84563052	-55.53473267
-88.70194524		-90.35712887	-89.30413565
-129.9354296		-135.0263099	-131.4267729
-179.0228628		-297.6242993	-182.5230680
-235.9642604			-244.5957644
-300.7596298			-530.5090590

Table III.3: Eigenvalues with Bessel basis approximation functions for the case $\eta = 5.10^{-7}$

III.3 Symplectic Galerkin scheme

In the previous simulations, we neglected the dependence of the electrical resistivity η with the time t and the spatial radial coordinate z. More precisely this resistivity is a function of the plasma state (noticeably of the plasma electronic temperature $T_e(z,t)$ and density $n_e(z,t)$, see [107] for details). Rather than including a multi-physics plasma model including the energy and mass material balance equations we will make use of an analytic expression for $\eta(z,t)$ (from [90]).

In this case, the chosen Bessel basis functions are no longer the eigenfunctions of the system, since the eigenfunctions are no more analytically solvable. The discretization method will be then called a symplectic Galerkin scheme since both the projection of the resistive diffusion equation and the cancellation of the corresponding residual are performed in the same approximation space generated by the chosen Bessel functions. The dissipation matrix R now has to be computed online due to the time variations of the resistivity $\eta(z,t)$. In fact, the resistivity values supplied from the experimental data may be used to set the values of $\eta_k(t)$ of the resistivity at the discrete quadrature points z_k used in the finite dimensional model. The dissipation R matrix is till (now online) computed by the Gauss quadrature formula (III.15) according to:

$$\begin{aligned} R_{ij}(t) &= \int_0^1 \frac{\eta(t,z)}{C_3} w_i^f(z) w_j^f(z) \mathrm{d}z \\ &= \frac{\pi}{2n} \sum_{k=1}^{n} \frac{\eta(t,z_k)}{C_3} w_i^f(z_k) w_j^f(z_k) . \sqrt{1-(2z_k-1)^2} \end{aligned} \tag{III.17}$$

The eigenvalues of the corresponding finite dimensional PCH model obtained with the proposed symplectic Galerkin method may now only be computed numerically. In fact, with a time varying resistivity, the meaning of the expression "theoretical eigenvalues" for the infinite dimensional resistive diffusion equation is far from clear. However one may check that the finite dimensional model

still has purely dissipative eigenvalues (as expected from a diffusion equation) and that these ones converge when N increased. The results are in table III.4. where the eigenvalues are computed at time $t = 11s$ for the Tore Supra discharge TS#47673.

Numerical eigenvalues			
N=5	N=8	N=10	N=20
-0.316349428	-0.315983205	-0.315877522	-0.315856805
-2.673789607	-2.372985846	-2.372985846	-2.371577391
-14.74424065	-6.357688599	-6.278320313	-6.267211833
-359.7443273	-14.08116991	-12.01718458	-11.87022206
	-36.20739521	-21.66293021	-19.46289366
	-129.9270811	-43.38740206	-30.44782740
	-1724.357267	-102.0884225	-50.82178655
		-309.9311502	-84.68730014
		-3355.769434	-138.8389938

Table III.4: Eigenvalues with Bessel base-functions and experimentally provided time varying and non uniform resistivity $\eta(z, t = 11s) \in [2.10^{-8}, 2.10^{-6}]$, discharge TS#47673

IV Comparison against experimental data

Accuracy of the time response for the selected scenario (Tore Supra discharge TS#47673) may not be evaluated only by simulation since experimental values have been used for the plasma resistivity. Therefore, in this section, we wish to present a validation of the global port-Hamiltonian modelling and symplectic reduction approach, for the plasma resistive diffusion problem, by comparing the simulation results with experimental data.

IV.1 Test case definition

In order to validate the presented model, it is compared to experimental data from Tore Supra discharge TS#47673 where plasma current steps are performed. The effort base functions size is chosen equal to $N = 5$, $m = 10$ Chebyshev points are used in the Gauss quadrature formula (III.15). The system input is the boundary condition V_{loop} and the output is the total plasma current I_p.

In the test case, the non-inductive current source J_{ni} is only the bootstrap current J_{bs} (external non-inductive sources are set to zero). This current source and the plasma resistivity are computed using experimental data and expressions based on the work [90].

Furthermore, in a tokamak, the loop voltage V_{loop} can't be set directly but is generated using the central solenoid coil voltage. Thus on Tore Supra, a simple proportional controller is implemented between the plasma current and the coil voltage. On the proposed model, this controller is replaced by a proportional controller between I_p and V_{loop}. The gain of the controller is tuned to get the same steady state error as on the real plant (see cf. figures IV.1.a and IV.1.c).

IV.2 Results

The figure IV.1 shows the simulation results compared with experimental data. The coherence between our model and the experimental facility leads to the comparability in the result of input-output signals. The simulated loop voltage V_{loop} is very closed to the real one, except on the begin of the pulse during the ramp-up phase when the shape of the plasma is not stable and so the minor and major radius of the plasma are time-dependent. This dependance is not taken into account in the port-Hamiltonian model and leads to the small observed difference in figure IV.1.b before $t < 3$s. A zoom of the plasma current I_p and loop voltage V_{loop} presents the step response of the system in figure IV.1.c. A small delay appears between the experimental plasma current and the simulated one. This delay is coming from the actuator simplification assumed on the model. The central solenoid controller dynamic is not modelled. This explains why the step response of the model is faster than the one of the real plant.

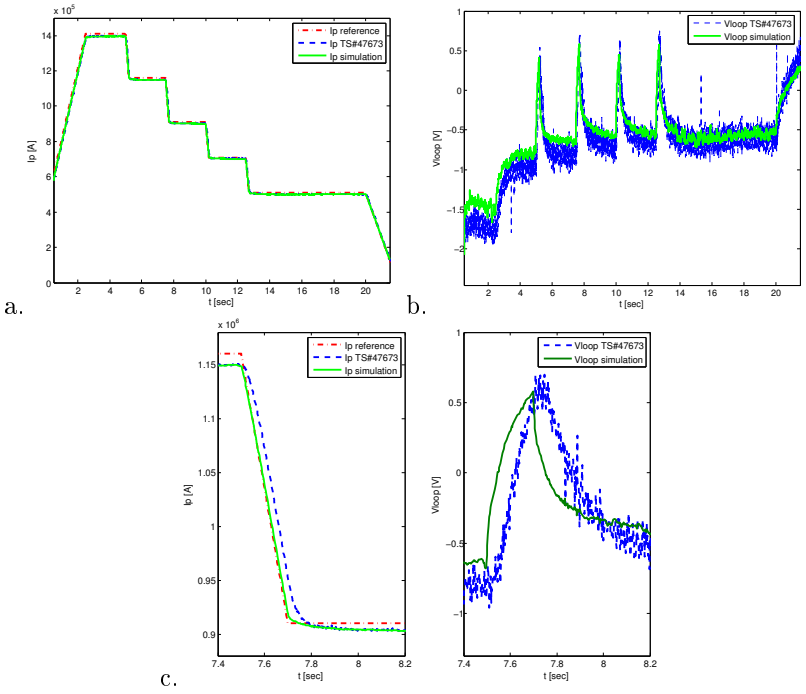

Figure IV.1: In-Output comparison
a. Plasma current I_p; b. Loop voltage V_{loop};
c. (I_p, V_{loop}) zoom at $t \in [7.4s, 8.2s]$

The safety factor q-profile (see section II.3) is given for several time shots in figure IV.2. The presented model safety factor is closed to the one provided by METIS despite the large difference of complexity between these two models. Since METIS is based on a finite difference discretization scheme of the resistive diffusion equation with some modifications to deal with the singularity in x = 0. These modifications in the model - using complex empirical expressions - at the edge and the center "boundaries" of the plasma explain the difference between the two $q-$profiles at the boundaries. Besides, due to the difficulty to obtain signification measurements of the q-profile in real plant and consequently to tune accurately the reconstruction code, the q-profile obtained with METIS could be only used as an indicator of the actual q-profile shape.

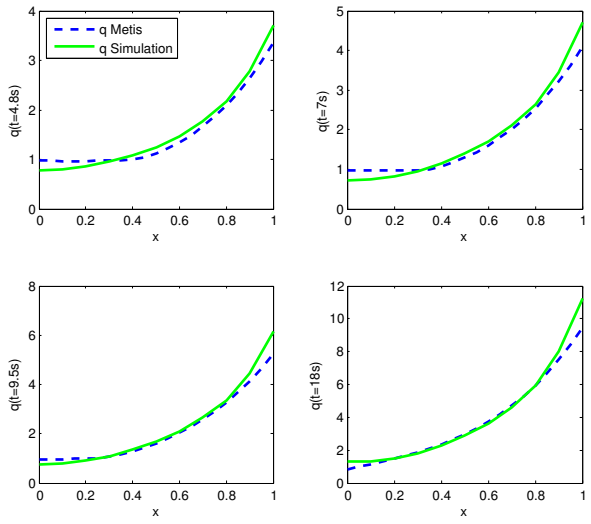

Figure IV.2: Safety factor q comparison

V Symplectic discretization applied to thermal diffusion equation

Following the same idea, the theoretical eigenfunctions of the thermal diffusion equation (in the simple case of uniform homogeneous thermal diffusion coefficient χ) are used to span the approximation bases hereafter. The discretization procedure does not differ from the previous case, although the obtained finite dimensional model for the thermal diffusion is given in implicit form only since there's just one conservation law for the entropy evolution. The constitutive relation of Fourier's law in equation (V.4) (chapter 3) is thus chosen to form a PCH system (see section V, chapter 3). Consequently, the control model derived from this system admits a singular value 0 in the state evolution . The Bessel functions of order 0 and 1 are still employed as the spaces of efforts and flows in this scheme. Nevertheless, the eigenvalues are not the same as those in the previous example due to the different boundary condition in this case (see section II in appendix E for the detail).

V.1 Thermal PCH discrete model

The thermal diffusion equation in (V.3), chapter 3 in the case of a uniform and constant diffusivity χ is also a Bessel equation (see section II appendix E for the derivation of this equation and further details on eigenvalues and eigenfunctions of the thermal diffusion operator). Therefore we may use as well Bessel functions for the approximation basis. The first kind Bessel functions of order 0, J_{B0}, and order 1, J_{B1}, will be used again to generate approximation bases for efforts and flows. The eigenvalues s_T for the thermal diffusion operator with uniform constant diffusivity χ may be as well derived from the zeros ξ_k of J_{B0} as:

$$s_{Tk} = \frac{2\chi}{3a^2}\xi_k^2,\ k = \overline{1..N-1} \tag{V.1}$$

Remark 12. In the general case, one may choose two different sets of approximation bases $w^f(z)$ and $w^e(z)$ for the coupled resistive and thermal diffusion equations. In this case, the port variables approximations between the two submodels have to be converted from one approximation space to the other through a fictitious numerical coupling. However, since we are considering here two diffusion systems, with Bessel functions as generating functions for the approximation bases in both cases and since we have no specific accuracy requirements for each of the two subsystems, we will use the same approximation spaces for both of them in order to simplify the calculus (and to avoid eventual undesired supplementary numerical effects).

Therefore, like the resistive diffusion equation (IV.8) (chapter 3), the $0D$ discrete scheme for the thermal diffusion equation (V.3) (chapter 3) is written using the input-output representation of the Dirac interconnection structure:

$$\begin{bmatrix} \begin{pmatrix} \mathbf{f}_1 \\ f_{\partial 1} \end{pmatrix} \\ \begin{pmatrix} \mathbf{e}_2 \\ -e_{\partial 0} \end{pmatrix} \end{bmatrix} = \begin{bmatrix} 0 & \begin{pmatrix} -D \\ w^e(1) \end{pmatrix}\begin{pmatrix} M^T \\ w^e(0) \end{pmatrix}^{-1} \\ \begin{pmatrix} -D \\ -w^e(0) \end{pmatrix}\begin{pmatrix} M^T \\ w^e(1) \end{pmatrix}^{-1} & 0 \end{bmatrix} \begin{bmatrix} \begin{pmatrix} \tilde{\mathbf{e}}_1 \\ e_{\partial 1} \end{pmatrix} \\ \begin{pmatrix} \tilde{\mathbf{f}}_2 \\ f_{\partial 0} \end{pmatrix} \end{bmatrix} + \begin{bmatrix} \begin{pmatrix} \overline{S} \\ 0 \end{pmatrix} \\ \begin{pmatrix} 0 \\ 0 \end{pmatrix} \end{bmatrix} \tag{V.2}$$

with the same derivative matrix $D = [\mathbb{I}_{N-1}|\,0] \in \mathbb{R}^{(N-1)\times N}$, the same integration matrix $M \in \mathbb{R}^{N\times(N-1)}$. The closure equations will be given by the projections of the constitutive relations in the same approximation bases and will be written as relations between the reduced variables $(\tilde{\mathbf{e}}_1, \mathbf{f}_1)$ and $\left(\mathbf{e}_2, \tilde{\mathbf{f}}_2\right)$.

V.2 Constitutive relations

The constitutive relations are here also obtained from to the projection of the power product (e, f) and the energy storage and dissipation relations in the previously chosen approximation bases.

Energy storage elements

Let us define e_{ex} the extended effort variable such as:

$$\overline{\mathcal{F}} \ni e_{ex} = \frac{3}{2}n\sqrt{g}T = \frac{3}{2}n\sqrt{g}\,e_1$$

then

$$\frac{de_{ex}}{dt} = \frac{3}{2} n\sqrt{g}\frac{dT}{dt} = n\sqrt{g}T\frac{ds}{dt} = f_1$$

in the considered case of time invariant particle density n, (see V.5). Considering both the power balance equation:

$$\frac{d\mathbb{H}_T}{dt} = \int_\Pi e_1 f_1 = \tilde{\mathbf{e}}_1^T \mathbf{f}_1 \tag{V.3}$$

and the projection of the storage constitutive relation :

$$\frac{d\mathbb{H}_T}{dt} = \int_\Pi e_1 f_1 = \int_\Pi \left(\frac{3}{2} n\sqrt{g}\right)^{-1} e_{ex}\, f_1 = \mathbf{e}_{ex}^T G_T \mathbf{f}_1 \tag{V.4}$$

with

$$(G_T)_{ij} = \int_0^1 \left(\frac{3}{2} n\sqrt{g}\right)^{-1} w_i^f(z) w_j^f(z),\ G_T = G_T^T \tag{V.5}$$

we deduce:

$$\tilde{\mathbf{e}}_1 = G_T \mathbf{e}_{ex} \tag{V.6}$$

with $e_{ex}^T = \sum_{k=1}^{N-1} \left(\mathbf{e}_{ex}^T(t)\right)_k w_k^f(z)$.

Energy dissipative element

Using the chosen port variable notations, the dissipated power in thermal domain reads:

$$\mathbb{P}_{Td} = \int_\Pi e_2\, f_2 = \mathbf{e}_2^T \tilde{\mathbf{f}}_2 \tag{V.7}$$

From the Fourier's law in (V.4): $f_2 = n\chi\dfrac{\sqrt{g_\theta g_\phi}}{\sqrt{g_\rho}} e_2$, one gets:

$$\mathbb{P}_d = \int_\Pi e_2\, f_2 = \int_\Pi e_2 n\chi\frac{\sqrt{g_\theta g_\phi}}{\sqrt{g_\rho}} e_2 = \mathbf{e}_2^T R_T \mathbf{e}_2 \tag{V.8}$$

where

$$R_{Tij} = \int_0^1 n\chi\frac{\sqrt{g_\theta g_\phi}}{\sqrt{g_\rho}} w_i^f(z) w_j^f(z); R_T = R_T^T > 0 \tag{V.9}$$

denotes the dissipation matrix. Therefore we will use the projected constitutive equation:

$$\tilde{\mathbf{f}}_2 = R_T \mathbf{e}_2 \tag{V.10}$$

Control model for thermal diffusion

The model in (V.2) including the constitutive relation (V.10) becomes:

$$\begin{pmatrix} \partial_t \mathbf{e}_{ex} \\ 0 \end{pmatrix} = \left[\begin{pmatrix} 0 & J_{T1} \\ J_{T2} & \end{pmatrix} - \begin{pmatrix} 0 & 0 \\ 0 & R_T^{-1} \end{pmatrix}\right] \begin{pmatrix} G_T \mathbf{e}_{ex} \\ \tilde{\mathbf{f}}_2 \end{pmatrix} + \begin{pmatrix} \overline{S} \\ J_{T4} T_1 \end{pmatrix} \tag{V.11}$$

The matrices J_{T1}, J_{T2} with $J_{T1} = -J_{T2}^T$ represent the spatial derivation operator ∂_z and its formal adjoint in the finite dimensional approximation spaces. J_{T4} is related to the boundary coefficient, while T_1 is the value of the average temperature at the boundary $z = 1$.

Remark 13. Since the thermal model (V.3) is not written in canonical PCH form, an implicit representation for discrete thermal scheme may be easily given using, for instance, the image representation of a Dirac structure given in (V.12).

$$\begin{pmatrix} \mathbf{f}_1 \\ \mathbf{e}_2 \\ e_{\partial 1} \\ e_{\partial 0} \end{pmatrix} = \underbrace{\begin{pmatrix} 0 & -D \\ -D & 0 \\ w^e(1) & 0 \\ w^e(0) & 0 \end{pmatrix}}_{E^T} \begin{pmatrix} \mathbf{e}_1 \\ \mathbf{f}_2 \end{pmatrix} + \begin{pmatrix} \begin{pmatrix} \overline{S} \\ 0 \end{pmatrix} \\ \begin{pmatrix} 0 \\ 0 \end{pmatrix} \end{pmatrix} \quad \text{and} \quad \begin{pmatrix} \tilde{\mathbf{e}}_1 \\ \tilde{\mathbf{f}}_2 \\ f_{\partial 1} \\ f_{\partial 0} \end{pmatrix} = \underbrace{\begin{pmatrix} M^T & 0 \\ 0 & M^T \\ 0 & w^e(1) \\ 0 & w^e(0) \end{pmatrix}}_{F^T} \begin{pmatrix} \mathbf{e}_1 \\ \mathbf{f}_2 \end{pmatrix} \tag{V.12}$$

The table V.1 here below compares the eigenvalues of the proposed discretization scheme with the theoretical ones, and the ones from a finite difference scheme. The symplectic scheme not only gets more accurate result but also avoids the creation of unstable modes (positive eigenvalue) or oscillating modes as it may be observed with the finite different scheme. The eigenvalues for the

Theoretical eigenvalues	Numerical eigenvalues N=5	N=8	N=10	FD with N=50
				7.234097
-120.483040	-120.702770	-120,524486	-120,504490	-118.141417
-634.817965	-641.754030	-635,901271	-635,313587	-748.190997
-1560.145974	-1619.180495	-1567,140230	-1563,180841	-1827.815893
-2896.672592	-4254.170952	-2924,070376	-2907,791802	-3355,212061
-4644.422992		-4731,088204	-4675,9536082	-5323,638574
-6803.403186		-7069,961051	-6881,489738	-7724,736935
-9373.615177		-15583,5718679	-9556,885491	-10548,547081
-12355.059784			-12807,004273	-13783,474351
-15747.737391			-27777,389374	-17416,282235

Table V.1: Eigenvalues with symplectic and finite different discretization scheme, with $n = 2.10^{19}[m^{-3}]$, $\chi = 5[m^2/s]$

energy transport in table V.1 are hundred of times larger than the ones obtained for the magnetic flux transport in table III.3. The hypothesis of two very different time scales in the plasma transport phenomena, mentioned in subsection II.2, is here correctly represented by the obtained *0D* (finite dimension) control models in PCH form for the two diffusion equations.

The figure V.1 shows the temperature profile comparison between the simulation results (right) and the experimental data from the tokamak Tore Supra (CEA Cadarache) ohmic shock TS #47673 (left) using experimental data. The different colors from green (under) to blue (upper) stand for the temperature profile from the center to the plasma edge. In this test, the pseudo-symplectic discrete scheme is employed with the non-uniform diffusion coefficient χ adapted to the test case. There is a difference between the two profiles at the center which is probably due to a poor estimation of the diffusivity coefficient χ estimated with the empirical formula proposed in [27]. The mismatch of temperature profiles are well-exposed in the figure V.2 at four different moments.

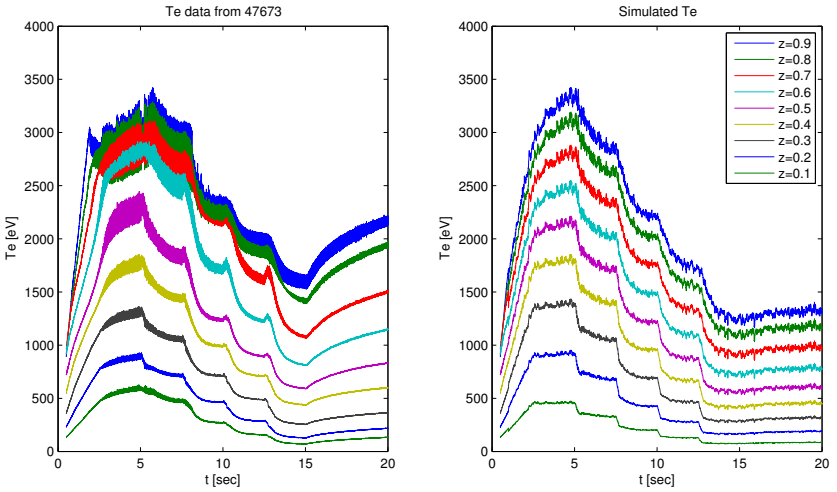

Figure V.1: Electronic temperature profiles - time evolution comparison

VI Conclusion

In this chapter we have suggested how classical pseudo-spectral methods for the spatial discretization of *1D* distributed parameter systems could be adapted in order to preserve the geometric structure of a class of Hamiltonian systems representing open physical systems, i.e. with energy flow through the boundary of their spatial domain. The resulting spatial discretization schemes preserve this structure after the reduction by projection on the chosen approximation spaces which

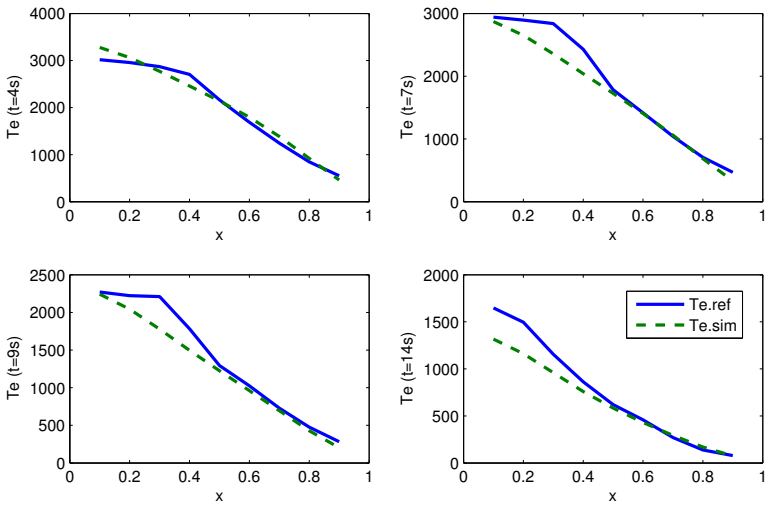

Figure V.2: Electronic temperature profiles - space evolution comparison

are differently chosen according to the degree of the differential forms that they approximate. Doing this, both the exterior derivative and the boundary operator may be exactly discretized and consequently the "mixed" schemes developed with the proposed methodology are symplectic (or geometric) while the methods used to generate these mixed schemes are not.

Another point of interest is the discussion about the selection of the approximation bases. This is a general problem for pseudo-spectral models. However in the case of "mixed" schemes, where several compatible approximation bases have to be selected, it was not obvious that interesting choices could happen. We claim that choosing, for one of the conjugated approximation bases, the set of eigenfunctions of a simplified problem may be an interesting choice. To illustrate the approximation base choice methodology, we selected the Galerkin scheme among the possible pseudo-spectral methods. Then we showed that the skew-symmetry of the Stokes-Dirac structure gives rise to a set of eigenfunctions (Bessel functions in our example) for which a conjugated compatible base can easily be found. Finally, in the resistive diffusion equation example, we showed that this approach may reduce numerical oscillations in the presence of non homogeneous initial conditions or sharp distributed control.

Our "geometric" discretization approach, based on the port-Hamiltonian formulation for open distributed parameter systems, has been used to generate a finite-dimensional approximation for a *1D* control model for plasma dynamics in tokamaks. This confirmed the effectiveness of the approach in preserving some desired physical properties of the actual *1D* model, namely spectral (eigenvalues and eigenfunctions) and energetic (conservativeness and passivity) properties. Moreover, although large simplification assumptions are made on the plasma geometry and properties to obtain the resistive diffusion equation, simulation results show good agreement with the experimental data and exhibit accuracy and qualitative behavior similar to the ones obtained from the "more complex" reference code (METIS) for such plasma simulations. Consequently, we may hope to derive from our discretized finite dimensional model, IDA-PBC (Interconnection and Damping Assignment, cf. [78]) controllers with a "reasonable" chance of success. This will be the topic of the next chapter 5.

Chapter 5

IDA-PBC Controller design

I Introduction

The Tokamak plasma control problems aim at many different objectives [83, 105, 2]. One of them consists in handling the MHD instabilities while maintaining some current, temperature and pressure density profiles. A suitable control model for these plasma dynamics is then a success key in the fusion research. One of the challenges is the control of the *1D* plasma safety factor profile which is an important parameter for both plasma stability and performance. The goal here is to reach some specific non-uniform radial profiles in order to avoid MHD instabilities and to improve the plasma confinement. Many investigations including some related to the ITER project - are currently dedicated to this issue[1], [39], [81]. In this context the *1D* resistive diffusion equation for the magnetic flux in the plasma ([10, Chap.6]) is a commonly used control model.

Readers could refer to [107] for investigations on this model for control purposes or to [81] for application to model-based predictive control. A similar model has been used to solve the current profile optimal tracking problem [80] or to design robust controller for the poloidal magnetic flux profile in [79]. Feedback control using Lyapunov approach in [1], or sliding mode in [39] are also proposed. Note also that two-time scale extensions have already been considered for simultaneous magnetic and kinetic (temperature) profile control in tokamak [28].

From the beginning of this thesis until now, our approach is to define a model which not only represents consistently the main physical properties and dynamical behaviours of the plasma but which is also simple enough to synthesize a model-based control for the internal profiles of the plasma. The presented model is based on a port-Hamiltonian formulation of the plasma TMHD in tokamaks developed in chapter 2 (section IV-VI). This model implies to modify the safety factor control problem into an equivalent magnetic field profile control problem. Spatial reduction and discretization methods, inspired from [70] and developed in chapter 3 and chapter 4, allow to reduce this *3D* TMHD model to a finite dimensional PCH model. These symplectic reduction and discretization methods preserve the qualitative spectrum properties (see chapter 4, table III.3-V.1). Another consequence is that the finite-dimensional PCH model derived in chapter 4 has the same invariants (for instance the total energy density) and model structure as the infinite-dimensional ones. Stored and dissipated energies in the finite dimensional model are simply approximation of the actual ones in the original distributed parameter model. Therefore, this finite-dimensional PCH model seems to be the ideal one for the design of a high performance IDA-PBC controller [78].

Here, the proposed IDA-PBC controller allows stabilizing *1D* profiles of the magnetic field - hence also the safety factor q-profile at the desired references directly by two actuators: the voltage at the boundary of the plasma (the loop voltage V_{loop}) and the distributed non inductive current-drive heating source J_{ext}. Besides, a third actuator, the external heating source S_{heat}, will be used as a supplementary actuator which modifies the plasma temperature, hence indirectly some physical parameters such as the resistivity η profile or the bootstrap current.

Challenges in this control problem not only arise from the time variation of some parameters usually badly estimated (such as the resistivity or diffusivity for instance), but also from the technological constraints and non-linearities in the actuator models. In the considered facilities - Tore Supra WEST and TCV - the distributed controls J_{ext} and S_{heat} have specific spatial profiles, pos-

sibly depending from the control variable values themselves. In fact, the controllable inputs are rather the total external current power P_{ext} and the total external heating power P_{heat}. The consequence is that the system is a finite rank input-output control system with both boundary and distributed control actions. The finite dimensional coupled control model may thus be considered as an under-actuated system in the sense that the number of actuators is less than the number of system states (more details on under-actuated PCH systems could be found in [76]).

Hence, only a limited (finite dimensional) set of safety factor profiles are reachable. In this work, the available control signals are used to regulate the q-profile at a finite number of points. On one side, the corresponding q-profile on the whole spatial domain for the radial coordinate, as well as the corresponding feedforward control are both computed in order to guarantee their compatibilities with the systems constraints. On the other side, the designed IDA-PBC feedback control aims at improving the system stabilization and convergence rate as well as at attenuating the approximation errors. Nevertheless, an integrator is still necessary to cancel the static error on the safety factor profile.

Two scenario are figured out in the sequel. In the first one the PCH model equivalent to the resistive diffusion equation (chapter 4, section I) is used with two control signals V_{loop} and P_{ext} to regulate the q radial profile at two positions. In the second one, the magneto-hydro-dynamic couplings and the thermal-electromagnetic model are investigated (see chapter 4, section V.1)). A third control signal P_{heat} is used in order to reach a given reference value for the$q$ radial profile at a third point.

The control approach is validated first in simulations for the Tore Supra WEST facility. These simulations are based on the model, parameters values and empirical laws presented in [107]. Then, other simulation results will be presented, they are based on the RAPTOR code for the TCV tokamak real-time control system. It is a *1D* transport code specially designed for a fast execution compatible with the needs for real-time control or for nonlinear optimization schemes [30, 29].

Besides, based on these previous simulation tests, the IDA-PBC controller has also been implemented and tested on the real TCV experimental facility. The first result obtained (before TCV has been stopped for a long period for maintenance and upgrade) is shown at the end of the chapter.

This chapter is organized as follows. In section II, the IDA-PBC design methodology is revisited and adapted to the specific studied case. The resistive diffusion model (from chapter 4 section II) is firstly used as a control model in section III. A non-linear feedforward control takes into account the system constraints in the WEST Tokamak case and a simple "linear" IDA-PBC feedback control is discussed with the help of some practical considerations. A criterion is derived which allows to give a variational (optimality) interpretation to the IDA-PBC parameters tuning. Some simulation and experimental (from Tokamak TCV shocks) results are then showed. In section IV, the coupled TMHD system is then used as a control model for the IDA-PBC controller design. An optimal IDA-PBC design is also proposed and tested with simulations. Later in chapter 6 we will make use of these early results to suggest an IDA-PBC-like controller designed with the *1D* infinite dimensional port-Hamiltonian model.

II IDA-PBC closed loop control

The IDA-PBC control design may be considered as the the most general one among passivity based control (PBC) designs for PCH systems. Readers may refer to [77] for an overview and connections between IDA-PBC controls and more particular types of PBC, such as energy shaping, power shaping, or control by interconnection. A brief reminder of the IDA-PBC design methodology (inspired from [78]) is given hereafter.

II.1 Methodology overview

Given a standard PCH system:

$$\dot{x} = \left[\mathcal{J}(x) - \mathcal{R}(x)\right] \frac{\partial \mathbb{H}(x)}{\partial x} + g(x)\, u \tag{II.1}$$

The main idea of the IDA-PBC method is to choose an appropriate feedback control law $u(x)$ so that the original system (II.1) is pulled back to a reference system with a set of desired properties.

Let us design a closed loop reference system:

$$\dot{x} = [\mathcal{J}_d(x) - \mathcal{R}_d(x)] \frac{\partial \mathbb{H}_d}{\partial x}(x) \tag{II.2}$$

with $\mathcal{J}_d = -\mathcal{J}_d^T$, $\mathcal{R}_d = \mathcal{R}_d^T \geqslant 0$ and a strict local minimum x_d for the closed loop Hamiltonian $\mathbb{H}_d$. This minimum x_d is a locally stable equilibrium since:

$$\dot{\mathbb{H}}_d = -\left(\partial_x \mathbb{H}_d\right)^T \mathcal{R}_d \left(\partial_x \mathbb{H}_d\right) \ \leq 0 \tag{II.3}$$

The static state feedback is then chosen such that the closed-loop system matches this reference PCH system by using the "tuning parameters" $\mathcal{J}_a(x)$, $\mathcal{R}_a(x)$, $\mathbb{H}_a(x)$ such that $\mathcal{J}_d(x) = \mathcal{J}(x) + \mathcal{J}_a(x)$, $\mathcal{R}_d(x) = \mathcal{R}(x) + \mathcal{R}_a(x)$ and such that $\mathbb{H}_d(x) = \mathbb{H}(x) + \mathbb{H}_a(x)$ has the minimum at x_d. This leads to a matching equation for the equivalence of (II.1) and (II.2) which reads:

$$(\mathcal{J} - \mathcal{R}) \frac{\partial \mathbb{H}}{\partial x} + gu = (\mathcal{J}_d - \mathcal{R}_d) \frac{\partial \mathbb{H}_d}{\partial x} \tag{II.4}$$

and leads to the feedback:

$$u = \left(g^T g\right)^{-1} g^T \left[(\mathcal{J}_d - \mathcal{R}_d) \frac{\partial \mathbb{H}_d}{\partial x} - (\mathcal{J} - \mathcal{R}) \frac{\partial \mathbb{H}}{\partial x}\right] \tag{II.5}$$

Besides, the following conditions are required for the solution:

i) *(Integrability)*

$$\frac{\partial^2 \mathbb{H}_d}{\partial x^2}(x) = \left[\frac{\partial^2 \mathbb{H}_d}{\partial x^2}(x)\right]^T \tag{II.6}$$

ii) *(Equilibrium assignment)*

$$\frac{\partial \mathbb{H}_d}{\partial x}(x_d) = 0 \tag{II.7}$$

iii) *(Lyapunov stability)*

$$\frac{\partial^2 \mathbb{H}_d}{\partial x^2}(x_d) > 0 \tag{II.8}$$

The first condition implies the existence of the scalar energy function $\mathbb{H}_d$, while the two others ensure respectively the existence of the minimum of $\mathbb{H}_d$ at the desired equilibrium value x_d and its stability. This general design methodology preserves many degrees of freedom since the controller is set only once $\mathcal{J}_a$, $\mathcal{R}_a$ and $\mathbb{H}_a$ have been chosen. We propose a particular design methodology for our system in the next subsections.

II.2 Integrator extension

An integral action may be added to the IDA-PBC control action in order to eliminate the static error due to the approximations or disturbances, while always conserving the PCH structure of the whole closed-loop system (a simple design for this integral action is proposed in [75, sec.6]). In this work, we have adapted this integrator into our system.

Proposition II.1. *Consider the system of equation (II.1) in closed-loop with $u = \beta(x) + v$:*

$$\begin{bmatrix} \dot{x} \\ \dot{x_I} \end{bmatrix} = \begin{bmatrix} \mathcal{J}_d(x) - \mathcal{R}_d(x) & K_I \\ -K_I^T & 0 \end{bmatrix} \begin{bmatrix} \partial_x W \\ \partial_{x_I} W \end{bmatrix} \tag{II.9}$$

where $x_I \in \mathbb{R}^k$ are the extended integral variables and $K_I \in \mathbb{R}^{n \times k}$ the corresponding integral gains. The extended Hamiltonian

$$W(x, x_I) \triangleq \mathbb{H}_d(x) + \mathbb{H}_I(x_I) \tag{II.10}$$

qualifies as a new Lyapunov function, in which $\mathbb{H}_I$ is considered as the energy function associated with the integral effect. It may be designed as the usual quadratic form:

$$\mathbb{H}_I = \frac{1}{2} x_I^T \mathcal{Q}_I x_I \quad \mathcal{Q}_I = Q_I^T \in \mathbb{R}_+^{k \times k} \tag{II.11}$$

The integral contribution in the control action is then derived:

$$v = -\left(g^T g\right)^{-1} g^T K_I \mathcal{Q}_I \int_0^t K_I^T \partial_x \mathbb{H}_d \tag{II.12}$$

Stability properties of x_d remain preserved since the augmented system (II.9) keeps the canonical PCH form.

II.3 Optimal control

How to choose the IDA-PBC design parameters is still largely an open issue (see the discussion in [78]). In our earlier work only an empirical proposal is made for the sake of simplicity and based on a prior qualitative knowledge of our process (the plasma dynamics). There is no guarantee for any optimal criteria to be satisfied for the closed loop system. Besides, the chosen added dissipation $\mathcal{R}_a$ doesn't (in general) satisfy the real actuator constraints neither specific MHD stability conditions for the plasma. To fix all these issues, we developed an optimal IDA-PBC design methodology in which the IDA-PBC parameters are chosen to minimize the error for the safety factor profile while the constraints on the inputs are still satisfied.

We will first reveal the equivalence between an optimal control law, u_{opt}, and the IDA-PBC one, u_{IDA}, by establishing in the same time the optimal criterion (cost function). In fact, from a pre-defined optimal criterion, the IDA-PBC parameters may be determined via the u_{opt} obtained from the well-known Riccati equation associated to the corresponding quadratic cost function.

The traditional optimal control principle (cf. [66]) is briefly revisited in the sequel. We consider the simple case, where the PCH system (II.1) can be regarded as a general linear system of the form:

$$\dot{x} = Ax(t) + Bu(t) \tag{II.13}$$

and also consider the standard quadratic cost function:

$$I = \int_0^{t_{fin}} x^T C x + u^T D u \tag{II.14}$$

where $C = C^T \in \mathbb{R}_+^{n\times n}$ and $D = D^T \in \mathbb{R}_+^{m\times m}$ are respectively the weight matrices for the regulation error and input values. The optimal feedback control law that minimizes the cost function I is written:

$$u_{opt} = -D^{-1}B^T P x \tag{II.15}$$

where $P = P^T \in \mathbb{R}_+^{n\times n}$ is the solution of Riccati equation:

$$PA + A^T P - PBD^{-1}BP + C = 0 \tag{II.16}$$

Hence, by replacing the optimal control u_{opt} given in (II.15) in the matching equation (II.4), one obtains another kind of "matching" condition written in terms of IDA-PBC designed parameter values. On the other hand, if both the system, $\mathbb{H}$, and desired, $\mathbb{H}_d$, Hamiltonian functions take the quadratic form:

$$\begin{aligned} \mathbb{H} &= \frac{1}{2} x^T \mathcal{Q} x \\ \mathbb{H}_d &= \frac{1}{2} x^T \mathcal{Q}_d x \end{aligned} \tag{II.17}$$

then by inserting $A = (\mathcal{J} - \mathcal{R})\mathcal{Q}$, the matching equation (II.4) can be simplified:

$$Ax + Bu = (\mathcal{J}_d - \mathcal{R}_d)\mathcal{Q}_d x \tag{II.18}$$

Substituting the optimal control law u_{opt} from (II.15) into this previous equation, we conclude that the control design parameters ($\mathcal{J}_d$, $\mathcal{R}_d$, $\mathcal{Q}_d$) must satisfy:

$$(\mathcal{J}_d - \mathcal{R}_d)\mathcal{Q}_d = A - BD^{-1}B^T P \ \ \forall x \tag{II.19}$$

together with the integrability, equilibrium and stability conditions (II.6-II.8). Assume that the desired total energy $\mathcal{Q}_d = \mathcal{Q}_d^T > 0$ of the closed loop system is set, then the other parameters $(\mathcal{J}_d, \mathcal{R}_d)$ may be computed by separating the symmetric and skew-symmetric parts of the matrix:

$$S = (\mathcal{J}_d - \mathcal{R}_d) = \left(A - BD^{-1}B^T P\right) \mathcal{Q}_d^{-1} \tag{II.20}$$

Indeed we may choose then:

$$\begin{cases} \mathcal{J}_d := & \frac{1}{2}\left(S - S^T\right) \\ \mathcal{R}_d := & -\frac{1}{2}\left(S + S^T\right) \end{cases} \tag{II.21}$$

Remark 14. Note that the choice $\mathcal{Q}_d = \alpha\mathcal{Q}$ with the scalar $\alpha > 0$ appears as an easy solution for equation (II.19). Besides, without energy shaping (i.e. $\mathcal{Q}_d \equiv \mathcal{Q}$) the proposed method qualifies as an "Interconnection and Damping assignment" control since only interconnection $\mathcal{J}_d$ and damping $\mathcal{R}_d$ matrices are modified.

Remark 15. The advantages of the proposed optimal design method when compared to the "traditional" empirical IDA-PBC design are the following:

- Saturation (constraints) on the actuators and the error convergence may be handled by tuning explicitly the weight matrices D and C.
- Diagonal matrices C and D are always easier to design than a probably full matrices $(\mathcal{J}_d,\ \mathcal{R}_d,\ \mathcal{Q}_d)$.
- There's no need to find a solution for matching partial differential equation (II.4) to define the IDA-PBC control parameters.

II.4 Control strategy

Besides the issue of the controller parameter choice, the non-linearities and actuator constraints still complicate the control synthesis. Regarding the distributed controls, the real action signals are the total powers $P_{ext}(t)$ and $P_{heat}(t)$ of the external current drive $J_{ext}(z,t)$ and the external heating source $S_{heat}(z,t)$ respectively (z denotes the spatial coordinate). The control deposit profiles are approximated as:

$$\begin{cases} J_{ext} & = P_{ext}(t)\, f_{ext}\,(z,t) \\ S_{heat} & = P_{heat}(t)\, f_{heat}\,(z,t) \end{cases} \tag{II.22}$$

where $f_{ext}\,(z,t)$ and $f_{heat}\,(z,t)$ are the specific spatial deposit shapes of these "distributed" controls (typically gaussian shapes in WEST and TCV). Notice also that in the Tore Supra WEST case, the gaussian shapes also depend on the source total powers; hence $f_{ext} := f_{ext}\,(z,t,P_{ext})$ and $f_{heat} := f_{heat}\,(z,t,P_{heat})$.

Consequently a feedforward control will be designed first which leads to a reachable steady state, then the closed-loop stabilization and the convergence rate will be improved via an IDA-PBC feedback control. This (usual) control strategy as summarized in the figure II.1.

For the design of the IDA-PBC feedback control, we will make use of the linearization of $g\,(x,u)$ around the equilibrium profile (x_d, u_d) (where u_d denotes the feedforward part of the control action which is designed with the non linear PCH model). This will help us to completely distinguish the feedforward and feedback effects, as well as allows us to apply the "traditional" IDA-PBC feedback design discussed in the previous subsection.

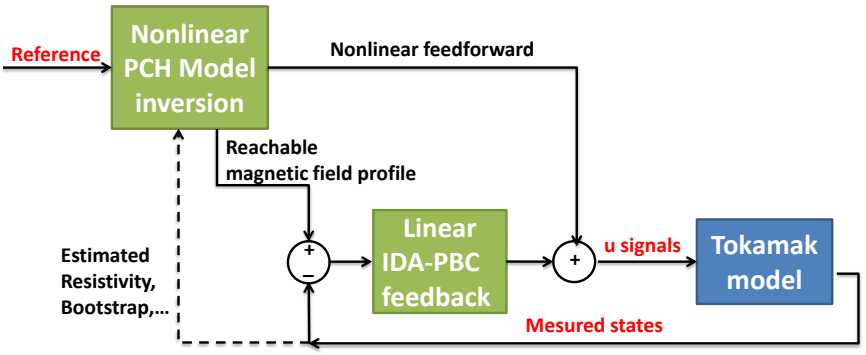

Figure II.1: The proposed control strategy: a nonlinear feedforward control and a feedback control designed with the help of the linearized model

Proposition II.2. *Assuming a good accuracy of the model, the feedback effect contribution is considered widely weaker than the feedforward one into the total control law $g(x,u)u$. Thus the feedforward part of the controller is computed using non-linear expression of the system and a linearization around the equilibrium point can be done for the computation of the feedback part:*

$$\begin{aligned} g(x,u)u = & \quad g\left(x_d, u_d + \delta u\right)\left(u_d + \delta u\right) \\ \approx & \quad g_d u_d + g_d \delta u \end{aligned} \tag{II.23}$$

where $g_d = g\left(x_d, u_d\right)$.

II.5 Robustness analysis

In this subsection, the robustness of the controller against two kinds of uncertainties is studied. The first one is on the system dissipation $\mathcal{R}$ coming from a bad estimation of the system parameters, such as the plasma resistivity η and the thermal diffusion coefficient χ. The second one concerns the uncertainty on the actuator profiles J_{ext}, S_{heat} as well as a bad knowledge of the bootstrap current J_{bs}. It can also include the approximation error during the linearization in (II.23):

$$g\left(x,u\right)u = g_d u_d + g_d \delta u + \underbrace{\delta g\ \left(u_d + \delta u\right)}_{\zeta} \tag{II.24}$$

We remind in the following lemma (see [8]) a condition of disturbance rejection for Port-Hamiltonian systems:

Lemma II.3. *Consider a Disturbed-port-Hamiltonian (DPCH) system with the bounded disturbance ζ:*

$$\dot{x} \quad = \quad \left[\mathcal{J}_d - \mathcal{R}_d\right]\partial_x \mathbb{H}_d + \zeta \tag{II.25}$$

Denote $\lambda_{min}\left[\mathcal{R}_d\right]$ the smallest eigenvalue of $\mathcal{R}_d \geq 0$, then the two following results hold:

- *If $\zeta = A\left(x\right)\partial_x \mathbb{H}_d$ then if $\left(R_d - A\right) \geq 0$, the perturbed system is still globally stable with the equilibrium x_d*
- *If $|\zeta| < \kappa\left|\partial_x \mathbb{H}_d\right|$ where $\kappa < \lambda_{min}\left[\mathcal{R}_d\right]$ then $\dot{\mathbb{H}}_d \leq 0$, and thus the system is still globally stable*

The disturbance defined via the uncertainty on the resistivity $\delta\eta$ and on the thermal diffusion coefficient $\delta\chi$ leads to an uncertainty $\delta\mathcal{R} = \delta\mathcal{R}^T$ applied on $\mathcal{R}$. The disturbed system can be defined as:

$$\dot{x} = \left[\mathcal{J}_d - \left(\mathcal{R}_d + \delta\mathcal{R}\right)\right]\partial_x H_d \tag{II.26}$$

This kind of disturbance corresponds to the first type defined in the previous lemma. Hence, the system is still stable as long as the total dissipation is positive, i.e. $\left[\mathcal{R}_d + \delta\mathcal{R}\right] > 0$.

The second kind of uncertainty on the control action spatial distribution and on the (bootstrap) current profile may be modelled as disturbances of the second type in lemma II.3. Nevertheless, it remains difficult to explicit quantitatively the bounding condition of these disturbances as well as to choose a non-linear Hamiltonian $\mathbb{H}_d$ that satisfies the condition in lemma II.3.

III First case study: the PCH resistive diffusion model

The proposed IDA-PBC controller allows to stabilize the safety factor profile at the desired reference using two controlled (scalar) variables: the loop voltage $V_{loop}(t)$ and the external current power source $P_{ext}(t)$. The feedforward control is designed by choosing the (reachable) desired steady state. In this example, a simple controller tuning for the IDA-PBC parameters is proposed. This tuning is equivalent to damping assignment and energy shaping. The simulations chosen to illustrate the approach are based on both the Tore Supra WEST and TCV facilities.

III.1 The resistive diffusion model

One obtains in chapter 4, section II the following time-dependent dissipative Port-Controlled Hamiltonian model equivalent to the resistive diffusion equation once discretized using our symplectic Galerkin scheme:

$$\partial_t \begin{pmatrix} \mathbf{d} \\ \mathbf{b} \end{pmatrix} = \left[\begin{pmatrix} 0 & -J_1 \\ -J_2 & 0 \end{pmatrix} - \begin{pmatrix} R^{-1}(\eta(z,t)) & 0 \\ 0 & 0 \end{pmatrix} \right] \begin{pmatrix} \partial_{\mathbf{d}} \mathbb{H}_{EM} \\ \\ \partial_{\mathbf{b}} \mathbb{H}_{EM} \end{pmatrix} - \begin{pmatrix} \mathbf{J}_{bs} + \mathbf{J}_{ext} \\ -J_4 V_{loop} \end{pmatrix} \tag{III.1}$$

The variables $\mathbf{d}$, $\mathbf{b}$, $\mathbf{J}_{bs}$ and $\mathbf{J}_{ext}$ are the time-varying coefficients of the expansions in the chosen approximation bases of respectively the electric field, the magnetic field, the bootstrap current density and the external current source density. Note that the boundary control $V_{loop}(t)$ is now embedded in the finite dimension state equation. The matrices J_1, J_2 with $J_1 = -J_2^T$ are obtained from the discretization (and reduction) of the spatial derivation ∂_z in the effort approximation basis while J_4 is related to the boundary coefficient of this approximation. The dissipation matrix R is determined by using the resistivity approximation in the same approximation bases $\eta(z,t)$. The total (approximate) energy function $\mathbb{H}_{EM}$ is defined as:

$$\mathbb{H}_{EM} = \frac{1}{2}\left(\mathbf{d}^T G_{el} \mathbf{d} + \mathbf{b}^T G_{mg} \mathbf{b}\right) = \frac{1}{2} x^T \mathcal{Q} x$$

where the matrices G_{el} and G_{mg} are diagonal and reduced to, respectively, the electric and magnetic permeability, $\frac{1}{\epsilon_0 C_3}$ and $\frac{C_2}{\mu_0}$, in the simple anisotropic case.. The coefficients C_2, C_3 are the toric coordinate coefficients defined by the plasma quasistatic equilibrium (chapter 4, subsection IV.2). The external current source is assumed equal to $\mathbf{J}_{ext} = f_{ext}(z) P_{ext}$ where $f_{ext}(z)$ is the external current source spatial distribution. Using these assumptions, the PCH model here above becomes:

$$\begin{aligned} \begin{pmatrix} \dot{\mathbf{d}} \\ \dot{\mathbf{b}} \end{pmatrix} = & \left[\begin{pmatrix} 0 & -J_1 \\ -J_2 & 0 \end{pmatrix} - \begin{pmatrix} R^{-1}(z,t) & 0 \\ 0 & 0 \end{pmatrix} \right] \underbrace{\begin{pmatrix} G_{el} & 0 \\ 0 & G_{mg} \end{pmatrix} \begin{pmatrix} \mathbf{d} \\ \mathbf{b} \end{pmatrix}}_{\partial_x \mathbb{H}_{EM}} \\ & + \underbrace{\begin{pmatrix} -f_{ext} - \frac{\mathbf{J}_{bs}}{P_{ext}} & 0 \\ 0 & J_4 \end{pmatrix}}_{g(z)} \underbrace{\begin{pmatrix} P_{ext} \\ V_{loop} \end{pmatrix}}_{u(t)} \end{aligned} \tag{III.2}$$

This reduced system is thus defined directly in the usual the explicit linear PCH form (II.1), except for the under-actuated non-linear mapping $g(z)$. A reachable equilibrium as well as the corresponding feedforward will be determined in the following subsection.

III.2 Reference state generation for the resistive diffusion model

The setting of the equilibrium point is restricted because of the actuator limitations previously discussed. To provide to the controller a reachable equilibrium profile, from two points of the reference q_{ref} used by the physicist, the steady state $x_d = (\mathbf{d}_d, \mathbf{b}_d)^T$ is computed (with $\mathbf{b}_d$ deduced from the inverse of the safety factor), and the corresponding feedforward control $u_d = (P_{ext.d}, V_{loop.d})$ is derived. The plasma resistivity is supposed to be known as well as other system parameters. The

equilibrium profiles x_d will be adapted online to take into account the variations of the actuators parameters $f_{ext.d}$ and the reference q_{ref}. We will make use of the relation between the q-profile and the magnetic field B_θ in [107] and of equation IV.15 in chapter 3 [1]. Using the geometric reduction in chapter 3, and the symplectic discretization method in chapter 4, this relation becomes in the chosen approximation spaces:

$$\overline{B}_\theta(z_i,t) = \mathbf{w}^f(z_i)\,\mathbf{b}_d(t) = 2\pi B_{\phi 0} a^2 \frac{z_i}{q_i} \tag{III.3}$$

where q_i denotes the values of q at the position z_i,$B_{\phi 0}$ the toroidal magnetic field intensity at $z=0$ and $\mathbf{w}^f(z_i) = \begin{pmatrix} w_1^f(z_i) & \dots & w_{N-1}^f(z_i) \end{pmatrix}$ the $N-1$ Bessel approximation functions defined in chapter 4, section 2. On the other hand, at the equilibrium $\dot{x}_d = 0$ and the equilibrium profiles must satisfy:

$$\begin{cases} J_1 G_{mg}\mathbf{b}_d + R^{-1}G_{el}\mathbf{d}_d + \mathbf{J}_{ext.d} + \mathbf{J}_{bs.d} &= 0 \\ -J_2 G_{el}\mathbf{d}_d + J_4 V_{loop.d} &= 0 \end{cases}$$

$$\Rightarrow \begin{cases} \mathbf{d}_d = \begin{pmatrix} 0 & (J_2G_{el})^{-1}J_4 \end{pmatrix} \begin{pmatrix} P_{ext.d} \\ V_{loop.d} \end{pmatrix} \\ \mathbf{b}_d = \underbrace{-(J_1G_{mg})^{-1}\begin{pmatrix} f_{ext.d} & R(t)^{-1}J_2^{-1}J_4 \end{pmatrix}}_{C(t)} u_d - (J_1G_{mg})^{-1}\mathbf{J}_{bs.d} \end{cases} \tag{III.4}$$

From (III.3) and (III.4), the feedforward control is therefore:

$$\begin{pmatrix} P_{ext.d} \\ V_{loop.d} \end{pmatrix} = \left(\begin{pmatrix} \mathbf{w}^f(z_1) \\ \mathbf{w}^f(z_2) \end{pmatrix} C(t) \right)^{-1} \times 2\pi \left(B_{\phi 0} a^2\right) \begin{pmatrix} z_1/q_1 \\ z_2/q_2 \end{pmatrix} \tag{III.5}$$

Remark 16. In practice, for the Tore Supra WEST case where the shape $f_{ext}(x,u)$ depends on control signal P_{ext}, an iterative loop is used at each time step to solve equation (III.5). This "loop" allows (also in the presence of disturbances and/or model deviations) to build reachable references and actuators requesting in steady state. However, there is no guarantee that the actuator requests based on the computation of both the feedforward and the feedback parts of the control law will be compatible with the system limitations during the transient phase (references tracking) or in case of disturbance.

III.3 Controller tuning

In the sequel, a non-linear "proportional" feedback control is proposed. The desired energy $\mathbb{H}_d = \mathbb{H} + \mathbb{H}_a$ is assumed to be the usual a quadratic form:

$$\mathbb{H}_d = \frac{1}{2}X^T\mathcal{Q}_d X = \frac{1}{2}X^T(\mathcal{Q}+\mathcal{Q}_a)X \tag{III.6}$$

with $X = x - x_d$ the state error and $\mathcal{Q}_d = \mathcal{Q}_d^T > 0$ (in such a way that $\mathbb{H}_d$ satisfies the integrability, equilibrium and stability conditions (II.6-II.8)). Two controller proposals are carried out in the sequel. The first one corresponds to a choice as simple as possible for the static damping assignment $\mathcal{R}_a$ (time-invariant) and the energy shaping $\mathcal{Q}_a$, derived from the matching equation (III.7). Nevertheless, this approach admits a large uncertainty on the designed $\mathcal{R}_a$ and do not handle the actuator saturation nor some MHD instability condition for the system itself. Hence, in the second proposal, an optimal criterion defined on the safety factor error and which handle the actuator capacity is figured out in order to deduce a smarter choice for the IDA-PBC parameters.

III.3.1 IDA-PBC simple choice: energy shaping and damping assignment

In the following, we choose $\mathcal{J}_a = 0$ since the interconnection structure $\mathcal{J}_d$ doesn't modify the convergence speed of the system total energy $\mathbb{H}_d$ in equation (II.3). The matrix $\mathcal{Q}_a$ shapes the

[1] when the toroidal magnetic flux Φ is assumed approximately constant, it takes the average value: $\Phi = -1/2 B_{\phi 0} a^2 z^2$ (cf. [107] or [10, p.255])

total energy storage function $\mathbb{H}_d$ of the closed loop system, while $\mathcal{R}_a$ plays the role of adding dissipation.

Since the initial system has dissipation $\mathcal{R}$ only on the electric field domain (linked to the first variable **d**), it's possible to add dissipation on the other field (linked to the second magnetic domain whose state is described by the variable **b**), via the matrix $\mathcal{R}_a$ by using the form $\mathcal{R}_a = \mathcal{R}_a^T = \begin{bmatrix} 0 & 0 \\ 0 & R_a \end{bmatrix}$, $0 \leqslant R_a \in \mathbb{R}^{n\times n}$ where R_a is chosen to be a diagonal matrix (damping on the whole system state) or eventually only has some non zero diagonal values corresponding to the two reference positions z_1 and z_2. The higher the value of $\mathcal{R}_a$ is, the faster the system will converge. However, the input power limitation on the loop voltage V_{loop} doesn't allow to set a huge value for $\mathcal{R}_a$.

The choice of $\mathcal{Q}_a$ is more complicated. The only condition to be satisfied is $\mathcal{Q}_d = \mathcal{Q} + \mathcal{Q}_a > 0$. One can refer to section 3 in [78] for a detailed discussion about how to choose $\mathcal{Q}_a$ so-that the matching equation could be (fully or partially) satisfied. An arbitrary choice of $\mathcal{Q}_a$ will anyway give an equivalent control signal by applying (II.5). However, the control law in this case doesn't fulfill the matching equation ($II.4$). This also means that the static feedback transforms the original system (II.1) into the desired one (II.2) with an unknown error coming from the matching equation error. Thus , nothing guarantees the existence of a control law agreeing with a particular choice of IDA-PBC parameters.

One of the approximating solutions proposed in [78] is to pre-multiply the matching equation (III.7) with the left annihilation $g^\perp$ of g_d (i.e. such that $g_d^\perp g_d = 0$), and to choose $\mathcal{Q}_a$ as the solution of the "linear" equation:

$$0 = \quad g_d^\perp g_d \delta u \quad = \quad g^\perp \left(\left[\mathcal{J} - (\mathcal{R} + \mathcal{R}_a) \right] \mathcal{Q}_a X - \mathcal{R}_a \mathcal{Q} X \right) \tag{III.7}$$

One should remark that $\mathcal{Q}_a$ defined in this way is time-dependent due to its dependence with $\mathcal{R}(z,t)$.

III.4 Simulation results

In the simulations, the presented IDA-PBC controller is tested first with a simple model of the Tore Supra WEST tokamak (from the CEA/Cadarache, see [107]) and then with the RAPTOR code developed for the TCV tokamak (cf. [30, 29]). The electronic temperature profile of the plasma is computed using a static *0D* model (with an analytic spatial distribution expression) in the Tore Supra WEST simulation and a thermal diffusion model in the RAPTOR/TCV case. The plasma resistivity mainly depends on this temperature whereas the bootstrap current is a function of its gradient.

Remark 17. The output signals are defined differently according to each system. They depends on the available measures of each Tokamak. In the WEST Tore Supra tokamak, both the safety factor q-profile and the plasma current at the boundary I_p ($\sim 1/q(z=1)$) are considered. In TCV, all the measures are based on the q-profile.

Different simulation scenarios - related to the "experimental reality"- are set up for the two tokamaks.

III.4.1 Results for the Tore Supra WEST configuration

The current-drive heating source is provided by Low-Hybrid (LH) launchers following non-linear scaling laws (given in [107]) and the plasma resistivity is computed using a non-linear model (also from [107]). The other plasma parameters can be found in appendix A or in [19].

Two reference values for the q-profile at the two extremities are considered as control objectives: q_1 at $z_1 = 0.001$ and I_p (which equivalently force the value of q_2) at $z_2 = 1$. Two separated step references of I_p at $t = 7s$ and q_1 at $t = 13s$ are used to illustrate the behaviour of this control law. The simulation results associated with the choices of $\mathcal{R}_a$ et $\mathcal{Q}_a$ discussed in the previous section are figured out.

First of all, since the system is naturally dissipative, we have the convergence of the open-loop system with the feedforward control (see figure III.1). The desired reference is reached at the

steady state. The response time is decreased by the feedback control action via non zero $\mathcal{R}_a$ and $\mathcal{Q}_a$ matrices (see figure III.2).

However, with the step references for I_p and q_1, the closed loop system with a large damping $\mathcal{R}_a$ over-responds to the sudden changes and produces impulses of P_{ext} and V_{loop} (figure III.2). A low-pass filter is therefore necessary and will be applied on the references to avoid this phenomenon. The different response times between I_p and q_0 illustrate the timescale effects of the different actuators. The boundary control action can immediately have an effect on the conjugated boundary output, whereas the distributed action needs, more time to affect the system state at the center. The integrator is not employed in this example since the small static error is neglected (it is indeed in this case negligible when compared to the uncertainty in the q-profile measurement).

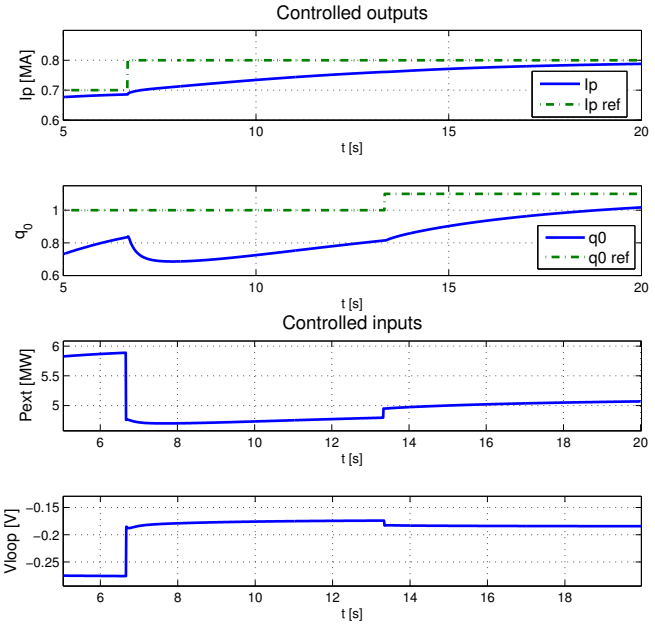

Figure III.1: Open loop system with only the feedforward part of the controller

III.4.2 Results for the TCV configuration

Two ECCD/ECRH clusters[2] (see chapter 2, section 1 for more details) are used to generate both the non-inductive current and the external heating source. The first one is used as a co-current source (to increase the total plasma current) and the second one as a counter-current source (to decrease the total plasma current). Both clusters are also used as external heating sources and are configured with their own profile shapes. Therefore distributed control actions have the forms:

$$\begin{aligned} J_{ext} &= f_{ext}P_{ext} &= f_{ext}\left(P_A - P_B\right) \\ S_{heat} & f_{heat}P_{heat} &= f_{heat}\left(P_A + P_B\right) \end{aligned} \tag{III.8}$$

The total heating source P_{heat} is kept unchanged during the plasma discharge in this section. We also consider that all the states are measurable or computable from measurements. Unlike in the case of the tokamak Tore Supra WEST, one can "correctly" estimate the whole profile of q in TCV.

[2]The details for the TCV actuators may also be found in the website https://crppwww.epfl.ch/crpp_tcv.html

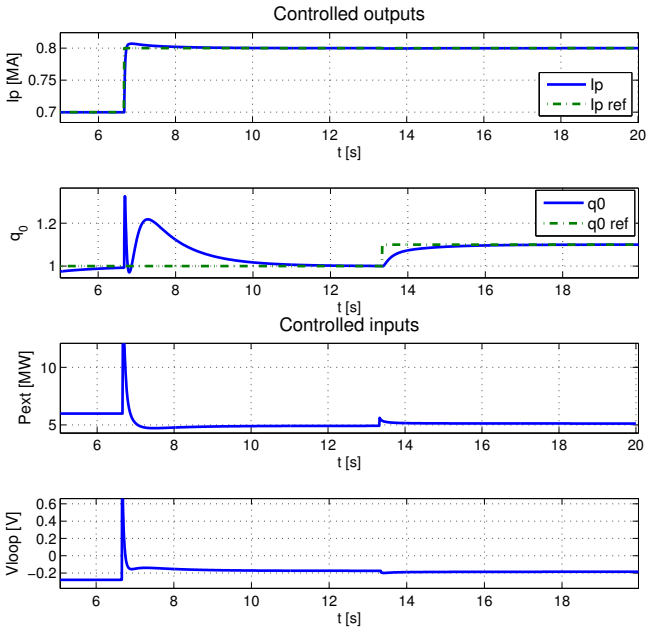

Figure III.2: Closed loop system with the full finite dimensional controller (feedforward and feedback parts)

From MHD stability and confinement considerations, it is desirable to keep the q-profile near the center as flat as possible. Therefore, two reference values for the safety factor q are defined at the radial relative coordinates $z_1 = 0.1$, and $z_2 = 0.4$ which are in the interesting zone. The feedforward calculus gives u_d as well as the reference profile q_d (corresponding to the two reference values and taking into account actuator limits). The IDA-PBC control determines the feedback signal δu from (II.23) to correct the error X.

Remark 18. In the TCV case, the output q-profile determined by RAPTOR is based on a finite element discretization method of the resistive diffusion model, while the one in our model comes from a symplectic geometric method (see chapter 4). This explains the non-perfect match of two q-profiles showed in the results figures. In other words, even in the best case there's still a q-profile error between the two profiles computed with the two different models. The controller objective is however only to regulate q at the two chosen positions (and only give the best possible approximation of the q-profile elsewhere).

In the figure III.3, the reference q profile is set with the values at the two points $z = 0.1, 0.4$ as $q_a = (0.85, 1.25)$. The heating power is switched on at $t = 0.2s$, the feedback control starts at $t = 0.45s$. Then at $t = 1.2s$, the reference is changed to the new desired profile $q_b = (1, 1.25)$. We denote *error* 1, 2 the gaps between q and q_{ref} profiles at two considered positions.

Since the system is naturally dissipative, the feedforward in figure III.3.a shows the convergence of the opened-loop system. Thanks to the re-computation of the equilibrium profile as in (III.4) at each step time, the q-profile reaches a steady state which is quite closed to the reference values. In figure III.4 and III.5, the response time is decreased by the feedback effect via the $\mathcal{R}_a$ damping and the $\mathcal{Q}_a$ energy shaping.

It's important to note that, in general the feedback effect does not significantly acts on the considered particular positions. It does ameliorate the whole q- profile when more damping assignment is added (see figure III.4 and III.5), although the control strategy is only based on two reference points of q- profile.

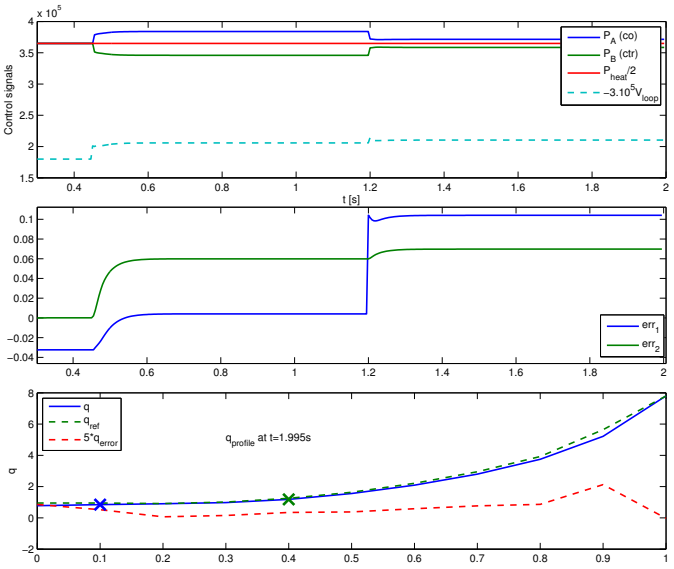

Figure III.3: Open-loop response with feedforward control

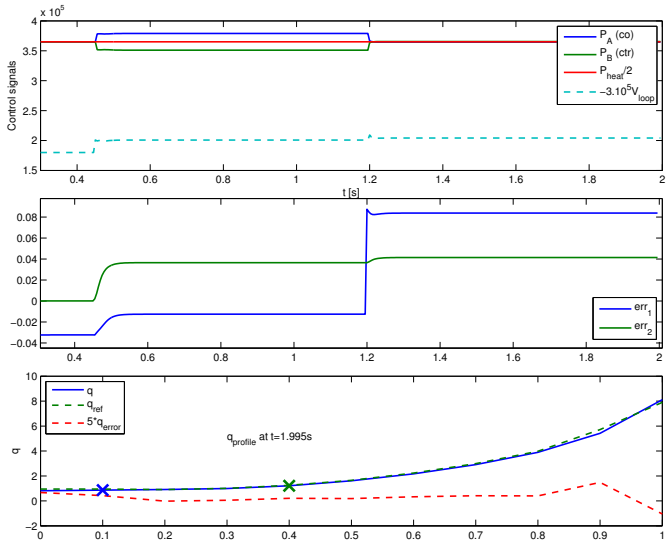

Figure III.4: The response of the closed loop system with an IDA-PBC controller and a small damping $\mathcal{R}_a$

Since there are always static errors caused by the approximations in the linearization (see subsection II.4) of the actuator distribution profile and in the state estimation in (III.8), an integrator is added to the studied scenario and results are shown in figure III.6.

Remark 19. The errors on the q-profile at the two considered positions are totally eliminated after $0.5s$. However, it is "expensive" in term of controller energy to compensate the gap on the two values of the q-profile below 0.05. Furthermore, P_A can't be technically set under the power of $150\,KW$ and consequently the absolute convergence seen in figure III.6 is unreachable in the reality. On the other hand, a small error on q-profile doesn't lead to a significant change in the behavior of the whole system.

In the figure III.7, two disturbances are added. An error of 0.5η is added on the measured resistivity at $t = 0.65s$ and an error of $0.5 f_{ext}$ is added on the estimated actuator profile at $t = 0.9s$. These perturbations are effectively rejected. As expected, the loop voltage V_{loop} predominantly

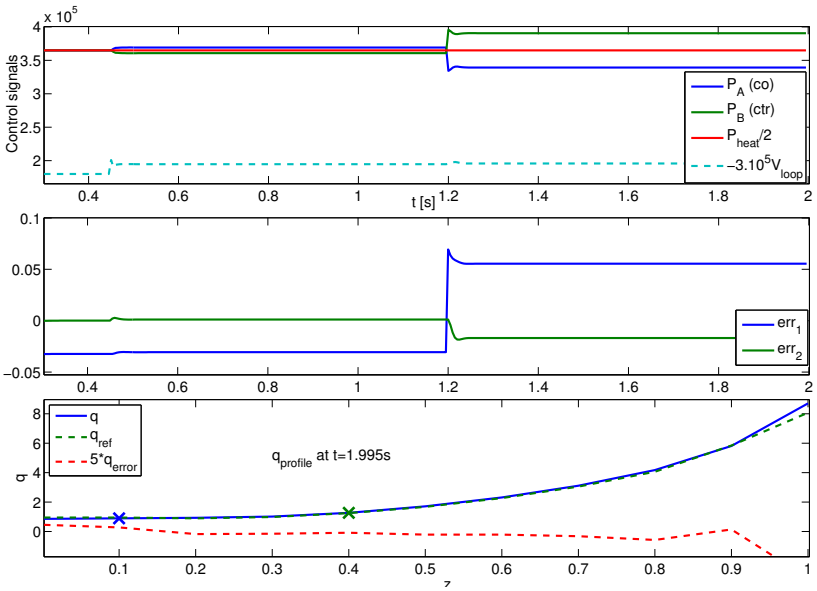

Figure III.5: The response of the closed loop system with an IDA-PBC controller and a larger damping $\mathcal{R}_a$

corrects the perturbation on resistivity while the external current source is used to compensate the distributed error on the current profile.

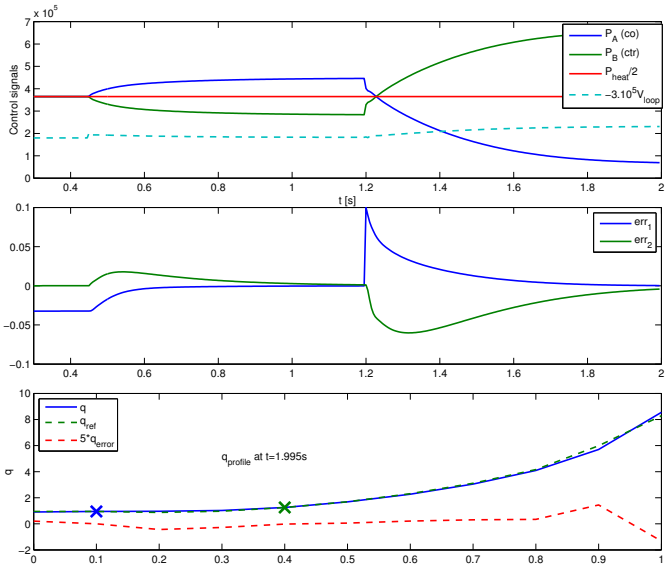

Figure III.6: Closed loop system with IDA-PBC controller with integrator effect

III.5 Experimental result

The IDA-PBC control with the simple damping and energy shaping in subsection III.3.1 was implemented on TCV Tokamak. The real experimental data are compared to the simulation one in the figure III.8. The test scenario is set as the same as our previous simulation in the subsection III.4.2.

The controller reacted as predicted in the first period around $0.5s$. The average control values are consistent with the simulation result for all P_A, P_B and V_{loop}. Unfortunately one of the cluster (the

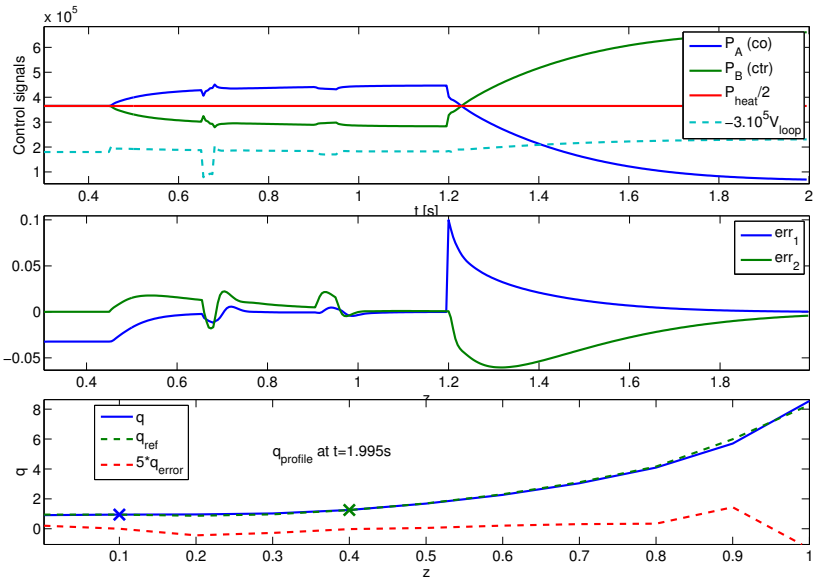

Figure III.7: Closed loop system with IDA-PBC controller (with the integrator) with perturbations on the resistivity and on the actuator spatial distribution

co-current source, cluster A) stopped working at $t = 0.8s$. From then we lost the control efficiency as the controller wasn't informed about this accident. However, the closed loop control at least acts in the "good direction" (using cluster B only) when q_{ref} profile reference changed until the end. We can remark at $t = 0.8s$, when P_A was cut off, the simulation realized the variation of q-profile, then reacted on $P_{B.sim}$, whilst in practice, it seemed that the controller didn't figure out the change. It maintained P_B until the reference moved to the new profile. One of the unexplained observation is that the real controller P_B responded more slowly than in simulation, even in comparing to the beginning of the feedback at $t = 0.45s$. It may come from the actuator performance itself.

The q- profile at two considered positions are also showed in the figure III.8. The feedback control is re-simulated based on the experimental average plasma density $\overline{n}$ from the shock 49514. Due to the fact that the control signals are equivalent in two cases, the q-profiles shows no differences but the measure noise between them. Furthermore, the measured values do match quite well the simulation ones.

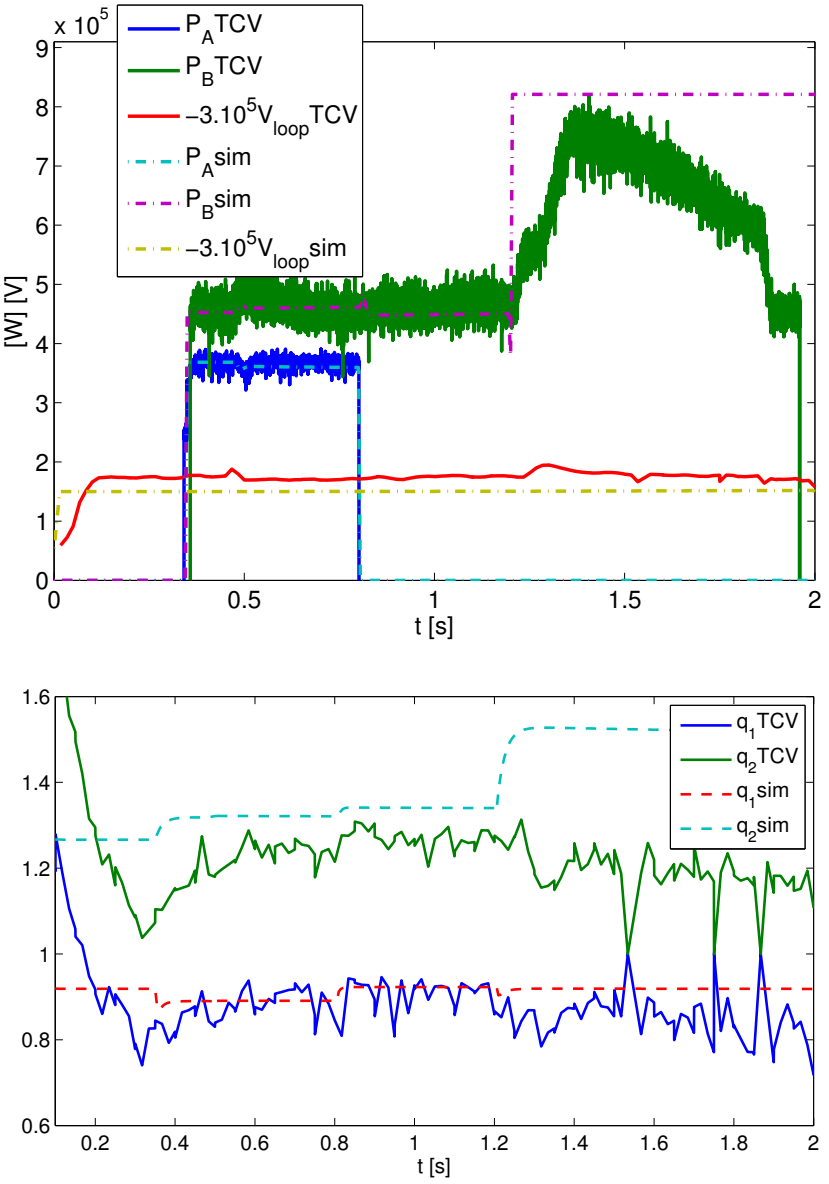

Figure III.8: TCV shock 49514

IV TMHD Coupled system

Actually, the resistive diffusion model used in the previous section is equivalent to the resistive diffusion equation which is widely used as a control model for the plasma (when one tries to regulate the security factor profile, for instance). However, as explained in chapter 2, section IV, the influence of the temperature T on certain parameters in electromagnetic domain, such as the resistivity $\eta(T)$ and the bootstrap non-inductive current $J_{bt}(\partial_z T)$, is not negligible. The MHD couplings between the electromagnetic and thermal domains are presented in chapter 2 in the irreversible entropy source term and in the bootstrap current source.

Therefore, a coupled control model made with the resistive diffusion submodel and the thermal diffusion submodel, is investigated hereafter. This finite dimensional control model is obtained with the coupling of the two finite dimensional approximations from the two diffusion models, using two geometric reduction schemes. Again, a feedforward control will be used to guarantee the compatibility of the designed control with the actuator constraints. Then, an IDA-PBC feedback law will be synthesized using the the linearized error system.

As the result of adding the thermal diffusion submodel, a third actuator, the external heating power source P_{heat}, will be involved. Then, due to the under-actuation of the studied system, only the values of the safety factors at three reference points z_1, z_2 and z_3, denoted respectively q_1, q_2 and q_3 will be assigned with the help of the three available control variables V_{loop}, P_{ext} and P_{heat}. However, the corresponding full radial profile reference for q-profile (hence for the state variables of our model) is required in order to define our IDA-PBC state feedback. This profile will be computed by taking into account at the same time the actuation constraints and the TMHD couplings. This procedure leads to an achievable steady state for the feedback design and, on the other hand, transforms the feedback design into a linearized IDA-PBC feedback control problem. The obtained numerical results are validated with the RAPTOR code.

IV.1 TMHD control system

The first resistive diffusion submodel is recalled in equation (III.1) in the previous section. The second submodel is the discrete thermal model derived from the *1D* port-Hamiltonian thermal diffusion model (V.3) (in chapter 4, section V), using the same discretization methodology as for the resistive diffusion submodel. This finite-dimensional approximation reads:

$$\begin{pmatrix} \partial_t \mathbf{e}_{ex} \\ 0 \end{pmatrix} = \left[\begin{pmatrix} 0 & J_{T1} \\ J_{T2} & 0 \end{pmatrix} - \begin{pmatrix} 0 & 0 \\ 0 & R_T^{-1} \end{pmatrix} \right] \begin{pmatrix} G_T \mathbf{e}_{ex} \\ \mathbf{f}_q \end{pmatrix} + \begin{pmatrix} \overline{S} \\ J_{T4} T_1 \end{pmatrix}$$
$$\mathbb{H}_T = \frac{1}{2} \mathbf{e}_{ex}^T \mathcal{Q}_T \mathbf{e}_{ex} \tag{IV.1}$$

where $\mathbf{e}_{ex}$, $\mathbf{f}_q \in \mathbb{R}^{N\times 1}$ are respectively the time dependent coefficients of TD_ts and of the heat flux f_q. The matrices J_{T1}, $J_{T2} \in \mathbb{R}^{N\times N}$ with $J_{T1} = -J_{T2}^T$ are obtained from the reduction of the spatial derivation operator ∂_z in the chosen finite dimensional spatial approximation bases. $\mathcal{Q}_T \in \mathbb{R}^{N\times N}$ is the positive definite matrix obtained from the discretization of the constitutive relation for the energy (i.e. between e_{ex} and T) and $R_T \in \mathbb{R}^{N\times N}$ is the thermal resistivity approximation which depends on the thermal diffusion coefficient χ. This thermal diffusivity coefficient (in our model) is used to write the dissipative constitutive relation between the thermal force F and the heat flux f_q. $J_{T4} \in \mathbb{R}^{N\times 1}$ is related to the boundary coefficient, T_1 is the fixed value of the average temperature at the boundary and $\mathbb{H}_T$ is the thermal energy.

Note that the PCH model for the thermal diffusion (IV.1) is given in implicit form only, since there's only one balance equation for the entropy. The second equation (used to close the constitutive equation with the skew-adjoint operator to form the Dirac structure) is the dissipative relation giving the thermal force.

The aggregation of the resistive diffusion and the heat transport submodels results in the finite dimensional TMHD model:

$$\begin{pmatrix} \partial_t \mathbf{d} \\ \partial_t \mathbf{b} \\ \partial_t \mathbf{e}_{ex} \\ 0 \end{pmatrix} = \left(\begin{bmatrix} -\begin{pmatrix} 0 & J_1 \\ J_2 & 0 \end{pmatrix} & 0 \\ 0 & \begin{pmatrix} 0 & J_{T1} \\ J_{T2} & 0 \end{pmatrix} \end{bmatrix} - \begin{bmatrix} \begin{pmatrix} R^{-1} & 0 \\ 0 & 0 \end{pmatrix} & 0 \\ 0 & \begin{pmatrix} 0 & 0 \\ 0 & R_T^{-1} \end{pmatrix} \end{bmatrix} \right) \times$$
$$\times \begin{pmatrix} G_{el}\mathbf{d} \\ G_{mg}\mathbf{b} \\ G_T \mathbf{e}_{ex} \\ \mathbf{f}_q \end{pmatrix} + \begin{pmatrix} -f_{ext} P_{ext} - \mathbf{J}_{bs} \\ J_4 V_{loop} \\ \overline{S} \\ J_{T4} T_1 \end{pmatrix} \tag{IV.2}$$

which is written in the (implicit) PCH-like form:

$$\begin{pmatrix} \dot{x} \\ 0 \end{pmatrix} = [\mathcal{J}(x) - \mathcal{R}(x)] \begin{pmatrix} \partial_x \mathbb{H} \\ \mathbf{f}_q \end{pmatrix} (x) + gu \tag{IV.3}$$

where $\mathcal{J} = -\mathcal{J}^T$ is a skew-symmetric interconnection matrix defining a corresponding Dirac structure while $\mathcal{R} = \mathcal{R}^T \geqslant 0$ is a symmetric positive semi-definite dissipation matrix which is nonlinearly depending on the state variables. The total energy function or Hamiltonian is simply the sum of electromagnetic and thermal energy: $\mathbb{H} = \mathbb{H}_{EM} + \mathbb{H}_T$. As a consequence of this port-Hamiltonian representation for the TMHD model, the IDA-PBC approach for nonlinear control may be applied

to the whole interconnected model as it was already the case for the electromagnetic part of it (equivalent to the resistive diffusion model).

The control of the interconnected system (resistive diffusion and thermal diffusion equations) is expected to take advantage of the explicit state space representation of the TMHD coupling analysis to improve the control performance through a better parameter estimations for the resistivity R (via a good approximation of $\eta(T_e)$ and of the bootstrap current $J_{bs}(T_e, \partial_z T_e)$), as well as for the thermal resistivity R_T (via the diffusion coefficient $\chi(\partial_z T, B)$).

Besides, the control actions are assumed to satisfy specific shapes (radial distribution) via the functions f_{ext} and f_{heat} (namely Gaussian distributions in the studied case). Therefore control variables are the scalar total external current power P_{ext} and heating power P_{heat}. As discussed in subsection II.4, this implies that only a limited set of equilibrium states $x_d = (\mathbf{d}_d, \mathbf{b}_d, \mathbf{e}_{ex})^T$ are reachable. Thus a feedforward control will be designed first which leads to a reachable steady state for which the closed loop convergence of the feedback diffusion system may be obtained via an IDA-PBC controller. Previously, a feedforward control $(P_{ext}, V_{loop})_d^T$ has been proposed to achieve the regulation for two reference points of the safety factor profile: at the center and at the boundary. Here, using the interconnected TMHD model will allows us to add a third reference point of q by the use of the new control action P_{heat}.

IV.2 Steady state generation for coupled TMHD model

The steady state x_d of (IV.2) satisfies:

$$\begin{cases} J_1 G_{mg} \mathbf{b}_d + R^{-1} G_{el} \mathbf{d}_d + f_{ext} P_{ext} + \mathbf{J}_{bs} &= 0 \\ -J_2 G_{el} \mathbf{d}_d + J_4 V_{loop.d} &= 0 \\ J_{T1} \mathbf{f}_{qd} + \overline{S} &= 0 \\ J_{T2} G_T \mathbf{e}_{ex} - R_T^{-1} \mathbf{f}_{qd} + J_{T4} T_1 &= 0 \end{cases} \tag{IV.4}$$

The following points could be noticed :

- The input signal T_1 is assumed constant in these equilibrium equations ($T_1 = 0$ for instant)
- The source term $\overline{S}$ includes the Joule effect $S_{Joule} = \eta J_{tot}(J_{tot} - J_{ni})$ (where J_{tot} is the total current density) and the external heating source S_{heat} which is controlled by the heating power P_{heat}.
- The TMHD couplings - including the terms $J_{bs}(B_\theta, T, \partial_z T)$, $\eta(T)$, and $\chi(\partial_z T, B_\theta)$ - are estimated by empirical analytic expressions given in chapter 3, section 4. With the assumption that the thermal steady state for T and $\partial_z T$ are quickly established and also assuming a constant particle density n, we can deduce from these expressions the following values for:
  - the resistivity coefficient :
  $$\eta(T) = C_\eta(\mathbf{b})\, T^{-3/2}$$
  - the thermal diffusion coefficient:
  $$\chi(\partial_z T, B_\theta) = C_\chi(\mathbf{b})\, \partial_z T$$
  - the discrete bootstrap current:
  $$\begin{aligned} \mathbf{J}_{bs} &= \frac{1}{\mathbf{b}} \left(\beta_1 \mathbf{e}_{ex} + \beta_2 R_T^{-1} \mathbf{f}_q\right) \\ &= \frac{1}{\mathbf{b}} \left(\beta_1 (J_{T2} G_T)^{-1} + \beta_2\right) (J_{T1} R_T)^{-1} \overline{S} \\ &= \frac{1}{\mathbf{b}} \left(\beta_1 (J_{T2} G_T)^{-1} + \beta_2\right) (J_{T1} R_T)^{-1} (S_{Joule} + S_{heat}) \end{aligned} \tag{IV.5}$$

    The Joule effect S_{Joule} may be considered as a measurable output assuming that the total current and the external non-inductive current are known. It's also one of the MHD couplings but in practice, it is negligible when compared to the external heating source. S_{heat} is given by the analytic expression $f_{heat} P_{heat}$ where f_{heat} is a chosen (known) Gaussian function of z which is a characteristic of the used actuator.

Due to the different orders of magnitude between T and $\mathbf{b}$ and to the fact that only small variations of the magnetic field are considered, the dependence of the bootstrap current, the plasma resistivity and the thermal diffusion coefficient with the magnetic field may be neglected. This allows a linearization for the feedforward computation, using, for the computation of these quantities, the measurement of the magnetic field instead of the foreseen reference $\mathbf{b_d}$. It has to be noticed however that doing so, the stabilization with the state feedback control will be obtained only locally, when the requested references will be close enough from the system initial state values.

Remark 20. One can remark that only the influence from the thermal domain to the electromagnetic one is represented and not the opposite sense. This choice however is justified by the assumption in chapter 3, section II.2 that the diffusion time-scales of each domain are separated by several orders of magnitude. The temperature establishes thousand times faster than the magnetic field does. In consequence, the magnetic field can be considered as "static" in the computation of the MHD couplings.

Finally, the feedforward is deduced from the steady state equation (IV.4) using the relation between the safety factor q and the magnetic state $\mathbf{b}$ in equation (III.3). The obtained feedforward u_d is:

$$\begin{pmatrix} P_{ext} \\ (P_{heat})^{3/2} V_{loop} \\ P_{heat} \end{pmatrix}_d = \left(\begin{pmatrix} w^f(z_1) \\ w^f(z_2) \\ w^f(z_3) \end{pmatrix} C \right)^{-1} \times \begin{bmatrix} 2\pi \left(B_{\phi 0} a^2\right) \left(\frac{z_1}{q_{1d}}, \frac{z_2}{q_{2d}}, \frac{z_3}{q_{3d}} \right)^T \\ + \begin{pmatrix} w^f(z_1) \\ w^f(z_2) \\ w^f(z_3) \end{pmatrix} (J_1 G_{mg})^{-1} C_{bs.d} S_{Joule} \end{bmatrix} \tag{IV.6}$$

where $C = -(J_1 G_{mg})^{-1} \begin{pmatrix} f_{ext} & C_R J_2^{-1} J_4 & C_{bs} f_{heat} \end{pmatrix}$; $C_R = R/(P_{heat})_d^{3/2}$, while z_1, z_2, z_3 are the three positions of the three references q_{1d}, q_{2d}, q_{3d} for the safety factor.

The feedforward control is thus derived from the steady state for the system obtained by the linearization at each time step of the non-linear parameters R, R_T, G_T and J_{bs}. The feedback control is then required not only to increase the convergence speed but also to overcome the errors caused by the linearization assumptions.

IV.3 Controller tuning

The interconnected system naturally converge to its equilibrium thanks to the two dissipations represented by the dissipation matrices R and R_T. We decide to preserve the interconnection structure $\mathcal{J}$ of the original system, hence not modifying the internal dynamical couplings ($\mathcal{J}_a = 0$). Our control design consists in setting $\mathcal{R}_a$ constant such that $\mathcal{R}_d = \mathcal{R}_d^T > 0$ (the desired dissipation rate) and then to determine the shaped Hamiltonian $\mathbb{H}_d$ and the feedback signal δu with the help of the matching equation (III.7) and the integrability, equilibrium and stability conditions (II.6-II.8).

The robustness of the controller with respect to two kinds of uncertainties is studied. The first kind of uncertainties are those on the system dissipation $\mathcal{R}$ resulting from poor estimations of the plasma resistivity η and the thermal diffusion coefficient χ. The second kind of uncertainties are related to the linearization assumptions made in the derivation the feedforward control and in the approximation of the bootstrap current $\mathbf{J}_{bs}$.

Briefly, with a choice of supplementary dissipation $\mathcal{R}_a$ such that $\mathcal{R}_d$ is sufficiently large, we can handle these uncertainties (see subsection II.5). Of course, the actuator power saturation will prevent us to compensate very large perturbations. Besides, the designed controller being basically a proportional controller, the choice of large values for the proportional gain may create undesired oscillations and instability for the closed loop system.

IV.4 Simulation

Three reference values for the safety factor q are defined respectively at the radial relative coordinates $z = 0.1$, 0.3, and 0.4. The feedforward calculus gives u_d, the whole reference profile q_d and

the average temperature profile T_d, corresponding to these three references and taking into account the actuators constraints. The IDA-PBC control determines the feedback signal δu from matching equation (II.4) to correct the error X. The IDA-PBC parameters are designed as discussed in the previous subsection, with the choice of $\mathcal{J}_a = 0$ and $\mathcal{R}_a$ such as:

$$\mathcal{R}_a = \begin{bmatrix} \begin{pmatrix} 0 & 0 \\ 0 & R_{a1} \end{pmatrix} & 0 \\ 0 & \begin{pmatrix} R_{a2} & 0 \\ 0 & 0 \end{pmatrix} \end{bmatrix} \tag{IV.7}$$

where the positive diagonal matrix R_{a1} and R_{a2} account for the dampings added in electromagnetic domain and thermal domain respectively. As a particular case one can set only three diagonal values for the matrices R_{a1} and R_{a2} which correspond to three chosen reference positions.

The proposed IDA-PBC controller is tested on the RAPTOR code with the TCV configuration. The simulation results are showed as below.

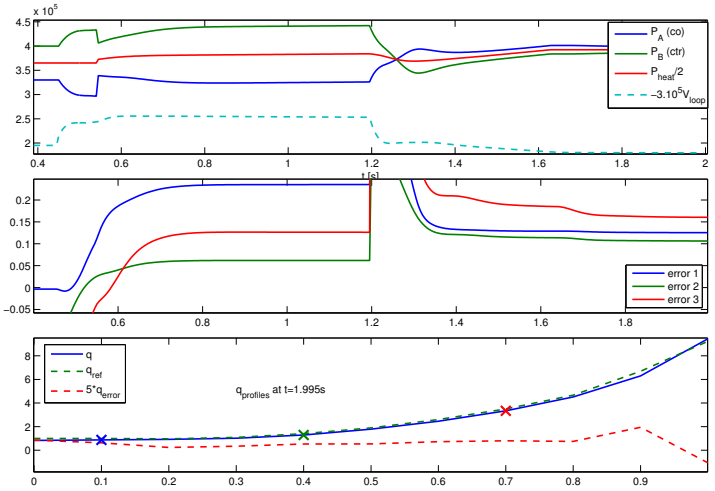

Figure IV.1: Feedforward control of coupled system

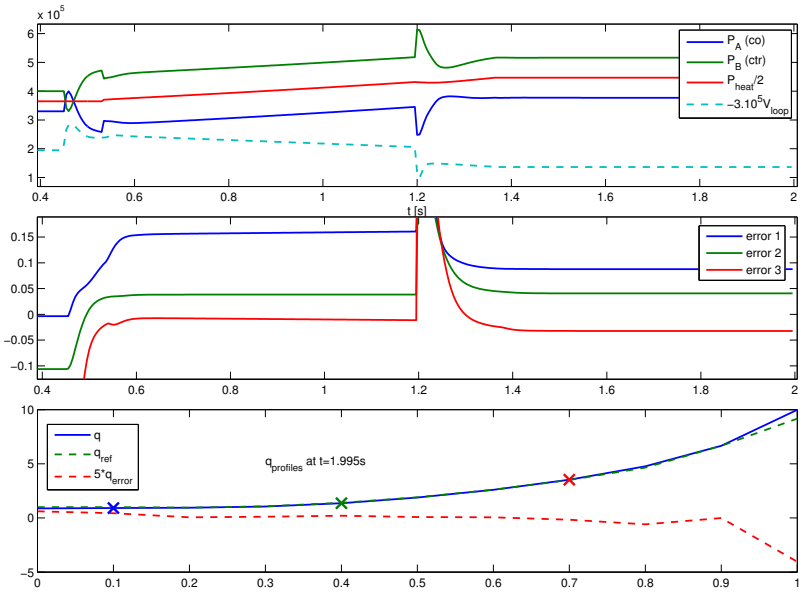

Figure IV.2: Feedback control of coupled system

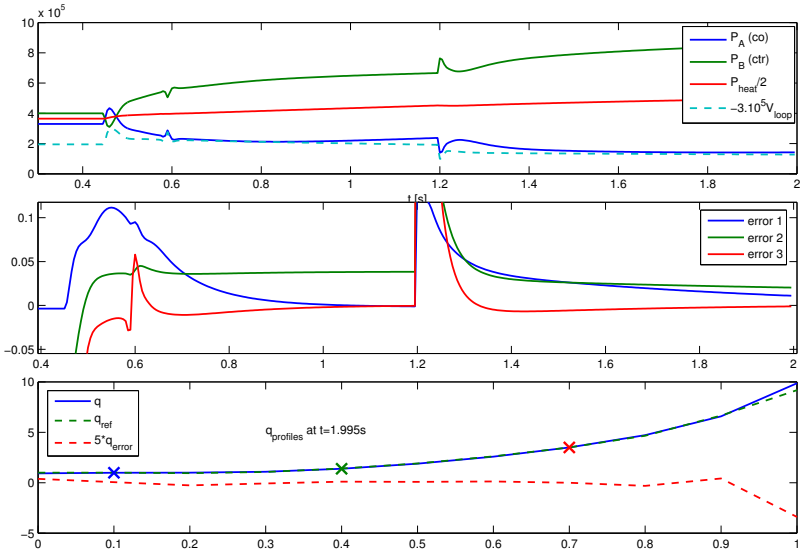

Figure IV.3: Feedback control of coupled system with a supplementary integrator

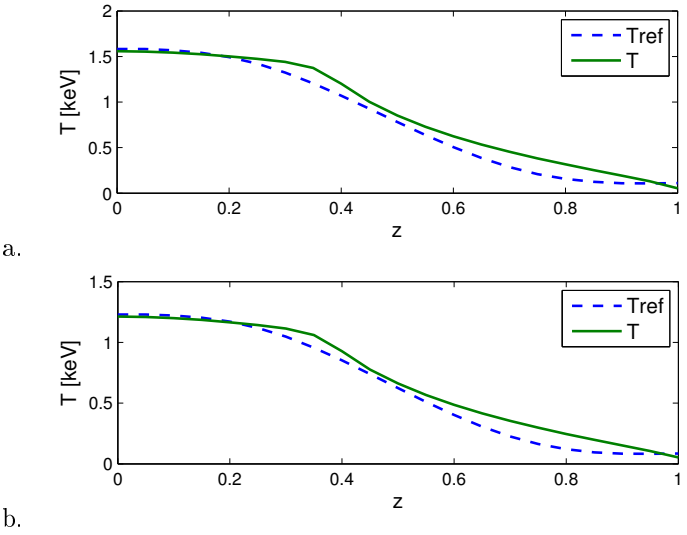

Figure IV.4: T profiles at $t = 0.7s$ (a) and $t = 1.5s$ (b)

Figures IV.1 and IV.2 show respectively the results obtained with the feedforward and the feedback controls. The heating actuator starts at $t = 0.2s$ with the initial values $(P_{ext}, V_{loop}, P_{heat})_{init}$= $(40kW, -0.6V, 300kW)$, whereas at $z = (0.1, 0.3, 0.7)$ the reference q-profile is set as $q_a = (0.85, 1.1, 2.4)$. Then at $t = 0.8s$, the reference is changed to $q_b = (1, 1.4, 3)$.

The feedforward does bring the q profile close to the reference values but the actuator values as well as the q profile oscillate around the equilibrium due to the parameter linearization and approximation. The feedback however makes effort to improve the result by continuing to react significantly on P_{heat}. However, it doesn't succeed in stabilizing the middle reference value for the q-profile. It is mainly regulated by P_{heat}, which continues to increase till the end. An integrator is implanted for the simulation presented in figure IV.3. A signification improvement is obtained for the first and the third points, which are directly affected by P_{ext} and V_{loop}, while P_{heat} makes impact indirectly to the second point via the TMHD couplings J_{bs}. The figure IV.4 shows the temperature profile vs the reference defined by the feedforward control at $t = 0.7s$ and $t = 1.5s$. Although these two profiles are built by two different discretization methods, they still match quite well to each other. On the other hand, these results lead to a discussion about the reference choice:

should we take two reference points for the q-profile and one for the T profile, the latter being directly affected by the heating source S_{heat}. The temperature profile control should be a major challenge in the burn control problem which is among the prospects of this work.

V Conclusion

In this chapter, a IDA-PBC feedback law is presented for the resistive diffusion of the magnetic flux and then for the coupled TMHD model - a set of two interconnected models for the resistive and thermal diffusions inside the tokamak plasma. The control methodology is based on IDA-PBC and the control law is derived from a PCH control model obtained from the geometric/ symplectic discretization of the corresponding coupled PDEs. An integrator is also successfully used in order to eliminate the static errors. The actuator constraints and limitations are taken into account in the equilibrium computation for the feedforward control action. The temperature profile and its influence on the resistivity coefficients are integrated into the control law via the Magneto-Hydro-Dynammics couplings. The controllers have been tested in simulations with the simple model of Tore Supra WEST and with the RAPTOR code, and compared against the experimental data. A convergence has been observed with the computed feedforward and feedback controls. Moreover, in the general case, one can consider the different profiles of the co-current drive and counter-current drive. This fact just leads to a supplement linear calculus to distinguish the actuator P_A and P_B afterward.

Chapter 6

IDA-PBC-like controller for infinite-dimensional PHS

I Introduction

Infinite dimensional port-Hamiltonian systems have recently become more and more popular either in the system theory community as a class of naturally well-posed (linear) systems (cf. [22, 108]) or suitable for control designs based on Casimir Functionals in [91], Control by Interconnection (CbI) in [58] or energy shaping in [53]. On the other hand, IDA-PBC methods have been successful in the control of nonlinear (and linear) finite dimensional Port-Controlled Hamiltonian systems in [78, 88]. It has also been used extensively in the control of finite dimensional PCH systems obtained via geometric spatial reduction of port-Hamiltonian systems, such as in the works on plasma current control for tokamaks developed previously in Chapter 5. Roughly speaking, it makes use of the feedback control to match the original system with a desired system written in the form of a closed loop asymptotically stable Hamiltonian systems.

In this chapter we propose in the first time an extension of this idea to infinite dimensional open port-Hamiltonian systems. More precisely, while keeping the geometrical interconnection structure (namely the Dirac structure) unchanged, we propose energy shaping and damping assignment to match a restricted class of closed loop port-Hamiltonian systems. In order to achieve this result, we need to use the finite rank distributed control in the state equation and the boundary control simultaneously.

In a second time, an IDA-PBC-like controller, similar to the one developed for the finite dimensional case, will be investigated. On one hand, in the infinite dimensional case there are many constraints on the choice of the design "parameters" (more precisely on the closed loop Hamiltonian functional, damping rate and interconnection structure). It's hard to find a general solution to the matching equation which also satisfies these constraints. On the other hand, if the proposed controller does not satisfy exactly the matching equation and the constraints, there is no guaranteed stability for the desired closed loop equilibrium. Therefore we propose hereafter an approximated solution to the matching equation such that the error (with respect to some "exact solution") may be compensated by another boundary control via a "propagation function" (or backstepping control) to be determined. A similar approach is carried out in [50], but in a different context since it is applied to "simple" diffusion or wave equations. In this latter work, the propagation function is referred to as the "k-kernel" used in the Volterra (or "backstepping" in [50]) transformation.

In our application case, the control is used to set the radial profile of the poloidal magnetic flux at some desired closed-loop non-uniform steady-state profile. Both the boundary (magnetic coils) and distributed (antennas) actuators are used. The non-inductive current injection plays the role of the distributed control while the loop voltage creates the boundary action. The distributed control is finite rank since only the total incoming power and the angle for the injected waves are controlled while the radial distribution (shape) of the control action is fixed for a given actuator. Unlike in the "traditional" boundary control methods where the boundary action is homogenized to appear in the system state evolution equation, the feedback distributed control is here used to match a system with an homogeneous state equation (no control term) and a new boundary control

action which includes both the original control and the propagation of the distributed control.

This chapter is organized as follows. In section 2 we define the class of controlled port-Hamiltonian systems, the class of target systems and the resulting matching equation for the control design. In section 3 we apply this idea to the example of the resistive diffusion equation for the poloidal flux in tokamaks. Both distributed non inductive current and boundary loop voltage are used as control variables. Damping assignment is performed in order to achieve some prescribed dissipation and the resulting asymptotic stability. In section 4, the boundary control steps into the IDA-PBC matching equation via the Volterra transformation. Some propositions are discussed to determine the designed parameters. Finally the feasibility of this control is discussed through some simulation examples.

II IDA-PBC control for infinite-dimensional port-Hamiltonian systems

The studied class of infinite dimensional port-Hamiltonian systems is presented in this section. The principle of IDA-PBC control is also adapted for the considered case. In the first time, we propose a simple control design, namely energy shaping and damping assignment for the subclass of linear port-Hamiltonian systems. The stability of the closed-loop system in the sense of Lyapunov is also demonstrated.

II.1 The class of considered original and target port-Hamiltonian systems

We will investigate the control problem for a class of distributed parameters port-Hamiltonian systems with both boundary and distributed finite rank controls defined as:

$$\left\{ \begin{array}{ccc} \dot{x} & = & \left[\mathcal{J}\left(x,t\right)-\mathcal{R}\left(x,t\right)\right]\dfrac{\partial \mathbb{H}}{\partial x}+g\left(x\right)u_1\left(t\right) \\ \left(\begin{array}{c} u_2 \\ y \end{array}\right) & = & \mathcal{B}x \end{array} \right. \tag{II.1}$$

where the "distributed" control u_1 is just a time dependent scalar signal $u_1(t)$. The control map $g(x)$ represents the spatial distribution of this control action. $\mathcal{J} = -\mathcal{J}^*$ is a formally skew-symmetric differential operator (cf. [57] Corollary 3.2). For the sake of simplicity we will consider only a restricted class of spatial operators of the form $\mathcal{J} = P_1\partial_z + P_0$, where $P_1 \in M_n(\mathbb{R})$ is a non-singular symmetric matrix and $P_0 = -P_0^T \in M_n(\mathbb{R})$ is a skew-symmetric one, although this class may be generalized to higher order spatial derivatives such as in [52, 102]. Denoting $\mathcal{Z} = [0;1]$, the spatial domain, the state space or space of configurations is chosen as $x \ni \mathcal{X} = L^2([0,+\infty)\times\mathcal{Z})$. The dissipation is defined using the non negative self-adjoint operator $\mathcal{R} \geqslant 0$, and the total energy stored in the system using the hamiltonian smooth function $\mathcal{H} : \mathcal{X} \to \mathbb{R}$ with

$$\mathbb{H} = \int_{\mathcal{Z}} \mathcal{H} \mathrm{d}V \tag{II.2}$$

where $\mathcal{H}$ is the energy density. $\mathcal{B}$ is a differential operator induced on the boundary $\partial\mathcal{Z} = \{0;1\}$ by the differential operator $\mathcal{J}$ in the sense of the following lemma [57].

Lemma II.1. *Consider a matrix differential operator L and denote by L^* its formal adjoint ([57] definition 3.2). Denote by U, V two sets of smooth functions from $\mathcal{Z}$ to $\mathbb{R}$. Then, for every functions $u \in U$ and $v \in V$, there exists a differential operator $\mathcal{B}_L$ defined on the boundary $\partial\mathcal{Z}$ such that:*

$$\int_{\mathcal{Z}} \left(v^T L u - u^T L^* v\right) dV = \int_{\partial\mathcal{Z}} \mathcal{B}_L\left(u,v\right) dA \tag{II.3}$$

We say that $\mathcal{B}_L$ is the differential operator induced on the boundary $\partial\mathcal{Z}$ by the differential operator L.

For example, if we consider the first order spatial derivative $L = \partial_z$ on the domain $\mathcal{Z} = [a; b]$, forall $u, v \in \mathcal{Z}$, then we get:

$$\int_{\mathcal{Z}} \left(v^T \partial_z u + u^T \partial_z v\right) \mathrm{d}z \quad = \quad \int_{\mathcal{Z}} \left(\partial_z \left(vu\right)\right) \mathrm{d}z \quad = \quad vu|_a^b \tag{II.4}$$

Therefore the boundary operator $\mathcal{B}_{\partial_z}$ induced by $L = \partial_z$ is here simply the evaluation of the inner product $\langle u, v\rangle = uv$ on the boundary $\partial\mathcal{Z} = \{a; b\}$. Such induced boundary operators may be constructed for a larger class of higher-order skew symmetric differential operators. The resulting class of systems of the form (II.1) together with the class of input-output variables which are admissible in order to define a well-posed linear problem and generate a contraction semigroup are defined in [108, 52, 102]. It must be noticed that the class of systems of the form (II.1) includes most classical hyperbolic examples such as wave, membrane, plates and beams equations, shallow water equation, Boussinesq, Korteg de Vries and Navier-Stokes flow equations, Maxwell field equations, etc. but also some parabolic examples as it will be shown hereafter with the plasma poloidal flux resistive diffusion equation.

The purpose of the designed feedback control is to match a target (or "desired") canonical passive port-Hamiltonian system of the form:

$$\left\{ \begin{array}{ccc} \dot{x} & = & \left[\mathcal{J}_d\left(x,t\right) - \mathcal{R}_d\left(x,t\right)\right] \dfrac{\partial \mathbb{H}_d}{\partial x} \\ \begin{pmatrix} \tilde{u}_2 \\ \tilde{y} \end{pmatrix} & = & \mathcal{B}_d x \end{array} \right. \tag{II.5}$$

where $\mathcal{J}_d = -\mathcal{J}_d^*$, $\mathcal{R}_d = \mathcal{R}_d^T \geqslant 0$ are respectively the desired system interconnection and damping operators. The desired closed-loop Hamiltonian $\mathbb{H}_d$ satisfies:

i) *(Equilibrium assignment)*

$$\frac{\partial \mathbb{H}_d}{\partial x}\left(x_d\right) = 0 \tag{II.6}$$

ii) *(Lyapunov stability)*

$$\frac{\partial^2 \mathbb{H}_d}{\partial x^2}\left(x_d\right) > 0 \tag{II.7}$$

$\mathcal{B}_d$ denotes a desired boundary operator which ensures that the couple $(\tilde{y},\, \tilde{u}_2)$ is a passive input-output pair for the target system with respect to the storage functional $\mathbb{H}_d$. Again the definition and parametrization of all admissible passive input-output pairs which lead to a well-posed boundary control system may be found in [53] or [103, 104]. Note that the passivity with the so-called impedance-passive input-output pairs of variables simply results from the energy balance equation which reads (due to the skew-adjoint differential operator $\mathcal{J}_d$ (cf. [57] Corollary 3.2 or lemma II.1):

$$\begin{array}{rcll} \dfrac{d\mathbb{H}_d}{dt} & = & \dfrac{\partial \mathbb{H}_d}{\partial x}^T \dot{x} & \\ & = & \tilde{y}^T \tilde{u}_2 - \dfrac{\partial \mathbb{H}_d}{\partial x}^T \mathcal{R}_d \dfrac{\partial \mathbb{H}_d}{\partial x} & \leq \tilde{y}^T \tilde{u}_2 \end{array} \tag{II.8}$$

Remark 21. Unlike the "traditional" approach which consists in homogenizing the boundary control to embed it in the system state equation and then handling it as a distributed control, the method presented in this work reverses the idea. In other words, the distributed control is used to transform the original system (II.1) into the target canonical port-Hamiltonian system (II.5) with a boundary control (usually not the same as the one in the original system).

Remark 22. A dissipative target port-Hamiltonian system, that is with $\mathcal{R}_d > 0$, is asymptotically stable even with an homogenous boundary condition $\tilde{u}_2 = 0$. Otherwise, when $\mathcal{R}_d \geq 0$ is only positive semidefinite, a simple "boundary damping" injection of the form $\tilde{u}_2 = -K_p \tilde{y}_2$, $K_p > 0$ ensures the stabilization. The matching equation:

$$g u_1 = \left[\mathcal{J}_d\left(x,t\right) - \mathcal{R}_d\left(x,t\right)\right] \frac{\partial \mathbb{H}_d}{\partial x} - \left[\mathcal{J}\left(x,t\right) - \mathcal{R}\left(x,t\right)\right] \frac{\partial \mathbb{H}}{\partial x} \tag{II.9}$$

then determines the "distributed" control $g u_1$.

II.2 Energy shaping and damping assignment for a subclass of linear port-Hamiltonian systems

We will now focus on a particular subclass of linear port-Hamiltonian systems, assuming that the energy function of the original system has the quadratic form $\mathcal{H} = \frac{1}{2}x^T\mathcal{Q}x$ (i.e. the system dynamic is linear) and that the canonical choice $(u_2,\, y_2) = (\partial_x\mathbb{H})\,|_{\partial\mathcal{Z}}$ of boundary input-output impedance-passive variables has been selected [102]. It may happen that the interconnection operator $\mathcal{J}$ has a suitable form which should remain unchanged in the target system. In fact, this is the most common case and the geometric interconnection structure of the actual model should not be changed in the target system unless some specific purposes are given since it affects the structural invariants and intrinsic dynamical behavior of the system. For instance, in the resistive diffusion equation example hereafter, the interconnection operator $\mathcal{J}$ is defined using the derivation operator

$$\mathcal{J}_d = \mathcal{J} = \begin{pmatrix} 0 & 1 \\ 1 & 0 \end{pmatrix} \partial_z \tag{II.10}$$

together with some given boundary conditions (see section 3) and should be preserved since it implies (with a dissipative closure equation) a purely dissipative input-output operator with a spectrum entirely lying on the negative real half-axis in the complex plane. In such cases where the interconnection structure of the actual system must remain unchanged, the target system is obtained by using only "energy shaping" and/or "damping injection":

- $\mathbb{H}_d = \int_{\mathcal{Z}} \frac{1}{2}x^T\mathcal{Q}_d x = \int_{\mathcal{Z}} \frac{1}{2}x^T\left(\mathcal{Q}+\mathcal{Q}_a\right)x = \mathbb{H}+\mathbb{H}_a;\ \mathcal{Q}_d > 0$
- $\mathcal{R}_d = \mathcal{R}+\mathcal{R}_a \geq 0$ with $\mathcal{R}_a = \mathcal{R}_a^T \neq 0$

The new "passive" boundary input (and the corresponding conjugated output) of the target system is determined via the chosen Hamiltonian $\mathbb{H}_d$ and thus may be related with the original system boundary control u_2:

$$\begin{aligned} \begin{pmatrix} \tilde{u}_2 \\ \tilde{y}_2 \end{pmatrix} = \begin{pmatrix} f_\partial \\ e_\partial \end{pmatrix} &= \left(\partial_x\mathbb{H}_d\right)|_{\partial\mathcal{Z}} \\ &= \left(\partial_x\mathbb{H}+\partial_x\mathbb{H}_a\right)|_{\partial\mathcal{Z}} \\ &= \begin{pmatrix} u_2 \\ y_2 \end{pmatrix} + \partial_x\mathbb{H}_a|_{\partial\mathcal{Z}} \end{aligned} \tag{II.11}$$

This new boundary input $\tilde{u}_2$ is thus modified only by the energy shaping $\mathcal{Q}_a$ and not influenced by the damping injection $\mathcal{R}_a$. Furthermore, in the considered linear case exponential stability will be achieved without any supplementary boundary control $\tilde{u}_2$. The stability of the target system may be proved via the first and second Arnold's stability theorems (see for instance [96]) by using a suitable norm. In our case, the norm associated with the energy stored in the target system results in very simple calculations to prove the asymptotic (exponential) stability with respect to this norm. Indeed, assume that the energy function of the target system is the quadratic form $\mathbb{H}_d = \frac{1}{2}\int_{\mathcal{Z}} x^T\mathcal{Q}_d x = \|x\|^2_{\mathcal{Q}_d}$, then $\partial_x\mathbb{H}_d\left(x^*\right) = \mathbb{H}\left(x^*\right) = 0$ at the equilibrium profile $x^* = 0$. Considering no boundary control $\tilde{u}_2 = 0$ in the system (II.5), the energy balance reads:

$$\begin{aligned} \frac{d}{dt}\mathbb{H}_d &= -\frac{\partial\mathbb{H}_d}{\partial x}^T\mathcal{R}_d\frac{\partial\mathbb{H}_d}{\partial x} \\ &= -\int_{\mathcal{Z}} x^T\mathcal{Q}_d\mathcal{R}_d\mathcal{Q}_d x \\ &= -\int_{\mathcal{Z}} x^T\mathcal{Q}_d\left(\mathcal{R}_d\right)^{1/2}\left(\mathcal{Q}_d\right)^{-1/2}\mathcal{Q}_d\left(\mathcal{Q}_d\right)^{-1/2}\left(\mathcal{R}_d\right)^{1/2}\mathcal{Q}_d x \\ &= -\left\|\left(\mathcal{Q}_d\right)^{-1/2}\left(\mathcal{R}_d\right)^{1/2}\mathcal{Q}_d x\right\|^2_{\mathcal{Q}_d} \\ &\leq -\Gamma\|x\|^2_{\mathcal{Q}_d} \end{aligned} \tag{II.12}$$

where $\Gamma = \min\left(\left(\mathcal{Q}_d\right)^{-1/2}\left(\mathcal{R}_d\right)^{1/2}\mathcal{Q}_d\right) > 0$, the minimum positive value of $\left(\left(\mathcal{Q}_d\right)^{-1/2}\left(\mathcal{R}_d\right)^{1/2}\mathcal{Q}_d\right)$ since $\mathcal{Q}_d > 0$, $\mathcal{R}_d > 0$. Then:

$$\frac{d}{dt}\mathbb{H}_d \leq -\Gamma \left\|x\right\|^2_{\mathcal{Q}_d} = -\Gamma\mathbb{H}_d \tag{II.13}$$

which proves exponential stability in the sense of Lyapunov with respect to the energy norm $\|.\|_{\mathcal{Q}_d}$.

The resistive diffusion of plasma poloidal flux in Tokamaks will be used in the next part as an example for the proposed energy shaping and damping assignment control design.

III Damping assignment design for the resistive diffusion equation

We consider in this section a very simple solution of the matching equation for the IDA-PBC control design for the resistive diffusion equation (see chapter 3, section IV). In this problem both the state equation (through the non inductive current source) and the boundary condition (through the loop voltage generated by external coils) are controlled. In the first step, if both the interconnection structure of the model and its Hamiltonian are kept unchanged in the target system, it becomes possible to solve explicitly the matching equation to design the damping assignment through the finite rank distributed control in the state equation.

III.1 Infinite-dimensional PCH formulation for the resistive diffusion equation

Let us recall the port-Hamiltonian formulation of the resistive diffusion equation (refer to chapter 3, section IV) in magnetic toric coordinates. This formulation reads:

$$\begin{cases} \partial_t \underbrace{\begin{pmatrix} \overline{D}_\phi \\ \overline{B}_\theta \end{pmatrix}}_{x} &= \left[\underbrace{\begin{pmatrix} 0 & 1 \\ 1 & 0 \end{pmatrix}\partial_z}_{\mathcal{J}} - \underbrace{\begin{pmatrix} \frac{C_3}{\eta} & 0 \\ 0 & 0 \end{pmatrix}}_{\mathcal{R}}\right] \underbrace{\begin{pmatrix} \frac{1}{\epsilon C_3} & 0 \\ 0 & \frac{C_2}{\mu} \end{pmatrix}\begin{pmatrix} \overline{D}_\phi \\ \overline{B}_\theta \end{pmatrix}}_{\partial_x\mathbb{H}} + \begin{pmatrix} -\overline{J}_{ext} - \overline{J}_{bs} \\ 0 \end{pmatrix} \\ \mathcal{B}\left(\partial_x\mathbb{H}\right) &= \begin{pmatrix} f_\partial \\ e_\partial \end{pmatrix}|_{z=1} = \begin{pmatrix} V_{loop} \\ I_{p1} \end{pmatrix} \end{cases} \tag{III.1}$$

where the flow variables here are $\partial_t\left(-\overline{D}_\phi\right)$, $\partial_t\left(-\overline{B}_\theta\right)$ and $\left(\overline{J}_{ext} + \overline{J}_{bs}\right)$ which correspond to the reduced *1D* variables for the electric intensity flow, the magnetic density flow and the total current density, the latter including the bootstrap current $\overline{J}_{bs}$ and the external current source $\overline{J}_{ext}$. The plasma resistivity η is normally a parameter varying significantly with the plasma temperature. However, since the Thermo-MagnetoHydroDynamic couplings are not considered in this chapter, the plasma resistivity is assumed to be a given spatially non uniform time varying parameter $\eta\left(z,t\right)$. ϵ and μ are respectively considered to be the void permittivity and void permeability (the tokamaks are operating at very low densities). The boundary variables correspond to the total plasma current at the edge I_{p1} and the loop voltage V_{loop} produced by the external electric coils. Note that there's no energy source at the center, hence $f_\partial e_\partial|_{z=0} = 0$. The total electromagnetic energy density is assumed to be a quadratic form:

$$\mathcal{H} = \frac{1}{2}x^T\mathcal{Q}x \tag{III.2}$$

With these assumptions, the PCH model for the resistive diffusion may be turned into the usual PCH form:

$$\begin{cases} \partial_t \begin{pmatrix} x_1 \\ x_2 \end{pmatrix} &= \left[\mathcal{J} - \mathcal{R}\right]\mathcal{Q}\begin{pmatrix} x_1 \\ x_2 \end{pmatrix} + gu_1 \\ \begin{pmatrix} u_2 \\ y_2 \end{pmatrix} &= \mathcal{Q}\begin{pmatrix} x_1 \\ x_2 \end{pmatrix}|_{z=1} \end{cases} \tag{III.3}$$

where $\begin{pmatrix} x_1 \\ x_2 \end{pmatrix}$ and $\begin{pmatrix} u_1 \\ u_2 \end{pmatrix}$ denote the system errors $\delta\begin{pmatrix} \overline{D} \\ \overline{B} \end{pmatrix}$ and feedback control $\delta\begin{pmatrix} P_{ext} \\ V_{loop} \end{pmatrix}$ of the resistive diffusion system in (III.1), and $g = \begin{pmatrix} -f_{ext} \\ 0 \end{pmatrix}$ is the control mapping.

Remark 23. This port-Hamiltonian model (III.3) states the error evolution of the origin system (III.1). The bootstrap current $\overline{J}_{bs}$, not a control signal, is thus taken into account in the feedforward computation.

Remark 24.
- The control gu_1 is not a "fully distributed" action in the sense that it is regulated only by the scalar power $u_1(t)$. Generally speaking (and in the particular case of the Tore Supra actuators, $g(x,t)$ is a function of the system state and time. A feedforward computation is necessary to determine the accessible steady state with respect to the actuator constraint g. The system error (III.3) is then defined using the linearization around the desired equilibrium as in the finite dimensional case.

- The original system (III.3) without the distributed control u_1 has the "usual" form with a Stoke-Dirac interconnection structure. Hence it which satisfies the passivity property (or power balance equation):
$$\frac{d}{dt}\mathbb{H} \leq u_2^T y_2 \tag{III.4}$$

- The system dissipation $\mathcal{R} \geq 0$ is not strictly positive definite but this may be modified by using the distributed control gu_1 (which also allows to improve the convergence speed).

Consequently, if one can prove that there exists a solution u_1 of the matching equation *(II.9)* which can bring the system to the stable target form (II.5), then the convergence speed can be further improved with the boundary control $\tilde{u}_2$. In other words, one determines a feedback control $u_1(t)$ without expliciting the choice of the control parameters $\mathcal{J}_d$, $\mathcal{R}_d$, and $\mathcal{H}_d$, but one only guarantees their existence.

III.2 Controller tuning

We will consider first a simple damping assignment for the error system (III.3), using only the distributed control to modify the system dissipation while preserving the stored energy (i.e. or $Q_a = 0$, no energy shaping). We thus want to perform the matching:

$$\begin{cases} \partial_t \begin{pmatrix} x_1 \\ x_2 \end{pmatrix} &= [\mathcal{J} - \mathcal{R}]\, \mathcal{Q} \begin{pmatrix} x_1 \\ x_2 \end{pmatrix} + g u_1 \\ \begin{pmatrix} u_2 \\ y_2 \end{pmatrix} &= \mathcal{Q} \begin{pmatrix} x_1 \\ x_2 \end{pmatrix} |_{z=1} \end{cases} \tag{III.5}$$

$$\longrightarrow \quad \begin{cases} \partial_t \begin{pmatrix} x_1 \\ x_2 \end{pmatrix} &= [\mathcal{J} - \mathcal{R}_d]\, \mathcal{Q} \begin{pmatrix} x_1 \\ x_2 \end{pmatrix} \\ \begin{pmatrix} u_2 \\ y_2 \end{pmatrix} &= \mathcal{Q} \begin{pmatrix} x_1 \\ x_2 \end{pmatrix} |_{z=1} \end{cases}$$

Let us denote now by $\mathcal{R}_d = \begin{pmatrix} r_1 & r_{12} \\ r_{12} & r_2 \end{pmatrix} > 0$, the desired strictly positive definite damping operator with:

$$\begin{cases} r_1 & > 0 \\ r_2 & > 0 \\ r_1 r_2 - r_{12}^2 & > 0 \end{cases} \tag{III.6}$$

and define $R_1 = \frac{C_3}{\eta}$; $\mathcal{Q} = \begin{pmatrix} Q_1 & 0 \\ 0 & Q_2 \end{pmatrix} = \begin{pmatrix} \frac{1}{\epsilon C_3} & 0 \\ 0 & \frac{C_2}{\mu} \end{pmatrix}$. In this simplest case, the matching of the distributed controller term gu_1 which ensures the desired dissipation $\mathcal{R}_d$ reads:

$$gu_1 = (\mathcal{R} - \mathcal{R}_d) \frac{\partial \mathbb{H}}{\partial x} = (\mathcal{R} - \mathcal{R}_d)\, \mathcal{Q} x \tag{III.7}$$

Therefore, one only has to prove the point-wise existence of this scalar control $u_1(t)$ for all x value. Meanwhile, the boundary control u_2 will be designed to accelerate the convergence of the solution.

The matching equation (III.7) leads to:

$$\begin{pmatrix} -f_{ext} \\ 0 \end{pmatrix} u_1 = \left(\begin{pmatrix} R_1 & 0 \\ 0 & 0 \end{pmatrix} - \begin{pmatrix} r_1 & r_{12} \\ r_{12} & r_2 \end{pmatrix} \right) \begin{pmatrix} Q_1 & 0 \\ 0 & Q_2 \end{pmatrix} \begin{pmatrix} x_1 \\ x_2 \end{pmatrix} \tag{III.8}$$

$$\iff \begin{cases} -f_{ext} u_1 &= (R_1 - r_1) Q_1 x_1 - r_{12} Q_2 x_2 \\ 0 &= r_{12} Q_1 x_1 + r_2 Q_2 x_2 \end{cases} \tag{III.9}$$

One can easily derive from (III.6) and (III.9) the solution:

$$\begin{cases} \dfrac{-f_{ext}}{Q_1 x_1} u_1 = (R_1 - r_1) + r_2 \left(\dfrac{Q_2 x_2}{Q_1 x_1} \right)^2 \\ r_1 > r_2 \left(\dfrac{Q_2 x_2}{Q_1 x_1} \right)^2 > 0 \end{cases} \tag{III.10}$$

with the constraints or "bounds" on u_1:

$$R_1 - r_1 < \frac{-f_{ext}}{Q_1 x_1} u_1 < R_1 \tag{III.11}$$

Once the value of u_1 is determined from the previous inequality for all x, one can ensure the existence of a positive definite damping $\mathcal{R}_d > 0$ (in the case $r_1 > R_1$, a trivial solution is $u_1 = 0$). The original system thus becomes the target system with the energy balance (II.8). Therefore a supplementary boundary damping injection $\tilde{u}_2 = -K_p \tilde{y}_2$, $K_p > 0$ will accelerate the convergence of the closed loop system to the equilibrium 0 (that is the convergence of the real system to the desired state used to design the feedforward control).

III.3 Simulation result

The above IDA-PBC control law is applied to the resistive diffusion model for the plasma. However, this model doesn't stand alone, since it requires the time-variant profiles of resistivity and bootstrap current. The plasma resistivity mainly depends on the temperature whereas the bootstrap current is mainly function of its gradient. For the Tore-Supra WEST configuration and for the considered simulation conditions, these plasma parameters may be found in [19].

Two separated step references of I_p at $t = 7s$ and q_0 (the plasma current at the center $z \approx 0$) at $t = 11s$ are used just like in chapter 5, section III.4.1 to illustrate the behavior of this control law. Comparing to the feedforward in figure III.1, chapter 5, the feedback control u_1, computed from the chosen r_1 and r_2 does indeed decreases the response time (see figure III.1). In fact, it doesn't allow to tune freely u_1 since it should strictly respect the condition (III.11). Nevertheless, the complete feedback control with (u_1, u_2) is showed up in figure III.2. The boundary plasma I_p quickly reach the reference as the boundary control V_{loop} affects directly the conjugated variable I_p. The boundary effect needs more time to propagate to the center, in order to converge q_0.

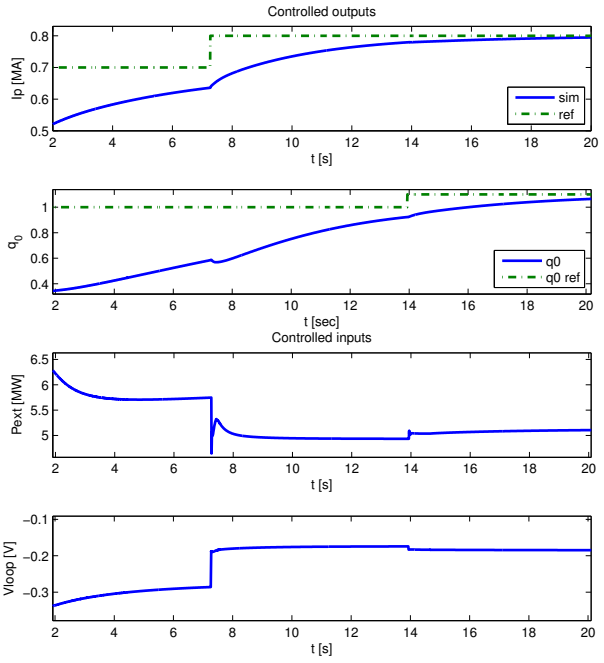

Figure III.1: Feedback with the distributed control u_1

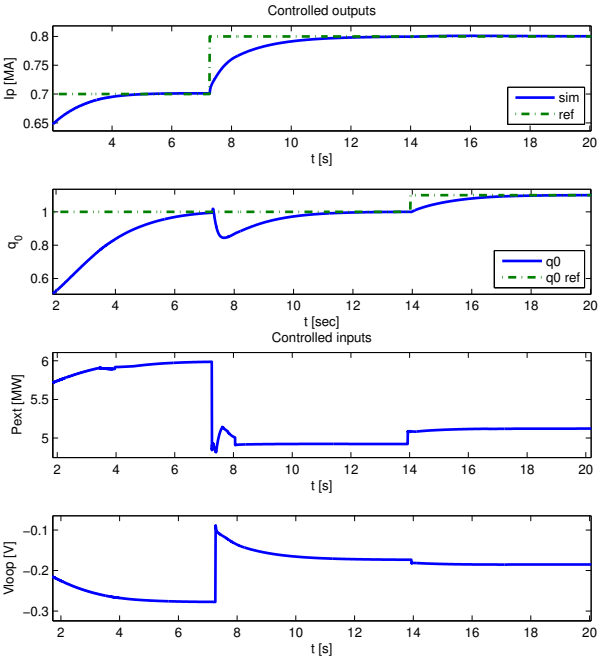

Figure III.2: Feedback with the distributed control u_1 and the boundary control u_2

In term of robustness, the same properties as those already observed for the finite dimensional IDA-PBC may be found here.

Remark 25. Similarly, a "strong" enough boundary damping $\tilde{u}_2 = -k\tilde{y}_2$, $k > 0$ will help to

compensate the disturbance effect ζ on the new conjugated boundary variable couples $\begin{pmatrix} f_\partial \\ e_\partial \end{pmatrix}_d$.

IV IDA-PBC boundary control

In the previous section, the very first and simple damping assignment is figured out as a solution of the IDA-PBC matching equation. When augmenting the solution to interconnection and energy shaping, the solution is far from trivial, among others due to the specific conditions that each "control parameter" ($\mathcal{J}_d$, $\mathcal{R}_d$, $\mathbb{H}_d$) must satisfy. On one hand, one can easily obtain an average solution of matching equation, although it doesn't guarantee the stability of the closed-loop system. On the other hand, the matching equation deduces only the distributed control law, the boundary control being thus still "free" to choose. This leads us to develop the IDA-PBC boundary control framework presented hereafter.

The action of the boundary control may spread into the whole domain and a propagation function will be used in order to stand for this effect. Although this influence is not as rapid and direct as the one from the "real" distributed control, it can somehow correct the error done in the matching equation. In fact, thanks to the Volterra transformation (or backstepping boundary control, according to the terminology in [50]), the system stabilization will be recovered despite of the error in the matching equation with the distributed control action. A relaxation in matching equation solution is thus proposed by using simultaneously the distributed and boundary controls.

IV.1 Average matching equation solutions

How to solve the matching equation (II.9) and how to parametrize the solutions are major concerns in the IDA-PBC literature even for the control design for finite dimensional systems [78]. Since in our case the distributed control is only finite rank, there is no solution in general for the matching equation in the infinite dimensional case. We present hereafter two approaches to "solve" this problem in some approximate senses.

- A first case occurs when there exists an adjoint function $g^\perp$ of g so-that their inner product $\langle g^\perp, g \rangle = 0$, and when two among the three control parameters $\mathcal{J}_d$, $\mathcal{R}_d$, and $\mathbb{H}_d$ are set a priory. Then the third target parameter is the solution of the linear equation:

$$\begin{aligned} 0 &= u_1 \int_0^1 g^\perp g \mathrm{d}z \\ &= \int_0^1 g^\perp \left[\mathcal{J}_d(x,t) - \mathcal{R}_d(x,t)\right] \frac{\partial \mathbb{H}_d}{\partial x} \mathrm{d}z - \int_0^1 g^\perp \left[\mathcal{J}(x,t) - \mathcal{R}(x,t)\right] \frac{\partial \mathbb{H}}{\partial x} \mathrm{d}z \end{aligned} \tag{IV.1}$$

  Note that the parameters set or computed in this way should respect the structural constraints $\mathcal{J}_d = -\mathcal{J}_d^*$, $\mathcal{R}_d = \mathcal{R}_d^T \geqslant 0$. and $\mathcal{H}_d = \mathcal{H}_d^T > 0$. It is not always feasible to guarantee the existence of a solution with these properties. However, it exists for the resistive diffusion equation in the case of some damping assignment control as it is carried out in section III. The idea there is to restrict sufficiently the class of admissible target systems.

- A second approach consists in solving the matching equation only in an average sense. Indeed the scalar value of $u_1(t)$, not depending on the spatial coordinate z, may be isolated from the control spatial distribution $g(z,t)$ in the matching equation when computing moments for this distribution. For instance for the average value, we get:

$$\begin{aligned} & \int_0^1 g(z,t)\, u_1(t)\, dz = \int_0^1 \left[\mathcal{J}_d(x,t) - \mathcal{R}_d(x,t)\right] \frac{\partial \mathbb{H}_d}{\partial x} dz - \int_0^1 \left[\mathcal{J}(x,t) - \mathcal{R}(x,t)\right] \frac{\partial \mathbb{H}}{\partial x} dz \\ \Leftrightarrow\ & u_1(t) \int_0^1 g(z,t)\, dz = \int_0^1 \left[\mathcal{J}_d(x,t) - \mathcal{R}_d(x,t)\right] \frac{\partial \mathbb{H}_d}{\partial x} dz - \int_0^1 \left[\mathcal{J}(x,t) - \mathcal{R}(x,t)\right] \frac{\partial \mathbb{H}}{\partial x} dz \\ \Leftrightarrow\ & u_1(t) = \frac{\int_0^1 \left[\mathcal{J}_d(x,t) - \mathcal{R}_d(x,t)\right] \frac{\partial \mathbb{H}_d}{\partial x} dz - \int_0^1 \left[\mathcal{J}(x,t) - \mathcal{R}(x,t)\right] \frac{\partial \mathbb{H}}{\partial x} dz}{\int_0^1 g(z,t)\, dz} \end{aligned} \tag{IV.2}$$

  Therefore the obtained control u_1 is the one which cancels the average value (on the whole spatial domain $[0,1]$) of the residual for the matching equation. The idea could be extended to higher moments of the matching error residual in the case where several control variables are available.

Remark 26. The previous proposed solution for the matching equation only solve it in an average sense. Therefore, one can not transform the original system into the target one, which is stable, with this control. The discussion then consists in knowing whether or not the boundary control $\tilde{u}_2$ can be used to stabilize this "matching error". The proposition in the next section will exploit this idea.

IV.2 IDA-PBC extension: matching equation relaxation

We suggest in the next proposition an extended version of IDA-PBC for infinite dimensional port-Hamiltonian systems, using both finite rank distributed control and boundary backstepping control actions.

Proposition IV.1. *We consider the closed loop system obtained with the average finite rank distributed control defined in the previous section*

$$\dot{x} = [\mathcal{J} - \mathcal{R}]\,\mathcal{Q}x + gu_1 = [\mathcal{J}_d - \mathcal{R}_d]\,\mathcal{Q}_d x + F(x) \tag{IV.3}$$

where $F(x)$ is the error from the matching equation (II.9). We define the Volterra (or backstepping) state space transformation transformation:

$$w = x - \int_0^z k(z,y)\,x(y,t)\,dy \tag{IV.4}$$

where $k(z,y)$ is the Volterra kernel. The boundary control u_2 in (II.1) becomes:

$$\begin{aligned} u_2 &= \mathcal{B}x = \mathcal{B}\left(w + \int_0^z k(z,y)\,x(y,t)\,dy\right) \\ &= \tilde{u}_2 + \mathcal{B}\left(\int_0^z k(z,y)\,x(y,t)\,dy\right) \end{aligned} \tag{IV.5}$$

The original system turns into a new system which is stable, if there exists a corresponding kernel $k(z,y)$ satisfying:

$$\begin{aligned} F(x,z) \quad & -\textstyle\int_0^z k(z,y)\,F(x,y)\,dy - \int_0^z k(z,y)\,[\mathcal{J}_d - \mathcal{R}_d]\,\mathcal{Q}_d(y)\,x(y)\,dy \\ & + [\mathcal{J}_d - \mathcal{R}_d]\,\mathcal{Q}_d \textstyle\int_0^z k(z,y)\,x(y,t)\,dy \qquad\qquad = 0 \end{aligned} \tag{IV.6}$$

Proof.

Combining the two previous equations (IV.3-IV.6), one gets:

$$\begin{aligned} \dot{w} &= \dot{x} - \textstyle\int_0^z k(z,y)\,\dot{x}(y,t)\,\mathrm{d}y \\ &= [\mathcal{J}_d - \mathcal{R}_d]\,\mathcal{Q}_d w \end{aligned} \tag{IV.7}$$

The system (IV.7), without boundary control ($\mathcal{B}w \equiv 0$), is asymptotically stable with $\mathcal{R}_d > 0$, according to the balance equation in (II.8). □

Remark 27. In equation (IV.5), the Volterra transformation kernel $k(z,y)$ describes the way the boundary control u_2 propagates inside the system domain $\mathcal{Z}$, how it allows to compensate the matching error $F(x)$ and to stabilize the closed-loop system when the condition in (IV.6) is satisfied. Furthermore, it's permitted to add a boundary damping via $\tilde{u}_2 = \mathcal{B}w$ defined as $\tilde{u}_2 = -K_p\tilde{y}_2$ in order to improve the stabilization of the system (IV.7), as well as the one of our original system (II.1).

Remark 28. The case where $F(x,z) = 0$ is the classical IDA-PBC design. However, when the kernel $k(z,y)$ is not zero, it helps to choose appropriate controller parameters ($\mathcal{J}_d$, $\mathcal{R}_d$, $\mathbb{H}_d$) such that:

$$\begin{aligned} & -\textstyle\int_0^z k(z,y)\,[\mathcal{J}_d - \mathcal{R}_d]\,\mathcal{Q}_d(y)\,x(y)\,dy \\ & + [\mathcal{J}_d - \mathcal{R}_d]\,\mathcal{Q}_d(z) \textstyle\int_0^z k(z,y)\,x(y,t)\,dy \quad = 0 \end{aligned} \tag{IV.8}$$

The presented methodology may be summarized in the following way:

$$\text{Original system} \quad \begin{cases} \dot{x} & = [\mathcal{J} - \mathcal{R}]\,\mathcal{Q}x + gu_1 \\ \begin{pmatrix} u_2 \\ y_2 \end{pmatrix} & = \mathcal{B}x \\ \mathbb{H} & = \dfrac{1}{2}x^T\mathcal{Q}x \end{cases} \tag{IV.9}$$

(IV.10)

$$\xrightarrow{u_1 \text{ IDA}} \begin{cases} \dot{x} & = [\mathcal{J}_d - \mathcal{R}_d]\,\mathcal{Q}_d x + F(z) \\ \begin{pmatrix} u'_2 \\ y'_2 \end{pmatrix} & = \mathcal{B}x \\ \mathbb{H}_d & = \dfrac{1}{2}x^T\mathcal{Q}_d x \end{cases} \tag{IV.11}$$

$$\xrightarrow{w = x - \int_0^z k(z,y)\,x(y,t)\,\mathrm{d}y} \begin{cases} \dot{w} & = [\mathcal{J}_d - \mathcal{R}_d]\,\mathcal{Q}_d w \\ \begin{pmatrix} \tilde{u}_2 \\ \tilde{y}_2 \end{pmatrix} & = \mathcal{B}w \\ \mathbb{H}_{dw} & = \dfrac{1}{2}w^T\mathcal{Q}_d w \end{cases} \tag{IV.12}$$

We will now derive the new matching equations to determine the system controls u_1 and u_2 together with the appropriate choice of the kernel $k(z,y)$ for the Volterra transformation and the IDA-PBC parameters ($\mathcal{J}_d$, $\mathcal{R}_d$, $\mathbb{H}_d$).

IV.3 Solving new matching equation

In this subsection, we try to solve the matching equation (IV.6) analytically, step by step.

We will make use of the notation $\mathcal{J}_d = \mathcal{J} = \begin{pmatrix} 0 & 1 \\ 1 & 0 \end{pmatrix}\partial_z = i\partial_z$, for compactness. We may transform the last element of equation (IV.6) in the following way:

$$\begin{aligned} [\mathcal{J}_d - \mathcal{R}_d]\,\mathcal{Q}_d \textstyle\int_0^z k(z,y)\,x(y,t)\,\mathrm{d}y &= \begin{array}{c} \mathcal{J}_d\mathcal{Q}_d \int_0^z k(z,y)\,x(y)\,\mathrm{d}y \\ -\mathcal{R}_d\mathcal{Q}_d \int_0^z k(z,y)\,x(y)\,\mathrm{d}y \end{array} \\ &= \begin{array}{c} i\partial_z \int_0^z \mathcal{Q}_d(z)\,k(z,y)\,x(y)\,\mathrm{d}y \\ -\int_0^z \mathcal{R}_d(z)\,\mathcal{Q}_d(z)\,k(z,y)\,x(y)\,\mathrm{d}y \end{array} \\ &= \begin{array}{c} i\mathcal{Q}_d(z)\,k(z,z)\,x(z) \\ +\int_0^z i\partial_z\left(\mathcal{Q}_d(z)\,k(z,y)\right)x(y)\,\mathrm{d}y \\ -\int_0^z \mathcal{R}_d(z)\,\mathcal{Q}_d(z)\,k(z,y)\,x(y)\,\mathrm{d}y \end{array} \end{aligned} \tag{IV.13}$$

since from Leibniz theorem $\partial_z \int_0^z f(z,y)\,\mathrm{d}y = f(z,z) + \int_0^z \partial_z f(z,y)\,\mathrm{d}y$. The third element of (IV.6) becomes:

$$\begin{aligned} -\textstyle\int_0^z k(z,y)\,[\mathcal{J}_d - \mathcal{R}_d]\,\mathcal{Q}_d(y)\,x(y)\,\mathrm{d}y &= \begin{array}{c} -\int_0^z k(z,y)\,i\partial_y\left(\mathcal{Q}_d(y)\,x(y)\right)\mathrm{d}y \\ +\int_0^z k(z,y)\,\mathcal{R}_d(y)\,\mathcal{Q}_d(y)\,x(y)\,\mathrm{d}y \end{array} \\ (\text{ integrate by part}) &= \begin{array}{c} -k(z,z)\,i\mathcal{Q}_d(z)\,x(z) + k(z,0)\,i\mathcal{Q}_d(0)\,x(0) \\ +\int_0^z \partial_y k(z,y)\,i\mathcal{Q}_d(y)\,x(y)\,\mathrm{d}y \\ +\int_0^z k(z,y)\,\mathcal{R}_d(y)\,\mathcal{Q}_d(y)\,x(y)\,\mathrm{d}y \end{array} \end{aligned} \tag{IV.14}$$

We get:

$$\begin{array}{ll} F(x,z) - \int_0^z k(z,y)\,F(x,y)\,\mathrm{d}y & +k(z,0)\,i\mathcal{Q}_d(0)\,x(0) \\ +\int_0^z \partial_y k(z,y)\,i\mathcal{Q}_d(y)\,x(y)\,\mathrm{d}y & +\int_0^z k(z,y)\,\mathcal{R}_d(y)\,\mathcal{Q}_d(y)\,x(y)\,\mathrm{d}y \\ +\int_0^z i\partial_z\left(\mathcal{Q}_d(z)\,k(z,y)\right)x(y)\,\mathrm{d}y + & -\int_0^z \mathcal{R}_d(z)\,\mathcal{Q}_d(z)\,k(z,y)\,x(y)\,\mathrm{d}y \quad = 0 \end{array} \tag{IV.15}$$

which can be reformulated as:

$$\begin{array}{c} \partial_y F(x,y) \\ +\partial_y k(z,y)\, i\mathcal{Q}_d(y)\, x(y) + i\mathcal{Q}_d(z)\, \partial_z k(z,y)\, x(y) \\ +k(z,y)\left(-F(x,y) + i\partial_z \mathcal{Q}_d(z)\, x(y) + \mathcal{R}_d(y)\, \mathcal{Q}_d(y)\, x(y) - \mathcal{R}_d(z)\, \mathcal{Q}_d(z)\, x(y)\right) = 0 \end{array} \tag{IV.16}$$

because, for all function $f(z,t)$ absolutely continuous in $\mathcal{Z}$:

$$f(z,t) = \int_0^z \partial_y f(y,t)\, \mathrm{d}y + f(0,t) \tag{IV.17}$$

Note that the following boundary condition holds:

$$F(x(0)) + k(z,0)\, i\mathcal{Q}_d(0)\, x(0) = 0 \tag{IV.18}$$

IV.3.1 $k(z,y)$ determination

The problem stated in (IV.16) admits an analytical solution by using the variable separation method only in the case where $\partial_y F(x,y) = 0$. Otherwise, the solution is not trivial. In the particular case where $k(z,y) = k(y)$, the boundary condition (IV.18) is satisfied, and the equation (IV.16) becomes:

$$\begin{cases} \partial_y F(x,y) + \partial_y k(z,y)\, i\mathcal{Q}_d(y)\, x(y) & \\ +k(y)\left(-F(x,y) + \mathcal{R}_d(y)\, \mathcal{Q}_d(y)\right) x(y) & = 0 \\ & \\ i\partial_z \mathcal{Q}_d(z) - \mathcal{R}_d(z)\, \mathcal{Q}_d(z) & = 0 \end{cases} \tag{IV.19}$$

The second condition in (IV.19) leads to an appropriate choice of IDA-PBC parameters, which will be studied in the next subsection. The spatial derivative equation of $k(y)$ (the first one of (IV.19)) will define the $k(y)$ kernel from the chosen $\mathcal{R}_d$, $\mathcal{Q}_d$ (which have to be solution of the second equation in (IV.19)):

$$\mathcal{A}(y)\, \partial_y k(y) + \mathcal{D}(y)\, k(y) + \mathcal{C}(y) = 0 \tag{IV.20}$$

Thus $k(y)$ may be computed explicitly:

$$k(y) = e^{-\alpha(y)} \left(\int \beta(y)\, e^{-\alpha(y)} dy + \kappa \right) \tag{IV.21}$$

with $\alpha(y) = \int \frac{\mathcal{D}(y)}{\mathcal{A}(y)} \mathrm{d}y$, $\beta(y) = -\frac{\mathcal{C}(y)}{\mathcal{A}(y)}$ and where κ is a constant of integration depending on the initial condition.

IV.3.2 Find $(\mathcal{R}_d,\, \mathcal{Q}_d)$

The control parameters $(\mathcal{R}_d,\, \mathcal{Q}_d)$ must be computed together with the kernel $k(y)$. Let us denote $\mathcal{R}_d = \begin{pmatrix} r_1 & r_{12} \\ r_{12} & r_2 \end{pmatrix} > 0$ and $\mathcal{Q}_d = \begin{pmatrix} q_1 & q_{12} \\ q_{12} & q_2 \end{pmatrix} > 0$ (note that the case where $q_{12} = 0$ is not possible with our differential operator $\mathcal{J} = i\partial_z$).

We will consider the simple case where $r_1, r_2 > 0$; $r_{12} = 0$ and $q_1 q_2 - q_{12}^2 > 0$. Then the condition for $(\mathcal{R}_d,\, \mathcal{Q}_d)$ in (IV.19) holds if:

$$\begin{cases} \partial_z q_{12} & = r_1 q_1 = r_2 q_2 \\ \partial_z q_1 & = r_2 q_{12} \\ \partial_z q_2 & = r_1 q_{12} \end{cases} \tag{IV.22}$$

Once r_1, r_2 are fixed, these conditions result in:

$$\frac{\partial_z q_1}{\partial_z q_2} = \frac{q_1}{q_2} = \frac{r_2}{r_1} = \alpha(z) > 0 \tag{IV.23}$$

Assume now that $q_2 = \beta(z)$ and $\partial_z \beta(z) \neq 0$. From (IV.23), we get:

$$\begin{cases} q_1(z) & = \alpha(z)\, \beta(z) \\ \partial_z q_1(z) & = \alpha(z)\, \partial_z \beta(z) \end{cases} \Rightarrow \alpha(z) = \alpha\, \text{constant} \tag{IV.24}$$

with the additional condition $-\sqrt{\alpha}r_1 < 0 < \frac{\partial_z q_1}{q_1} < \sqrt{\alpha}r_1$ guaranteeing $\mathcal{Q}_d > 0$. Hence we get

$$q_1(z) = Ce^{\int_0^z (\sqrt{\alpha}r_1 - \epsilon)dz} \tag{IV.25}$$

where C and $\epsilon = \sqrt{\alpha}r_1 - \frac{\partial_z q_1}{q_1} > 0$ are tuning constants.

IV.4 Simulation

The RAPTOR code is employed this time on the example system (III.1). For the sake of simplicity, the control signals are two scalars: the heating power $u_1 = P_{ext}(t)\,(= P_A - P_B)$ of the non-inductive current $\overline{J}_{ext}$ and the loop voltage $u_2 = V_{loop}(t)$.

Using the same scenario test as in subsection III.4.2, chapter 5. Two reference values for safety factor q are defined at $z = 0.1$, and 0.4. The feedforward calculus gives u_d and the equilibrium profile q_d, corresponding to the references and taking into account actuators limits and non-linearities. The boundary IDA-PBC control presented in the previous section defines the feedback signals with the choice of desired dissipation:

$$\mathcal{R}_d = \begin{pmatrix} r_1 & 0 \\ 0 & r_2 \end{pmatrix} > 0$$

where $r_1 = \frac{C_3}{\eta}$ and the ratio $\alpha > 0$ is fixed (we choose $\alpha = 10^{-9}$ since one can only add a very small damping into the magnetic domain via $r_2 > 0$). Then the other IDA-PBC parameters (r_2 and $\mathcal{Q}_d$) are determined based on the conditions in subsection IV.3, equations (IV.22-IV.25). The "distributed" control u_1 is computed from equation (IV.2), as well as the matching error $F(x,z)$ in (IV.3). Finally, the Volterra kernel $k(y)$ is figured out as in (IV.21), that leads to the boundary control value u_2 from (IV.5) when a boundary damping $\widetilde{u}_2 = -K_p\tilde{y}_2$, $K_p > 0$ is also taken on.

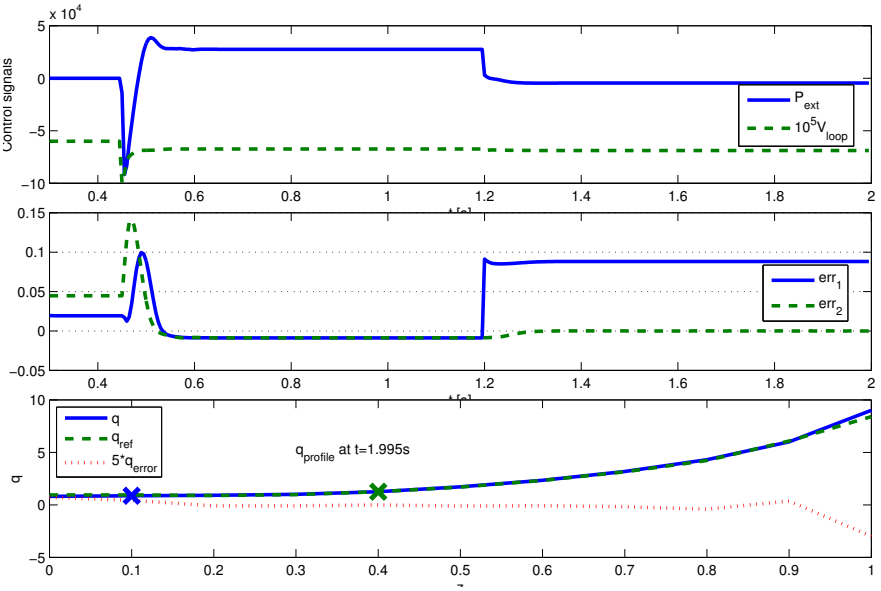

Figure IV.1: Simulation result of boundary IDA-PBC control for infinite dimensional resistive diffusion equation in Tokamaks

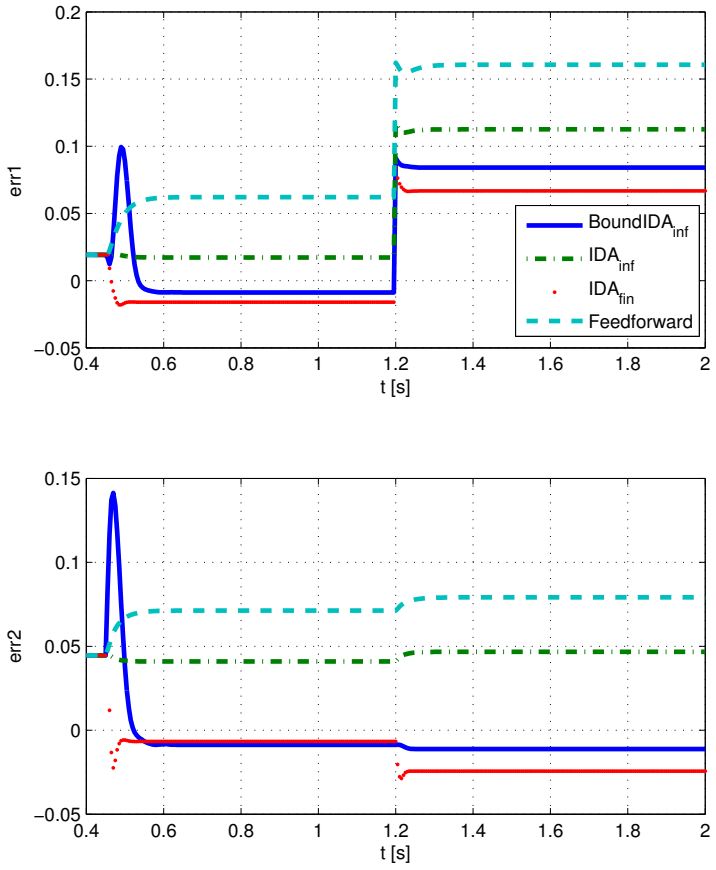

Figure IV.2: Error comparison between the presented method, the infinite IDA without boundary control, the (traditional) finite IDA-PBC and the feedforward control

The figures IV.1 shows the results obtained with the proposed control laws. The controller starts at $t = 0.45s$ with the initial values $(P_{ext},\, V_{loop})_{init} = (0,\, -0.65V)$, whereas at $z = (0.1,\, 0.4)$ the reference q profile is set as $(q_{1a}, q_{2a}) = (0.85,\, 1.25)$. Then at $t = 1.2s$, the reference is changed to $(q_{1b}, q_{2b}) = (0.95,\, 1.25)$.

In figure IV.2, the system errors are examined. The feedforward brings the q profile near to the reference values, but there are still significant static error coming from the linearization and the errors on the system parameter measurements. Three feedback controllers are compared in this work. They are our boundary IDA-PBC control with both $(u_1, u_2)^T$, the only average distributed IDA-PBC control u_1, the finite dimensional IDA-PBC control developed in chapter 5. All the considered feedback controls improve the precision of the closed-loop. Using only u_1 obviously leads to a better result in comparing to the feedforward control but it can't optimize the system errors. The boundary IDA-PBC control $(u_1, u_2)^T$ has nearly the same precision with the finite IDA-PBC control at the center $z = 0.1$ and it gives the best results at the second point near the edge $z = 0.4$ thanks to the possibility of adding boundary damping $\tilde{u}_2 = -K_p \tilde{y}_2$.

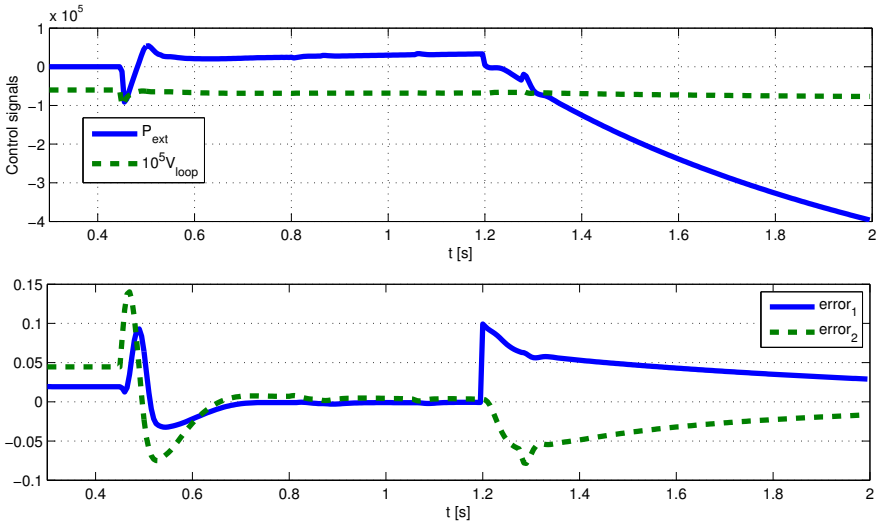

Figure IV.3: Simulation result of boundary IDA-PBC control with integrator

Furthermore, one can also use an integrator (which is similar to the case in II.2 chapter 5) to eliminate the static errors as in the figure IV.3. The equilibrium is quickly reached in the first stage when $t < 1.2s$, and step by step approached in the second stage $t \geq 1.2s$. Nevertheless, it's much more expensive on actuator cost only to get rid of a small static error. Besides, the required control value $P_{ext} = -4.10^5 MW$ at $t = 2s$ is out of the actuator operating range. However, in practice, a small gap on q- profile is still acceptable since it doesn't change much the physical properties of the system.

V Conclusion

In this chapter, a boundary IDA-PBC control for infinite dimensional port-Hamiltonian system is investigated. The distributed control is determined by the "traditional" IDA-PBC principle, while the boundary control is employed to compensate the error from the matching equation. The Volterra transformation is used to prove the stability of the target system.

An energy shaping and damping assignment control has been designed for the resistive diffusion model of the poloidal magnetic flux in tokamak reactors, using the distributed finite rank control u_1 and the boundary control u_2. The actuator spatial distribution has been included in the control design and the matching of the resulting controlled system with the asymptotically stable target system is guaranteed. This is not the case when we use some average matching method for the infinite dimensional system or any finite dimensional IDA-PBC controller.

The proposed controller has been tested on RAPTOR simulation tool developed for the TCV configuration. Numerical experiments show that indeed asymptotic convergence is reached with this feedback control.

Chapter 7

Conclusion and perspectives

In this thesis, a complete methodology has been proposed for the modelling, reduction and control design for finite and infinite dimensional port-Hamiltonian systems. The plasma dynamics in tokamaks has been selected as the particular demonstrating example throughout the thesis.

The port-Hamiltonian framework has been used to build a *3D* model for each subdomain in the tokamak system, including the electromagnetic field volume domain and the moving material domain (for the mass, entropy and momentum balance equations). A complete *3D* port-Hamiltonian model has been built by adding several multidomain MHD couplings. A graphical representation of this model has been proposed using Bondgraph notations which clarify the structure of power exchanges throughout the system, as well as some interdomain couplings of some phenomena such as the bootstrap current or the irreversible entropy in resistive $\mathcal{R}$- field.

A spatial geometric symplectic reduction has been proposed to reduce *3D* port-Hamiltonian models into *1D* control models by using symmetries in the system geometry (i.e. coordinates). The method is based on the power product conservation. The "new" *1D* variables are defined in such a way that simultaneously all power products and interconnection structures are preserved (i.e. transformed into "analogous" *1D* interconnection structures). These ideas has been applied on the tokamak example to get *1D* control models both for the poloidal magnetic flux radial diffusion and for the head radial diffusion.

Based on these control models, the direct and indirect approaches have been investigated for the control design. Therefore both finite and infinite-dimensional IDA-PBC control designs have been proposed.

For the indirect approach, a symplectic discretization method has been developed to get a *0D* continuous PCH control system. Using similar ideas as for the *3D-1D* reduction, the *1D-0D* transformation aims at keeping unchanged the physical properties (energy, spectrum and system structure) of the original system. A symplectic Galerkin scheme has been proposed with different choices for the effort and flow approximation spaces. The method has been validated with Bessel's approximation functions for the resistive diffusion equation and for the heat equation separately and coupled together. Numerical results exhibits excellent spectral properties, the expected dynamical behaviours and qualitative dynamical properties as well as a good agreement with the "experimental" data from the METIS open-loop simulations for real shocks.

Two feedback IDA-PBC control laws have been developed from the obtained finite dimensional PCH tokamak models, respectively for the the resistive diffusion equation of the magnetic flux first and for the coupled TMHD model next. The control objective was the safety factor q-profile regulation. The used feedforward control also handle the actuators saturations and non-linearities. A supplementary integrator eliminates the static errors. The developed control laws have been experimented on the TCV machine and gave quite good results in the single experimental section.

For the direct control approach, a boundary IDA-PBC-like control design has been proposed from the *1D* infinite dimensional port-Hamiltonian model for the resistive diffusion equation. Simultaneous distributed and boundary control actions have been considered. An approximate IDA-PBC matching equation has been used to determine the finite rank distributed control law. The corresponding matching error is then compensated by the backstepping boundary control. The boundary control effect propagating into the whole system domain is settled by the kernel of a Volterra transformation. The proposed method was proved to be asymptotically stable in the sense

of Lyapunov. A simple test on the resistive diffusion equation demonstrates the effectiveness of this infinite boundary IDA-PBC control.

Many perspectives of this work have been outlined, on theoretical as well as on practical aspects. The tokamak modelling should be improved in the material domain in order to take into account the material injection and the fusion reaction phenomena. The idea of system state observer and parameter estimator (i.e. the resistivity, diffusivity, bootstrap current,...) in real time using the PCH framework can be also considered as a possible issue for the next modelling stage since the precision of the mesure obviously plays an important role to facilitate the control synthesis. In other words, a more general tuning methodology for the IDA-PBC parameters could be proposed, as an extension of the optimal design proposed in this thesis. The developed controllers are expected to be experimented on the new configurations of WEST and TCV. The raise of the burn control problem in the port-Hamiltonian formulation is also an important objective for the future works.

Appendix A

Tokamak plasma parameters

Most of the relevant parameters of tokamak plasma which are fixed in the tests are given in the following table.

notation	name	value of WEST	value of TCV	unit
a	small radius of the torus	0.4	0.28	m
z	normalized radius	$[0, 1]$	$[0, 1]$	m
R_0	big torus radius	2.5	0.88	m
B_0	toroidal magnetic field at $z = 0$	3.8	1.45	T
η	homogenous plasma resistivity	5×10^{-7}	10^{-5}	Ωm
$\overline{n}$	average plasma density	4×10^{19}	2×10^{19}	m^{-3}
ϵ	permittivity	8.854×10^{-12}		Fm^{-1}
μ	permeability	$4\pi \times 10^{-7}$		Hm^{-1}

Table .1: Fixed parameters of tokamak plasma

The table .2 summarizes all the significant varying parameters used as system states or system varying parameters in this thesis.

notation	name	unit
B_θ	poloidal magnetic field	T
D	electric field	NC^{-1}
E	electric field intensity	Vm^{-1}
H	magnetic field intensity	Am^{-1}
J	total plasma current density	Am^{-2}
J_Ω	Ohmic current density	Am^{-2}
J_{ni}	non-inductive current density	Am^{-2}
$\mathbb{H}$	total energy of domain	J
$\mathcal{H}$	energy density	Jm^{-3}
ψ	poloidal magnetic flux	Wb
Φ	toroidal magnetic flux	Wb
I_p	plasma current	A
v	average plasma velocity	ms^{-1}
T	average plasma temperature	eV
P	average plasma pressure	Pa
χ	average thermal diffusion coefficient	m^2s^{-1}
C_2, C_3	toric coordinate coefficients	

Table .2: Varying parameters of tokamak plasma

Appendix B

Covariant form

This appendix supplements the recall of the co-variant form in subsection III.1 with the examples and the calculus detail in the *3D* domain $\Omega \in \mathbb{R}^3$.

I Differential forms

Differential forms whose definition is in (III.1) are an approach to multi-variable calculus that is independent of coordinates. Differential forms provide a unified approach to defining integrands over curves, surfaces, volumes, and higher-dimensional manifolds in the mathematical fields of differential geometry and tensor calculus. It has many applications, especially in geometry, topology and physics.

Differential *k-forms* are endowed with a product which we use to compute the power and define the passivity properties, i.e expression of a *k-form* in a space whose has the base $(dz^1, dz^2, ..., dz^n)$:

$$\omega = \sum a_H dz^{h_1} ... dz^{h_k},\ a_H \text{ constants}$$

we also write it in form:

$$\omega = \sum a_H(z^1, ..., z^n) dx^H = \sum a_H dz^H$$

It is antisymmetric in each pair of entries.

$$a(..., dz^i, ..., dz^j, ...) = -a(..., dz^j, ..., dz^i, ...)$$

I.1 Exterior product

Note that the notation $\wedge$ is used in differential forms as exterior multiplication. In the other words, it is applied just on the basis dz^i, for examples in a *3D* space (dx, dy, dz):

- a *0-form* is a function on Ω
- a *1-form* is a vector field
$$\omega^1 = \omega_1 dx + \omega_2 dy + \omega_3 dz$$
- a *2-form* is a flux
$$\omega^2 = \omega_1 dy \wedge dz + \omega_2 dz \wedge dx + \omega_3 dx \wedge dy$$
- a *3-form* is a density
$$\omega^3 = \omega_1 dx \wedge dy \wedge dz$$

For computation, the usual rules of arithmetic are used except the antisymmetry, in particular $dx \wedge dy = -dy \wedge dx$ and $dx \wedge dx = 0$

The **exterior product** is simply the wedge product with the particular rules in differential forms.

$$\wedge : \ \Lambda^p(\Omega) \times \Lambda^q(\Omega) \quad \rightarrow \quad \Lambda^{p+q}(\Omega)$$

Thus if $\omega \in \Lambda^1(\Omega)$ and $\eta \in \Lambda^2(\Omega)$:

$$\omega^1 \quad = \quad \omega_1 dx + \omega_2 dy + \omega_3 dz$$

and

$$\eta^2 \quad = \quad \eta_1 dy \wedge dz + \eta_2 dz \wedge dx + \eta_3 dx \wedge dy$$

So their exterior product will be:

$$\omega^1 \wedge \eta^2 = (\omega_1\eta_1 + \omega_2\eta_2 + \omega_3\eta_3) dx \wedge dy \wedge dz \in \Lambda^3(\Omega)$$

I.2 Exterior Derivative

The **d operator** named exterior derivative turn each *k-form* ω into a *(k+1)-form* $d\omega$.

$$\mathrm{d} : \ \Lambda^k(\Omega) \quad \rightarrow \quad \Lambda^{k+1}(\Omega)$$

In $\mathbf{\Omega} = \mathbb{R}^3$ it will be:

$$\mathrm{d}f^0 = \frac{\partial f}{\partial x}dx + \frac{\partial f}{\partial y}dy + \frac{\partial f}{\partial z}dz$$

Then for a *1-form*:

$$\begin{aligned}\mathrm{d}\omega^1 = &\left(\frac{\partial \omega_1}{\partial x}dx + \frac{\partial \omega_1}{\partial y}dy + \frac{\partial \omega_1}{\partial z}dz\right) \wedge dx + \left(\frac{\partial \omega_2}{\partial x}dx + \frac{\partial \omega_2}{\partial y}dy + \frac{\partial \omega_2}{\partial z}dz\right) \wedge dy \\ &+ \left(\frac{\partial \omega_3}{\partial x}dx + \frac{\partial \omega_3}{\partial y}dy + \frac{\partial \omega_3}{\partial z}dz\right) \wedge dz \\ = &\left(\frac{\partial \omega_3}{\partial y} - \frac{\partial \omega_2}{\partial z}\right) dy \wedge dz + \left(\frac{\partial \omega_1}{\partial z} - \frac{\partial \omega_3}{\partial x}\right) dz \wedge dx + \left(\frac{\partial \omega_2}{\partial x} - \frac{\partial \omega_1}{\partial y}\right) dx \wedge dy\end{aligned}$$

At last ,when ω is a *2-form:*

$$\begin{aligned}\mathrm{d}\omega^2 = &\left(\frac{\partial \omega_1}{\partial x}dx + \frac{\partial \omega_1}{\partial y}dy + \frac{\partial \omega_1}{\partial z}dz\right) \wedge dy \wedge dz + \left(\frac{\partial \omega_2}{\partial x}dx + \frac{\partial \omega_2}{\partial y}dy + \frac{\partial \omega_2}{\partial z}dz\right) \wedge dz \wedge dx \\ &+ \left(\frac{\partial \omega_3}{\partial x}dx + \frac{\partial \omega_3}{\partial y}dy + \frac{\partial \omega_3}{\partial z}dz\right) \wedge dx \wedge dy \\ = &\left(\frac{\partial \omega_1}{\partial x} + \frac{\partial \omega_2}{\partial y} + \frac{\partial \omega_3}{\partial z}\right) dx \wedge dy \wedge dz\end{aligned}$$

Roughly speaking, the d operator in *3 dimension* is considered as the ordinary *gradient* ∇, *curl* $(\nabla\times)$ *and divergence* $(\nabla.)$.

II Hodge star operator

Let's take Ω^n a *n-dimensional space, the Hodge Star Operator* applying to a *k-form:*

$$\star : \ \Lambda^k \quad (\Omega) \rightarrow \quad \Lambda^{n-k}(\Omega)$$

In Ω^n with the orthogonal basis $dx^1 \wedge ... \wedge dx^n$, take $I = (i_1, ...i_k)$ and the complementary $J = (j_1, ..., j_{n-k})$, thus we have

$$\star(dx^I) = \pm dx^J$$

The sign $\pm$ depends on the computation rules of differential forms.

For examples in Ω^3:

$$\star f^0 = f\, dx \wedge dy \wedge dz \in \Lambda^3(\Omega)$$

$$\star\omega^1 = \omega_1 dy \wedge dz + \omega_2 dz \wedge dx + \omega_3 dx \wedge dy = \omega^2 \in \Lambda^2(\Omega)$$

III Interior product and Contraction

Definition III.1. If v is a vector and α is a *k-form,* the *interior product* is defined:

$$i_v : \Lambda^k(\Omega) \rightarrow \Lambda^{k-1}(\Omega)$$

this interior product of v and α has the same principle of their like vectorial product which has components $v^j a_{i_1 \ldots i_k}$ and its contraction $v^j a_{j i_2 \ldots i_k}$ defining a covariant tensor. They call it a special machinery for contracting vectors and forms.

The explicit way to write this product:

$$i_v \alpha = \sum_{i_2 < \ldots < i_k} \sum_j v^j a_{j i_2 < \ldots < i_k} dx^{i_2} \wedge \ldots \wedge dx^{i_k}$$

The interior product satisfies the following properties:

- $i_{a+b} = i_a + i_b$ and $i_{ca} = c i_a$ with c constant
- i_v is an anti-derivation, like exterior product:

$$i_v(\alpha^p \wedge \beta^q) = (i_v \alpha^p) \wedge \beta^q + (-1)^p \alpha^p \wedge (i_v \beta^q) \tag{III.1}$$

In the following part, we develop explicitly this kind of product applied to different form of α. First, we can denote that:

$$i_v \alpha = \sum_j v_j i_{\partial_j} \alpha$$

Note that $i_v \alpha^0 = 0$ with every $\alpha \in \Lambda^0$ and not like exterior product, this one gets the same orthogonal basis of v and α like this way:

$$i_{\partial_i} \mathrm{d}x^i = 1$$

$$i_{\partial_i} \mathrm{d}x^j = 0$$

But pay attention, from III.1 we have:

$$i_{\partial_i} \left(\mathrm{d}x^j \wedge \mathrm{d}x^i \right) = i_{\partial_i} \left(-\mathrm{d}x^i \wedge \mathrm{d}x^j \right) = -\mathrm{d}x^j$$

Therefore, it does reduce the degree of a *k-form* to a *(k-1)-form.*

III.1 Contraction and corresponding

Let's take some simple examples of contraction calculus. Our goal is to find out the relationship between the exterior, interior and vectorial product (concluding dot product and cross product). Define hereafter the vector field v as a *1-form* and α^k *k-form* $\left(k = \overline{0..3}\right)$ in $\mathbb{R}^3$:

$$v^1 = v_1 dx + v_2 dy + v_3 dz$$

$$\alpha^1 = \alpha_1 dx + \alpha_2 dy + \alpha_3 dz$$

$$\alpha^2 = \alpha_1 dy \wedge dz + \alpha_2 dz \wedge dx + \alpha_3 dx \wedge dy$$

$$\alpha^3 = \alpha_0 dx \wedge dy \wedge dz = \star \alpha^0$$

Note that $\star \alpha^0 = \alpha^3$, and $\star \alpha^1 = \alpha^2$. Before all the product calculations, it's so important to identify a vector associated to an *k-form* α^k in the coordinate of three orthogonal basis (dx, dy, dz). In particular, the *0-form* and *3-form* of α are considered as a scalar function α^0, whereas the *1-form* and *2-form* correspond vector $\overrightarrow{\alpha} = \alpha_1 dx + \alpha_2 dy + \alpha_3 dz$. Hence, the interior product can be written for α^1 as:

$$i_v \alpha^1 = \sum_{i=1}^{3} v_i i_{\partial_i} \left(\alpha^1 \right) = \sum_{i=1}^{3} v_i i_{\partial_i} \left(\alpha_1 dx + \alpha_2 dy + \alpha_3 dz \right) = v_1 \alpha_1 + v_2 \alpha_2 + v_3 \alpha_3$$

So we can see that : $i_v\alpha^1 \equiv \star(v \wedge \star\alpha^1)$ in exterior product term, and $i_v\alpha^1 = \overrightarrow{v}.\overrightarrow{\alpha}$ in vectorial term. In the same manner, we have:

$$\begin{array}{rcl} i_v\alpha^2 & = & \sum_{i=1}^{3} v_i i_{\partial_i}\left(\alpha^2\right) \\ & = & \sum_{i=1}^{3} v_i i_{\partial_i}\left(\alpha_1 dy \wedge dz + \alpha_2 dz \wedge dx + \alpha_3 dx \wedge dy\right) \\ & = & (v_3\alpha_2 - v_2\alpha_3)dx + (v_3\alpha_1 - v_1\alpha_3)dy + (v_2\alpha_1 - v_1\alpha_2)dz \\ & = & -(\star(v^1 \wedge \star\alpha^2)) \end{array}$$

and:

$$\begin{array}{rcl} i_v\alpha^3 & = & \sum_{i=1}^{3} v_i i_{\partial_i}\left(\alpha^3\right) \\ & = & \sum_{i=1}^{3} v_i i_{\partial_i}\left(\alpha_0 dx \wedge dy \wedge dz\right) \\ & = & \alpha_0(v_1 dy \wedge dz + v_2 dz \wedge dx + v_3 dx \wedge dy) \\ & = & \star\left(v^1 \wedge \star\alpha^3\right) \end{array}$$

The correspondence of these products is summarized in the table III.1, chapter 3. This equivalence was also studied in [20, V.A.,p.295-296] for two *1-forms* α^1 and β^1 in $\mathbb{R}^3$: $\alpha = \sum_{i=1}^{3} \alpha_i dx^i$ and $\beta = \sum_{i=1}^{3} \beta_i dx^i$.

Remark 29. In this work, the product $\star(\alpha \wedge \beta)$ may be identified component-wise with the vector product $\begin{pmatrix} \alpha_1 \\ \alpha_2 \\ \alpha_3 \end{pmatrix} \wedge \begin{pmatrix} \beta_1 \\ \beta_2 \\ \beta_3 \end{pmatrix}$. Thereby we can express the magneto-hydrodynamic coupling relations using this expression. In the first instance we write the Lorentz force (IV.6) using the Hodge star product and the exterior product $E_L = i_v B$ and the electromagnetic pressure (V.21) as $\sigma_P = -i_{(\star J)}B$.

Appendix C

Microscopic model (Transport equations)

Based on Boltzmann equation (V.1) (chapter 3), we integrate the products of that equation with 1, mv, and $\frac{mv^2}{2}$ respectively over the velocity domain, in order to deduce the mass, momentum, and energy balances (cf. [16]).

I Equation of continuity (particle transport equation)

When integrating equation (V.1) (chapter 3) over velocity, we get the particle transport equation:

$$\begin{aligned} \int \left(\frac{\partial f_a}{\partial t} + \frac{\partial}{\partial x_\beta} \left(v_\beta f_a \right) + \frac{\partial}{\partial v_\beta} \left(\frac{F_{a\beta}}{m_a} f_a \right) \right) dv &= 0 \\ \Leftrightarrow \frac{\partial n_a}{\partial t} + \frac{\partial}{\partial x_\beta} \left(n_a \overline{v}_a \right) &= 0 \end{aligned} \tag{I.1}$$

Thus it holds:

$$\frac{\partial n_a}{\partial t} + \nabla . \left(n_a \overline{v}_a \right) = 0 \tag{I.2}$$

where $a = e$ or i. It's reduced thanks to the "mass conservation" without external source, and the assumption that the third term of (V.1) (chapter 3) vanishes rapidly as $v \to \infty$. With:

$$\frac{d}{dt} = \frac{\partial}{\partial t} + \overline{v} \nabla \tag{I.3}$$

then:

$$\begin{aligned} \frac{dn_a}{dt} &= \frac{\partial n_a}{\partial t} + \overline{v}_a \nabla . n_a \\ &= -\nabla . \left(n_a \overline{v}_a \right) + \overline{v}_a \nabla . n_a \\ &= -n_a \nabla . \overline{v}_a - \overline{v}_a \nabla n_a + \overline{v}_a \nabla . n_a \\ &= -n_a \nabla . \overline{v}_a \end{aligned} \tag{I.4}$$

as given in equation (V.5) (chapter 3).

II Equation of motion (momentum transport)

Take Boltzmann equation (V.1)$\times mv$, then integrate over velocity:

$$\begin{aligned} m \int v \left(\frac{\partial f_a}{\partial t} + \frac{\partial}{\partial x_\beta} \left(v_\beta f_a \right) + \frac{\partial}{\partial v_\beta} \left(\frac{F_{a\beta}}{m_a} f_a \right) \right) dv &= 0 \\ \Leftrightarrow \frac{\partial \left(mn \overline{v}_a \right)}{\partial t} + \nabla . \left(mn \left\langle v_a v_\beta \right\rangle \right) - en \left(E_a + \frac{1}{c} \left[\overline{v}_a B \right]_a \right) &= 0 \end{aligned} \tag{II.1}$$

Note that e_a takes the value of $e_e = -e$. Now denote $v = \overline{v} + v'$, with the mean velocity $\overline{v}$ and a random velocity v' whose $\langle v' \rangle = 0$, then:

$$\langle v_a v_\beta \rangle = \overline{v}_a \overline{v}_\beta + \left\langle v'_a v'_\beta \right\rangle \tag{II.2}$$

and the second term of (I.2) is:

$$\begin{aligned} \nabla.\left(mn\left\langle v_a v_\beta \right\rangle\right) = & \quad \nabla.\left(mn\overline{v}_a\overline{v}_\beta\right) + \nabla.\left(mn\left\langle v'_a v'_\beta \right\rangle\right) \\ = & \quad mn\overline{v}_\beta \nabla.\left(\overline{v}_a\right) + m\overline{v}_a \nabla.\left(n\overline{v}_\beta\right) + \\ & + \nabla.\left(mn\left\langle v'_a v'_\beta \right\rangle\right) \end{aligned} \tag{II.3}$$

and the pressure tensor is determined:

$$\mathbf{P}_{a\beta} = \int m v'_a v'_\beta f dv = mn\left\langle v'_a v'_\beta \right\rangle = P\delta_{a\beta} + \tau_{a\beta} \tag{II.4}$$

where P denotes the scalar pressure and τ the stress tensor, whereas:

$$\begin{cases} P & = nm\left\langle v'^2 \right\rangle /3 = nT \\ \tau_{a\beta} & = nm\left\langle v'_a v'_\beta - \left(v'^2/3\right)\delta_{a\beta} \right\rangle \end{cases} \tag{II.5}$$

On the other hand, thanks to the continuity equation in (I.2), the first term of equation (II.1) is derived:

$$\begin{aligned} \frac{\partial\left(mn\overline{v}_a\right)}{\partial t} & = mn\frac{\partial \overline{v}_a}{\partial t} + m\overline{v}_a\frac{\partial n}{\partial t} \\ & = mn\frac{\partial \overline{v}_a}{\partial t} - m\overline{v}_a\left[\nabla.\left(n\overline{v}_\beta\right)\right] \end{aligned} \tag{II.6}$$

Then from (III.3-II.6), and (I.3) the momentum transport can be rewritten as:

$$nm\frac{d\overline{v}_a}{dt} = -\nabla P - \nabla \times \tau + en\left(E_a + \frac{1}{c}\left[\overline{v}B\right]_a\right) \tag{II.7}$$

III Energy transport

Take equation (V.1)$\times\dfrac{mv^2}{2}$, then integrate over velocity:

$$\begin{aligned} \int \frac{mv^2}{2}\left(\frac{\partial f_a}{\partial t} + \frac{\partial}{\partial x_\beta}\left(v_\beta f_a\right) + \frac{\partial}{\partial v_\beta}\left(\frac{F_{a\beta}}{m_a}f_a\right)\right)dv & = 0 \\ \Leftrightarrow \frac{\partial}{\partial t}\left(\frac{mn}{2}\left\langle v^2 \right\rangle\right) + \nabla.\left(\frac{mn}{2}\left\langle v^2 v_\beta \right\rangle\right) - en\left(E\overline{v}\right) & = 0 \end{aligned} \tag{III.1}$$

In first term, the total energy ϵ includes the kinetic and potential energy due to equation (II.5):

$$\begin{aligned} \epsilon = \frac{mn}{2}\left\langle v^2 \right\rangle = & \quad \frac{mn}{2}\overline{v}^2 + \frac{mn}{2}\left\langle v'^2 \right\rangle \\ = & \quad \frac{mn}{2}\overline{v}^2 + \frac{3}{2}nT \end{aligned} \tag{III.2}$$

The second term corresponds to the divergence of energy flux:

$$\begin{aligned} \left\langle v^2 v_\beta \right\rangle & = \left\langle \left(\overline{v} + v'\right)^2\left(\overline{v}_\beta + v'_\beta\right)\right\rangle \\ & = \overline{v}^2\overline{v}_\beta + \left\langle v'^2\right\rangle\overline{v}_\beta + 2\overline{v}\left\langle v'v'_\beta\right\rangle + \left\langle \left(v'\right)^2 v'_\beta \right\rangle \\ & = \overline{v}^2\overline{v}_\beta + \frac{\left(3nT\right)\overline{v}_\beta}{nm} + \frac{2\left(\tau + nT\right)\overline{v}}{nm} + \frac{2\mathbf{q}}{nm} \end{aligned} \tag{III.3}$$

hence thanks to the definition of pressure P and stress tensor τ in (II.5), with the heat flux density:

$$\mathbf{q} = \int \frac{m}{2} v'^2 v f dv = mn \left\langle \frac{v'^2}{2} v \right\rangle$$

The energy balance equation in (III.1) is then equivalent to:

$$\begin{aligned} \frac{\partial}{\partial t}\left(\frac{mn}{2}\overline{v}^2 + \frac{3}{2}nT\right) + \nabla.\left\{\left(\frac{mn}{2}\overline{v}^2 + \frac{5}{2}nT\right)\overline{v}_\beta + \tau\overline{v} + \mathbf{q}\right\} \\ -en\left(E\overline{v}\right) = 0 \end{aligned} \tag{III.4}$$

The formula of derivative in (I.3) is used again as:

$$\begin{aligned} \frac{d\epsilon}{dt} &= \frac{\partial \epsilon}{\partial t} + \nabla.\left(\epsilon \overline{v}_\beta\right) \\ &= -\nabla.\left[\left(\epsilon + nT\right)\overline{v}_\beta + \tau\overline{v} + \mathbf{q}\right] + en\left(E\overline{v}\right) + \nabla.\left(\epsilon\overline{v}_\beta\right) \\ &= -\nabla.\left[nT\overline{v}_\beta + \tau\overline{v} + \mathbf{q}\right] + en\left(E\overline{v}\right) \end{aligned} \tag{III.5}$$

IV Equation of internal energy (heat balance equation) and entropy equation

The so-called heat balance equation (or internal energy balance) is derived by means of equation of continuity and motion, the kinetic energy is eliminated in equation (III.4). We first remind the kinetic rate term:

$$\begin{aligned} \frac{d}{dt}\left(\frac{mn}{2}\overline{v}^2\right) &= \left(\frac{m\overline{v}^2}{2}\right)\frac{d}{dt}n + mn\overline{v}\frac{d}{dt}\left(\overline{v}\right) \\ &= -\left(\frac{m\overline{v}^2}{2}\right)\nabla.\overline{v} + \\ &\quad +\overline{v}\left(-\nabla P - \nabla\times\tau + en\left(E + \frac{1}{c}\left[\overline{v}B\right]\right)\right) \\ &= -\frac{3}{2}nT\nabla.\overline{v} + \overline{v}\left(-\nabla P - \nabla\times\tau + enE\right) \end{aligned} \tag{IV.1}$$

due to (I.4) and (II.7), and the fact that $\overline{v}\left[\overline{v}B\right] = 0$. Then (III.5) becomes:

$$\frac{d}{dt}\left(\frac{mn}{2}\overline{v}^2\right) + \frac{d}{dt}\left(\frac{3}{2}nT\right) = -\nabla.\left[P\overline{v} + \tau\overline{v} + \mathbf{q}\right] + en\left(E\overline{v}\right)$$

$$\Leftrightarrow -\frac{3}{2}nT\nabla.\overline{v} + \frac{d}{dt}\left(\frac{3}{2}nT\right) = -P\nabla.\overline{v} - \tau\nabla.\overline{v} - \nabla.\mathbf{q} \tag{IV.2}$$

$$\Leftrightarrow \frac{3}{2}n\frac{d}{dt}T = -P\nabla.\overline{v} - \tau\nabla.\overline{v} - \nabla.\mathbf{q}$$

Finally, the internal energy equation is deduces:

$$\frac{3}{2}n\frac{d}{dt}T = -P\nabla.\overline{v} - \tau\nabla.\overline{v} - \nabla.\mathbf{q} \tag{IV.3}$$

Appendix D

Magnetic toric coordinate

The toric coordinate (r, θ, ϕ) as we mentioned in chapter 3, subsection II.3 is not convenient to modelize the Tokamak system in *1D* model. Instead, we use the magnetic toric coordinate (ρ, θ, ϕ) which is considered *the deformed toric coordinate*, then $r = r(\rho, \theta)$ and $dr = \dfrac{\partial r}{\partial \rho} d\rho + \dfrac{\partial r}{\partial \theta} d\theta$. We develop hereafter the derivative operators in this coordinate.

I From Cartesian to magnetic toric coordinate transformation

We remind here after the relation between Cartesian coordinate (x, y, z) and magnetic toric coordinate (r, θ, ϕ) (figure I.1) . A point at (x, y, z) is equivalent at (r, θ, ϕ) in the new coordinate:

$$\begin{array}{c} x = (R_0 + r cos\theta)\, cos\phi \\ y = (R_0 + r cos\theta)\, sin\phi \\ z = r\, sin\theta \end{array} \tag{I.1}$$

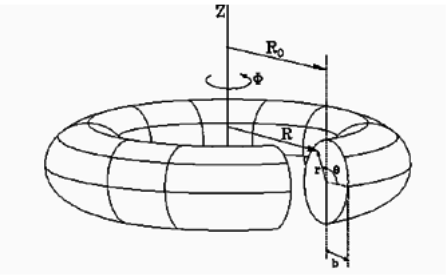

Figure 1. Schematic view of a tokamak.

Figure I.1: Geometric toric coordinate

Let's note $\lambda = R_0 + r cos\theta$, $\delta_\rho = \dfrac{\partial r}{\partial \rho}$, and $\delta_\theta = \dfrac{\partial r}{\partial \theta}$ to simplify the calculation. We compute now a line element in coordinate (x, y, z):

$$\begin{array}{rcc} dl & = & dx.1_x + dy.1_y + dz.1_z \\ & = & \begin{array}{c} (\delta_\rho cos\theta cos\phi\, d\rho + (\delta_\theta cos\theta cos\phi - r sin\theta cos\phi)\ d\theta - \lambda sin\phi\, d\phi)\, 1_x + \\ + (\delta_\rho cos\theta sin\phi\, d\rho + (\delta_\theta cos\theta sin\phi - r sin\theta sin\phi)\ d\theta + \lambda cos\phi\, d\phi)\, 1_y + \\ + (\delta_\rho sin\theta\, d\rho + (\delta_\theta sin\theta + r cos\theta)\ d\theta)\, 1_z \end{array} \end{array} \tag{I.2}$$

Equivalently, we have the new coordinate base (ρ, θ, ϕ):

$$\begin{array}{rcc} e_\rho & = & \delta_\rho \left(cos\theta cos\phi.1_x + cos\theta sin\phi.1_y + sin\theta 1_z\right) \\ e_\theta & = & \left(\delta_\theta cos\theta cos\phi - r sin\theta cos\phi\right) 1_x + \left(\delta_\theta cos\theta sin\phi - r sin\theta sin\phi\right) 1_y + \left(\delta_\theta sin\theta + r cos\theta\right) 1_z \\ e_\phi & = & \lambda \left(-sin\phi 1_x + cos\phi 1_y\right) \end{array} \tag{I.3}$$

Thus the conversion coefficients g can be obtained as:

$$\Longrightarrow \begin{cases} g_\rho = & (e_\rho)^2 = (\delta_\rho)^2 \\ g_\theta = & (e_\theta)^2 = \delta_\theta^2 + r^2 \\ g_\phi = & (e_\phi)^2 = \lambda^2 \end{cases}$$

$$\Longrightarrow g = g_\rho g_\theta g_\phi = (\delta_\rho)^2 \left(\delta_\theta^2 + r^2\right) \lambda^2 \tag{I.4}$$

Then a volume element is written:

$$\begin{array}{rcc} dV & = & \sqrt{g}\, d\rho\, d\theta\, d\phi \\ & = & \delta_\rho d\rho.\sqrt{(\delta_\theta^2 + r^2)} d\theta.\lambda d\phi \end{array} \tag{I.5}$$

On the other hand, we have a common formula to calculate the volume element in the new coordinate:

$$\begin{array}{rcc} dV & = & det\dfrac{(x,y,z)}{(\rho,\theta,\phi)} d\rho\, d\theta\, d\phi \\ & = & r\lambda\, d\rho\, d\theta\, d\phi \end{array} \tag{I.6}$$

whereas $det\dfrac{(x,y,z)}{(\rho,\theta,\phi)}$ is called the determinant of the Jacobian of the transformation from (x, y, z) to (ρ, θ, ϕ) coordinate. As the result, they prove that:

$$\sqrt{g_\rho g_\theta} = \delta_\rho \sqrt{(\delta_\theta^2 + r^2)} = r \tag{I.7}$$

II Derivative operators in magnetic toric coordinate

The following part will develop the expression of *del* operators. Applying on a function f and a vector $A = A_\rho 1_\rho + A_\theta 1_\theta + A_\phi 1_\phi$ in the magnetic toric coordinate:

- Computation of ∇f

$$\begin{array}{rcc} \nabla f & = & \dfrac{1}{\sqrt{g_\rho}} \dfrac{\partial f}{\partial \rho} 1_\rho + \dfrac{1}{\sqrt{g_\theta}} \dfrac{\partial f}{\partial \theta} 1_\theta + \dfrac{1}{\sqrt{g_\phi}} \dfrac{\partial f}{\partial \phi} 1_\phi \\ & = & \dfrac{1}{|\delta_\rho|} \dfrac{\partial f}{\partial \rho} 1_\rho + \dfrac{1}{\sqrt{(\delta_\theta)^2 + r^2}} \dfrac{\partial f}{\partial \theta} 1_\theta + \dfrac{1}{\lambda} \dfrac{\partial f}{\partial \phi} 1_\phi \end{array} \tag{II.1}$$

- Computation of $\nabla \times A$

$$\nabla \times A = \frac{1}{\sqrt{g}} \begin{bmatrix} \sqrt{g_\rho} 1_\rho & \sqrt{g_\theta} 1_\theta & \sqrt{g_\phi} 1_\phi \\ \dfrac{\partial}{\partial \rho} & \dfrac{\partial}{\partial \theta} & \dfrac{\partial}{\partial \phi} \\ \left(\sqrt{g_\rho} A_\rho\right) & \left(\sqrt{g_\theta} A_\theta\right) & \left(\sqrt{g_\phi} A_\phi\right) \end{bmatrix} \tag{II.2}$$

  Remind that we used the notation 3×3 matrix II.2 to simplify the rotation expression, that means the equivalent result is calculated as the determinant of that matrix.

- Computation of $\nabla . A$

$$\nabla \cdot A = \frac{1}{\sqrt{g}} \left[\frac{\partial \left(\sqrt{g_\theta g_\phi} A_\rho\right)}{\partial \rho} + \frac{\partial \left(\sqrt{g_\rho g_\phi} A_\theta\right)}{\partial \theta} + \frac{\partial \left(\sqrt{g_\rho g_\theta} A_\phi\right)}{\partial \phi} \right] \tag{II.3}$$

Appendix E

Theoretical eigenvalues for the diffusion operator

In this appendix we present the calculations needed to obtain eigenvalues and eigenfunctions of the simplified resistive diffusion equation (with homogeneous boundary condition and uniform resistivity). These eigenvalues are compared, in chapter 3, with the numerical ones in order to prove the symplecticity of the proposed discretization schemes and their "spectral" accuracy. The corresponding eigenfunctions are used to generate conjugate compatible bases for the developed symplectic Galerkin method.

I Theoretical eigenvalues for the resistive diffusion equation

From the reduced sub-system in (IV.8), chapter 3, the diffusion model is figured out as:

$$\begin{pmatrix} f_{el\phi} \\ f_{mg\theta} \end{pmatrix} = \begin{pmatrix} 0 & -\dfrac{\partial}{\partial\rho} \\ -\dfrac{\partial}{\partial\rho} & 0 \end{pmatrix} \begin{pmatrix} e_{el\phi} \\ e_{mg\theta} \end{pmatrix} + \begin{pmatrix} 1 \\ 0 \end{pmatrix} f_{d\phi} \tag{I.1}$$

where $f_{mg\theta} = -\partial_t \left(R_0 B_\theta\right) = -\partial_t \tilde{B}_\theta$. For the considered case $f_{el\phi} = 0$, $j_{ni} = 0$, using the constitutive relation (IV.11), chapter 3, we get:

$$\begin{pmatrix} f_{d\phi} \\ -\dfrac{\partial}{\partial t}\tilde{B}_\theta \end{pmatrix} = \begin{pmatrix} 0 & \dfrac{\partial}{\partial\rho} \\ -\dfrac{\partial}{\partial\rho} & 0 \end{pmatrix} \begin{pmatrix} e_{el\phi} \\ e_{mg\theta} \end{pmatrix} = \begin{pmatrix} 0 & \dfrac{\partial}{\partial\rho} \\ -\dfrac{\partial}{\partial\rho} & 0 \end{pmatrix} \begin{pmatrix} \eta\dfrac{R_0}{\rho} & 0 \\ 0 & \dfrac{1}{\mu}\dfrac{\rho}{R_0} \end{pmatrix} \begin{pmatrix} f_{d\phi} \\ \tilde{B}_\theta \end{pmatrix} \tag{I.2}$$

The eigenvalues $-s$ of the resistive diffusion equation are those complex values such that the second order equation:

$$-s\tilde{B}_\theta = \frac{1}{a^2}\frac{\partial}{\partial x}\left(\frac{\eta}{x}\left(\frac{\partial\dfrac{1}{\mu}x\tilde{B}_\theta}{\partial x}\right)\right) = \mathcal{L}\tilde{B}_\theta \text{ where } x := \frac{\rho}{a} \tag{I.3}$$

has a non trivial solution (see the boundary conditions hereafter). In the case of constant coefficients (uniform permittivity and resistivity), the differential operator $\mathcal{L}$ is the classical Laplace operator in toric coordinates:

$$\frac{1}{a^2}\frac{\partial}{\partial x}\left(\frac{\eta}{x}\left(\frac{\partial\dfrac{1}{\mu}x.}{\partial x}\right)\right) \tag{I.4}$$

In this case, one can prove using Green formula (on a disc coordinate cross section of the tokamak) that $-s$ is real and negative. These eigenvalues are calculated hereafter. For the case η and μ

constant, equation (I.3) becomes:

$$x^2\frac{\partial^2}{\partial x^2}\tilde{B}_\theta + x\frac{\partial}{\partial x}\tilde{B}_\theta + \tilde{B}_\theta\left(\frac{\mu s}{\eta}x^2 - 1\right) = 0 \tag{I.5}$$

Let $z^2 = \frac{\mu s}{\eta}x^2$ (where $s > 0$). Then the equation has the standard form of a Bessel equation:

$$z^2\frac{\partial^2}{\partial z^2}\beta + z\frac{\partial}{\partial z}\beta + \beta\left(z^2 - 1\right) = 0 \tag{I.6}$$

whose general solution is:

$$a_0 J_1(z) + a_1 Y_1(z) \tag{I.7}$$

where $J_1(z)$ and $Y_1(z)$ are 1^{st} order Bessel functions of the first and second kind. In particular, $J_1(z)$ can be written:

$$\begin{aligned} J_1(z) &= \frac{1}{\pi}\int_0^\pi cos(\tau - zsin\tau)\,d\tau \\ &= \frac{1}{2\pi}\int_{-\pi}^{\pi} e^{-i(\tau - zsin\tau)}d\tau \\ &= \sum_{m=0}^{\infty}\frac{(-1)^m}{2^{2m+1}m!\,(m+1)!}z^{2m+1} \end{aligned} \tag{I.8}$$

The boundary conditions help us to determine the coefficient a_0 and a_1. The condition at $x = 0$ forces $a_1 = 0$ as $Y_1(z)$ is unbounded when $z \to 0$. The other boundary condition $\partial_x(x\beta)|_1 = 0$ implies:

$$\frac{\partial(zJ_1(z))}{\partial z}\Big|_{z=\sqrt{\frac{s\mu}{\eta}}} = zJ_0(z)\Big|_{z=\sqrt{\frac{s\mu}{\eta}}} = 0 \tag{I.9}$$

Since Bessel functions satisfy:

$$\frac{\partial(zJ_1)}{\partial z} = zJ_0 \tag{I.10}$$

the eigenvalues may be calculated explicitly from the roots of the Bessel function $J_0(z)$. These zeros are represented on figure I.1 hereafter.

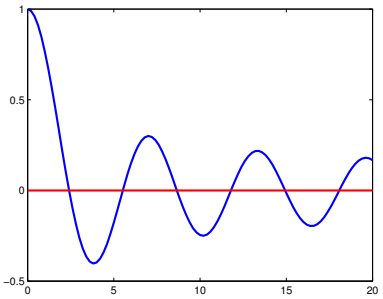

n	1	2	3	4	5
z	2.40482555769577	5.52007811028631	8.65372791291101	11.7915344390142	14.9309177084877

Figure I.1: The Bessel function $J_0(z)$ and its first zeros values

II Theoretical eigenvalues for the thermal diffusion equation

The actual infinite *1D* model for thermal diffusion states in equation (V.6), chapter 3:

$$\sqrt{g}\frac{3}{2}\frac{\partial nT}{\partial t} = \partial_\rho\left(\frac{\sqrt{g_{\theta\theta}g_{\phi\phi}}}{\sqrt{g_{\rho\rho}}}(n\chi\partial_\rho T)\right) + \overline{\sigma}_{\mathbf{s}} \tag{II.1}$$

Let assume in the uniform torus coordinate:

$$\begin{cases} g_\rho & \approx 1 \\ g_\theta & \approx \rho^2 \\ g_\phi & \approx R_0^2 \end{cases} \tag{II.2}$$

where R_0 is the nominal toroidal radius (at $x = 0$) of the torus, and suppose also that the density profile n is time invariant. Then the PDE for effort variable T can be written as:

$$\frac{3}{2}\rho\left(-s_T\right)T = \partial_\rho\left(\rho\chi\left(\partial_\rho T\right)\right) = \mathcal{L}_T T \tag{II.3}$$

where $(-s_T)$ denotes the eigenvalues of the previous diffusion operator $\mathcal{L}$ by Laplace transformation. Remark that the equation (II.3) can also be written:

$$\rho^2\left(\partial_\rho^2 T\right) + \rho\left(\partial_\rho T\right) + \frac{3}{2}\frac{\rho^2 s_T}{\chi}T = 0 \tag{II.4}$$

with $\rho \neq 0$. Let $\lambda^2 = \dfrac{3}{2}\dfrac{\rho^2 s_T}{\chi}$ (where $s, \chi > 0$, $\rho > 0$). Then the equation has the standard form of a Bessel equation:

$$\lambda^2\frac{\partial^2}{\partial\lambda^2}\beta + \lambda\frac{\partial}{\partial\lambda}\beta + \beta\left(\lambda^2 - 0\right) = 0 \tag{II.5}$$

Thus temperature T obviously takes the Bessel function J_{B0}, the solution of the previous order 0 Bessel equation[1].

Like the previous case, the eigenvalues s_T are derived from the zeros of Bessel function order 0 J_{B0} showed on figure I.1.

[1] Note that the general solution of equation (II.5) is $a_0 J_{B0}(\lambda) + a_1 Y_{B0}(\lambda)$, and the condition $\lambda = 0$ forces $a_1 = 0$ as $Y_{B1}(\lambda)$ is unbounded when $\lambda \to 0$

Appendix F

Error analysis of Symplectic Collocation method

I Influence of collocation point choice

It is obvious that the different collocation points get different precisions. We try then to recalculate the eigenvalues with the uniform, Legendre and Chebyshev collocation points. Thanks to the comparison table I.1, the Chebyshev points exhibits more precision then the two others. Furthermore, another remark is that the choice of effort collocation points seem to be more important than those of flux, as all the calculus are based on the effort base functions $w_i^e(x)$, $(i = 1..N)$.

Theoretical eigenvalues	Numerical eigenvalues		
	Uniform points	Legendre points	Chebyshev points
-2.301056852	-2,4122190	-2,3034030	-2.304769649
-12.12413006	-18,6087633	-11,8201217	-12.23545753
-29.79659326	-44,4229304	-27,9562188	-30.39891094
-55.32237139	-92,0432864	-52,8780494	-56.51610868
-88.70194524	-160,4467269	-86,8450446	-88.81543981
-129.9354296	-323,5578853	-131,9484170	-127.9699944
-179.0228628	354,1681743	-208,9253302	-176.7315844
-235.9642604	-627,2508525	-330,3620033	-317.0613604
-300.7596298	-2863,2871125	-2453,3789667	-2547.963503

Table I.1: Comparison the precision of the different collocation point choice among the points uniform, Legendre, Chebyshev $\eta = 5.10^{-7}$

Otherwise, although the variance due to the collocation point choices do affect the precision but it is not really the principle reason of the oscillation in our model. We investigate the second possibility hereafter concerning to the base function choice.

II Influence of eigenfunction, base function choice

We try now to investigate the approximation precision in eigenfunctions aspect. The error computation is refered to [85]. The theoretical eigenfunctions are calculated from the Bessel function of order 1 J_1 just like in equation (III.10), chapter 4:

$$y_k(x) = J_1(\lambda_k x) \tag{II.1}$$

where $\lambda_k = \sqrt{s_k \frac{\eta}{\mu}}$, $k = 1, ...N-1$. The approximating functions are indicated by the Lagrange method:

$$\hat{y}_k(x) = \sum_{j=1}^{N-1} y_k(\xi_j) w_j^f(x) \tag{II.2}$$

with ξ_j, $j = 1...N-1$ are the flux collocation points, $w_j^f(x)$ are the flux base functions. Approximating errors are:

$$E_k(x) = y_k(x) - \hat{y}_k(x) \tag{II.3}$$

Then $E_k(\xi_j) = 0$, $\forall j$ if w^f are orthogonal functions:

$$w_k^f(\xi_j) = \begin{cases} 1 & \text{if } j = k \\ 0 & \text{else} \end{cases} \tag{II.4}$$

II.1 Symplectic collocation with boundary constraints

The base functions chosen in this case are presented in subsection III.1.1, chapter 4.

$$w_i^e = 1 - x^2\zeta_i^2 l_i, \;\; l_i = \prod_{j=1\neq i}^{N} \frac{x-\zeta_j}{\zeta_i-\zeta_j} \tag{II.5}$$

where ζ_i, $i = 1..N$ are the collocation points for efforts, then $deg(w^e) = N+1$.

The flux base functions are indicated from the effort ones as:

$$w^f = (\partial_x w^e) D^+ \tag{II.6}$$

with pseudo inverse $D^+ = D'(DD')^{-1}$, then $deg(\hat{y}) = deg\left(w^f\right) = N$, and remind to the orthogonality of flux base functions $w_j^f(0) = 0$, $\forall j$.

Let's take N degree polynomials $p(x) = x\prod_{j=1}^{N-1}(x-\xi_j)$, so $p(x)$ vanishes at 0 and $N-1$ flux collocation points ξ_j: $p(0,\xi_j) = 0$. Then define a function $F(z)$ which is:

$$F(z) = y(z) - \hat{y}_k(z) - [y_k(x) - \hat{y}_k(x)]\frac{p(z)}{p(x)} \tag{II.7}$$

We have $\{0,\xi_j\}$ and x are $N+1$ roots of $F(z)$. It's possible thus to apply N times the Rolle's theorem on $F(z)$, we get:

$$F(z)^{(N)} = y(z)^{(N)} - \hat{y}(z)^{(N)} - [y(x) - \hat{y}(x)]\frac{N!}{p(x)} \tag{II.8}$$

then there's at least a $\zeta \in [0,\xi_{N-1}]$ satisfies $F(\zeta) = 0$. In orders words:

$$E(x) = y(x) - \hat{y}_k(x) = \left[y(\zeta)^{(N)} - \hat{y}(\zeta)^{(N)}\right]\frac{p(x)}{N!} \tag{II.9}$$

However, as $deg(\hat{y}) = N$, so the constant $\left(y(\zeta)^{(N)} - \hat{y}(\zeta)^{(N)}\right)$ also has an important effect on $E(x)$. The figure II.1 shows the very significant error in eigenfunction approximation, this polynomial base function choice just sticks at the collocation points, such as with the first and the fifth eigenvalues, but not elsewhere.

II.2 Symplectic collocation without boundary constraints

Once realizing that the constant error left in the previous base function choice, consider now the case without integrating boundary conditions, we simply take effort base function equal to the Lagrange polynomials of degree $N-1$, $deg(w^e) = N-1$:

$$w_i^e = l_i, \;\; l_i = \prod_{j=1\neq i}^{N} \frac{x-\zeta_j}{\zeta_i-\zeta_j} \tag{II.10}$$

Similar to the previous case, flux base functions w^f has the degree of $N-2$:

$$deg(\hat{y}) = deg\left(w^f\right) = N-2 \tag{II.11}$$

This time the polynomials $p(x)$ is taken as:

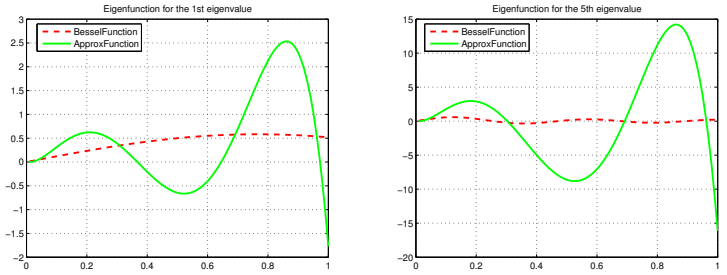

Figure II.1: The first and fifth calculated eigenfunctions with boundary conditions $w_i^e = 1 - x^2\zeta_i^2 l_i$ vs theoretical Bessel eigenfunctions

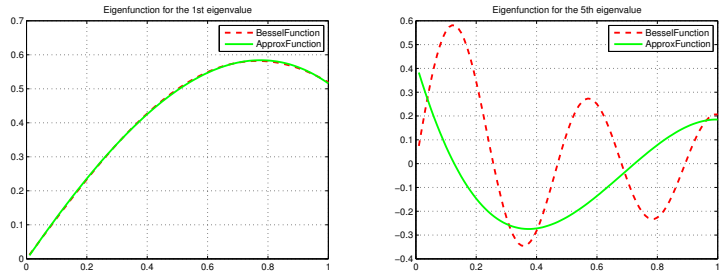

Figure II.2: Simulation for the case of $we_i = le_i$ with constant $\eta = 5.10^{-7}$, without boundary conditions

$$p(x) = \prod_{j=1}^{N-1} (x - \xi_j) \tag{II.12}$$

where $deg(p) = N - 1$ and of course $p(\xi_j) = 0$.

With the same function $F(z)$ as before:

$$F(z) = y(z) - \hat{y}_k(z) - [y_k(x) - \hat{y}_k(x)] \frac{p(z)}{p(x)} \tag{II.13}$$

We have now N roots (ξ_i and x) of $F(z)$, then $N - 1$ times the Rolle's theorem is applied:

$$F(z)^{(N-1)} = y(z)^{(N-1)} - \hat{y}(z)^{(N-1)} - [y(x) - \hat{y}(x)] \frac{(N-1)!}{p(x)} \tag{II.14}$$

then there's at least a $\zeta \in [\xi_1, \xi_{N-1}]$ satisfies $F(\zeta) = 0$. In orders words:

$$E(x) = y(x) - \hat{y}_k(x) = \left[y(\zeta)^{(N-1)} - \hat{y}(\zeta)^{(N-1)} \right] \frac{p(x)}{(N-1)!} \tag{II.15}$$

In this case $\hat{y}(z)^{(N-1)} = 0$ since $deg(\hat{y}) = N - 2$, the approximation error is thus of order of $y^{(N)} = J_1^{(N)}$, and it has the order of 10^{-5} with $N = 10$. In the figure II.2, the eigenfunction is better approached with the first eigenvalue, and has the same magnitude order with the fifth eigenvalue. But of course, the boundary condition can't be satisfied.

In conclusion, symplectic collocation method used to achieve in many PCH discretization model, with this example of parabolic plasma resistive diffusion, it even gives a very good eigenvalue approximation. However, the bad eigenfunction approximation, caused by the boundary condition integrating in the base function choice, leads strange numerical oscillation in the simulation.

Appendix G

Finite difference approximation scheme

In section III, chapter 4, a finite-difference scheme is used for the spatial discretization of the resistive diffusion equation written in the port-Hamiltonian form. The accuracy of the spectrum approximation obtained with this scheme is then compared with the one derived from the symplectic collocation and Galerkin schemes. To achieve a fair comparison, a very special case has to be considered. First, the grid points for the finite difference scheme are zeros of Chebyshev polynomials. Besides, the spectrum accuracy is maximal with Chebyshev points. Then, homogeneous boundary conditions have to be considered. Indeed, whatever the choice of discretization points is, the finite difference scheme is not symplectic at all (with respect to the bilinear power product used to defined the Stokes-Dirac structure) for open systems (with non autonomous boundary conditions). This will result in unstable and oscillating modes (and meaningless values for the spectrum) in the finite difference approximated model while the resistive diffusion model itself is of course purely dissipative. The finite difference scheme used to solve the resistive diffusion equation (for the unknown function $\tilde{B}_\theta = R_0 B_\theta$) with these assumptions is presented hereafter. We start from the simplified resistive diffusion equation:

$$\begin{array}{rcl} \dfrac{\partial \tilde{B}_\theta}{\partial t} & = & \dfrac{\eta}{\mu a^2}\dfrac{\partial}{\partial x}\left(\dfrac{1}{x}\dfrac{\partial}{\partial x}\left(x\tilde{B}_\theta\right)\right) - \eta\dfrac{\partial}{\partial x} j_{ni} \\ & = \dfrac{\eta}{\mu a^2} & \left(\dfrac{1}{x^2}\tilde{B}_\theta + \left(\dfrac{1}{x}+1\right)\dfrac{\partial}{\partial x}\tilde{B}_\theta + x\dfrac{\partial^2}{\partial x^2}\tilde{B}_\theta\right) - \eta\dfrac{\partial}{\partial x} j_{ni} \end{array} \tag{.1}$$

By denoting $\mathbf{b_i}$, $(i = 1..N)$ the approximated values of $\tilde{B}_\theta$ at the discretization points x_i (zeros of the $(N-2)^{th}$ order Chebyshev polynomial, completed with the two boundary values, in our case), one gets:

$$\begin{array}{rcl} \dfrac{\partial \mathbf{b}_i}{\partial t} & = & \dfrac{\eta}{\mu a^2}[-\dfrac{1}{x_i^2}\mathbf{b}_i + \left(\dfrac{1}{x_i}+1\right)\dfrac{\mathbf{b}_{i+1}-\mathbf{b}_{i-1}}{\delta_{i+1}+\delta_i} \\ & & +2x_i\dfrac{\mathbf{b}_{i+1}-2\mathbf{b}_i+\mathbf{b}_{i-1}}{\delta_{i+1}^2+\delta_i^2}] \;\; \forall i = 2..(N-1) \end{array} \tag{.2}$$

where

$$\left\{\begin{array}{rcl} \delta_{i+1} & = & x_{i+1} - x_i \\ \delta_i & = & x_i - x_{i-1} \end{array}\right.$$

The boundary conditions give the missing values for $\mathbf{b}_1$ and $\mathbf{b}_N$:

$$\left\{\begin{array}{rcl} \tilde{B}|_{x_1=0} = 0 & \Rightarrow & \mathbf{b}_1 = 0 \\ \partial_x\left(x\tilde{B}\right)|_{x_N=1} = 0 & \Rightarrow & \mathbf{b}_N = \dfrac{\mathbf{b}_{N-1}}{2-x_{N-1}} \end{array}\right. \tag{.3}$$

Written in matrix form (convenient for instance for eigenvalues computations) the diffusion equation becomes:

$$\frac{\partial \mathbf{b}}{\partial t} = \frac{\eta}{\mu a^2} \underbrace{\begin{bmatrix} \beta_2 & \gamma_2 & & & 0 \\ \ddots & \ddots & \ddots & & \\ & \alpha_i & \beta_i & \gamma_i & \\ & & \ddots & \ddots & \ddots \\ 0 & & & \alpha_{N-1} & \left(\beta_{N-1} + \frac{1}{2 - x_{N-1}}\gamma_{N-1}\right) \end{bmatrix}}_{A} \mathbf{b} \tag{.4}$$

with $\mathbf{b} := (\mathbf{b}_2, \ldots, \mathbf{b}_{N-1})^T$ and where:

$$\begin{cases} \alpha_i &= \left(-\dfrac{\frac{1}{x_i} + 1}{\delta_{i+1} + \delta_i} + 2\dfrac{x_i}{\delta_{i+1}^2 + \delta_i^2} \right) \\ \beta_i &= \left(-\dfrac{1}{x_i^2} - \dfrac{4x_i}{\delta_{i+1}^2 + \delta_i^2} \right) \qquad \forall i = 2..(N-1) \\ \gamma_i &= \left(\dfrac{\frac{1}{x_i} + 1}{\delta_{i+1} + \delta_i} + 2\dfrac{x_i}{\delta_{i+1}^2 + \delta_i^2} \right) \end{cases} \tag{.5}$$

As it has been noticed, this finite difference scheme with over $N = 200$ points has spectral properties (see table III.1), chapter 4 which are comparable to those obtained with the collocation method with about $N = 10$ discretization points (see table III.2), chapter 4. Basically, the eigenvalues calculated from the characteristic matrix A in the equation .4 (which is however a tri-diagonal matrix) converge to the theoretical values as $\frac{1}{N}$, while those obtained with the collocation method (and its full matrix) as $\frac{1}{N^2}$.

Bibliography

[1] F.B. Argomedo, C. Prieur, E. Witrant, and S. Brémond. A strict control lyapunov function for a diffusion equation with time-varying distributed coefficients. *IEEE Transactions on Automatic Control*, 2012.

[2] M. Ariola and A. Pironti. *Magnetic Control of Tokamak Plasmas.* Advances in Industrial Control. Springer Verlag, London, 2008. ISBN 978-1-84800-323-1.

[3] J.F. Artaud and al. The cronos suite of codes for integrated tokamak modelling. *Nuclear Fusion*, 50(4), 2010.

[4] A. Baaiu, F. Couenne, D. Eberard, C. Jallut, Y. Le Gorrec, L. Lefevre, and M. Tayakout-Fayolle. Port-based modelling of mass transfer phenomena. *Mathematical and Computer Modelling of Dynamical Systems*, 15(3):233–254, 2009.

[5] A. Baaiu, F. Couenne, D. Eberard, C. Jallut, Y. Legorrec, L. Lefèvre, and B. Maschke. Port-based modelling of mass transport phenomena. *Mathematical and Computer Modelling of Dynamical Systems*, 22(1):1–22, 2009.

[6] A. Baaiu, F. Couenne, L. Lefevre, Y. Le Gorrec, and M. Tayakout-Fayolle. Structure-preserving infinite dimensional model reduction: Application to adsorption processes. *Journal of Process Control*, 19:394–404, 2009.

[7] A. Baaiu, F. Couenne, Y. Legorrec, L. Lefèvre, and M. Tayakout. Structure-preserving infinite dimensional model reduction application to adsorption processes. *Journal of Process Control*, 19(3):394–404, 2009.

[8] M. Becherif and E. Mendes. Stability and robustness of disturbed-port controlled hamiltonian systems with dissipation. In *Proceedings of the 16th IFAC world congress*, Praha, Cesch Republic, 2005.

[9] G. Blankenstein and A.J. van der Schaft. Symmetry and reduction in implicit generalized hamiltonian systems. *Rep. Math. Phys.*, 47(1):57–100, December 15-17 2001.

[10] J. Blum. *Numerical Simulation and Optimal Control in Plasma Physics.* Gauthier-Villars, 1989.

[11] A.H. Boozer. Onsager symmetry of transport in toroidal plasmas. *Phys.Fluids*, 4(9):2845–2853, September 1992.

[12] A. Bossavit. *Computational Electromagnetism.* Academic Press, 1998.

[13] M.D. Boyer, J. Barton, E. Schuster, and et al. First-principles-driven model-based current profile control for the diii-d tokamak via lqi optimal control. *Plasma Physics and Controlled Fusion*, (55), 2013.

[14] M.D. Boyer and E. Schuster. Adaptive nonlinear burn control in tokamak fusion reactors. *American Controls Conference, Montréal, Canada*, June 2012.

[15] M.D. Boyer and E. Schuster. Nonlinear burn control in tokamak fusion reactors via output feedback. *19th IFAC World Congress, Capetown, South Africa*, August 2014.

[16] S.I. Braginskii. *Reviews of Plasma Physics, M.A. Leontovich editor*, volume 1, chapter Transport Processes in a Plasma, pages 205–311. Consultants Bureau, New York, 1965.

[17] T.J Bridges. Multi-symplectic structures and wave propagation. *Math. Proc. Camb. Phil. Soc.*, 121:147–190, 1997.

[18] T.J. Bridges. Multi-symplectic integrators: numerical schemes for Hamiltonian PDEs that conserve symplecticity. *Physics Letters A*, 284:184–193, June 2001.

[19] J. Bucalossi, A. Argouarch, V. Basiuk, and all. Feasibility study of an actively cooled tungsten divertor in tore supra for iter technology testing. *Fusion Engineering and Design*, (86):684–688, 2011.

[20] Y. Choquet-Bruhat and C. De Witt-Morette. *Analysis Manifolds and Physics*. North-Holland Publ. Co., revised edition, 1982.

[21] T.J. Courant. Dirac manifolds. *Trans. American Math. Soc. 319*, pages 631–661, 1990.

[22] R.F. Curtain and H.J. Zwart. *An introduction to Infinite-Dimensional Linear System Theory*. Springer-Verlag, i edition, 1995. ISBN 0-387-94475-3.

[23] M. Dalsmo and A.J. van der Schaft. On representations and integrability of mathematical structures in energy-conserving physical systems. *SIAM Journal of Control and Optimization*, 37(1):54–91, 1999.

[24] S.R. de Groot and P. Mazur. *Non-equilibrium thermodynamics*. Dover Books on Physics. Dover Publications, 2nd edition edition, 1984. ISBN 0486647412.

[25] F. Delebecque, J.-P. Quadrat, S. Bremond, A.Witrant, and J-F Artaud. Simple modeling and control of plasma current profile. Oct. 2008.

[26] F.L. Waelbroeck E. Tassi, P.J. Morrison and D. Grasso. Hamiltonian formulation and analysis of a collisionless fluid reconnection model. *Plasma Physics and Controlled Fusion*, (50), may 2008.

[27] M. Erba, T. Aniel, V. Basiuk, A. Becoulet, and X. Litaudon. Validation of a new mixed bohm/gyro-bohm for electron and ion heat transport against the iter, tore supra and start database discharges. *Nuclear Fusion*, 6(7):2835–2839, July 1998.

[28] D. Moreau et al. A two-time-scale dynamic-model approach for magnetic and kinetic profile control in advanced tokamak scenarios on jet. *Nuclear Fusion*, 48(10):1–38, July 2008.

[29] F. Felici and O. Sauter. Non-linear model-based optimization of actuator trajectories for tokamak plasma profile control. *Plasma Physics and Controlled Fusion*, 54, 2012.

[30] F. Felici, O. Sauter, S. Coda, B.P. Duval, T.P. Goodman, J.M. Moret, J.I. Paley, and the TCV Team. Real-time physics-model-based simulation of the current density profile in tokamak plasmas. *Nuclear Fusion*, 51, 2011.

[31] B.A. Finlayson. *The method of weighted residuals and variational principles*. Academic Press, 1972.

[32] B. Fornberg. *A Practical Guide to Pseudospectral Methods*. Cambridge University Press, 1996.

[33] A. Franco, P. Schott, C. Jallut, and B.M. Maschke. Multi-scale bond graph model of the electrochemical dynamics in a fuel cell. In *Proceedings of the of the 5th MathMod conference*, Vienna, Autsria, 2006.

[34] A.A Franco, P. Schott, C. Jallut, and B.M. Maschke. A multi-scale dynamic mechanistic model for transient analysis of pefcs. *Fuel Cells: From Fundamentals to Systems*, 7(2):99–117, April 2007.

[35] T. Frankel. *The Geometry of Physics : an Introduction*. Cambridge University Press, Cambridge, 2nd edition edition, 2004. ISBN 0-521-53927-7.

[36] A.J. van der Schaft G. Golo, V. Talasila and B. Maschke. Hamiltonian discretization of the the Telegrapher's equation. *Automatica*, 2004.

[37] B. Maschke G. Nishida, K. Takagi and T. Osada. Multi-scale distributed parameter modeling of ionic polymer-metal composite soft actuator. *Control Engineering Practice*, 19(4):321–334, 2011.

[38] X. Garbet and et al. Thermodynamics of neoclassical and turbulent transport. *Plasma Phys. Control. Fusion*, (54), April 2012.

[39] O. Gaye, E. Moulay, S. Brémond, L. Autrique, R. Nouailletas, and Y. Orlov. Sliding mode stabilization of the current profile in tokamak plasmas. *CDC*, December 2011.

[40] G. Golo, V. Talasila, A.J. van der Schaft, and B. Maschke. Hamiltonian discretization of boundary control systems. *Automatica*, 40(5):757–771, 2004.

[41] E. Hairer, C. Lubich, and G. Wanner. *Geometric numerical integration : structure-preserving algorithms for ordinary differential equations*, volume 31 of *Springer Series in Computational Mathematics*. Springer-Verlag, Berlin Heidelberg, 2002. ISBN 3-540-43003-2.

[42] B. Hamroun, L. Lefevre, and E. Mendes. Port-based modelling for open channel irrigation systems. *Transactions on Fluid Mechanics*, 1(12):995–1009, 2006.

[43] B. Hamroun, L. Lefevre, and E. Mendes. A port-controlled hamiltonian approach to geometric reduction of distributed parameters systems - application to the shallow water equations. *International Journal of Numerical Methods in Engineering*, 2009.

[44] B. Hamroun, L. Lefevre, and E. Mendes. Control by interconnection and energy-shaping methods of port Hamiltonian models - application to the shallow water equations. *European Journal of Control*, 16(5):1–19, 2010. DOI: 10.3166 / EJC.16.1-19.

[45] B. Hamroun, L. Lefevre, and E. Mendes. Port-based modelling for open channel irrigation systems. In *Proceedings of the 2nd IASME/WSEAS Int.ernational Conference on Water Resources, Hydraulics and Hydrology*, Portorose, Slovenia, May 2007.

[46] F.L. Hinton and R.D. Hazeltine. Theory of plasma transport in toroidal confinement systems. *Review of Modern Physics*, 48:239–308, 1976.

[47] P.E Hydon. Multisymplectic conservation laws for differential and differential-difference equations. *Proceedings of the royal society A*, 461:1627–1637, 2005.

[48] A. Weinstein J.E. Marsden, T. Ratiu. Semidirect products and reduction in Mechanics. *Trans. American Math. Society*, (281):147–177, 1984.

[49] D.C. Karnopp, D.L. Margolis, and R.C. Rosenberg. *System Dynamics: Modeling and Simulation of Mechatronic Systems*. John Wiley and Sons, 2006.

[50] M. Krstic and A. Smyshlyaev. *Boundary control of PDEs: A course on Backstepping designs*. Advances in Design and Control, SIAM, Philadelphia, 2008.

[51] A. Kugi. *Non-linear Control Based on Physical Models: Electrical, Hydraulic and Mechanical Systems*, volume 260 of *Lecture Notes in Control and Information Science*. Springer, London, Great Britain, 2000. ISBN 978-1852333294.

[52] Y. Le Gorrec, H. Zwart, and B.M. Maschke. Dirac structures and boundary control systems associated with skew-symmetric differential operators. *SIAM J. of Control and Optimization*, 44(5):1864–1892, 2005.

[53] A. Macchelli. Boundary energy shaping of linear distributed port-hamiltonian systems. *European Journal of Control*, 19:521–528, 2013.

[54] A. Macchelli and B.M. Maschke. *Modeling and Control of Complex Physical Systems - The Port-Hamiltonian Approach*, chapter Infinite-dimensional Port-Hamiltonian Systems, pages 211–272. Springer, Sept. 2009. ISBN 978-3-642-03195-3.

[55] A. Macchelli and C. Melchiorri. Modeling and control of the Timoshenko beam. the Distributed Port Hamiltonian approach. *SIAM Journal On Control and Optimization*, 43(2):743–767, 2004.

[56] A. Macchelli and C. Melchiorri. Control by interconnection of mixed port hamiltonian systems. *IEEE Transactions on Automatic Control*, 50:1839–1844, 2005.

[57] A. Macchelli, A.J. van der Schaft, and C. Melchiorri. Port hamiltonian formulation of infinite dimensional systems. i. modeling. *Proc. 50th IEEE Conference on Decisions and Control (CDC04)*, 2004.

[58] A. Macchelli, A.J. van der Schaft, and C. Melchiorri. Port hamiltonian formulation of infinite dimensional systems. ii. boundary control by interconnection. *43rd IEEE Conference on Decisions and Control (CDC04)*, 2004.

[59] J.E. Marsden, T. Ratiu, and A. Weinstein. Reduction and hamiltonian structures on duals of semidirect product Lie algebras. *AMS Contemporary Mathematics*, 28:55–100, 1984.

[60] J.E. Marsden and T.S. Ratiu. Reduction of poisson manifolds. *Lett. in Math. Phys.11*, pages 161–170, 1986.

[61] J.E. Marsden, T.S. Ratiu, and A.Weinstein. Reduction and hamiltonian structures on duals of semidirect product lie algebras. *Cont. Math. AMS 28*, pages 55–100, 1984.

[62] J.E. Marsden and A. Weinstein. The Hamiltonian structure of the Maxwell-Vlasov equations. *Physica D: nonlinear phenomena*, 4(3):394–406, 1982.

[63] B. Maschke and A.J. van der Schaft. *Advanced Topics in Control Systems Theory. Lecture Notes from FAP 2004*, chapter Compositional modelling of distributed-parameter systems, pages 115–154. Lecture Notes on Control and Information Sciences. Springer, 2005.

[64] B.M. Maschke and A. J. van der Schaft. Canonical interdomain coupling in distributed parameter systems: an extension of the symplectic gyrator. In *Proc. Int. Mechanical Engineering Congress and Exposition*, New- York, USA, Nov. 2001. ASME.

[65] B.M. Maschke and A.J. van der Schaft. Port controlled Hamiltonian systems: modeling origins and system theoretic properties. In *Proc. 3rd Int. IFAC Conf. on Nonlinear Systems' Theory and Control,, NOLCOS'92*, pages 282–288, Bordeaux, June 1992.

[66] J. Mikles and M. Fikar. *Process modelling, identification, and control.* Springer, 2007.

[67] D. Moreau, F. Crisanti, X. Litaudon, and et al. Real-time control of the q-profile in jet for steady state advanced tokamak operation. *Nuclear Fusion*, 46:870–882, August 2003.

[68] P.J. Morrison. Hamiltonian description of the ideal fluid. *Rev. Mod. Phys.*, 70(2):467–521, Apr 1998.

[69] P.J. Morrison and J.M. Greene. Noncanonical Hamiltonian density formulation of hydrodynamics and ideal magnetohydrodynamics. *Phys. Rev. Lett.*, 45(10):790–794, Sep 1980.

[70] R. Moulla, L. Lefèvre, and B. Maschke. Pseudo-spectral methods for the spatial symplectic reduction of open systems of conservation laws. *Journal of Computational Physics*, 231(4):1972–1992, December 2012.

[71] G. Nishida and N. Sakamoto. Port-based modeling of magnetohydrodynamics equations for tokamaks. *IEEE Control Applications (CCA)*, pages 842–847, September 2010.

[72] G. Nishida, K. Takagi, and B.M. Maschke. Multiscale distributed port-hamiltonian representation of ionic polymer-metal composite (ipmc). In *Proc. IFAC World Congress 2008*, pages 2300–2305, Seoul, Korea,, July 6-11 2008.

[73] P.J. Olver. *Applications of Lie Groups to Differential Equations*, volume 107 of *Graduate texts in mathematics*. Springer, New-York, ii edition, 1993. ISBN 0-387-94007-3.

[74] L. Onsager. Reciprocal relations in irreversible processes. *Phys. Rev.*, 2265(38), December 1931.

[75] R. Ortega and E. Garcia-Canseco. Interconnection and damping assignment passivity-based control: A survey. *Eur. J Control*, 10:432–450, 2004.

[76] R. Ortega and Mark W. Spong. Stabilization of underactuated mechanical systems via interconnection and damping assignment. *Automatic Control*, 47:1218 – 1233, 2002.

[77] R. Ortega, A.J. van der Schaft, F. Castanos, and A. Astolfi. Control by interconnection and standard passivity-based control of port-hamiltonian systems. *IEEE Trans. on Automatic Control*, 53(11):2527–2542, 2008.

[78] R. Ortega, A.J. van der Schaft, B. Maschke, and G. Escobar. Interconnection and damping assignment: passivity-based control of port-controlled Hamiltonian systems. *Automatica*, 38(4):585–596, 2002.

[79] Y. Ou, C. Xu, and E. Schuster. Robust control design for the poloidal magnetic flux profile evolution in the presence of model uncertainties. *IEEE Transactions on Plasma Sciences*, 32(3):375–382, March 2010.

[80] Y. Ou, C. Xu, E. Schuster, T.C. Luce, J.R. Ferron, M.L. Walker, and D.A. Humphreys. Optimal tracking control of current profile in tokamaks. *IEEE Transaction on Control Systems Technology*, 19(2):432–441, March 2011.

[81] H. Ouarit, S. Brémond, R. Nouailletas, E. Witrant, and L. Autrique. Validation of plasma current profile model predictive control in tokamaks via simulations. *SOFT*, September 2010.

[82] R. Pasumarthy and A.J. van der Schaft. On interconnections of infinite dimensional port-hamiltonian systems. In *Proc. Sixteenth International Symposium on Mathematical Theory of Networks and Systems, MTNS2004*, Leuven, Belgium, July 5-9 2004.

[83] A. Pironti and M. Walker. Fusion, tokamaks and plasma control. *IEEE Control Systems Mag.*, 25:30–43, 2005.

[84] M. Polner and J.J.W. van der Vegt. A hamiltonian vorticity-dilatation formulation of the compressible euler equations. *Nonlinear Analysis*, (109):113–135, July 2014.

[85] A. Ralston and P. Rabinowitz. *A first course in numerical analysis*. Dover Publication,Inc, Mineola, Newyork, 2nd edition, 2001.

[86] S. Reich. Multi-symplectic Runge-Kutta collocation methods for Hamiltonian wave equations. *Journal of Computational Physics*, 157:473–499, 2000.

[87] R.Moulla, L. Lefevre, and B. Maschke. Geometric pseudo-spectral method for spatial integration of dynamical systems. *Mathematical and Computer Modelling of Dynamical Systems, special issue on Modelling, Analysis and Control of Distributed Parameter Systems*, 17(1):85–104, 2011. Kurt Schlacher and Markus Schoberl editors.

[88] R.Ortega and E.Garcia-Canseco. Interconnection and damping assignement passivit-based control: A survey. *European Journal of Control*, 110, 2003.

[89] A. Jamiolkowski R.S. Ingarden. *Classical Electrodynamics*. PWN-Polish Sc. Publ. Elsevier, Warszawa, Poland, 1985.

[90] O. Sauter, C. Angioni, and Y.R. Lin-Liu. Neoclassical conductivity and bootstrap current formulas for general axisymmetric equilibria and arbitrary collisionality regime. *Physic of Plasma*, 6(7):2835–2839, July 1999.

[91] M. Schöberl and A. Siuka. On casimir functionals for field fheories in port-hamiltonian description for control purposes. *50nd IEEE Conference on Decision and Control, Orlando, FL, USA*, December 12-15 2011.

[92] E. Schuster and M. Krstic. Control of a nonlinear pde system arising from non-burning tokamak plasma transport dynamics. *International Journal of Control*, 76(11):1116–1124, 2003.

[93] E. Schuster, M. Krstic, and G. Tynan. Nonlinear lyapunov-based burn control in fusion reactor. *Fusion Engineering and Design*, (63-64):569–575, 2002.

[94] E. Schuster, M. Krstic, and G. Tynan. Burn control in fusion reactors via nonlinear stabilization techniques. *Fusion Science and Technology*, (43), 2003.

[95] S. Stramigioli. *Modeling and IPC Control of Interactive Mechanical Systems: a Coordinate-free Approach*, volume 266 of *Lect. Notes in Control and Information Sci.* Springer, London, Great Britain, 2001. ISBN 1-85233-395-2.

[96] G.E. Swaters. *Introduction to Hamiltonian fluid dynamics and stability theory.* Chapman & Hal/CRC, 2000.

[97] A.J. van der Schaft. *L_2-Gain and Passivity Techniques in Nonlinear Control.* Springer Communications and Control Engineering series. Springer-Verlag, London, 2nd revised and enlarged edition, 2000. first edition Lect. Notes in Control and Inf. Sciences, vol. 218, Springer-Verlag, Berlin, 1996.

[98] A.J. van der Schaft and B.M. Maschke. The Hamiltonian formulation of energy conserving physical systems with external ports. *Archiv für Elektronik und Übertragungstechnik*, 49(5/6):362–371, 1995.

[99] A.J. van der Schaft and B.M. Maschke. Hamiltonian formulation of distributed parameter systems with boundary energy flow. *J. of Geometry and Physics*, 42:166–174, 2002.

[100] J. Vankerschaver, H. Yoshimura, M. Leok, and J.E. Marsden. Stokes-dirac structures through reduction of infinite-dimensional dirac structures. *49th IEEE Conference on Decision and Control, Hilton Atlanta Hotel, Atlanta, GA, USA*, December 15-17 2010.

[101] S. Stramigioli V.Duindam, A. Macchelli and H. Bruyninckx eds. *Modeling and Control of Complex Physical Systems - The Port-Hamiltonian Approach.* Springer, Sept. 2009. ISBN 978-3-642-03195-3.

[102] J. Villegas, H. Zwart, Y. Le Gorrec, and B.M. Maschke. Stability and stabilization of a class of boundary control systems. *IEEE Transaction On Automatic Control*, 54:142–147, January 2009.

[103] J.A. Villegas, , H. Zwart, Y. Le Gorrec, B. Maschke, and A.J. van der Schaft. Stability and stabilization of a class of boundary control systems. In *Proc. 44th IEEE Conference on Decision and Control and European Control Conference ECC 2005*, pages 3850 – 3855, Seville, Spain, December 12-15 2005.

[104] J.A. Villegas, Y. Le Gorrec, H. Zwart, and B. Maschke. Boundary control for a class of dissipative differential operators including diffusion systems. In *Proc. 7th International Symposium on Mathematical Theory of Networks and Systems*, pages 297–304, Kyoto, Japan,, July 24-28 2006.

[105] M.L. Walker, D.A. Humphreys, D. Mazon, D. Moreau, M. Okabayashi, T.H. Osborne, and E. Schuster. Emerging applications in tokamak plasma control. *IEEE Control Systems Mag.*, 26:35–63, 2006.

[106] J. Wesson. *Tokamaks. Third edition.* Oxford Science Publications, 2004.

[107] E. Witrant, E. Joffrin, S. Brémond, G. Giruzzi, D. Mazon, O. Barana, and P. Moreau. A control-oriented model of the current profile on tokamak plasma. *Plasma Physics and Controlled Fusion*, 49:1075–1105, 2007.

[108] H. Zwart, Y. Le Gorrec, B. Maschke, and J. Villegas. Well-posedness and regularity of hyperbolic boundary control systems on a one-dimensional spatial domain. *ESAIM: Control, Optimisation and Calculus of Variations*, August 2009. Published Online: DOI: 10.1051/cocv/2009036.